UNIVERSITÉ CATHOLIQUE DE LOUVAIN

Thesis submitted to fulfil the requirements for the degree of PhD in biomedical and pharmaceutical sciences

Towards the discovery and synthesis of new Arginase 1 inhibitors

Julien R. C. Prevost

Promoter:

Pr. Raphaël Frédérick (UCLouvain, Belgium)

Jury members:

Pr. Olivier Feron (**President**) (UCLouvain, Belgium)
Pr. Didier Lambert (UCLouvain, Belgium)
Pr. Lionel Pochet (University of Namur, Belgium)
Pr. Pascal De Tulio (University of Liège, Belgium)
Dr. Marc Pudlo (University of Franche-Comté, France)
Pr. Johan Wouters (University of Namur, Belgium)

REMERCIEMENT

*Je tiens à remercier en premier lieu le **Prof. Raphaël Frédérick**, mon promoteur pour m'avoir offert l'opportunité de réaliser mon doctorat au sein de son groupe, mais aussi pour ses conseils et la patience qu'il a eu pour corriger cette thèse et les autres manuscrits qui ont rythmé ces années de recherche. Merci pour la grande liberté scientifique qu'il m'a octroyée tout au long de ce projet. Cela m'a permis d'améliorer considérablement mon background scientifique tout en gagnant en maturité et en autonomie.*

*Je voudrais remercier aussi les membres du comité d'accompagnement, ainsi que les membres additionnels qui forme le jury : **Prof. Olivier Feron, Prof. Didier Lambert, Prof. Lionel Pochet, Prof. Pascal de Tulio, Dr. Marc Pudlo** et **Prof. Johan Wouters**. Je voudrais ajouter à cette liste le **Prof. Giulio Muccioli**, qui a été présent lors du comité d'accompagnement. Je tiens à les remercier pour leurs encouragements et leurs soutiens dans ce projet ainsi que pour leurs nombreuses remarques scientifiques pertinentes. C'est grâce à leurs remarques constructives que ce travail a pu avancer et s'améliorer.*

*Je voudrais remercier tout particulièrement toutes les personnes qui ont travaillé sur ce projet et en particulier **Arina** et **Arnaud** qui se sont beaucoup impliqués dans le cadre de la synthèse des bromothiazoles et dans leurs évaluations avec **Bouazza**. Un tout grand merci à nos collaborateurs de Namur, de UCLouvain et de Berlin, avec qui nous avons pu travailler pour faire avancer la recherche dans le domaine de l'arginase. Grâce à leurs expertises dans leur domaine, nous avons pu compléter nos travaux par des données d'analyses (X-ray, Mass Spectrometry…) mais aussi pu discuter de nos résultats respectifs afin d'avancer en équipe. Merci aussi aux différents étudiants chercheurs : **Nicolas**, **Raphaël**, et **Reda,** qui se sont succédés au fil des ans sur ce projet difficile et qui ont fait preuve de résilience.*

Je remercie également tous mes collègues du laboratoire pour leur bonne humeur, les discussions scientifiques et le soutien qu'ils ont pu m'apporter : les doctorants ***Quentin***, ***Urbain***, ***Léopold***, ***Marine(1)***, ***Romain***, ***Chiara***, ***Perrine***, ***Juhans***, ***Marine(2)***, ***Darius, Yonghua***, ***Giuditta*** *et* ***Séraphin****, sans oublier, les post-doct'* ***Séverine***, ***Simon***, ***Max*** *et* ***Karine*** *qui nous ont donné de très bons conseils tout en nous faisant profiter de leur bonne humeur.*

Quentin*, je n'oublie pas que je te dois une partie de Magic. C'est la moindre des choses vu le nombre de fois où je t'ai empêché de dormir à cause de mes ronflements lors des congrès. N'oublie pas que j'ai toujours ton vin dans ma cave.*

Léo*, après ton départ, le bureau n'a jamais été le même. Il y manquait une odeur particulière à laquelle je m'étais habitué. Mais merci pour tous les moments où j'ai pu te parler sans que tu m'écoutes ou que tu partes faire autre chose avant la fin de notre échange.*

Merci à ***Arina*** *et* ***Mar1*** *pour nos conversations de filles et tous ces moments de commérages. Merci Arina d'avoir relu ce manuscrit et pour les brunchs et soirées jeux de sociétés avec Léo. Mar1, merci d'avoir été là durant la période du Covid pour partager pizzas et autres mets après notre TD du lundi soir. On aura passé de bons moments lors des TP où les étudiants pensaient qu'on était mariés ensemble.*

Merci ***Darius*** *et* ***Max*** *pour ces moments sur Warzone. On aura quand même fini par faire un top1 malgré notre niveau catastrophique et mes lagues. Max, j'espère pouvoir faire rapidement notre sortie à Pairi Daiza ou à Nausicaa avec* ***Juliette***, ***Marie*** *et les enfants.*

Je n'oublierai pas non plus les soirées foot, rugby ou toute autre excuse avec ***Séverine***, ***Romain***, ***Quentin, Jacques*** *et* ***Urbain****. Ces moments de partage et de gastronomie m'ont laissé des souvenirs impérissables.*

Merci ***Chiara*** *de nous avoir fait découvrir Rome. Nous ne serions pas aller voir « il buco della serratura » sans toi. Merci à* ***Perrine*** *pour les longues*

discussions sportives mais aussi de me rappeler que ma région natale me manque parfois. Merci à ***Mar2*** *pour sa bonne humeur mais aussi pour les discussions autour de la formule 1 et cette espèce de rivalité bon enfant qui s'est créé entre nous qui supportions des écuries et des pilotes différents.*

Merci à ***Simon*** *pour ses découvertes cinématographiques et musicales aussi variées que douteuses.*

Merci à ***Karine*** *pour nos discussions de « vieux » et pour avoir pu partager ensemble nos craintes et d'autres choses qui me tenaient parfois à cœur.*

Merci à ***Yonghua****,* ***Giuditta*** *et* ***Séraphin*** *d'avoir partagé vos cultures, vos valeurs mais surtout votre bonne humeur.*

Merci à ***Juhans*** *d'avoir repris la relève sur le projet arginase. Je te souhaite beaucoup de courage dans la suite de ce projet, en espérant que tu auras plus de chance que paparginase. Merci aussi pour tous ces debriefs de footeux les lendemains de ligue des champions. Merci aussi à* ***Jacques****, pour ses discussions et aux techniciens du groupe :* ***Bouazza****,* ***Jonathan****,* ***Gwen****,* ***Esra*** *et* ***Assia****, pour le travail qu'ils ont effectué au laboratoire. Bouazza et Esra, merci pour les petits déjeunés et les moments café lors desquels on a pu échanger sur nos cultures et convictions personnels. Malgré qu'il ne reste que très peu de temps, je voulais aussi remercier nos autres étudiants-chercheurs, ainsi que tous nos stagiaires qui ont participé à nos recherches.*

Je voudrais aussi remercier tous mes collègues de l'enseignement : ***Béatrice****,* ***Pascale****,* ***Ahmed****,* ***Bernadette****,* ***Mickael****,* ***Lionel****,* ***Corentin****,* ***Jérôme****,* ***Ricky****,* ***Axel****,* ***Marine****,* ***Martin****,* ***Sharon****,* ***Ramazan*** *et* ***Sarah****. Et surtout Mohamed Ayadim pour ses nombreux conseils.*

Bien sûr, je n'oublie pas de remercier tout particulièrement ma famille. Merci ***Papa*** *et* ***Maman*** *pour votre soutien indéfectible lors de la réalisation de cette thèse, mais aussi tout au long de ma vie en général. Merci d'avoir toujours cru en moi, et de m'avoir laissé le choix de faire ce que je désirais sans aucun à priori. Il est évident de dire que sans vous je ne serais pas là où j'en suis à l'heure*

actuelle. Vous m'avez permis de me développer et de m'accomplir pleinement, de réaliser les projets qui me tenaient à cœur. Il n'y a pas de mot assez fort pour vous exprimer toute ma gratitude. Je ne le dis pas souvent et je l'écrirai encore moins mais sachez que je vous aime. Je voudrais aussi remercier celle avec qui j'ai fait mes études et qui partage maintenant ma vie. Merci Marie d'avoir été là dans les mauvais moments, tout comme dans les bons. Mais surtout, merci de m'avoir offert le plus beau des cadeaux : ma fille ***Élise****, qui illumine mes journées depuis le 11 décembre 2020.*

Merci aussi à mes amis : ***Aurélien****,* ***Florian****,* ***Julie****,* ***Geoffrey****,* ***Fanny****,* ***Enzo****,* ***Guillaume, Marion****… pour ne citer qu'eux, pour leur soutien et leur amitié inconditionnels. Vous êtes les meilleurs amis qu'on puisse rêver.*

Je suis aussi très reconnaissant à l'Université catholique de Louvain (UCLouvain) de m'avoir accordé le financement pour effectuer cette recherche.

Merci à tous et pour tout

Julien

Pour mes Parents, ma femme et ma fille
Advienne que pourra

PREAMBLE

The enzyme arginase is a hydrolase existing as two different isoforms that is responsible for the hydrolysis of L-arginine to urea and L-ornithine. It is particularly important in the urea cycle and in the immune system. Many studies demonstrated that arginase 1 (Arg1) is upregulated in various types of cancers and plays crucial roles in tumor growth and metastasis through various mechanisms such as regulating L-arginine metabolism and influencing tumor immune microenvironment. Arg1 is thus a particularly attractive target for cancer therapy. So far, the more potent Arg1 inhibitors reported are characterized by a boronic acid warhead that is linked *via* aliphatic linkers to an amino-acid tail. Although some of these compounds are very potent on Arginase 1 (Arg1), only one Arg1 inhibitor is currently being evaluated in clinical settings and, in fact, no Arg1 inhibitor was approved yet. The search for new Arg1 inhibitors possibly characterized with better pharmacokinetic properties is thus still the subject of intense research.

In this thesis, our aim was to discover new arginase inhibitors that would be more amenable to preclinical experiments compared to existing Arginase inhibitors that usually encompass a boronic acid warhead limiting pharmacokinetic properties. Hence this research program was initiated some time before the starting of this PhD thesis through collaborative works with the team of Medicinal Chemistry at the University of Namur. A first screening of an in-house library of compounds at University of Namur notably led to the identification of a first new hit compound on Arg1 characterized by a 5-bromo-aminothiazole scaffold. At the very beginning of the PhD thesis our aim was thus to pursue that particular scaffold and optimize its structure to reach a higher Arg1 inhibition. Because the inhibition of Arg1 by this compound could not be confirmed, we next envisioned a molecular modelling approach to detail Arg1 inhibition and possibly help the discovery of new Arg1 inhibitors.

Chapter one is an introduction providing a comprehensive overview of the physiological and biological roles of arginase and its implication in cancer progression. The reported Arginase 1 inhibitors are also described, as well of the different existing enzyme assays to determine Arginase activity and inhibition.

After introducing the general aim and the strategies used in this thesis in **chapter two**, the results will be presented in three different chapters.

In **chapter three**, our experiments to setup and validate a reliable Arg1 inhibition assay are presented. This includes our works to produce and purify Arg1, and the development of a radiometric Arg1 inhibition assay. This assay was validated using reference inhibitors. The use of this assay to measure Arg1 inhibition of the compounds with a 5-bromo-Aminothiazole previously identified at UNamur, in fact, overturned this series that revealed to be false-positive compounds probably because of aggregation issues.

In **chapter four**, a molecular modelling approach aiming at understanding Arg1 inhibition and identifying new Arg1 inhibitors was undertaken. For this, a thorough bibliographic search on the currently available structural knowledge on Arg1 was performed and led to the development of an original dynamic pharmacophore, called *dynophore*. This original *dynophore* reflects the enzyme plasticity and the limited possibility in terms of drug design to discover new Arg1 inhibitor. It also constitutes an original tool to possibly identify new Arg1 inhibitors.

In **chapter five**, this dynamic pharmacophore was used in a fragment-based drug discovery approach to possibly identify new Arg1 inhibitors deprived of the boronic acid head. The compounds identified virtually were experimentally assessed but unfortunately no hit could be obtained, hence revealing the crucial role of the boronic acid head to inhibit Arg1 and the challenge to find new Arg1 inhibitors.

Based on the knowledge gathered following the development of the *dynophore* and what we learned from the unsuccessful screening experiments, we finally investigated novel original boronic acid compounds including novel non-aliphatic chemical linkers between the boronic acid warhead and the amino-acid tail.

In fact, our aim was to take advantage of two imidazoles from two histidine residues delineating the Arg1 cavity in the region of the linker to tentatively improve the potency of Arg1 inhibitors.

In **chapter six**, an attempt to optimize two hits discovered using the data collected in the previous chapters is presented. The challenges to synthesize furan derivatives is illustrated.

In **chapter seven**, the conclusions of this work are summarized, and the perspectives are outlines to respond to the different challenges encountered.

Finally, although the 5-bromo-aminothizoles initially investigated as Arg1 inhibitor were not pursued, their chemical synthesis remained very interesting. A part of the time of this thesis was thus devoted to detail the chemical synthesis of these 5-bromo-aminothiazoles. This part of the work is presented in annex to this thesis.

TABLE OF CONTENTS

Table of abbreviations

2AH	L-2-aminohistidine
A1P	2-(S)-amino- 5-(2-aminoimidazol-1-yl)pentanoic acid
A4P	2-amino-5-(2-aminoimidazol-4-yl)pentanoic acid
ABH	2-(S)-amino-6-boronohexanoic acid
AHD	(S)-2-aminoheptanedioic acid
ANH	(S)-2-amino-6-nitrohexanoic acid
AOH	(S)-2-amino-7-oxoheptanoic acid
Arg1	arginase 1
Arg2	arginase 2
ASH	(S)-2-amino-6-sulfonamidohexanoic acid
BEC	S-(2-boronoethyl)-L-cysteine
CD3ζ	ζ chain of the cluster of differentiation 3
CHES	*N*-Cyclohexyl-2-aminoethanesulfonic acid
DFMO	2-(difluoromethyl)-L-ornithine
DPM	disintegrations per minute
*e*NOS	endothelial nitric oxide synthase
FABH	2-amino-6-borono-2-(difluoromethyl)hexanoic acid
FBDD	fragment-based drug design
FDA	food and drug administration
HPLC	high-performance liquid chromatography
IC_{50}	half maximal inhibitory concentration
IFN	interferon
IL	interleukin
*i*NOS	inducible nitric oxide synthase or NOS2
*K*a	acid dissociation constant

k_{cat}	apparent unimolecular rate constant
K_D or K_d	dissociation constant
Ki	inhibition constant
K_M	Michaelis constant
L-NAME	Nω-nitroarginine methyl ester
L-NOHA	Nω-hydroxy-L-Arginine
MABH	6-borono-2-methylhexanoic acid
MDSCs	myeloid-derived suppressor cells
NF-κB	nuclear factor kappa-light-chain-enhancer of activated B cells
NOHA	Nω-hydroxy-L-Arginine
nor-NOHA	Nω-Hydroxy-nor-L-Arginine
NOS	nitric oxide synthase
PDB	Protein Data Bank
PGE2	prostaglandin E_2
pIC_{50}	half maximal inhibitory concentration at logarithmic scale
pKa	acid dissociation constant at logarithmic scale
pKi	inhibition constant at logarithmic scale
quant.	quantitative
R_f	retention factor
RMSD	root-mean-square deviation
RMSF	root-mean-square fluctuation
RP2D	recommended phase 2 dose
SBDD	structure-based drug design
SEC	S-(2-sulfonamidoethyl)-L-cysteine
TAM	tumor-associated macrophage
TGF-β	transforming growth factor beta
Tm	unfolding midpoint temperature

TNF	tumor necrosis factor
TOGA	thioornithine generation assay
T_{reg}	regulatory T cells
Tris	tris(hydroxymethyl)aminomethane
V_{max}	maximum rate achieved by the system

1 INTRODUCTION

1.1 ARGINASE, A PROMISING THERAPEUTIC TARGET FOR ANTICANCER IMMUNOTHERAPY: STRUCTURES, FUNCTIONS, AND PHYSIOLOGICAL ROLES

1.1.1 Structures and functions

Arginase is a hydrolase that exists as two isoenzymes, arginase 1 (Arg1) and arginase 2 (Arg2), catalyzing the same reaction. Arg1 and Arg2 are trimeric enzymes[1] that use L-arginine **1** as a substrate. They are similar from a structural point of view and share a similar mechanism of catalysis. (Figure 1)

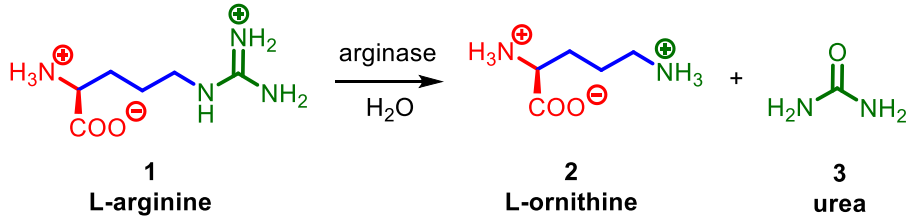

*Figure 1: Hydrolysis catalyzed by Arginase. L-arginine **1** is converted to L-ornithine **2** and urea **3**.*

1.1.1.1 Comparison between Arg1 and Arg2

The distinct characteristics of these two isoenzymes are listed in Table 1.

Table 1:characteristics of arginase isoenzymes.

	Arginase 1	Arginase 2
Uniprot entry	P05089	P78540
Chromosomal location	6q23.2	14q24.1
Number of Residues	322	354
Cellular localization	Cytosol	Mitochondrion
Tissue specificity	liver, red blood cell, immune system, placenta	Kidney, prostate, intestinal tract, mammary gland, myometrium, immune and nervous systems,
	Endothelium	

Two different genes encode Arginase isoenzymes. Sequence alignment and comparison show that isoenzymes have an overall 54% sequence identity (190 over the 354 amino acids) with a 100% identity in their active sites. Arg1 and Arg2 have 190 conserved amino acids, and 94 residues are homologs. Arg2 differs from Arg1 by cellular location. Arg2 is a mitochondrial enzyme and thus possesses a transit sequence allowing its recognition and import into the mitochondria. The identity of both isoenzymes can reach 57% without considering the 22 amino acids transit peptide. It is also interesting to note that Arg1 is very well conserved in mammals, and human Arg1 has high homology with the rat Arg1 (86%) widely used for research purposes. Both Arg1 and Arg2 possess a carboxy-terminal S-shaped domain (81% identity) that allows oligomerization.[2] Arg-308 is particularly important for oligomerization by stabilizing the trimers.[3] (Figure 2)

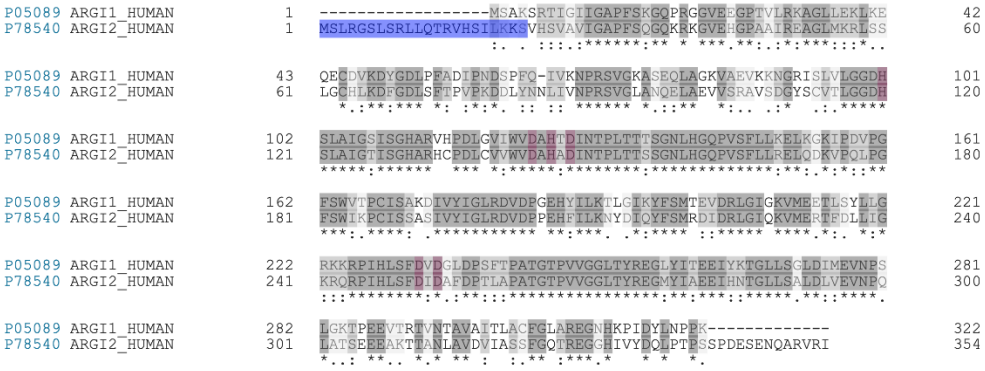

Figure 2: UniProt Protein alignment for Arg1 and Arg2. ***Blue****: transit peptide,* ***pink****: metal binding.* ***dark grey**** *conserved residue,* ***grey.*** *strongly similar properties,* ***light grey:*** *weakly similar properties*

Their respective roles differ as well as their locations. Arg1 is generally considered a hepatic enzyme. However, it is also found in red blood cells, the placenta, and cells of the immune system. Arg1 plays an essential role in inflammation, immune regulation, and tumor escape mechanisms. HIF-α production and immune suppression are crucial in ontogeny, especially placenta formation and development. On the other hand, Arg2, also known as mitochondrial or renal, is

found in endothelial cells and peripheral tissues such as the kidney, prostate, small intestine, nervous system, myometrium, or mammary gland during lactation.

Despite their different locations, the function of both isoenzymes is paired with a Nitric Oxide Synthase (NOS); The inducible *i*NOS for Arg1 and the constitutive endothelial *e*NOS for Arg2. The role of NOS is to control the release of nitric oxide (NO) for reactive oxygen species (ROS) production in immune mechanisms and vasodilation in the endothelial function.

1.1.1.2 Structure of Arg1

The enzyme is relatively compact with an approximate dimension of 40x50x50 Å. 8 parallel β sheets and 9 α helixes constitute the secondary structures of the enzyme. The arginase is an homotrimer[4] and belongs to the α/β protein class[5] with a globular structure. (Figure 3)

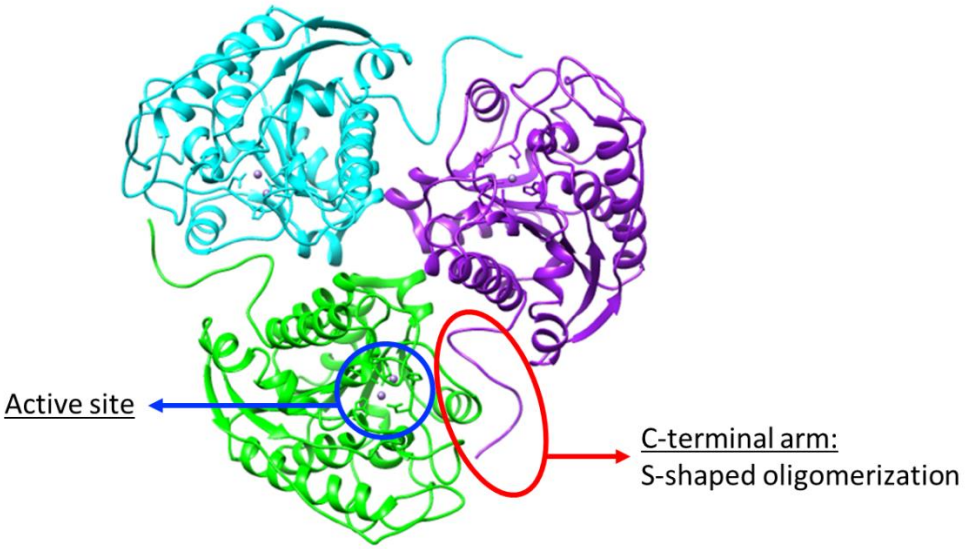

Figure 3: ribbon representation of the homotrimer of human Arg1. Mn^{2+} are represented in purple (PDB: 2pha)

At the carboxy-terminus, the unusual S-shaped oligomerization motif of around 20 residues is represented and is responsible for the 54% of the intermonomer contact in the rat enzyme.[6]

Each monomer has a catalytic site with a binuclear manganese cluster buried 15 Å deep in the active site. Arg1 and Arg2 active sites are identical in all respects. This area is very conserved between species, and the specific physiological requirement for the Mn^{2+} cations is well documented.[7] Indeed, other metalloenzymes can function with other transition metals (i.e., Mg^{2+} instead of Mn^{2+}) but Mn^{2+} is more favorable for arginase.[8] The active site cavity of the human Arg1 is composed of a rigid, narrow, and deep channel leading to the buried manganese-bound hydrophilic pocket. [86, 210] The 350 $Å^3$ channel displays a pipe shape structure with only a 10 Å length from the cavity's entry to the oxygen of the hydroxide ion and no more than 6 Å wide. (Figure 4)

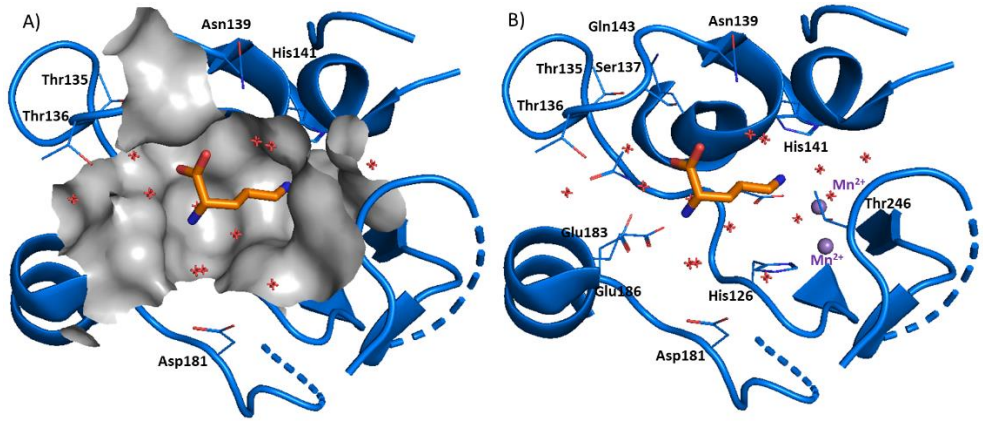

*Figure 4: View of L-ornithine **2** (in orange) in the Arg1 active site. (PDB: 3GMZ)A) Receptor surface is represented in transparency displaying the narrow pipe-shaped channel of approximately 350 $Å^3$. B) Interaction between **2** and residues of the catalytic pocket. H_2O molecules are represented by red stars.*

The two manganese (II) are linked by the side-chains of aspartate residues 124, 128, 232, and 234, and histidines 101 and 126.[9] These metal cations have an octahedral geometry which gives them a low spin character.[10] An hydroxide anion, originating from the deprotonation of a bound water molecule, is present between

the manganese and is required for hydrolysis. The manganese facilitates this deprotonation by lowering water's pK_a in the vicinity of the metal cations. [11] The pK_a of this hydroxide should have a value considerably lower than 10.5,[12] which is the pK_a of a hydroxide bound to a single Mn^{2+}.[13] In the literature, manganese ions of the catalytic site were removed to study the structural changes in the protein conformation and substituted by other metals such as Cobalt,[94] Nickel and Zinc[8, 14] to study the structure and the mechanism.

1.1.1.3 Mechanism of Arg1

Arg1 and Arg2 have a common hydrolysis mechanism that relies on a catalytic triad involving glutamate, histidine, and aspartate residues. According to the mechanism proposed for Arg1 by Kanyo et al. in 1996,[6] the hydroxide ion bridged between the two manganese of the active site allows the hydrolysis to occur. (Figure 5)

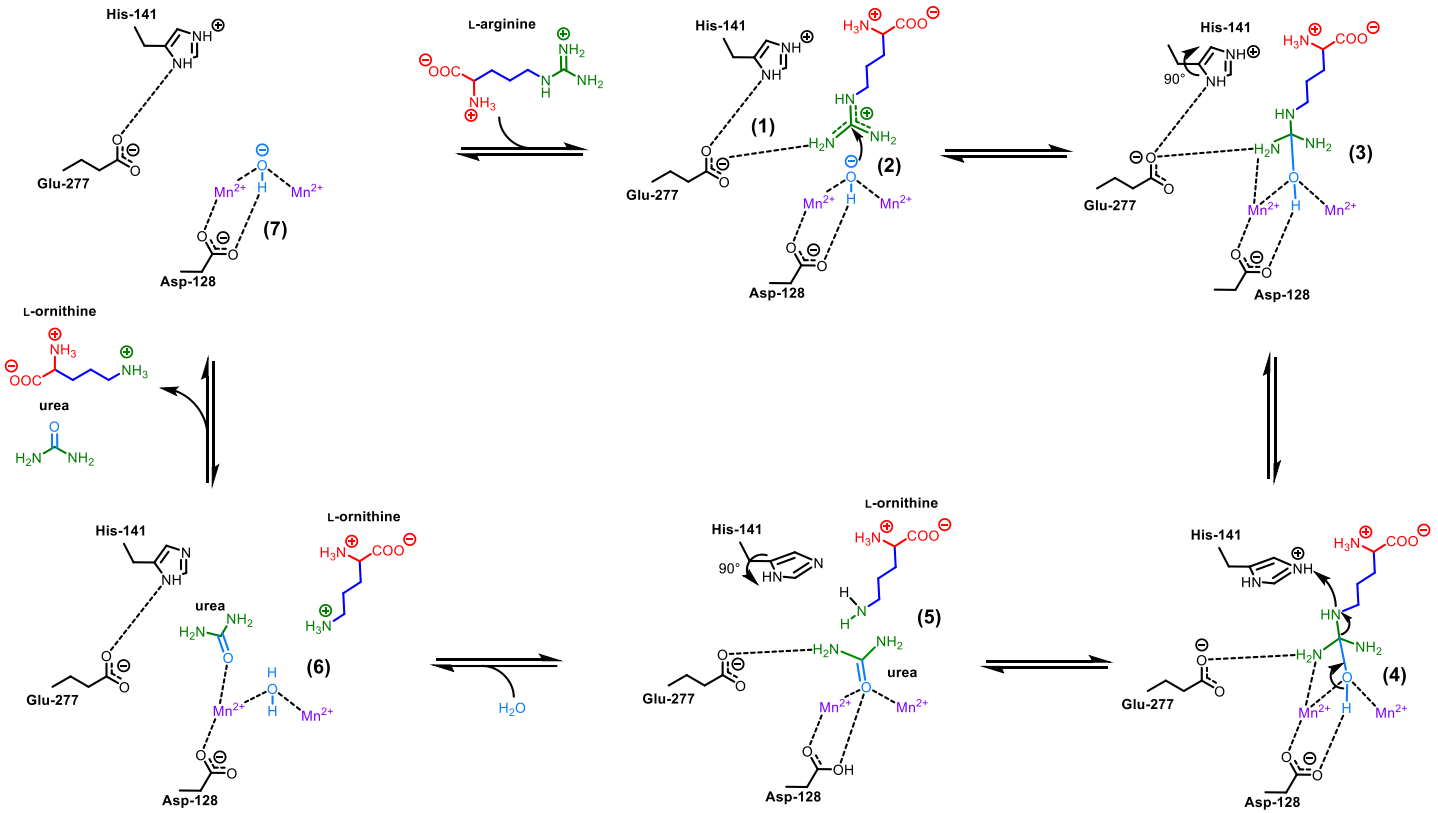

Figure 5: Proposed mechanism of Arginase (adapted from Kanyo, Z. F.; et al. Nature 1996, 383, 554–557 and Di Costanzo, L.; et al. Proc. Natl. Acad. Sci. U. S. A. 2005, 102, 13058–13063)

Following the substrate's entry, the sp2 carbon of arginine's guanidium group is activated by hydrogen bond formation with the carboxylate of the glutamate 277 (1). Then, this guanidinium carbon undergoes a nucleophilic attack by the hydroxide (2). This nucleophilic attack results in a tetrahedral transition state (3) with an sp3 carbon. By donating a proton, Histidine 141 serves as a general acid catalyst for the departure of the leaving group. Histidine 141 side-chain rotates approximately 90° and creates a new hydrogen bond with the substrate, making the rearrangement possible. (4). The covalent bond breakage leads to the reformation of the sp2 carbon forming urea, while the carboxylate of the Aspartate 128 side-chain captures the hydrogen of the hydroxide (5). The entry of a new water molecule allows urea and ornithine to leave the active site (6). Finally, the new water molecule is deprotonated, and the protonation of the Histidine 141 imidazole restores the base/proton shuttle to restart the process (7).[15] This mechanism is consistent with the importance of Histidine 141 and data related to its mutation by a leucine, leading to hyperargininemia in hereditary disease of liver arginase deficiency.[16] α-amino and α-carboxylate groups of the substrate and inhibitors are also required for higher binding potency. Deletion of one of these two groups results in a 5000-fold reduction in k_{cat}/K_M.[17]

Product of the transformation L-ornithine **2** causes negative feedback, regulating Arg1.[18] L-ornithine (K_i = 1.3 mM), is a weak reversible competitive inhibitor[19] and co-crystallographic data with Arg1 was reported in 2011, allowing a complete understanding of the binding inside the active site. (Figure 6)

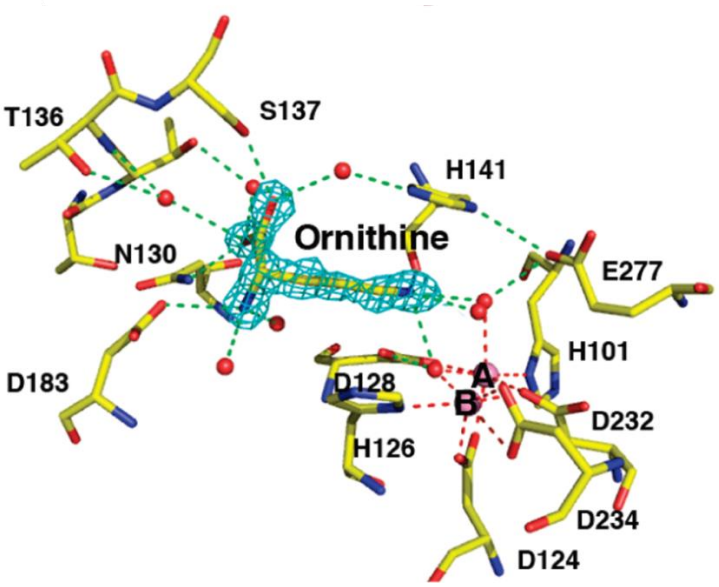

*Figure 6: Simulated annealing omit electron density map of the Arg2-L-ornithine complex (cyan, contoured at 3.3σ). Atoms are color-coded as follows: C = yellow, O = red, N = blue, F = black; Mn2+ ions and water molecules are purple and red spheres, respectively. Metal coordination and hydrogen bond interactions are indicated by red and green dashed lines, respectively. (Figure and legend from Ilies et al. J Med Chem, **2011**, 54; 5432) (PDB: 3GMZ)*

The difference in interaction compared to the substrate comes from the ammonium function which makes π-cation interactions with His141 and His126 but also bounds through nearby water molecules, between the manganese and the ligand.

This product also inhibits cationic amino acid transporters involved in cellular uptake of L-arginine and thus limits the availability of the substrate as illustrated bellow in Figure 8.

1.1.2 Physiological roles of arginases

As represented in Table 1, the two isoenzymes of arginase have different localizations, but they also have different roles. Arg2 is involved in endothelial function by allowing the production of NO, crucial for smooth muscle relaxation. [20, 21] Arg2 also has a role in controlling autophagy in the endothelial system,[22]which is important to maintain cellular and tissue homeostasis and provides a mechanism to adapt to extracellular cues and metabolic stressors.[23] Similarly, Arg1 is also essential

to regulate erectile function via NO production by *i*NOS.[24] The inhibition of Arg1 has been widely studied in treating erectile dysfunction as its inhibition leaves more substrate for *i*NOS. Arg1 is also involved in the urea cycle and immune system regulation, developed in the two subsequent sections.

1.1.2.1 Urea cycle

Arg1 is essential, and the deletion of Arg1 in a murine model has dramatic consequences**.**[25] Partial single knockout (KO) Arg1 gene and double knockout of Arg1 substantially affect argininemia and ammonemia.[26] In the case of a double KO or complete inhibition of liver Arg1, lethality is observed within approximately three weeks of development, resulting in mice dying approximately two weeks after birth.[27] Mutations of Arg1 in humans have less severe effects because of Arg2's ability to compensate. Indeed, in the case of a malfunction or absence of one isoform, the other can be overproduced or overactivated. In the murine model, however, this compensation cannot be done due to the existence of only one isoform. The urea cycle eliminates ammonium ions from protein catabolism, which are toxic to the body. Thanks to this biological process, the ammonium ions are converted into urea. Urea is then excreted in the urine. This process occurs following a series of four enzymatic transformations. (Figure 7)

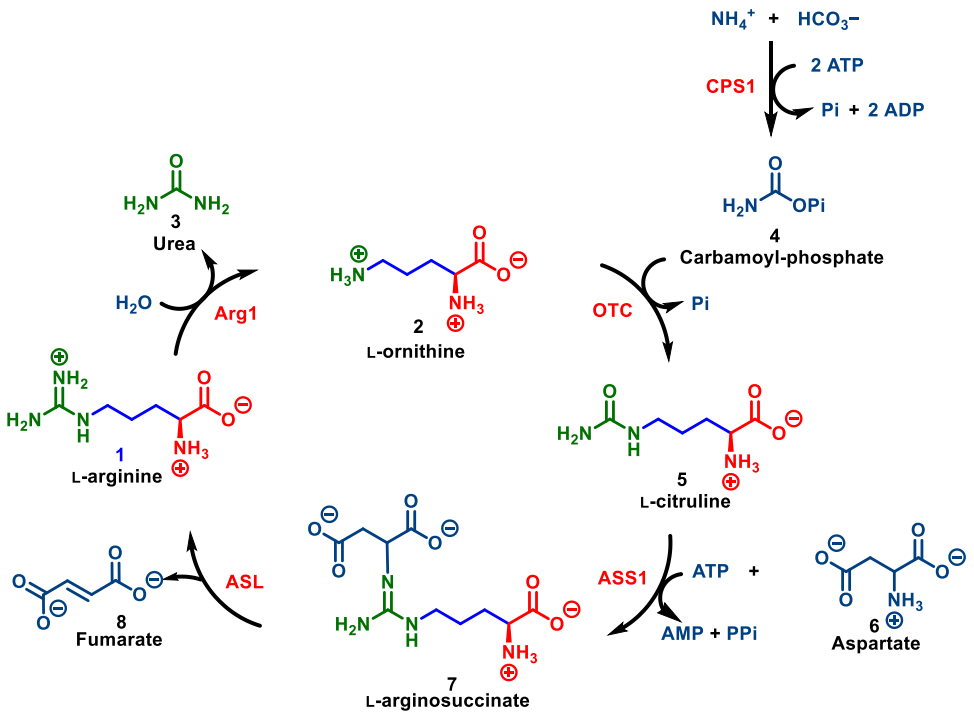

*Figure 7: Diagram of the urea cycle. L-ornithine **2** and carbamoyl-phosphate are converted to L-citrulline **5** by ornithine transcarbamoylase (OTC). The resulting L-citrulline **5** is transformed by argininosuccinate synthetase (ASS1) to L-arginosuccinate **7**, which is converted then to L-arginine **1** by argininosuccinate lyase (ASL). Arginase 1 (Arg1) catalyzes the last transformation to L-ornithine **2** and urea from L-arginine **1**.*

Excess ammonium ions are transformed by carbamoylphosphate synthetase I (CPS1) in the hepatocyte mitochondria into carbamoyl phosphate **4**. The first reaction in the cycle is catalyzed by ornithine transcarbamoylase (OTC). OTC transfers the carbamoyl group to L-ornithine **2** to form L-citrulline **5**. This reaction is the only one to occur in the matrix of the mitochondria, whereas the others take place in the cytosol. In the second reaction, L-citrulline **5** is taken up by argininosuccinate synthetase 1 (ASS1). The reaction requires ATP and aspartate **6** to form L-arginosuccinate **7**. Then, argininosuccinate lyase (ASL) cleaves L-arginosuccinate **7** into L-arginine **1** and fumarate **8**. And fumarate **8** can be converted in the TCA cycle later. L-arginine **1** is then cleaved into L-ornithine **2** and urea **3** by arginase 1 (Arg1), allowing the cycle to continue.[28]

1.1.2.2 Immune modulation

Arginine consumption by Arg1 is at the core of a complex relationship with the immune response. L-arginine **1** can be metabolized by two different enzymes involved in immune modulation. Inductive Nitric Oxide Synthase (iNOS or NOS2) transforms L-arginine **1** to Nω-hydroxy-L-Arginine (NOHA) in a first step, then in L-citrulline **5** and nitric oxide (NO). Macrophages use this pathway to kill abnormal cells by damaging DNA, lipids, and proteins of target cells by producing reactive oxygen species (ROS) and reactive nitrogen oxide species (RNOS).[29] The oxidative condition triggers the cells to evolve towards cell death pathways such as apoptosis.[30] (Figure 8)

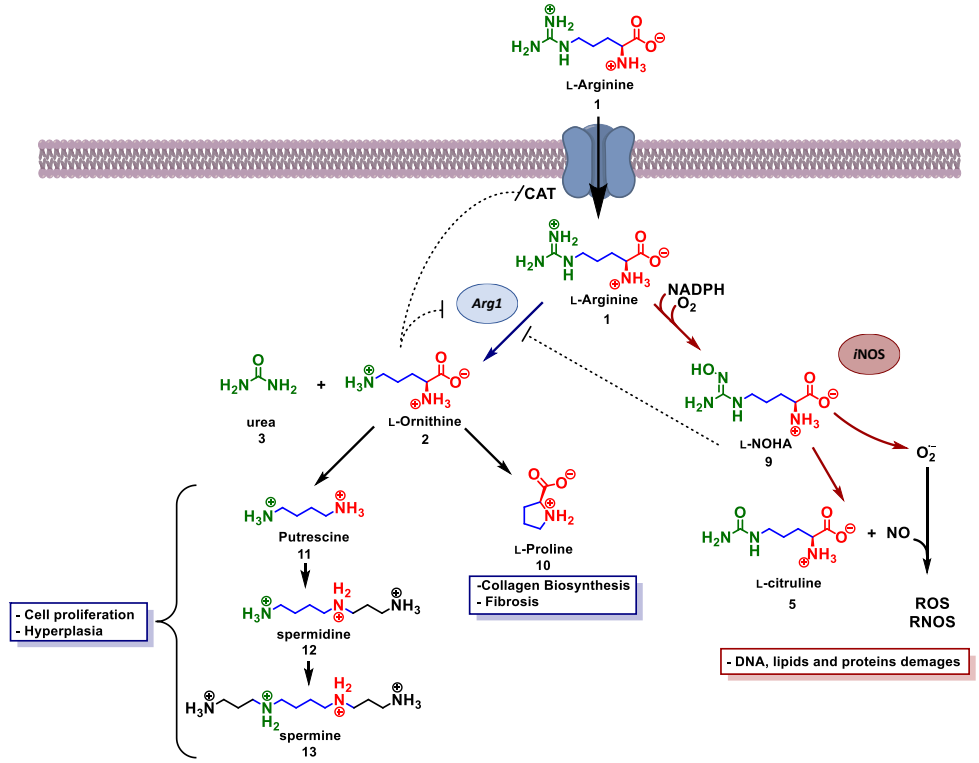

Figure 8: Pathways of L-arginine consumption with the biological effects of the products. L-arginine 1 from the diet, protein turnover, or de novo synthesis enters the cell by cationic amino acid transporter (CAT). Two enzymes can convert 1 in the cytosol: Arg1 (left) and iNOS (right). iNOS transformation gives nitrogen monoxide and damages DNA, lipids, and proteins by Reactive Oxygen Species (ROS) and Reactive Nitrogen Species (RNS). Arg1 conversion results in L-ornithine 2 production. 2 is essential in healing mechanisms. L-proline 10 is a building block for collagen biosynthesis and is involved in constituting the fibrotic tumor stroma. Polyamines (11, 12 and 13) obtained after the de decarboxylation of 2 help the proliferation of tumor and associated cells.

The second pathway of L-Arginine **1** transformation is performed by Arg1 to give L-Ornithine **2** and urea **3**. L-Ornithine **2** is a crucial intermediate in healing processes. L-Proline **10** used in collagen biosynthesis and fibrosis is obtained from **2** after ornithine cyclodeaminase (EC 4.3.1.12) transformation.[31] L-Ornithine **2** is also the precursor of polyamines putrescine **11**, spermidine **12**, and spermine **13**. L-Ornithine **2** is converted to putrescine **11** by ornithine decarboxylase (ODC, EC 4.1.1.17). Spermidine synthase (EC 2.5.1.16) converts putrescine **11** to spermidine **12**. Spermine synthase (EC 2.5.1.22) converts spermidine **12** to spermine **13**.[32]

The use of polyamines by cells leads to proliferation and hyperplasia. In tumor cells, polyamines support tumor growth and proliferation of immune suppressive cells, such as myeloid-derived suppressors cells (MDSCs) and tumor-associated macrophages (TAMs).[33]

A complex system regulates Arg1 and *i*NOS. Products of *i*NOS and Arg1 inhibit Arg1, avoiding disorders. L-Ornithine **2** inhibits *i*NOS as a substrate analog. The same effect is seen on Arg1 by NOHA **9**. These mechanisms allow to avoid overactivation of the immune system, resulting in an immune response adequate to the threat. Moreover, this complex system is also regulated by multiple immunological factors such as cytokines (IFN-ω, TNF, TGF-β) and prostanoids.[34]

1.1.3 Pathological roles of arginases

Due to its regulatory roles in endothelial and immune functions, arginase activity is linked to numerous pathologies. Thus the following pathologies may be associated with its endothelial role: hypertension,[35] erectile dysfunction,[36] atherosclerosis,[21] diabetes,[37] vascular aging,[38] myocardial ischemia/reperfusion and pulmonary artery hypertension,[39] obesity.[40] On the other hand, its overexpression is the starting point for the development of infectious diseases,[41] such leishmaniasis, and tumorigenesis.[42]

1.1.4 The implication of arginase in cancer

The metabolism of arginine sustains an immunosuppressive state within the tumor microenvironment. The results in cancer development are a polarization to the M2 macrophage phenotype of MDSCs where Arg1 is activated and *i*NOS downregulated. M2 phenotype is generally associated with healing and repair processes, but associated in cancer with pro-tumoral and immunosuppressive mechannisms.[43] MDSCs show an increase in the production of interleukins IL6 and

IL10, TGF-β, HIF-α. Paracrine and autocrine regulations stop the migration of MDSCs, block their apoptosis and activate the differentiation to TAMs and angiogenesis.[44] (Figure 9)

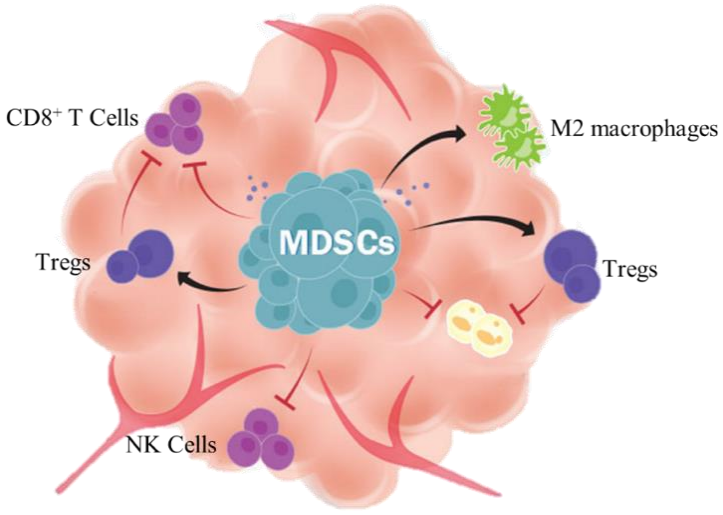

Figure 9: Immunosuppression mechanisms by MDSCs. MDSCs create an M2 phenotype polarization environment, with M2-MDSCs, M2-macrophages, and conversion of T cell into Tregs lymphocytes. Inhibition of NK cells and effective $CD8^+$ T cells block the immune response and participate in the generation of a pro-cancer environment, where Arg1 is involved. (Figure from Tavazoie, M.F. et al. Cell, 2018, 172, 825)

The first biological pathway described in Arg1 overexpression involves cyclooxygenases (COX2) by tumor cells. COX2 increases the production of PGE2 prostaglandin from arachidonic acid.[45] Once released into the extracellular medium, PGE2 binds to Prostaglandin E2 receptor 4 (EP4), a G protein-coupled receptor present at the surface of the MDSCs. Fixation to EP4 activates adenylate cyclase, the protein kinase A (PKA), and the 5' AMP-activated protein kinase (AMPK). The effect on the cells is a stop in cell migration and a polarization to the M2 phenotype of MDSCs where these cells overexpressed Arg1.[46] (Figure 10)

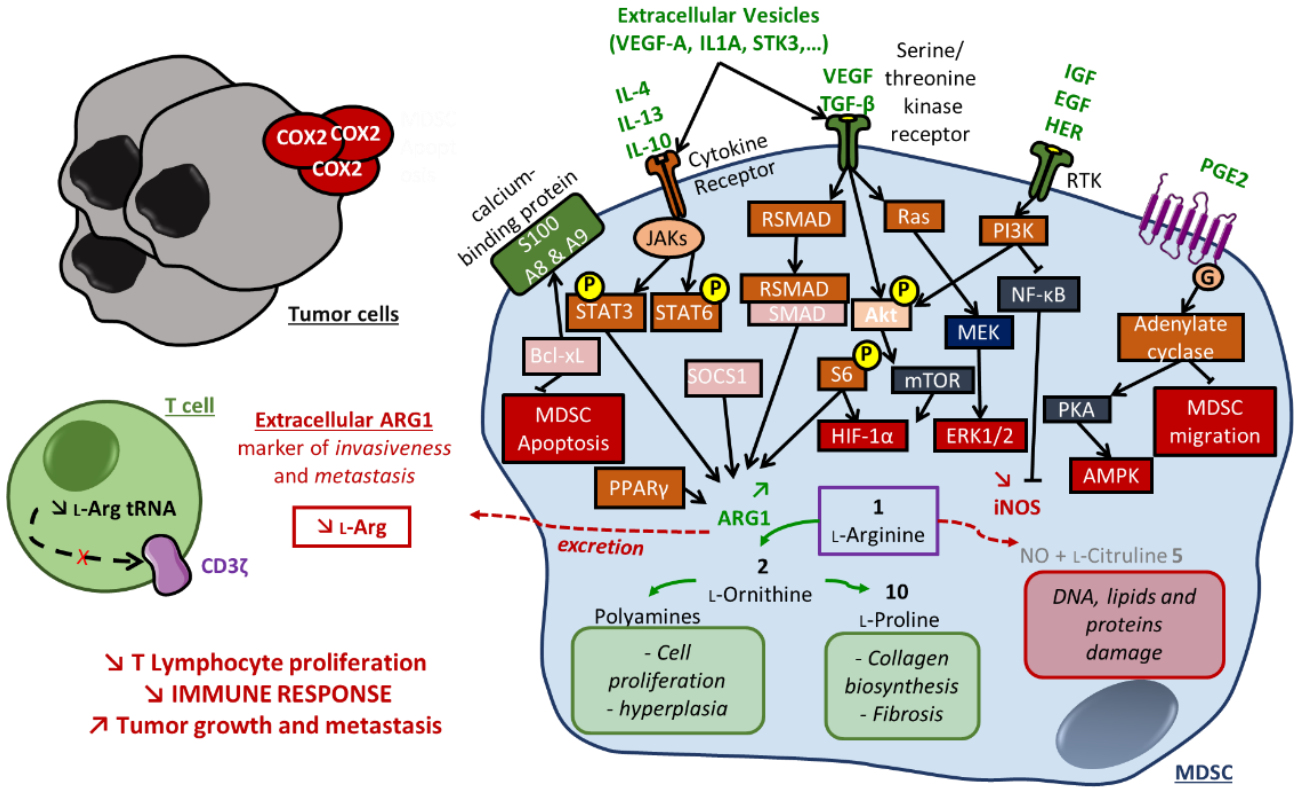

*Figure 10: L-arginine is a key intermediate in the regulation of T lymphocyte activity. The concentration of intra- and extracellular L-arginine **1** is dependent on the expression and activity of Arg1 and iNOS by myeloid-derived suppressor cells (MDSCs). Cytokine receptors, Serine/threonine kinase receptors, Prostaglandin E2 receptor 4, calcium-binding protein S100, and Receptor Tyrosine Kinase are involved in the Arg1 overexpression. Arg1 excretion occurs at high levels of intracellular Arg1*

Interleukins IL4, IL8, IL10, and IL13 activate the phosphorylation of signal transducer and activator of transcription STAT3 and STAT6.[47] Activation of STAT3 stops the apoptosis of MDSCs through B-cell lymphoma-extra large (Bcl-xL) transmembrane molecule transactivation. STAT6 acts on suppressor of cytokine signaling 1 (SOCS1), leading to Arg1 overexpression.[48]

Receptor Tyrosine Kinase (RTK) via insulin-like growth factor (IGF), epidermal growth factor (EGF), and receptor tyrosine-protein kinase (HER) activates the phosphoinositide 3-kinase (PI3K) pathway leading to Arg1 expression and the repression of nuclear factor kappa-light-chain-enhancer of activated B cells (NF-κB), inhibiting iNOS expression.[49] PI3K also phosphorylates protein kinase B (Akt).[50] Akt acts on 40S ribosomal protein S6 and mammalian target of rapamycin (mTOR), leading to various effects, such as angiogenesis with hypoxia-inducible factor 1-alpha (HIF-1α) activation.[51] vascular endothelial growth factor (VEGF) and transforming growth factor beta (TGF-β) fixation on serine/threonine kinase receptors also lead to Akt phosphorylation.[52] However, mothers against decapentaplegic signal transducer of TGF-β (SMAD) and extracellular signal-regulated kinase1/2 (ERK1/2) pathways can also be both involved with serine/threonine kinase receptor activation.[53]

In more recent literature, extracellular vesicles with factors such as VEGF-A, IL1A, serine/threonine-protein kinase 3 (STK3) were demonstrated to support the overexpression of Arg1. Tumor necrosis factor (TNF) expression restricts or blocks the production of *i*NOS, allowing more substrate for Arg1.[54]

Arg1 overexpression induces a substantial increase in the hydrolysis of L-arginine **1**, thus leading to an excess of L-ornithine **2** and urea **3**. The extensive intracellular L-arginine **1** depletion is compensated by the induction of the cationic amino acid transporters 2 (CAT2) at the MDSCs cell surface leading to L-arginine uptake into the cytoplasm. The intracellular deficiency thus quickly spreads outside MDSCs and down-regulates the immune system. The resulting lower L-Arg extracellular concentration reduces the protein synthesis.[45, 55] As an example, plasma

arginine concentrations were lower in patients with cancer (breast cancer: 80 ± 3 µmol/L compared with 103 ± 9 µmol/L; colonic cancer: 80 µmol/L compared with 96 ± 7 µmol/L; pancreatic cancer: 76 ± 5 µmol/L compared with 99 ± 7 µmol/L).[56] T lymphocytes are sensitive to amino acids depletion, which directly affect their proliferation and activity.[57] The L-arginine depletion also blocks the biosynthesis of some proteins in T cells. The lack of L-arginine has a very high impact on the immune system as this immune cell lineage is very sensitive due to the high consumption of this semi-essential amino acid. The repressed expression of the CD3 ζ chain inhibits the T-cell receptor (TCR) complex formation, and the activation signal cannot be transmitted. Because the activation is not possible, the differentiation and the proliferation of active T cells cannot occur.[58]

In these conditions, T cells tend to differentiate into regulatory T cells (Tregs). CD4+ or CD8+ Tregs can down-regulate the immune system by the production factors such as IL-10. Tregs population supports the immunosuppressive role of MDSCs and the immune escape. However, Tregs can be differentiated into effector T cells by interferon gamma (IFN-γ). Such differentiation stops the production of immunosuppressive factors and reactive the production of factors against tumors.

In conclusion, Arg1 is not only able to decrease the immune response but also supports tumor development. The expression of Arg1 and tumor development are closely related. Polyamines (**11**, **12** and **13**) and L-proline **10** productions are needed to form the capsule around the tumor cells cluster. Moreover, the production of other factors such as HIF-α supports tumor vascularization[59] with the M2 polarization.[60]

Inhibition of Arg1 clearly appears to be a relevant target to fight immune escape and tumor growth.[61]

1.2 ARGINASE INHIBITORS DESCRIBED IN THE LITERATURE

Since the discovery of arginase in 1904, molecules that inhibit its activity have been described.[62] We can discriminate synthetic derivatives from natural products and more simple chemical entities such as ions.[63]

Although these molecules sometimes seem to have an inhibitory constant (K_i) in the same range, it is important to note that their direct comparison cannot always be made. Indeed, the expression of K_i is a mathematical calculation whose expression depends on the mode of action. The inhibitors described here have different modes of action with mainly two types of inhibition: 1) inhibitors leading to a covalent bond with the manganese cores (sometimes described as a dative bond) such as for the boronic acid and sulfonamides inhibitors and 2) inhibitors binding to the enzyme through non-covalent intermolecular interactions. Moreover, in many articles, only the half-inhibitory concentration (IC_{50}) is described. In this case, the IC_{50} value also depends on the experimental conditions and therefore hamper a direct comparison. To illustrate this, one can cite the example of irreversible inhibitors, also known as suicide inhibitors, for which the IC_{50} increases with incubation time. In conclusion, comparing the inhibitory potency of compounds described in the literature is not always possible and should only be considered with care. It is in practice only possible to make these comparisons within a single chemical series, or at best, for compounds sharing the same mechanism and described by the same research group using similar experimental conditions.

1.2.1 Known modulators of Arg1 activity

1.2.1.1 Anions

Arg1 activity can be modified by the nature of the metals in the catalytic pocket as described previously, but anions can also be inhibitors. Anions substitute the hydroxide in the catalytic pocket, making the enzyme unable to perform the hydrolysis. The inhibitory effects of anions, such as N_3^-, NO_2^-, BO_3^-, SCN^-,

CH_3COO^-, SO_2^-, ClO_4^-, $H_2PO_4^-$, CN^-, I^-, Br^-, Cl^- and F^-, on the hydrolysis of L-arginine by rat liver arginase, was studied. Inhibition is obtained if the ligand bound to the two metals is strong enough. Of all these anions, only fluoride exhibited an apparent inhibitory effect in the mM range.[64] Inhibition by fluorine also depends on pH. Inhibition is facilitated at neutral pH (1.2 mM at pH 7.0) and lower in basic conditions (19 mM at pH 10).

1.2.1.2 Natural products

Most of the natural products described against arginase are extracted from plants, based on traditional medicine against *Plasmodia* and *Leishmania* parasites. Various scaffolds were described demonstrating low to moderate effect on Arg1 and are mainly used against Leishmania arginase, an enzyme used by a parasite to survive in the host. (Figure 11)

Flavonoids,[65] such as (+)-catechin **14** and (-)-Epicatechin **15**,[66] demonstrated a moderate effect on Arg2 activity. However, flavones such as sauchinone **16** and hydroxysauchinone **17**, and flavanones such as derivatives **24** and **25** demonstrated better inhibition values on Leishmania arginase. Gallic acid derivatives of flavonoids also show a wide range of inhibition against Leishmania arginase with or without inhibition of human isoenzymes Arg1 and Arg2. This difference in activity is easy to explain by significant differences in parasitic and human Arginase. Human and Leishmania arginase are structurally different. Inhibition seen on the parasite enzyme cannot be related to the human isoenzymes.[67]

More compounds such as orientin **21**, chlorogenic acid **19**, and obacunone **23** were described as only active on Leishmania arginase without human Arg1 activity.[68] Galloylquinic acids, the esters of gallic acid **18** and (-)-quinic acid, Piceatannol-3-O-β-D-glucopyranoside **27**, sauchinone **16** and hydroxyl derivative **17**, salvianolic acid **26** are the most studied in the literature.[69]

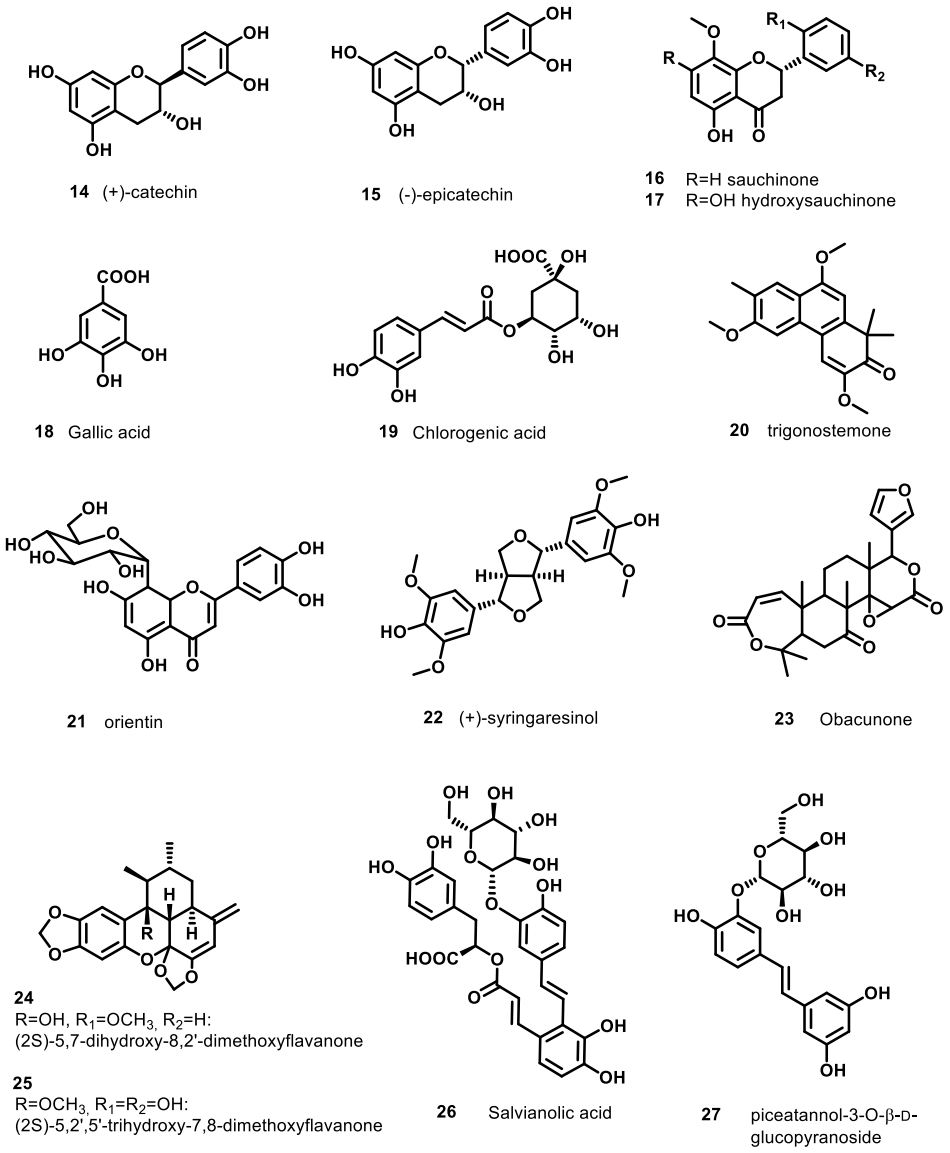

Figure 11: Natural products showing inhibition of human or leishmania arginases.

These molecules possess hydroxyl group(s) or carboxylic acid that are required for the inhibition of arginase.[70] The majority of the molecules reported in the literature possess aromatics hydroxide, such as catechols. Docking experiments were investigated to understand possible binding modes. Most of the molecules were

shown to coordinate Mn^{2+} cations in the catalytic pocket. However, no co-crystal structures of such compounds within Arg1 or parasite arginase are reported so far.

Purine-based molecules: adenosine, inosine, adenine, and uric acid were also described as weak competitive inhibitors of bovine liver arginase with K_i of respectively 30, 40, 14, and 9 μM. Pyrimidine based compounds display better affinities but are described as noncompetitive inhibitors with K_i of 5 μM for cytidine and 0.9 μM for cytosine.[71]

1.2.2 Inhibitors discovered via the SOSA approach

Existing drugs were also evaluated to find new starting points for a drug discovery program on arginase by following the Selective Optimization of Side Activities (SOSA) approach.[72] Selective optimization of side activities of drug molecules (the SOSA approach) is an efficient strategy to discover new active entities.[73] Approved drug molecules, for which bioavailability and toxicity studies have already been performed, are screened. After a hit is found and confirmed, optimization is performed so that the initial "side activity" is then transformed into the "main activity" and, conversely, the initial "main activity" is significantly reduced or abolished. This strategy has a high probability of yielding safe, bioavailable, original, and patentable analogues.[73]

This approach highlighted chloroquine with reversible and competitive inhibition of bovine liver arginase around 10 μM.[74] Complementary studies on chloroquine in human erythrocytic Arg1 revealed a dose-dependent inhibition with inhibition constants (K_i) of respectively 23.0 ± 0.04 μM and 41.0 ± 0.016 μM at pH of 6.8 and 7.4.[75]

In 2016, Lisi *et al*, reported Arg1 inhibition for antiretroviral drugs. (Figure 12)

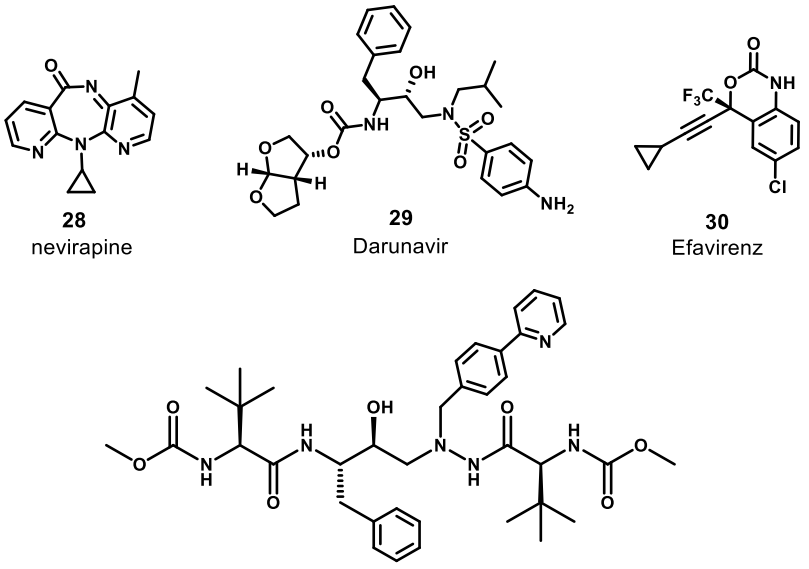

*Figure 12: Structures of antiretroviral agents nevirapine **28**, darunavir **29**, efavirenz **30**, and atazanavir **31**.*

Nevirapine **28**, darunavir **29**, efavirenz **30**, and atazanavir **31** are described altogether to be able to reduce ARG activity by about 50%, with a concentration of 1 nM (efavirenz **30**), 100 pM (darunavir **29**, atazanavir **31**), and 1 μM (efavirenz **30**). Docking experiments were performed to try to understand the binding of such derivatives.[76]

1.2.3 Substrate and transition state analogs

Research on Arg1 activity focuses mainly on inhibitors targeting the catalytic pocket with the substrate or product analogs.[77]

Amino acids were the first molecules described to show inhibition of Arg1. Aliphatic α-amino acids: glycine, alanine,[78] proline,[79] valine, leucine, and isoleucine[80] are weak arginase inhibitors. Lysine,[81] L-cysteine, and L-glutamic acid are also inhibitors of arginase although with very weak activities.[82] L-ornithine (K_i = 1.3 mM), which is the product of the catabolism of L-arginine, demonstrated

to be a weak reversible competitive inhibitor. This product inhibition regulates the enzyme activity through feedback inhibition limiting its over-activation as seen previously in part 1.1.1.3.[19] Short aliphatic chains and hydrophilic functions on the side-chains seems favored for the inhibition. Nω-hydroxy-L-arginine (NOHA) **9**, an intermediate produced by NOS, shows the same negative feedback effect on Arg1.[83]

Many active site-binding inhibitors have already been described and are based on the α-amino acid scaffold. (Figure 13)

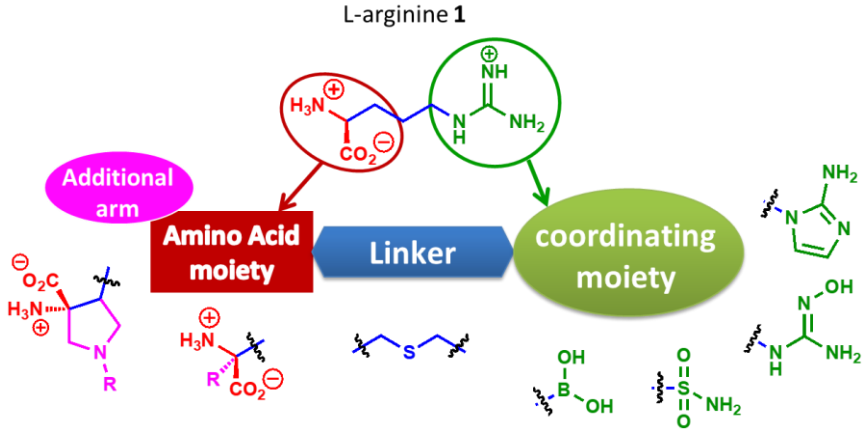

Figure 13: Substrate and modifications of the α-amino acid scaffold reported in inhibitors

The first rationally designed molecules are Nω-Hydroxyamino-α-amino acids based on the NOS intermediate product: L-NOHA **9**. L-NOHA IC_{50} were reported to be 20 µM on rat arginase[84] and 150 µM[77] on bovine liver arginase (BLA). This compound was shown to act as a competitive inhibitor. However, L-NOHA **9** is also a substrate of NOS which oxidizes the molecule to L-citrulline **5** and NO. Analogs were expected to be more active and more stable. Racemic amidoxime *N*ω-OH-DL-indospicine (NOHI, **32**) improves a little the activity with IC_{50} value on bovine liver arginase (BLA) of 5 µM. Ketoximes and aldoximes did not demonstrate any inhibition lower than the millimolar range. However, hydroxylamines showed

to be more interesting with micromolar inhibition such as *N*ω-OH-L-lysine with 11 ± 2 μM.[85, 86]

The very active research group of Professor David W. Christianson from the University of Pennsylvania published numerous articles in the field of arginase inhibition from the late 90s. (Table 2) A structure-based approach led them to describe several inhibitors families with different coordinating functions. From the articles of the Christianson group, modification of the guanidinium part was performed with sulfonamides,[87] 2-aminoimidazoles,[88] aldehydes,[89] nitro[90] and carboxylic acid derivatives,[90] epoxy compounds,[91] or even trifluoromethylketone, thanks to its crystallographic resolution of Arg1.[92] Crystallographic data with inhibitor-enzyme complexes had a major impact with the determination of the mechanism and allowed a better understanding of the interaction between ligands and the active cavity but also to design new inhibitors rationally.[93]

Table 2: Inhibitors in the literature with Arg1 activity and Arg2 activity[94]

Compounds	Biological activity	Reference
<u>*N*ω-hydroxyl-amino acids:</u> NOHA **9** 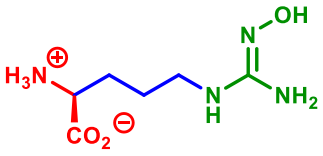 *N*ω-OH-DL-indospicine **32** 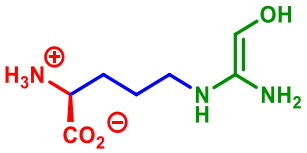 Nor-NOHA **33** 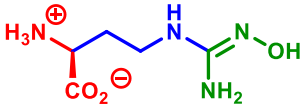	*Arginase 1:* K_i: 10 ± 2 µM (rat liver arginase, pH 7.4) [95] and 150 µM (BLA) K_d: 3.6 µM (pH 8.5)[77] *Arginase 2:* K_i: 1.6 µM (pH 7.5) K_i: 2 µM (pH 9.5) *Arginase 1:* K_i: 5 µM (BLA)[84] *Arginase 1:* K_i: 0.5 ± 0.1 µM (rat liver arginase, pH 7.4) K_d: 0.5 µM (pH 8.5) *Arginase 2:* K_i: 51±8 nM (pH 7.5)	**Custot *et al.*, 1996,[86] 1997[85]**
<u>Sulfonamides:</u> ASH **34** 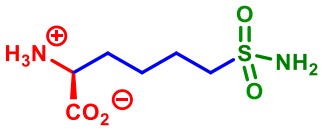 SEC **35** 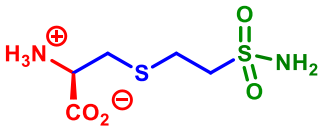	*Arginase 1:* K_i: 90 µM (rat liver arginase) *Arginase 2:* K_i: 67 µM *Arginase 1:* K_i: 52 µM (rat liver arginase)	**Cama, *et al.*, 2003[87]**

Compounds	Biological activity	Reference
2-aminoimidazoles: 2AH **36** 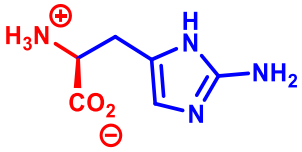 A1P **37** 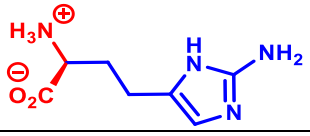	*Arginase 1:* K_i: 300±20 µM (pH 9.5) *Arginase 1:* K_i: 4.0±0.2 µM (pH 9.5) K_d: 2±0.1 µM (pH 8.5)	**Ilies, *et al.*, 2003**[88]
Aldehydes: AOH **38** 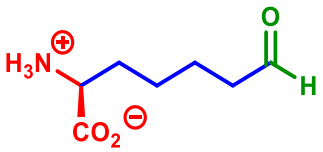	*Arginase 1:* ND *Arginase 2:* K_i: 60±8 µM (rat liver arginase)	**Shin, *et al.*, 2004**[89]
Nitro: ANH **39** 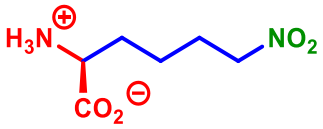	*Arginase 1:* K_d: 60 µM	**Zakharian, *et al.*, 2008a**[90]
Carboxylic acids: AHD **40** 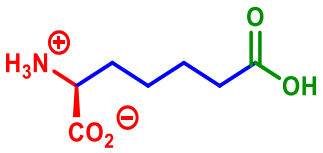	*Arginase 1:* K_d: 30 mM	**Zakharian, *et al.*, 2008a**[90]
Epoxides: **41** 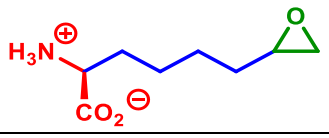	only co-crystalized, no inhibition determined	**Zakharian, *et al.*, 2008b**[91]

Compounds	Biological activity	Reference
Boronic acids: 2(*S*)-amino-6-boronohexanoic acid (ABH) **42** 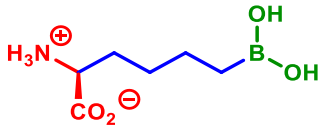 	*Arginase 1:* K_d: 5 nM *Arginase 2:* K_i: 0.25 µM (pH 7.5) K_i: 8.5 nM (pH 9.5)	**Baggio, *et al.*, 1997**[96]
S-(2-boronoethyl)-L-cysteine (BEC) **43** 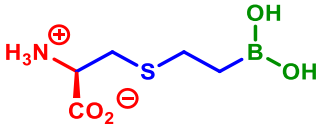 	*Arginase 1:* *Ki*: 0.4-0.6 µM, K_d: 2.56 µM *Arginase 2:* K_i: 0.31 µM (pH 7.5) K_i: 30 nM (pH 9.5)	**Kim, et al., 2001**[97]

Among all these inhibitors, the most potent are unquestionably the boronic acid compounds. The reference compound in this series, the (S)-2-amino-6-boronohexanoic acid (ABH) **42** has a K_d of 5 nM on human Arg1 and was shown to mimic the transition state. Later, S-(2-boronoethyl)-L-cysteine (BEC) **43** was reported as a modified version of **42** with sulfuryl function in the chain linker between the α-amino-acid moiety and the boronic acid.[97]

1.2.4 Boronic acids in Arg1 inhibition

The boronic acid inhibitors ABH **42** and BEC **43** were reported as competitive slow binding transition-state inhibitors.[98] Boronic acid-containing compounds mimic arginine, which just underwent the nucleophilic attack of the hydroxide ion, as seen previously with the mechanism (Figure 5, step 3). The boronic acid function reacts in the catalytic pocket with the hydroxide bridged between the two manganese. The nucleophilic attack of the hydroxide on the boron generates the conjugate boronate function. The binding in the active site is also very similar to the transition state. (Figure 14).

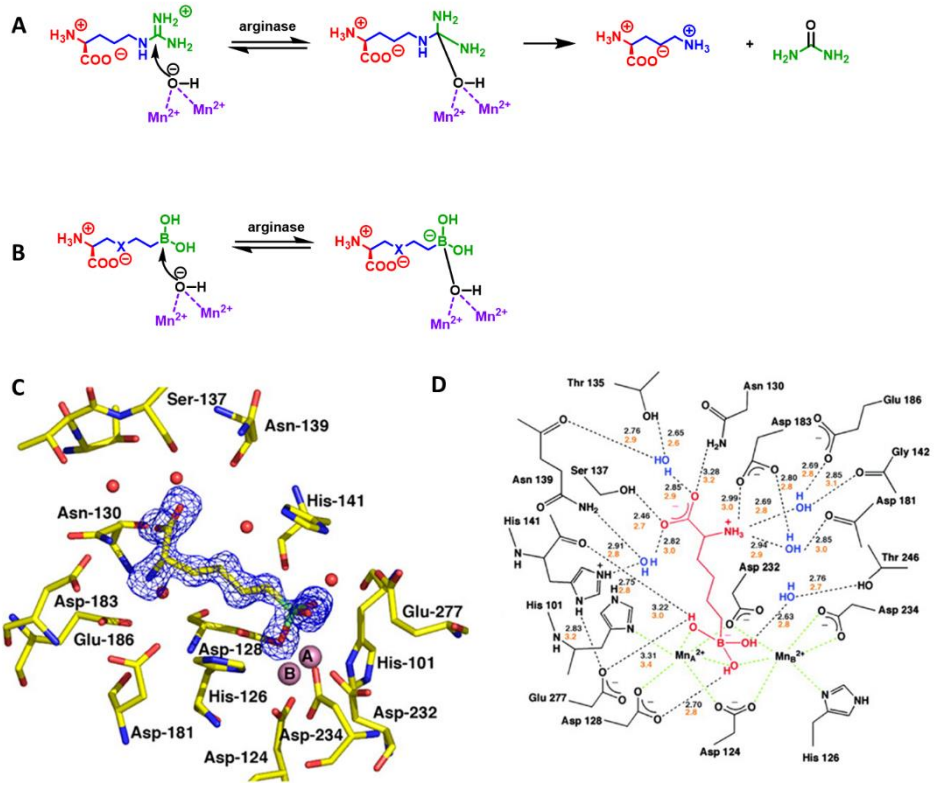

*Figure 14: Comparison of interactions of ABH **42**, arginase 1 inhibitor A: hydrolysis mechanism of L-arginine **1**. B: Inhibition mechanism of ABH (X=C) **42** and BEC (X=S) **43**. C: Co-crystallographic data of **42** and Arg1.*[97] *D: interaction map.*[98]

The amino acid part is very well superimposed compared to the transition state or L-ornithine **2**. Deeper in the pocket, the hydroxyl of the boron matches the -NH_2 and -OH functions of the transition state. Hydrogen bonds and ionic interactions strongly stabilize the inhibitor in the cavity.

However, the binding and inhibition data depend on the experimental conditions. In fact, affinity and kinetics of inhibition are strongly dependent on the pH, for example. Inhibitors are often reported at the optimum pH of the enzyme (pH 9.5) or physiological pH (pH 7.4) and show very different inhibition values are usually obtained. For instance, regarding ABH **42**, an inhibition constant (K_i) of 88 nM and 11 nM at pH 7.5 and 9.5, are reported. In a recent article, this difference in the affinity was explained by a modification of the enzyme conformation, adopting

a more symmetrical coordination structure and a higher abundance of hydroxide ions.[99] Some active site residues (Asp232 and Asp234) show some changes, and the enzyme metals were also more symmetric regarding their coordination at pH 9.0. The boronate of ABH **42** was shown to rotate upon an increase in pH as illustrated in Figure 15A. As a result, the coordination distances of -OHs of boronate become shorter at pH 9.0, in magenta, compared to pH 7.0 in cyan in Figure 15B.

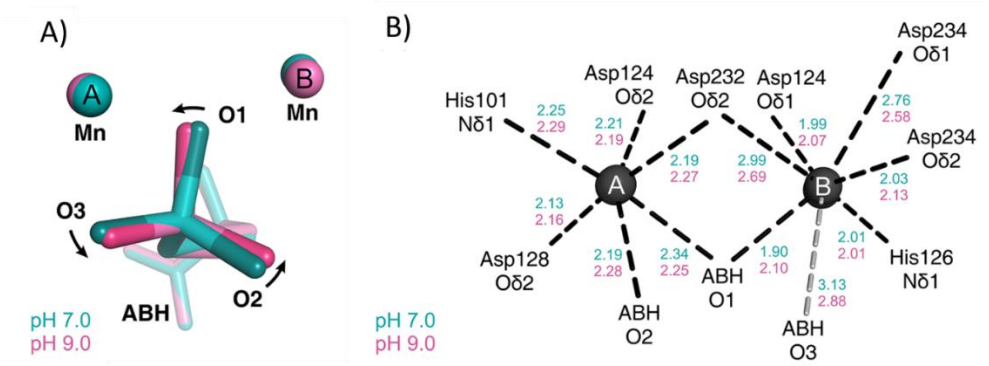

*Figure 15: Structural differences between the active sites of the Arginase-1/ABH **42** complexes at pH 7.0 in cyan and 9.0 in magenta. A) Detail of the **42** boronate anion bound near the manganese cluster B) Schematic representation of **42**-Arg1 complex. Dashed lines indicate coordination interactions with the metal ions, while dotted lines indicate hydrogen-bond interactions made by **42**. Distances between atoms are described for pH 7.0 and 9.0, with respective colors. (from Grobben, Y.; et al. J. Struct. Biol. X 2020, 4, 100014.)*

The ionization of the coordinating function is essential to consider.[100] For example, the p*K*a of the boronic acid side-chain is reported to be 9.3 for BEC **43** (Figure 16A).[94] It means that at the optimum pH of 9.5, the boronic acid function is very close to the pK_a. Consequently, we should expect almost half as boronate and another half as boronic acid.

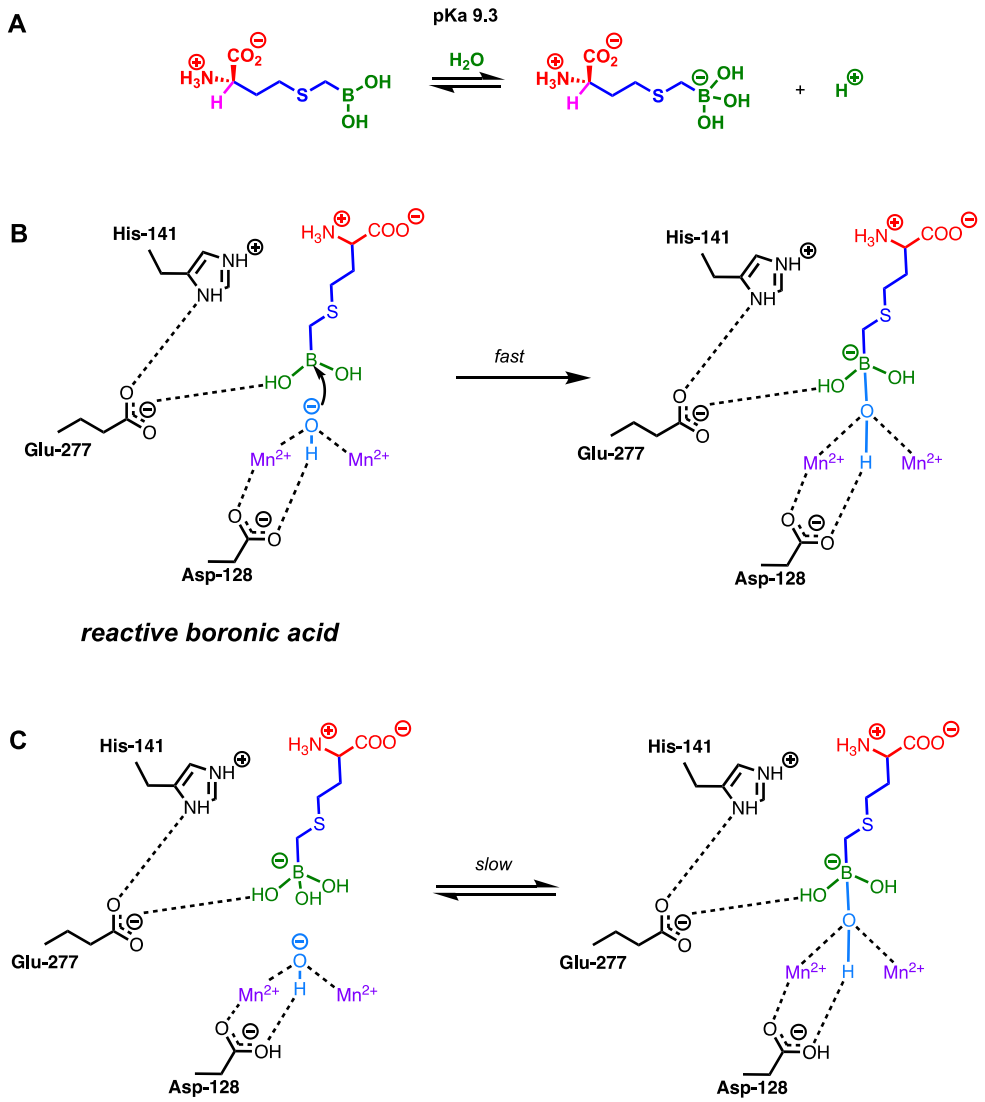

*Figure 16: A. pH equilibrium of boronic acid inhibitor BEC **43**. B. schematic representation of the possible fast nucleophilic attack of the hydroxide on the boronic acid function, compared the unreactive boronate function and proposed slow exchange (C).*

To inhibit the enzyme, the boronic acid must react with the hydroxide of the catalytic site, as illustrated in Figure 16B and 15C. However, inhibition is faster with boronic acid compared to boronate. Indeed, at a more neutral pH, the more abundant

boronic acid form can be attacked by hydroxide to bind to the enzyme covalently. However, the boronate must exchange an -OH group to form the same tetrahedral intermediate, which is a slower equilibrium. This explains the slower inhibition observed at alkaline pH, such as pH 9.5.[99]

Furthermore, displacing the hydroxide and coordinating the metal cores appear facilitated in a more neutral pH when functions are less prone to react with the hydroxide. This new parameter is due to the enzyme conformation and its stability. At pH 9.5, the enzyme showed a slightly higher melting temperature (Tm, determined by thermal shift assay) than pH 7.4.

1.2.5 Towards the next generations of boronic acids-based inhibitors

The presence of the boronic acid function does not reveal any side effects that could be expected with this function or boron in general. Indeed, the presence of the electronic vacancy could lead to nucleophilic attacks and the formation of covalent bonds. Overall, boron is not common in medicinal chemistry and is rarely used to design new chemical entities.

Boronic acid derivatives developments were the strategy and patented in the late 2000 and 2010s period, as reviewed in 2014 by Ivanenkov and Chufarova.[101] During this period, ABH **42** and BEC **43** were improved, resulting in several generation of inhibitors. (Figure 17)

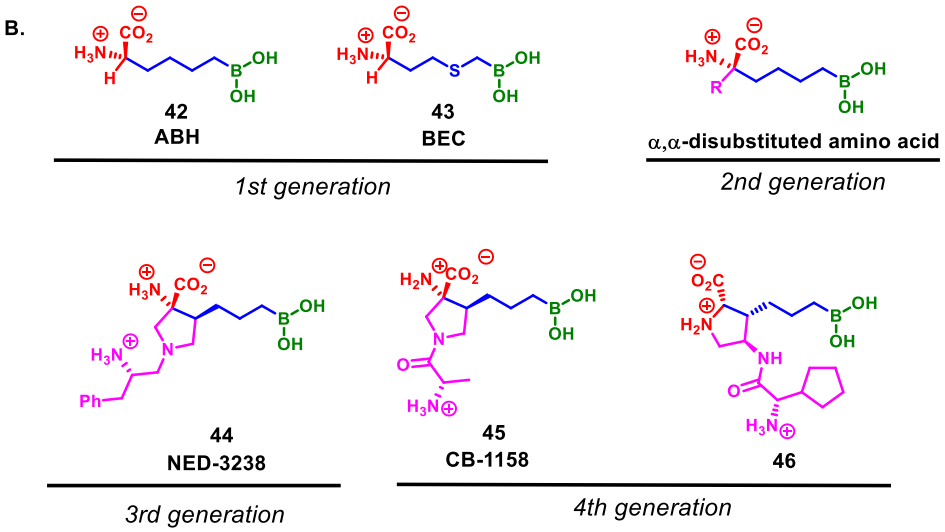

Figure 17: structures of the boronic acid inhibitors of Arg1 from the 1st to the4rd generation.

α-α-disubstituted amino acids are the second generation of inhibitors. They were designed by Ilies *et al.* to make new intermolecular interactions in the enzyme's outer active site.[102]

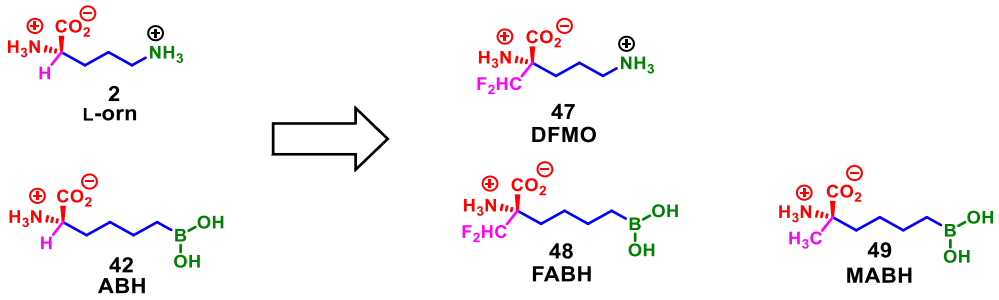

Figure 18: α-α-disubstituted amino acids designed from L-ornithine and first-generation inhibitor ABH.

From L-ornithine **2** and first-generation inhibitor ABH **42**, 2-(difluoromethyl) **47** and **48** and methyl **49** substituted compounds (Figure 18) were synthesized and evaluated on isolated human Arg1 and parasite-derived arginase (*Plasmodium falciparum* Arginase). The results of this study are depicted in Table 3.

Table 3: Enzymatic activity on human Arg1 and parasite arginase of α-α-disubstituted amino acids compared to ABH. (Result table from Ilies, M. et al, J Med Chem 2011, 54, 5432–5443)

inhibitor	**human Arginase 1** K_i (μM)	***Plasmodium falciparum* Arginase** K_i (μM)
ABH 42 (S-isomer)	0.018 ± 0.001	10 ± 1
FABH 48 (racemic)	34 ± 2	2000 ± 200
MABH 49 (racemic)	0.88 ± 0.02	260 ± 20

A decreased affinity of FABH **48** and MABH **49** compared to the parent inhibitor ABH **42** was reported. But the authors reported that a more polar substituent would be more favorable with the presence of potential hydrogen bonding groups in this region of the Arg1 active site. Additionally, a longer substituent might be better suited to capture additional binding interactions. Later, van Zandt *et al.* designed molecules following this way, as outlined in Figure 19.[103]

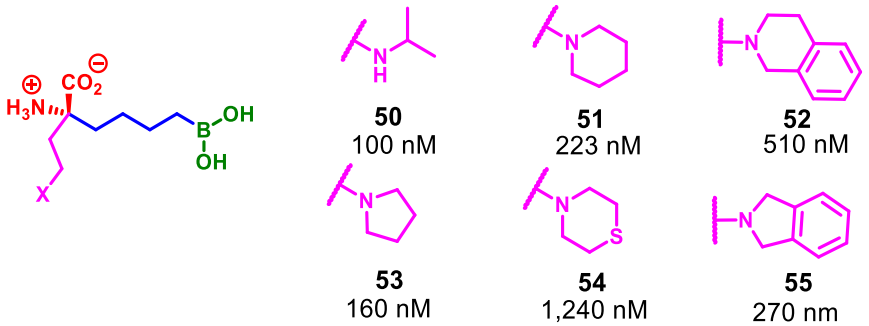

Figure 19: improved α-α-disubstituted amino acids elaborated by van Zandt, et al. IC_{50} on human arginase 1 are reported bellow each substituent to compare to ABH (1,450 mM).

From this study, such modification can clearly improve the inhibition potency. This series was expanded by various modifications of the α-substituent, and patented but did not lead to any compound in clinical trial.

Third-generation compounds are of similar structure but with a cyclization between α and β at the amino acid tail. Such modifications resulted in very active compounds on Arg1 with some selectivity versus Arg2.[104] (Figure 20)

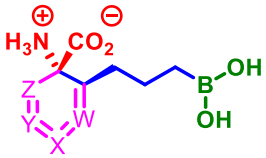

Figure 20: Markush structure for the third-generation compounds found in patents.

Among all the compounds synthesized, CB-1158 **45**, also named INCB001158 for clinic trial, has demonstrated great interest. Although it has a ring and can be classified in the 3rd generation, its dipeptide structure classifies it in the fourth generation. Indeed, the distinction between 3rd and 4th is made by the peptide character of the compounds. CB-1158 **45** has a reported IC_{50} of 86 nM on human Arg1 and 296 nM on human Arg2.[105] In contrary to other inhibitors, CB-1158 **45** is active *in cellulo* and *in vivo* as adjuvant but also as a single agent.[106-107]

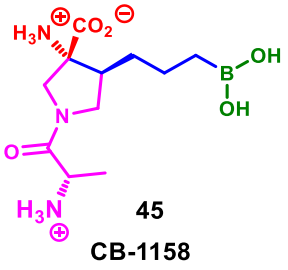

45

CB-1158

Figure 21: structure of CB-1158 studied in clinical trials

The same approach led to the development of **NED-3238**[104] **44**, up to 1000-fold more potent in comparison to ABH **42** (IC_{50} on human Arg1 of 1.3 nM vs 1,547 nM, respectively). **50**, **51**[108] and other proline-derived inhibitors[109] were reported recently with similar results.

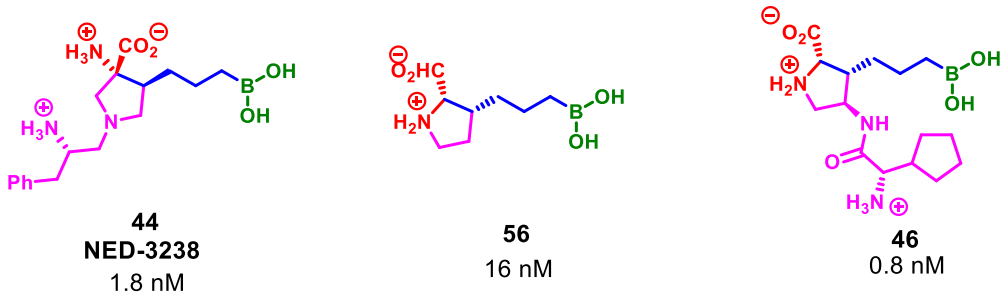

Figure 22: Structures of NED-3238 ***44****, proline-derived inhibitor* ***56*** *and* ***46****,*

Proline-derived inhibitors are reported with IC_{50} on Arg1 in the nanomolar range and below (**56**: IC_{50} = 16 nM). **46** was among patented compounds [110] and reported an IC_{50} of 0.8 nM. 6-membered cycle derivatives were also studied.[111]

Bicyclic compounds similar to CB-1158 **45** were also developed by Mitcheltree, *et al.* to inhibit Arg1 to enhance cancer immunotherapy.[112] (Figure 23)

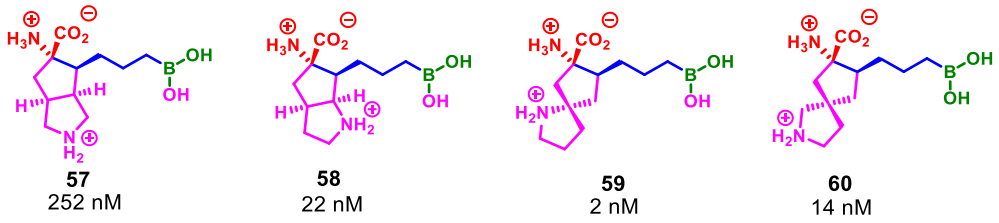

Figure 23: Structures of bicyclic derivatives designed for Arg1 inhibition and IC_{50}

In their assays, all the molecules from Figure 23 have inhibitory potency with IC_{50}s from 2 to 252 nanomolar, compared to 311 nM for ABH **42**. In addition, these molecules were also co-crystallized inside the Arg1 binding cleft. A new series was then synthesized to improve the bioavailability (Figure 24).

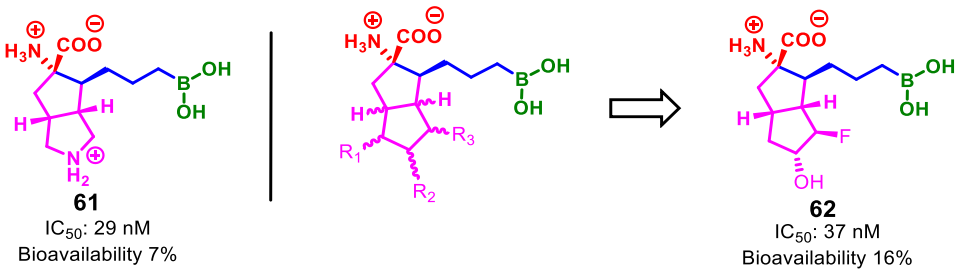

Figure 24: pharmacomodulation for improving the bioavailability.

In this study, pyrrolidine nitrogen was substituted or removed to improve bioavailability. Deletion of the nitrogen led to a loss in activity but improved the bioavailability significantly. The loss in activity was restored with the addition of other substituents (R_1, R_2 or R_3 in Figure 24) on the cycle. The best compound **62** has an IC_{50} of 37 nM and a bioavailability of 16%, which is more than double compared to the initial compound **61** for almost the same IC_{50} (29 nM and 7%).

In the same article, the authors highlighted another interesting characteristic of their compounds. The boronic acid function is closed enough to react with the amine of the amino-acid function. (Figure 25)

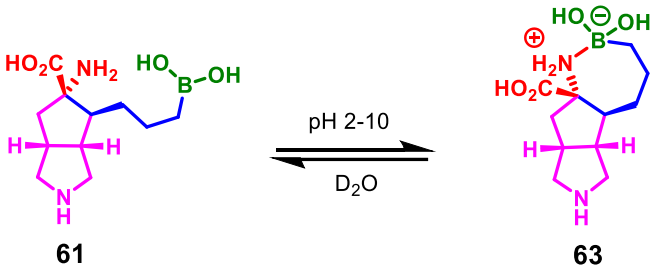

*Figure 25: dependent equilibrium with boronic acid **61** forming a cyclic aminoboronate **63**.*

This propriety can offer the possibility of having prodrugs that can be opened under certain conditions. This can protect the compound from potential degradation but also from side effects by avoiding off-target interactions. In addition, drug targeting could be considered with the opening of the ring, releasing the active

form of the drug into the site of action. This was mentioned in a previous patent released in 2018, where the boronic acid was protected by the carboxylic acid and amine functions, much like the N-methyliminodiacetic acid (MIDA) protection.[113]

A difference in the inhibition is thus observed depending on the pH and the nature of the inhibitor. (Table 4)

*Table 4:comparision of the Arg1 inhibitory potency for ABH **42**, nor-NOHA **33**, and CB-1158 **45** at pH 9.5 and pH 7.4*

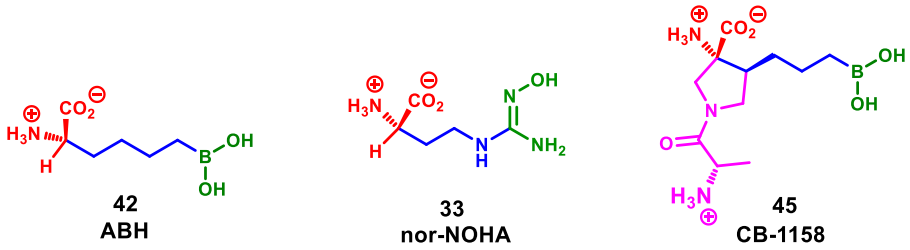

	Inhibitor	IC_{50} (nM) (95% CI)[a]	K_i (nM) (95% CI)[a]
pH 9.5	Buffer control		
	ABH	22 (19 – 26)	11 (9.4 – 13)
	nor-NOHA	109 (91 – 130)	54 (45 – 64)
	CB-1158	132 (109 – 159)	65 (54 – 79)
pH 7.4	Buffer control		
	ABH	184 (171 – 198)	88 (82 – 95)
	nor-NOHA	59 (50 – 70)	28 (24 – 34)
	CB-1158	8.6 (8.4 – 8.9)	4.1 (4.0 – 4.3)

[a] *Average IC_{50} and K_i values and 95% confidence intervals (95% CI) are reported using the pIC_{50} and pKi values of the individual experiments.*

As described in Table 4, ABH **42** is slightly more potent at pH 9.5, on the contrary to nor-NOHA **33** or CB-1158 **45**, a third-generation inhibitor in clinical study presented in the next part (1.2.6). However, the inhibition data reflects several parameters, such as the affinity and the kinetics of association and dissociation. Boronic acid inhibitors have a generally slow association and dissociation kinetics, as described in Table 5.

*Table 5: Kinetic parameters of Arg1 inhibition ABH **42**, nor-NOHA **33**, and CB-1158 **45** at pH 9.5 and pH 7.4*

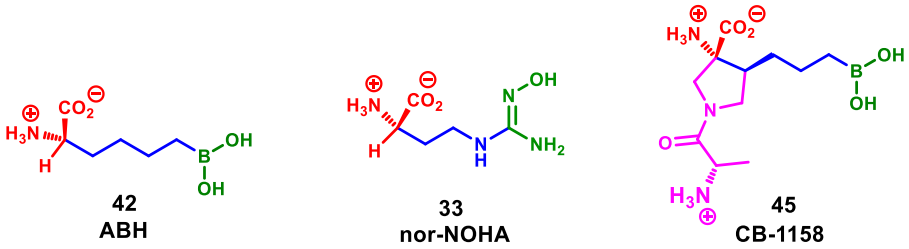

	Inhibitor	k_a (M^{-1} s^{-1})	log(k_a)	SD log(k_a)	k_d (s^{-1})	log(k_d)	SD log(k_d)
pH 9.5	ABH	5.1×10^3	3.71	0.03	1.4×10^{-4}	−3.86	0.03
	nor-NOHA	3.6×10^4	4.55	0.15	6.2×10^{-3}	−2.21	0.15
	CB-1158	1.3×10^3	3.11	0.04	9.2×10^{-5}	−4.04	0.04
pH 7.4	ABH	1.2×10^4	4.09	0.21	9.9×10^{-3}	−2.00	0.21
	nor-NOHA	1.2×10^4	4.09	0.21	1.9×10^{-2}	−1.73	0.21
	CB-1158	4.8×10^3	3.68		1.8×10^{-4}	−3.74	

The association rate constants (k_a) were determined by SPR of all three inhibitors at pH 9.5 and 7.4. CB-1158 **45** at pH 9.5 has the slowest formation of the enzyme-inhibitor complex with k_a of 1.3×10^3 M^{-1} s^{-1} and the slowest dissociation kinetics with a k_d of 9.2×10^{-5} s^{-1}. The dissociation rate constants (k_d) vary up to 200-fold among the inhibitors and pH conditions. nor-NOHA **33** has the fastest association and dissociation kinetics at both pH values. Such differences in inhibition and kinetics highlight pH as a crucial parameter to consider.

1.2.6 Arginase inhibitors in preclinical and clinical trials

1.2.6.1 Preclinical studies

OATD-02 or OAT-1746 (structure not disclosed, OncoArandi Therapeutics), is a dual arginase 1/2 inhibitor studied to improve the efficacy of immune checkpoint inhibitors.[114] This compound is a dual inhibitor with IC_{50} of 20 nM and 48 nM for Arg1 and Arg2, respectively, and demonstrated very low clearance, a long half-life, and moderate oral bioavailability in animal models.

OATD-02 was evaluated as a monotherapy and in combination with checkpoint inhibitors (gemcitabine, and IDO inhibitor) in various mouse models (colorectal, lung, ovarian cancers, melanoma, and leukemia). Tumor growth inhibition was in the range of 34-56% for monotherapy (50 mg/kg, twice a day), and combinatorial therapy of OATD-02 resulted in tumor growth inhibition in the range of 61-87%.

1.2.6.2 Phase 1 clinical trials

A study started in 2017 to evaluate the safety, tolerability, and antitumor activity of CB-1158 **45** plus Epacadostat (an IDO1 inhibitor), with or without pembrolizumab (PD-1 antibody), in advanced solid tumors.[115] However, at the end of the study in May 2020, the trial was inconclusive due to the insufficient numbers of patients enrolled (only one person in cohort 2), and no patients completed the study (3 deaths/4 patients in cohort 1 and 1 death/1patient on cohort 2).

Another arginase inhibitor, CB-280 (structure not disclosed, Calithera Biosciences), was studied in phase 1b (NCT04279769). The study's estimated primary completion was expected for the end of December 2021, so results should follow in the next few months.[116] In a tumor model compound (30 mg/kg), the compound demonstrated 30 % tumor growth inhibition in monotherapy and 87 % when combined with anti-PD-L1 (10 mg/kg). A regression of 7/10 tumors was also observed. [117]

1.2.6.3 Phase 2 clinical study

The only candidate to be currently widely involved in clinical trials is CB-1158 **45**. The molecule was then tested to ensure the safety of use in the human model and started a phase 1 trial in September 2016 as a monotherapy agent. CB-1158 **45** is also orally available and has good pharmacokinetics with a half-life of 6 hours (supports twice a day takes) and follows prediction for renal clearance. From preliminary data, exposure was over IC_{90} at 100 mg, and the plasma concentration

of arginine increased. Later, patients with advanced/metastatic solid tumors were enrolled in escalating monotherapy doses to determine the Recommended Phase 2 Dose (RP2D). Combination with anti-PD-1 therapy was also evaluated.[106]

A phase 1/2 study in combination with chemotherapy in subjects with solid tumors also started the same year.[118, 119] Preliminary results of a phase 1/2 study of CB-1158 **45** plus chemotherapy (gemcitabine/cisplatin) in patients with advanced biliary tract cancers suggest the combination of CB-1158 **45** 100 mg BID + gemcitabine/cisplatin was tolerable and did not result in significant added toxicity. Response rates and progression-free survival suggest that some patients may benefit from this combination.[119] Estimated study completion was expected for the end of March 2022, meaning results should become available in the next few months.

Results for CB-1158 **45** combined with Daratumumab in multiple myeloma are expected for mid-2022 (estimated primary completion: expected for the end of March 2022).[115]

CB-1158 **45** as a single agent and in combination with immune checkpoint therapy (Pembrolizumab, an antibody targeting programmed cell death protein 1 (PD-1) expressed on activated T-cells, monocytes, B-cells, natural killer (NK T-cells and dendritic cells) in patients with advanced/metastatic solid tumors has been investigated since 2016, and conclusions were initially expected for the end of 2021. Significant number of patients did not complete the full study due to withdrawal or switch in therapy. Adverse events reported in mid-May 2022 highlight that the combination led to low to moderate side effects: constipation (CB-1158 alone), diarrhea, nausea, and vomiting (CB-1158+ Pembrolizumab). However, outcomes regarding the effects of the treatments are not yet reported and estimate completion is expected for end of June 2022.[120]

The last study (INCMGA00012) with CB-1158 **45** and the combination of both in Japanese participants with advanced solid tumors ended in December 2021, but the results are not yet been reported either.[107]

It is important to note that many of these studies have had their results reports delayed due to the Covid-19 pandemic (limited number of recruited patients, limited resources…).

Overall, a few numbers of Arginase 1 inhibitors are just entering on first steps of clinical trials. Only CB-1158 went further with evaluations in combination with different treatments. No drugs are currently on the market.

1.2.7 General remarks on current arginase inhibitors

As described in the previous parts, most of the more potent Arg1 inhibitors are boronic acid compounds. These boronic acid inhibitors act as transition-state analogs by forming *in situ* a tetrahedral boronate function by addition, on the boronic acid head, of the catalytic hydroxide ion buried between the two manganese in the Arg1 binding cleft. (Figure 26A)[15, 77, 87-90] To summarize, these compounds can be structurally devised into three parts: (1) a boronic acid head responsible for the formation of the tetrahedral transition-state intermediate, represented in green in Figure 26, (2) an amino acid tail, colored in red, and (3) an aliphatic chain linker, in blue. In the last generation, an additional arm, colored in pink was added.

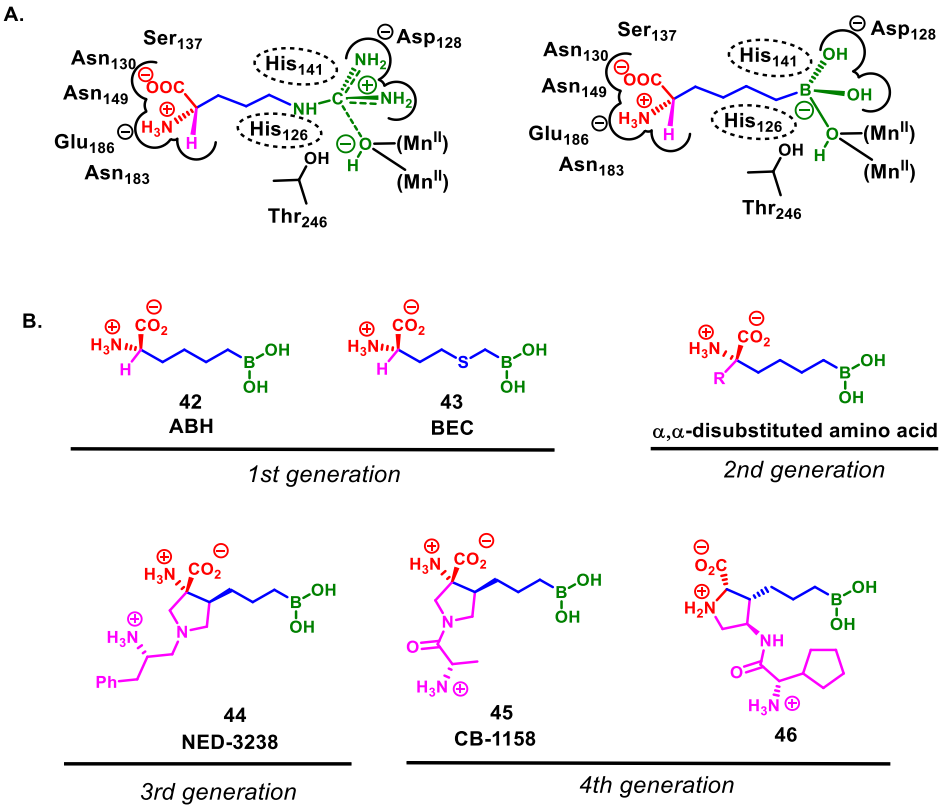

Figure 26: A. schematic representations of the transition-state of L-arginine and boronic acid inhibitors with Arg1.Boronic acid function mimic the transition state after the formation of boronate. B. reported transition-state Arg1 inhibitors in the recent literature.

Although they represent promising arginase inhibitors whose efficacies are, for some of them, currently being evaluated *in vivo*, the structural diversity among them is indeed very minimal, and the discovery of novel scaffolds remains very attractive, notably to elaborate backup strategies in case these boronic acids compounds failed in clinical evaluation. Moreover, these boronic acid-based Arg inhibitors generally suffer from poor bioavailability, limiting their use.[112] Most of these compounds are also very hydrophilic (logP close to or below zero), making their crossing through the cellular membrane difficult. In vivo, this compound was demonstrated to increase the plasma concentration of L-Arginine in cancer patients. However, it was also demonstrated that CB-1158 acts only on exocytosed Arg1.[105] This characteristic has advantages and drawbacks.

The main advantage of acting in the extracellular environment is the selectivity observed for these molecules. Being inefficient in membrane crossing prevents the compounds from inhibiting intracellular Arg, as illustrated by CB-1158. Hepatocytes do not seem to be affected by CB-1158, therefore avoiding some important side-effects related to the inhibition of the urea cycle. It could also mean the inhibition could not be observed on other Arg1-regulated pathways, or at least not lead to significant side-effect. Secondly, being localized in the mitochondria, Arg2 should not be touched. Accordingly, looking for a selective Arg1/Arg2 seems irrelevant or seems to be a minor concern. In addition, other off-target effects could be avoided by not entering the cells.

However, several drawbacks can also be discussed. Indeed, having such hydrophilic compounds involved some issues in pharmacokinetics. Such parameters are not often in the literature, with only the focus on the inhibition potency. But mean residence time, clearance, apparent volume of distribution, and oral bioavailability have started to be reported as in the development of bicyclic inhibitors published by Mitcheltree, *et al*. (Table 6).[112]

*Table 6: Pharmacokinetic profile of **61** in CL57BL/6 Mice*

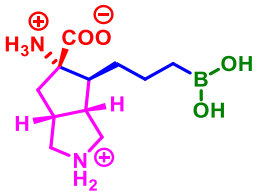

61

IC_{50}: 29 nM

Route of delivery	i.v.	p.o.
Dose (mg/kg)	1	10
Area under the curve (µM.h)	6.4	4.8
Concentration at 1h (µM)	0.91	1.2
Mean residence time (h)	1.4	3.6
Clearance (mL/min/kg)	10	/
Volume of distribution (L/kg)	0.84	/
Oral bioavailability (%)	/	7%

1.3 EXISTING ASSAYS IN THE LITERATURE

All the molecules that have been presented in the previous section (1.2) have been evaluated as Arg1 inhibitors using various biochemical assays. Hence, several experimental methods are described in the literature to evaluate arginase activity. Different strategies are possible to follow the enzyme activity. First, the disappearance of the starting material, or alternatively, the apparition of one of the products (L-ornithine **2** and urea **3**), can be monitored. Furthermore, an isostere of the natural substrate can be used. In this case, the release of an alternative product is followed. Nevertheless, no activity assay currently available can distinguish the arginase isozymes.

1.3.1 Assays measuring the formation of L-Ornithine 2

1.3.1.1 Quantification of L-Ornithine 2 by ninhydrin

Francis P. Chinard first described the colorimetric determination of **2** in 1952 via reaction with ninhydrin **64**[121] (Figure 27)

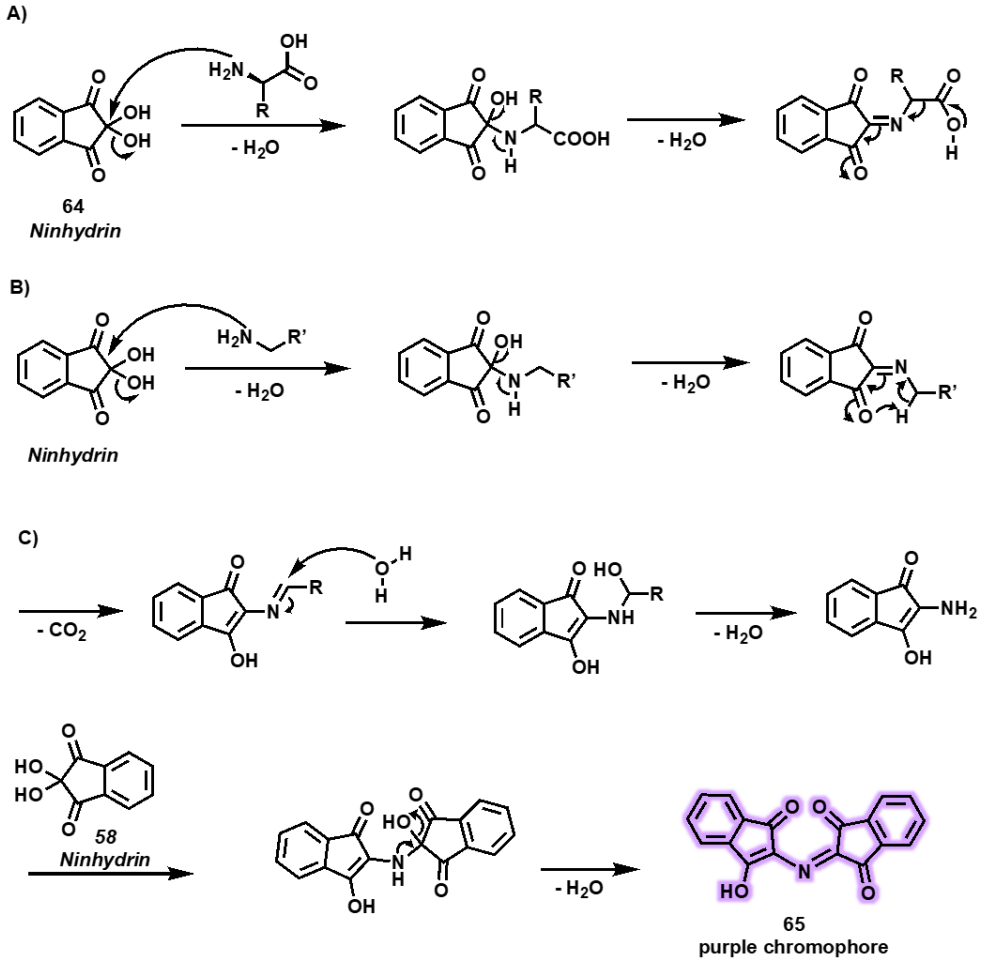

Figure 27: Reaction of L-ornithine 2 with ninhydrin 64 A) Pathway of amino acid moiety, with R= $CH_2CH_2CH_2NH_2$ B) pathway for the primary amine of the side-chain, with R'= $CH_2CH_2CH(NH_2)COOH$. C) continuation of A) and B). The product is purple (Ruhemann's purple 65), and its formation is followed by reding the absorbance between 400 and 505 nm.

In this method, L-ornithine **2** is quantified after reaction with ninhydrin **64** leading to the Ruhemann's purple **65**.[122] L-ornithine can react with its two amine functions: the amino acid function (Figure 27A) and the side-chain function (Figure 27B). Both form a purple chromophore with a maximum absorption value at a wavelength of 440 nm. So, via Beer-Lambert law, the concentration of **2** and, hence, the enzyme activity can be extrapolated from calibration curves.[123]

The main drawback of this quantification method is the need to heat up to 95°C for the formation of the chromophore. A lack of specificity with the reaction with ninhydrin is also observed. **2** shows the best coloration among all other amino acids, but reactions with other amines are not described. Interferences giving false-positive results are then often obtained with this method.[124]

1.3.1.2 Quantification by HPLC-MS or UPLC-MS

Another method of analysis consists of measuring the amount of L-ornithine **2** by HPLC-MS.[125] Deuterated L-ornithine (L-orn-d_6) or L-[U-^{13}C]ornithine are used as internal standards for quantification. The area under the chromatogram's UV curve is measured for m/z equal 133.11 Da corresponding to the parent ions ($[MH]^+$) of **2**. Concentrations are extrapolated from the area under the curves (AUC) of calibration curves obtained with known concentrations of **2**. This method offers several advantages, such as a good sensibility with low interferences.

1.3.2 Assays measuring the formation of urea

Regarding the methods for measuring urea, there are two possibilities for quantifying the enzymatic activity. First, urea can be derivatized into chromophores for direct colorimetric assessment. Alternatively, urea **3** can also be converted by urease into ammonia **66** and carbon dioxide, which are quantified.

1.3.2.1 *Assay with Berthelot's reagent*

With Berthelot's reagent, the ammonia **66** is transformed into indophenol **67** quantifiable by determining the absorbance at 630 nm.[126] (Figure 28)

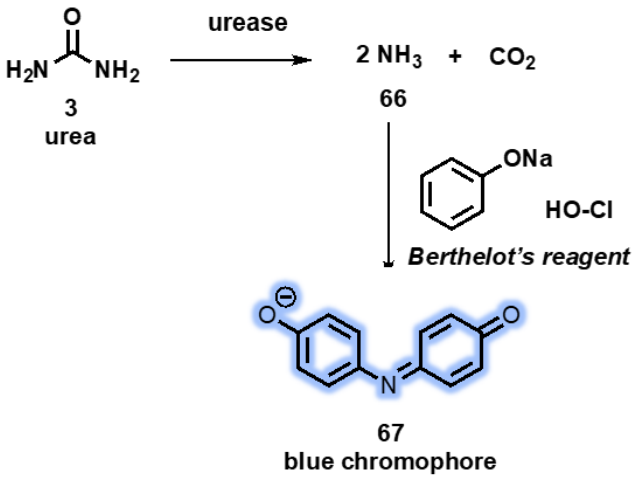

*Figure 28: General principle of the colorimetric assay with urease. Formation of a blue chromophore: indophenol **67** is followed by reading the absorbance between 570 and 630 nm.*

The quantification requires a second enzyme, increasing the incubation times (2 x 30 minutes) necessary to complete both transformations. The effect of positive molecules must be verified on the second enzyme activity, i.e., urease. Direct titration of urea seems thus more attractive, avoiding a secondary assessment of the inhibition. Moreover, amines can interfere with this test as well as organic solvents.

1.3.2.2 *Assay with the Ehrlich's reagent or p-dimethylamino-benzaldehyde 68 (PDAB or DMAB)*

In 1952, Watt and Chrisp described a spectrophotometric method that they used to quantify urea **3**.[127] The technique is based on developing a yellow-green color by adding an ethanolic solution of p-dimethylamino-benzaldehyde **68** with dilute acidic conditions. The method was improved several times and is sometimes referred to as the quantification with Ehrlich's reagent.[128] (Figure 29)

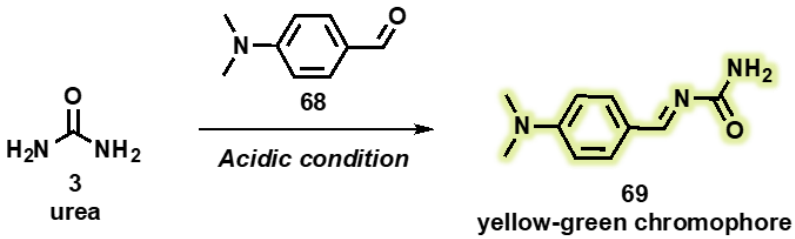

*Figure 29: General principle of the colorimetric assay with **68**. The formation of a yellow-green chromophore **69** is followed by reading absorbance between 420 nm and 435 nm.*

Numerous interactions are reported with p-dimethylamino-benzaldehyde **68** and other substances forming red, orange, violet, and yellow complexes,[129] making this test inadequate for testing libraries containing diverse chemical functions.

1.3.2.3 Assay with Diacetylmonoxime (DAM) and α-isonitrosopriopiophenone 70

The diacetylmonoxime (DAM) can also react with urea to form the chromophore that can be read at ~500 nm.[130] The color is developed at 95°C, but the diacetyl is volatile. In addition, the adduct degrades with sunlight making this test light-sensitive and tricky to use. Later, Archibald updated this method with α-isonitrosopriopiophenone **70** (α-ISO) to avoid the coloration's disappearance with light.[131] (Figure 30)

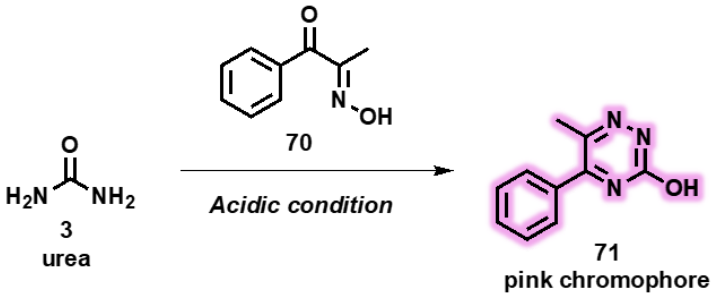

*Figure 30: General principle of the colorimetric assay with α-isonitrosopriopiophenone **70**. The formation of a pink chromophore **71** is followed by reading the absorbance at ~500 nm.*

However, heating at 95°C for 45 minutes is needed to reveal the coloration before the reading at 500 nm, making this test more inconvenient in practice. Such heating can also interfere due to the degradation of compounds, generating false-positive and false-negative results. Thus, confirmation with orthogonal methods or a study of potential inhibitors' structure is needed to avoid biased analysis.

1.3.2.4 Assay with xanthydrol 72

Greenberg, *et al.* proposed an assay with xanthydrol **72** for the derivatization of urea **3**. (Figure 31).[132]

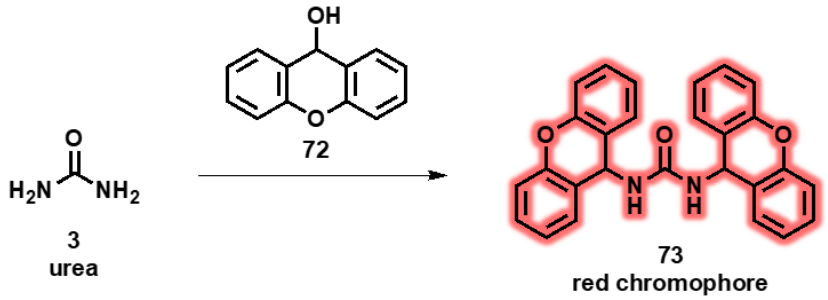

*Figure 31: General principle of the colorimetric assay with xanthydrol **72**. The formation of a red chromophore **73**, soluble in 50% sulfuric acid solution, is followed by reading the absorbance in a Klett-Summerson photoelectric colorimeter with a blue filter or in a Coleman Junior spectrophotometer.*

This test is barely described in articles and is not widely used because we measure the absorbance of the yellow solution produced when the precipitate is dissolved in 50% sulfuric acid. Unfortunately, a similar color was obtained from the unreacted xanthydrol **72**, which had to be washed from chromophore prior to adding the acid. This approach also suffered from poor reproducibility and interferences from numerous functions such as primary amides.[133] The other drawback of this method is the need to freshly synthesize the reagent from xanthone, also making this test inadequate for screening a large number of molecules.[134] Xanthydrol **72** can also be used to quantify urea by HPLC-MS.[135]

*1.3.2.5 Assay with o-*phtalaldehyde 74 *(OPA).*

This colorimetric reaction of urea uses a mix of *o*-phthalaldehyde **74** (OPA) and N-(1-naphthyl)ethylenediamine **76** (NED) in acidic conditions (sulfuric acid and boric acid solution).[136] (Figure 32)

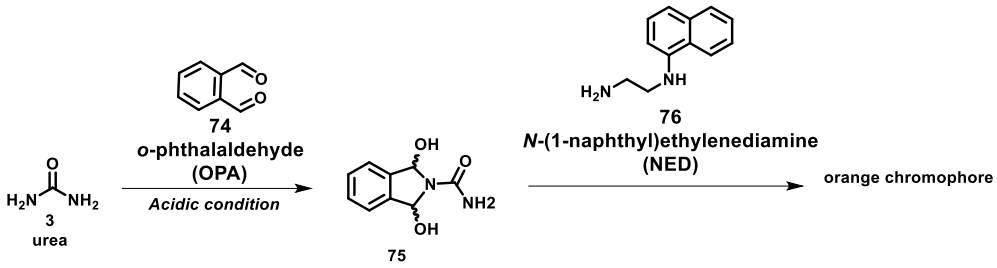

*Figure 32: General principle of the colorimetric assay with o-phthalaldehyde **74** (OPA) and N-(1-naphthyl)ethylenediamine **76** (NED). The formation of an orange chromophore is followed by reading the absorbance generally at 505 nm (480-540 nm range). The chromophore's structure is still unknown.*

This technique does not require elevated temperatures for color development, uses nonvolatile and stable reagents. The specificity is also comparable to the diacetyl reaction (DAM) described in 1.3.2.3. The chromophore obtained with OPA **74** and NED **76** is detected at 505 nm (480-540 nm range), but its structure is not known and is still debated. The substantial toxicity of NED **76** was resolved by using primaquine, an analog of NED **76**.[137]

There are several limitations of this test. First, the lower concentration requires more time for color development but does provide a more stable color. Interactions are present with some chemical functions. Several compounds: citrulline **5**, 3-ureidopropionic acid, sulfanilamide, and sulfanilamide derivatives (sulfa drugs), interfere by producing a color similar to the one obtained with urea, making this test inadequate for screening of such chemical series.

1.3.2.6 Assay with radiolabeled L-arginine 1 with the production of radioactive urea 3*.*

Urea quantification can also be performed using radiolabeled substrates. Several radiolabeled L-arginines are commercially available, including the L-arginine-[guanido-^{14}C] **1***. In 1980, Rüegg and Russell assessed for the first time the arginase activity with L-arginine-[guanido-^{14}C] **1***.[138] (Figure 33)

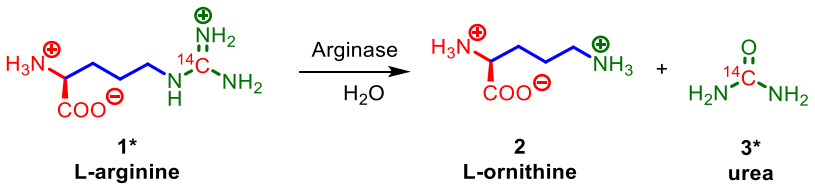

*Figure 33: General principle of the radioactive test. L-arginine-[guanido-^{14}C] **1*** is hydrolyzed by Arg1 catalysis to L-ornithine **2** and radioactive urea **3***. Arginase activity is then assessed by the determination of the radioactivity of urea.*

The use of a radiolabeled substrate makes the test very sensitive. This specific test using L-arginine-[guanido-^{14}C] **1*** is now widely used by different groups and, mainly, by the Christianson's group that developed several transition-state inhibitors.[15, 77, 96] This assay is seen as one of the most reliable ones.[139] Numerous publications report this assay, and so facilitate the stage of development. This test also offers the advantage of having high sensitivity and allows excellent reproducibility. However, it has a negative side that resides in the need to separate the products from the reagents. Because a radioactive substrate is used, the cost is high, but this drawback can be lower by the low need for radioactivity per test. The initial investment should typically last for an extended period in the use of ^{14}C radiolabeled ligands.

1.3.3 Assays using an alternate-substrate

1.3.3.1 Ellman's reagent-based end-point assay

Otherwise, tests exist based on the dosage of products derived from isosteric substrates of L-arginine **1**. In this type of test, the enzyme is in the presence of a

molecule capable of being a substrate and is forming products whose appearance can be easily followed.

Among these tests, L-thioarginine **77** can also be used. The test is usually abbreviated as TOGA, for thioornithine generation assay. Arg1 in the presence of L-thioarginine **77** forms L-thioornithine **78**. L-thioornithine **78** is revealed by reaction with 5,5'-dithiobis-2-nitrobenzoic acid **79** (DTNB), also known as the Ellman's reagent.[140] (Figure 34)

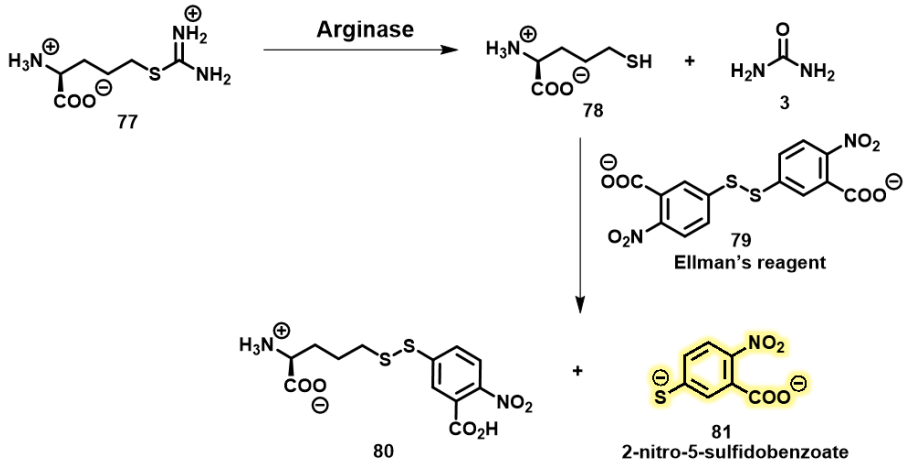

*Figure 34: General principle of the colorimetric assay with L-thioarginine **77**. L-thioarginine **77** is transformed to L-thioornithine **78** and urea **3** by Arg1. Then, L-thioornithine **78** reacts with Ellman's reagent **79** to form 2-nitro-5-sulfidobenzenoate **81**. 2-nitro-5-sulfidobenzenoate **81** is a yellow chromophore that is followed by reading the absorbance at 412 nm.*

After the obtention of L-thioornithine **78** with Arg1, L-thioornithine **78** reacts with Ellman's reagent **79** to form 2-nitro-5-sulfidobenzenoate **81**. 2-nitro-5-sulfidobenzenoate **81** is a yellow chromophore that is followed by reading the absorbance at 412 nm. The coloration appears at room temperature, making this test convenient to perform. Unfortunately, L-thioarginine **77** is commercially available, but only a few suppliers offer it as a kit, making assays with **77** expensive. This cost makes this test inadequate for the screening of large libraries. Moreover, the synthesis is also a bit long, making access difficult to **77**.

1.3.3.2 Continuous assay with direct determination.

All previously described assays are discontinuous since the reaction needs to be stopped to measure the enzymatic activity, known as fixed points assays. On the other hand, continuous assays allow the direct and continuous determination of product formation or remaining substrate. Thus, such approaches are more suitable for kinetics experiments.

-nitro-3-guanidinobenzene **82** (NGB) is an example of an alternative substrate. Its Michaelis-Menten constant (K_M) with 1.6 ± 0.2 mM is almost similar to the natural substrate. It leads after catalysis to the formation of urea **3** and a chromophore: *m*-nitroaniline **83**.[141] (Figure 35)

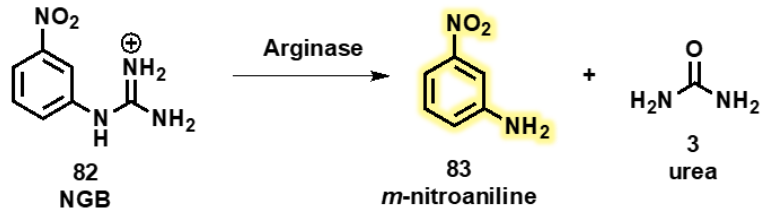

*Figure 35: General principle of the assay with alternative substrate: 1-nitro-3-guanidinobenzene (NGB) **82**. m-nitroaniline **83** is obtained after hydrolysis by Arginase, and absorption at 372 nm of this product allows quantitative and qualitative estimation of urea by spectroscopy at 372 nm (extinction coefficient of 109 $M^{-1}.cm^{-1}$).*

m-nitroaniline **83** formation can be measured by absorption at 372 nm. K_M value of NGB **82** is nearly identical to that of the biological substrate arginine even though NGB **82** lacks the α-amino and α-carboxylate groups of arginine that engage in extensive enzyme-substrate hydrogen-bond networks. The k_{cat} value for NGB hydrolysis (k_{cat} = 0.09 ± 0.02 min^{-1}) is much lower than that reported for arginine hydrolysis (k_{cat} = 15,000 ± 1200 min^{-1}).

Recently, 6-aza-2-thiothymine-stabilized gold nanoparticle **85** (ATT-AuNP)-Based Fluorescent Assay of Arginase Activity was developed.[142] The Gold Nanoparticles (AuNPs) act as a nanoswitch. The change in fluorescence is controlled

by a host−guest system, where ATT-AuNPs specifically recognize guanidium moiety of L-arginine **1**. When **1** is bound to the ATT-AuNPs **85** (= L-arg/ ATT-AuNPs **84**), fluorescence is observed with the emission of green light (526 nm) after the excitation at 472 nm.[143] But, **1** is in competition for ATT-AuNP **85** and arginase. With the enzymatic transformation, the guanidium moiety of **1** is hydrolyzed and cannot be recognized anymore by the ATT-AuNPs **85**. Thus, fluorescence decreases with the enzymatic reaction. (Figure 36)

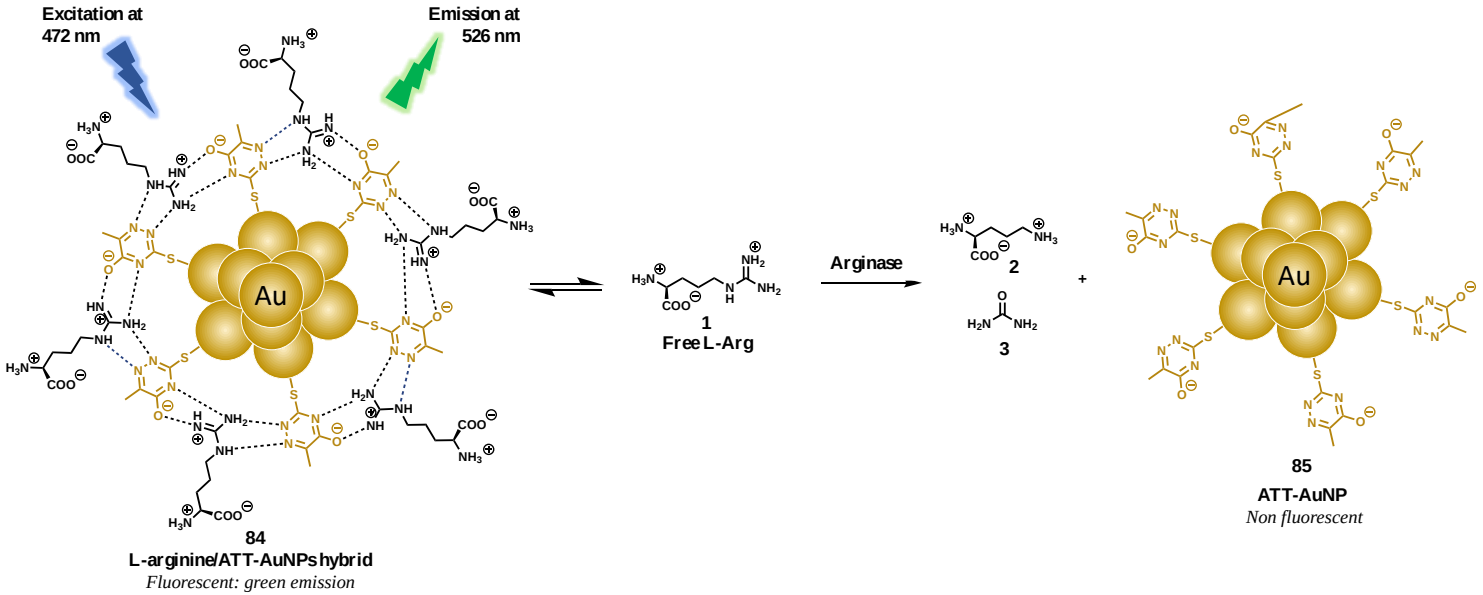

Figure 36: General principle of the 6-aza-2-thiothymine-stabilized gold nanoparticle ***85*** *(ATT-AuNP)-Based Fluorescent Assay of Arginase Activity.*

Although this method is described as a facile method of determining arginase activity, we can indicate some drawbacks. This procedure avoids the multiple technical manipulations involved in existing traditional measurements, but ATT-AuNPs **85** and L-arg/ ATT-AuNPs **84** need to be produced. The synthesis pathway is quite accessible, but it involves gold nanoparticles (AuNPs) obtention skills and grafting these gold nanoparticles from $HAuCl_4$ solution or citrate-AuNPs.[144] The use of gold also makes this test expensive to run, especially with many compounds to screen. L-arg/ ATT-AuNPs **84**. Moreover, L-arg/ ATT-AuNPs **84** are stable for months in a fridge. L-arg/ ATT-AuNPs **84** and ATT-AuNPs **85** are light sensitive and need to be synthesized and stored in the dark.

1.4 PREVIOUS PRELIMINARY WORKS ON ARGINASE

The search for Arg1 inhibitors was initiated before the starting of this PhD thesis at the Namur Medicine & Drug Innovation Center (NAMEDIC) at the University of Namur (UNamur). As the objective was to discover potent Arginase 1 inhibitors that could be amenable to experiments in preclinical settings, the first steps of the drug discovery program were started and led to the production and purification of Arg1 and the screening an *in house* (proprietary) library at NAMEDIC using the ninhydrin assay described in the previous chapter. This NAMEDIC library is composed of historical, original, compounds that were prepared in the context of other drug discovery programs. It contains few thousands of compounds.

This tentative screening on Arg1 using the *in house* NAMEDIC chemical library revealed only very few hits and particularly the 5-bromo-2-amino-thiazole **89** with a promising Arg1 inhibition of > 90% inhibition at a concentration of 100 µM. But unfortunately, due to a lack of time and human resources dedicated to this project, the IC_{50} of this compound **89** on Arg1 could not be determined and hence

the Arg1 inhibition of this compound could not be confirmed. Still, if validated, this compound could constitute one of the very first Arg1 inhibitor series deprived of the boronic acid head, and the scaffold could thus be the basis of a completely new series of Arg1 inhibitors endowed with a novel mechanism of action.

It should moreover be noted that this 5-bromo-2-amino-thiazole scaffold was, in fact, initially identified by serendipity by Dr. Eduard Dolušić (UNamur) during a tentative synthesis of the 2-amino-thiazole-*N*-oxide **90**. However, it was found that treatment of 2-aminothiazoles **88** with *m*-chloroperoxybenzoic acid (*m*CPBA) in ethanol afforded the corresponding 5-bromo-2-amino-thiazole **89** instead of the *N*-oxide product **90** in a very good yield (> 90%) (Figure 37).[145] Because **89** was thought to be a potential novel hit compound on Arg1 with a novel mechanism of action and moreover the route to access this series is particularly original, the first part of our thesis was dedicated to validate the Arg1 inhibition of **89** and to detail and possibly expand the synthesis of this series to generate diversely-substituted analogues of **89**.

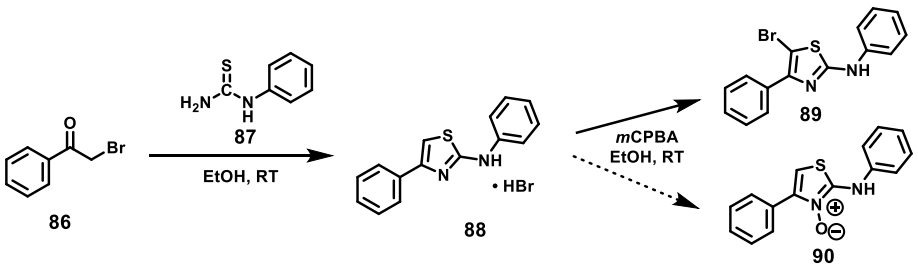

*Figure 37: mCPBA-mediated 5-bromo-2-amino-1,3-thiazole formation **89***

2 OBJECTIVES AND STRATEGIES

As presented previously in part 1.2, the most potent inhibitors are transition-state inhibitors bearing a boronic acid function. Despite many advantages, several important disadvantages were presented and discussed. To overcome these disadvantages is an appealing strategy to design better arginase inhibitors. Two different approaches to solving these problems can be envisioned:

- First, research can be aimed at discovering new scaffolds that are intrinsically more viable from a pharmacokinetic point of view, i.e., more lipophilic or without zwitterion, making the molecules able to cross membranes more effectively, a decreased clearance or a higher bioavailability for *per os* administration.
- Secondly, rational optimization can be performed from existing inhibitors or described scaffolds. With this type of approach, we are not starting from scratch, and the designed molecules may see a significant increase in their inhibition or pharmacokinetic parameters, as seen in the past with the addition of the additional arm or cycle.

Both approaches can lead to molecules capable of penetrating cells and would allow the study of cytosolic inhibition and allow the study of intracellular inhibition of Arg1 and Arg2 and their regulation. Such data should result in a better understanding of complex intracellular mechanisms.

In the present work, we thus aimed at discovering **new families of Arginase 1 inhibitors that could eventually be used in preclinical settings.** Both previously described approaches will be used in our work to contribute to the development of new original Arg1 inhibitors. It should constitute a first step towards the design of novel original anti-cancer agents in the field of immunotherapy. Moreover, since

arginase is involved in other pathologies such as vascular disease and asthma as presented in 1.1.3, these compounds could lead to new treatments for these diseases.

To reach this goal, our strategy comprised three complementary steps that could be pursued in parallel. (Figure 38)

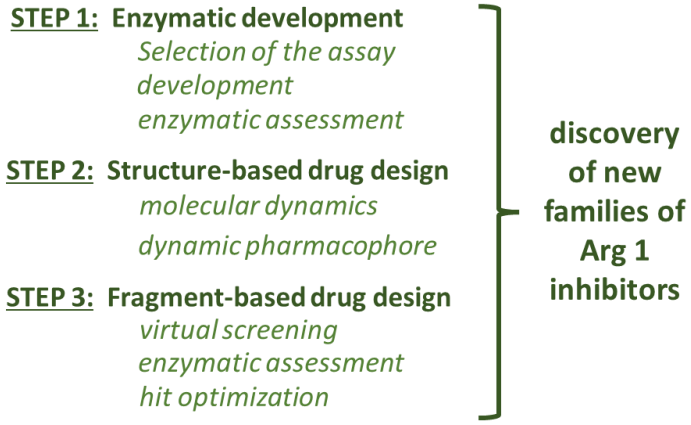

Figure 38: Strategy of the arginase research project for discovering new families of Arg1 inhibitors.

STEP 1. Firstly, based on preliminary results generated earlier (collaboration with the university of Namur), a reliable enzymatic evaluation method will be developed to investigate the potency of some 5-bromo-2-amino-thiazoles characterized with a somehow promising Arg1 inhibition (IC_{50} Arg1 inhibition around 100 µM using the ninhydrin colorimetric test). This yet unknown scaffold to inhibit Arg1 could thus potentially lead to a novel series of Arg1 inhibitors that would be deprived of a chelating moiety.

STEP 2. A molecular modeling approach using the current knowledge from the literature will be investigated to understand better the possibilities and possible limitations in the design of Arg1 inhibitors. This step will include the elaboration of a tentative dynamic pharmacophore that could potentially be used in the second step to screen for potential new fragments hits.

STEP 3. A ligand-based approach will be started using the dynamic pharmacophore elaborated in step 2 and all other collected data. Thus, a Fragment-Based Drug Design (FBDD) will be developed based on the inhibitors described in the literature. Screenings of various chemical libraries will be performed to tentatively find new original hits.

The next chapters will thus be organized as follow:

- In *chapter 3*, the production and purification protocols of the arginase enzymes, and the development of a radiolabeled enzyme assay will be presented, as well as the enzymatic assessments of the 5-bromo-2-aminothiazoles series.
- In *chapter 4*, the *in-silico* structure-based drug design approach will be detailed. Molecular dynamics and the so-called dynaphores will be presented.
- In *chapter 5*, the Fragment-Based Drug Design approach will be presented, with a focus on *in silico* and *in vitro* screenings.
- In *chapter 6*, the optimization of our best fragments will be pursued, and a challenging chemistry is discussed

3 PRODUCTION OF ARG1 AND SELECTION & DEVELOPMENT OF AN ARG1 INHIBITION ASSAY

In this first chapter, the works that were undertook to produce Arginase 1 and develop a suitable Arginase 1 inhibition assay amenable to screening experiments are presented.

3.1 ARGINASE 1 PRODUCTION AND EVALUATION

3.1.1 Enzyme production

The recombinant human arginase 1 used in our assay was either from a commercial vendor (batch of 20 µg of arginase 1 from Enzo Life Sciences) or produced in collaboration by the University of Namur.

Nowadays, the enzyme is also produced in our laboratory at UCLouvain. The protocol was setup in collaboration with Juhans Dechenne, based on the protocol used at UNamur and our existing methods from other projects developed in our group. The protocol is described below.

Recombinant Arg1 gene is inserted in a pET-28a+ plasmid vector, ordered from Genecust. The recombinant plasmid was transferred into the Escherichia coli strain BL21 (DE3) (Rosetta 2). The transformant was selected from a single colony on a LB kanamycin agar plate and was used to inoculate in a TB medium (50 µg/mL kanamycin and 34 µg/mL chloramphenicol) and was cultured at 37°C with an agitation of 120 rpm until an optical density of 0.8 was reached. The expression of *h*Arg1 was induced by isopropyl β-D-1-thiogalactopyranoside (IPTG), with a final concentration of 1 mM. The culture was grown at 20°C for 20h. Cells were harvested by centrifugation at 5000 rpm, 4 °C for 25 min. Cell pellets were resuspended in a lysis buffer (Tris-HCl 50 mM, pH 8.5, $MgCl_2$ 10 mM, $MnCl_2$ 1 mM, NaCl 300 mM, imidazole 5 mM, and glycerol 10%) supplemented with cOmplete™, EDTA-free protease inhibitor cocktail (Roche) and 1 mM of phenylmethylsulfonyl fluoride

(PMSF) and then disrupted by sonication, followed by centrifugation at 4°C and 10,000 rpm for 30 min. The supernatant was collected, and to 1 µL of β-mercaptoethanol per mL of the supernatant was added and loaded onto 1 mL His-trap FF-crude columns (GE Healthcare) according to the manufacturer's instructions for the purification by affinity chromatography. Purified *h*Arg1 was then dialyzed overnight in a pH 8 buffer containing 20 mM Tris, 100 mM NaCl, 1 mM DTT, 20% glycerol. All aliquots were freeze dry with liquid nitrogen, and then conserved at -80°C. All aliquots were used with the same number of freezing-unfreezing cycles.

In a last step, apoenzyme and holoenzyme were separated. The fraction with Arg1 recovered after purification was heated at 60°C for 20 min. Centrifugation at 10,000 rpm for 30 min removed the apoenzyme that is less stable that the holoenzyme and precipitated after its unfolding. Nano differential scanning Fluorimetry (NanoDSF) on a Tycho NT.6 device (NanoTemper Technologies) was used to assess the melting temperature of our batches before and after purification. NanoDSF is a modified method of the differential scanning fluorimetry for determining the protein stability thanks to intrinsic tryptophan or tyrosine fluorescence, as for thermal shift assay (TSA). A linear temperature increase is used to unfold the protein and a shift in intrinsic fluorescence is observed. The thermal stability of a protein is typically described by the 'melting temperature' or 'Tm', at which 50% of the protein population is unfolded, corresponding to the midpoint of the transition from folded to unfolded. According to the standard manufacturer's procedures, samples were poured into capillaries and heated up to 95°C in 3 min while following fluorescence emission at 330 and 350 nm. Melting temperatures were extracted from the derivative of the 350/330 nm fluorescence ratios upon increasing temperature. As observed on Figure 39, whereas two melting transitions are observed before purification by heating (red curve), only one melting event is observed after purification with a Tm value of 85.6°C corresponding to the holoenzyme.

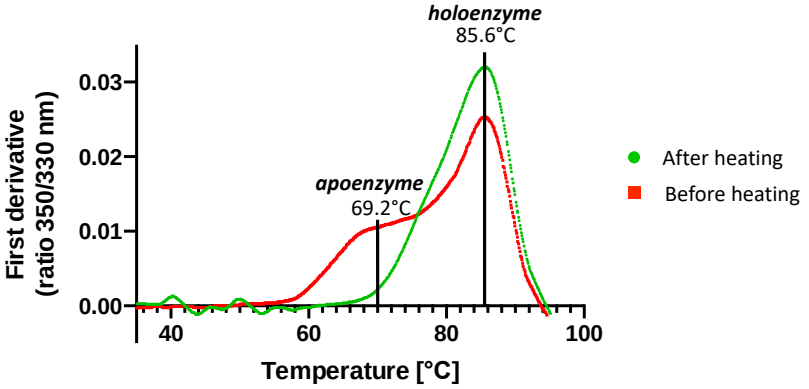

Figure 39: Effect of the purification by heating the protein after dialysis, observed by nanoDSF. Before heating, a mixture of apoenzyme holoenzyme is observed because Arg1 did not totally integrate Mn^{2+}. Less stable apoenzyme was removed by centrifugation after heat degradation. (Courtesy of Juhans Dechenne)

3.1.2 Evaluation of the enzyme quality

Protein concentrations were measured using the Bradford method with the Biorad protein assay kit, and sample homogeneity was assessed using sulfate-polyacrylamide gel electrophoresis with Coomassie brilliant blue as a staining agent. (Figure 40)

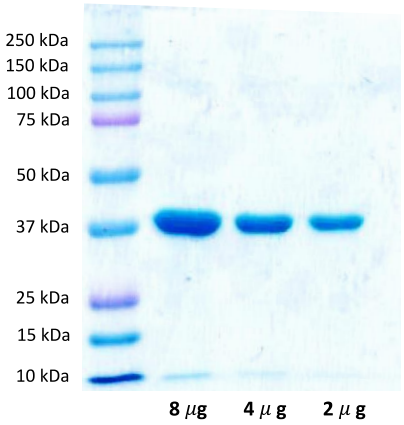

Figure 40: Electrophoresis gel of produced human Arg1 at 3 different concentrations.

A band corresponding to a molecular weight around 37 kDa that is coherent with the theorical MW of 36.5 kDa expected for the enzyme is obtained.

To ensure about the quality and proper folding of the purified Arg1, nano differential scanning fluorometry experiments were performed on a Tycho NT.6 device (NanoTemper Technologies). Change in fluorescence were seen at the inflection temperature of 86°C for Arg1 holoenzyme, from the storage buffer (20 mM Tris pH 8, 1 mM $MnCl_2$, 20% glycerol, 100 mM NaCl). (Figure 41B)

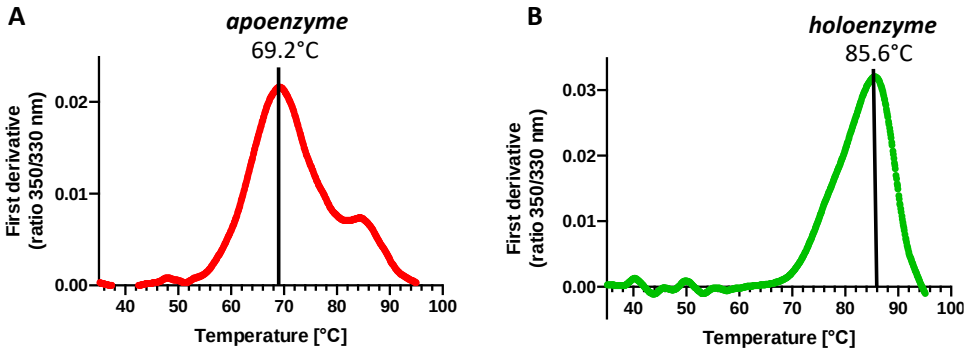

Figure 41: Nano differential scanning fluorimetry (nanoDSF) showing a melting temperature of 69°C for apoenzyme Arg1 (A) and 86°C for holoenzyme Arg1 (B). (Courtesy of Juhans Dechenne)

It is important to note that the melting temperature for TSA and the inflection temperature recorded by the nanoDSF are influenced by several parameters: the nature of the buffer and its concentration, the presence or not of $MnCl_2$ or other salts, the pH, the purity and the concentration of Arg1 sample.[146] A 15-16°C difference was observed when $MnCl_2$ is absent or present. In absence of $MnCl_2$ during the enzyme production (lysis buffer), melting temperature was measured at 69°C (Figure 41A), and which is in agreement with the literature. Values of 73 and 77°C are reported in recent literature by thermal shift at pH 7.4 and 9.5, respectively, in slightly different buffer conditions (0.2 mg/mL in 50 mM glycine pH 9.5 or 50 mM Na_2HPO_4 pH 7.4, without $MnCl_2$ in both case).[147]

3.2 DEVELOPMENT OF AN ARG1 INHIBITION ASSAY.

3.2.1 Preliminary results and issues with previous test using ninhydrin

The search for Arg1 inhibitors at the Namur Medicine & Drug Innovation Center (NAMEDIC) at the University of Namur (UNamur) was initiated with the production and purification of Arg1. The ninhydrin assay described in the previous chapter was setup and a screening of an *in house* library planned.

As a result, from this initial screening, 5-bromo-2-aminothiazoles were identified as promising hit compounds on Arg1 with, for the most promising hit, > 90% Arg1 inhibition at 100 µM. Due to a lack of time and human resources, these compounds have not however been confirmed by the evaluation of IC_{50}'s on Arg1.

Regarding the ninhydrin assay that was used to identify this new series of compounds, it should be noted that this assay is practical, easy to setup, and relatively inexpensive, but it has also revealed many drawbacks and limitations, including reproducibility issues and inconsistencies regarding the data obtained. One of the concerns dealt with the need to heat at relatively high temperature (90°C) and for a long time (1h) the mixture after the addition of the ninhydrin for the revelation step. During this heating, the test tubes must be opened to avoid overpressure. In our hands, we could not find experimental conditions with well-monitored solvent evaporation. This was also true with calibration curve rendering the extrapolation inaccurate. Another concern dealt with the potential presence of amine functions on the inhibitors that could lead to interference during the assay. Interferences are reported with other amino acid than L-ornithine **2** as discussed in 1.3.1.1, but it is also the case with other amines, carbamates and even amides after strong heating. Finally, a last weakness of the ninhydrin assay dealt with the difficulty to visually inspect the different wells on the plates for potential aggregation phenomenon. Aggregation is a common phenomenon leading to false positives during screening assays. Here the dark color generated with ninhydrin is a limitation to observe precipitation.

3.2.2 Selection of the assay

Because it was needed to make a relevant choice among the available Arg1 inhibition assays, we have decided to consider Arg1 inhibition assays that rely on a direct measure of the Arg1 activity instead of an indirect assessment that would rely on urease and/or secondary screening for instance, in order to limit potential artefacts or counter screening assays.

Although less easy to setup than a colorimetric assay, we envisioned to use a radiolabeled assay. This method offers several pros and cons. The most important pros is the high sensitivity of this test. It also has an excellent reproducibility. The low consumption of Arg1 enzyme in this assay is also an advantage. Moreover, this test is commonly used in the literature, and our lab has the chance to be equipped with a scintillation counter to detect radiolabeled compounds.

3.2.3 Implementation of the radioisotopic test

This radiolabeled assay was also described in numerous publications of Christianson's group.[87, 89] We thus set out to implement this radiolabeled assay in our lab. The principle and the procedure are summarized below. (Figure 42)

Briefly, the molecules are dissolved, generally in DMSO, for maximum solubilization of organic compounds. Then, 5 µL are deposited in a 1.5 mL microtube. Then, 40 µL of a mixture containing the buffer, *N*-Cyclohexyl-2-aminoethanesulfonic acid (CHES) at 50 mM, $MnCl_2$ (100 µM), and the substrate is added. The nature of the buffer is adapted to the desired pH. In our case, CHES is used to fit with the optimum pH of the enzyme. CHES buffer has a p*K*a of 9.3, which is very close to the optimum pH of 9.5 reported for Arg1. Next, $MnCl_2$ is added in a small amount to ensure there is enough of the cofactor (Mn^{2+}). The substrate is a mix of unlabeled and radioactive ligand. The amount of radioactivity is calculated to get an adequate number of disintegrations per minute (DPM). In this case, 0.05 µCi of

L-arginine-[guanido-14C] **1*** is necessary to follow the reaction. The addition of the 5 µL enzyme solution (10 µL/mL) initiates the reaction. 400 µL of a STOP solution interrupts the enzyme reaction after incubation at 37°C. The latter contains 0.25 mM acetic acid to obtain an acidic pH, 7 M urea, and 10 mM unlabeled L-arginine to ensure that the reaction is stopped and will not continue. A 1:1 (v/v) mixture of water/Dowex 50WX8, a cation exchange resin, is also added with this solution. Dowex 50WX8 efficiently separates the non-hydrolyzed radiolabeled arginine **1*** from the radioactive urea **3*** formed. Radiolabeled urea **3*** remains in the supernatant, where 200 µL are harvested and transferred to counting flasks. 3 mL of scintillation liquid (UltimaGold™ LSC cocktail) are then added. Counting can be done within one hour after addition. All vials are counted for 10 minutes, and the counting results are expressed in disintegrations per minute (DPM).

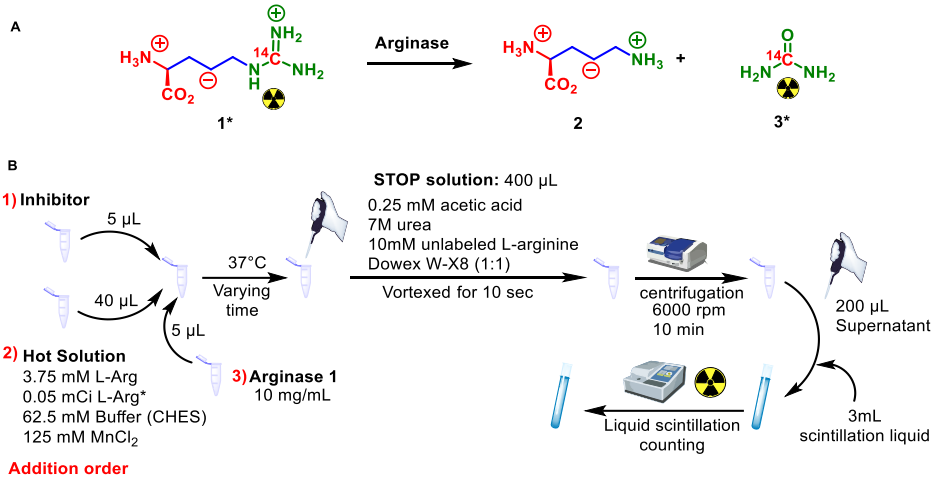

*Figure 42: A) Principe of the enzymatic assays. L-arginine-[guanido-14C] **1*** is hydrolyzed by Arg1 catalysis to L-ornithine **2** and radioactive urea **3***. B) Experimental protocol of the test. Addition of the inhibitor solution followed by the hot solution before the enzymatic reaction starts with the addition of the enzyme solution. The reaction is then stopped by the addition of "stop solution" after incubation. Next, the suspension is vortexed for 30 seconds before centrifugation to separate the resin of the supernatant. Finally, 200 µL of the supernatant is taken and added to 3 mL of scintillation liquid. After 1 hour, 10 minutes of counting is performed.*

3.2.4 Optimization of the assay

3.2.4.1 Evaluation of the effect of pH

To guarantee the highest enzymatic activity, it was necessary to determine the optimal pH to perform the assays. The conditions are alkaline for arginases due to the need of a hydroxide ion in the catalytic site. In the literature, most authors report a pH between 9 and 10 for assaying the recombinant human arginase. The pH of this enzymatic test with a radioligand is generally carried out at pH 9.5. *N*-cyclohexyl-2-aminoethanesulfonic acid (CHES) is the most suitable buffer, with a pK_a of 9.3 and an effective range between 8.3 and 10.3 (pK_a ± 1). Buffer at pH 8.5, 9.5 and 10.5 were prepared to maintain the same ionic force, and the enzyme activity was measured (50mM CHES buffer, 3 mM of unlabeled L-arginine, 0.05 Ci radiolabeled Arg, 100 µM $MnCl_2$). (Figure 43).

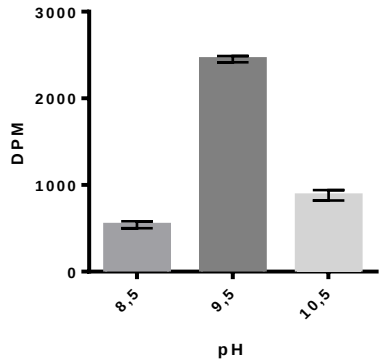

Figure 43: Quantity of product formed estimated in DPM as a function of the buffer's pH. All values are means (n = 3) +/- standard deviation.

Radioactivity measurements associated with the ^{14}C-urea **3*** formed revealed a higher catalytic activity at pH 9.5. The use of CHES as a buffer is thus confirmed. A comparison of enzyme activity was performed at the optimum pH of 9.5 and pH of 7.4. (Figure 44) The CHES buffer was selected to perform the assay at pH 9.5, as discussed previously. For pH 7.4, tris(hydroxymethyl)aminomethane,

also known as Tris, was used. Tris has a pK_a of 8.07 at 25°C and can be used with an effective pH range of 7.1 and 9.1 (pK_a ± 1).

In part 1.1.1, we discussed on the structure of arginase and highlighted the presence of a hydroxide anion in the catalytic site. This anion comes from the deprotonation of a water molecule near the manganese cores of the catalytic site. Although the deprotonation is facilitated by the coordination to metals, it is even more easily achieve at alkaline pH. However, in cancer, the tumor microenvironment is generally associated with a lower pH, due to glucose metabolism to lactate. [148]

We observed that pH has a significant impact on Arg1, being more active at pH 9.5 than 7.4. Although several research teams do report the use of pH 9.5 in their experimental assay of Arg1 activity, this alkaline pH not only misrepresents the tumor microenvironment, but also raises the question of the ionization state of molecules. Working at pH 7.4 or lower would better model what is happening in the tumor microenvironment but leads to experimental conditions with a slower reaction and a less stable enzyme and thus requires larger enzyme quantities. Therefore, we decided to perform our screenings at a pH of 9.5 to limit the consumption of enzyme, At this pH, we also ensure the presence of the hydroxide in the active site. Working at lower pH would limit the reaction with boronic acids that react with the hydroxide to form the bound boronate, for example. It is one of the explanations why boronic acid inhibitors are generally more potent at alkaline pH as described in part 1.2.4.

In addition to our screenings at pH 9.5, we also planned to investigate the most interesting compounds with additional tests: competition, reversibility, and orthogonal biophysical methods, but also at other pH such as 7.4.

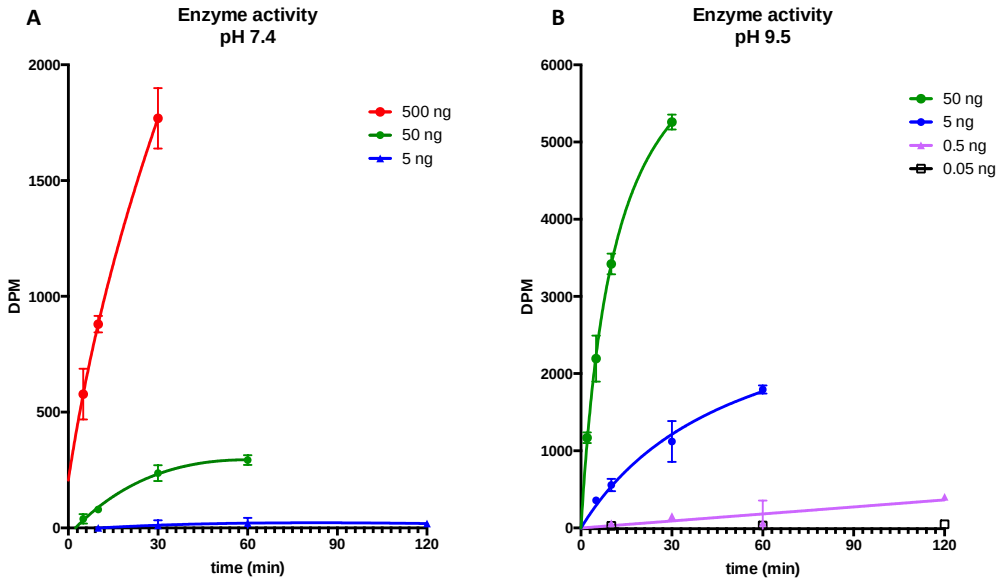

Figure 44: Enzyme activity at pH 7.4 (A) and pH 9.5 (B). Activity in DPM is the function of time (minutes) and for different enzyme amounts. All values are means (n = 3) +/- standard deviation.

In this experience, the comparison between pH 7.4 and 9.5 shows a clear difference in enzyme activity. For the same amount of enzyme, a lower value of DPM is observed for pH 7.4. Therefore, a test at pH 7.4 can be adapted by increasing the amount of enzyme and the incubation time from 5 min to 10 min.

3.2.4.2 Enzyme concentration

Like any chemical reaction, the higher the amount of catalyst, the faster the reaction will be. Limiting the enzyme concentration is also essential to decrease the cost per test. Different amounts of Arg1 between 1 and 100 ng were tested to find the appropriate conditions generating enough product to be reproducible. The incubation time must stay within the initial velocity where the product formation is linearly related to time. (Figure 45)

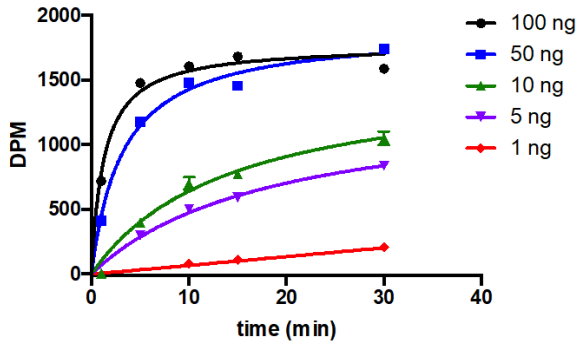

Figure 45: Study of the product formation over incubation time in function of enzyme amount in solution. All values are means (n = 3) +/- standard deviation. Conditions of this assay are the same as described at the beginning of the part 3.2.3(Figure 42). Substrate concentration is fixed at 3 mM, buffer at 50 mM and $MnCl_2$ at 100 µM. pH 9.5

The general recommendation for enzymatic assays is to stay with a substrate conversion of less than 15% to avoid other limiting factors such as product inhibition. It is important because regarding arginase, L-ornithine is a product inhibitor. However, substrate concentration must also be determined.

3.2.4.3 Michaelis-Menten Constant (KM) determination

It is also necessary to set the optimal concentration of L-Arginine **1**. The concentration is determined by measuring initial velocity at different concentrations of L-arginine **1**. The Michaelis-Menten constant (K_M) is determined by the substrate concentration for which the initial reaction rate is equal to half the maximal initial rate. The substrate concentration is essential for the screening of libraries because it affects the test's sensibility and can introduce a bias. The concentration of the substrate matters regarding the type of inhibition (competitive, non-competitive, uncompetitive, or mixed inhibitors). Competitive inhibitors bind to the active site where the substrate usually occupies the enzyme. In other words, if the concentration of the substrate is higher than the K_M, the screening favors the detection of non-competitive inhibitors. Furthermore, if this concentration is lower, the detection of competitive inhibitors is preferred. Therefore, operating the test with substrate

concentrations close to the K_M value constitutes the compromise allowing the detection of different inhibition modalities and the best choice for screening.

Urea amount production was calculated as developed by Kepka-Lenhart *et al.* adapted from the original calculation of Rüegg & Russell in 1980.[138] (Equation 1)

*Equation 1: Determination of urea **3** amount in mmol. DPM_{sample} corresponds to the disintegrations per minute of [^{14}C]urea **3*** produced in the sample reaction. $DPM_{radioactivity}$ corresponds to the total disintegrations per minute of L-arginine-[guanido-14C] **1*** in reaction. DPM_{blank} is dpm in the blank reaction. [L-arg] is the L-arginine **1** concentration in mmol.L^{-1}*

$$\boldsymbol{urea\ amout\ (mmol)} = \frac{\mathbf{2.25\ (DPM_{sample} - DPM_{blank})}}{\mathbf{(DPM_{radioactivity} - DPM_{blank})}}\mathbf{[L\text{-}arg]}$$

Initial velocity was obtained after incubation of 2 min with a concentration range of L-arginine from 0.1 to 10 mM. (0.1, 0.25, 0.5, 1.0, 2.5, 5.0, 7.5, 10 mM). (Figure 46)

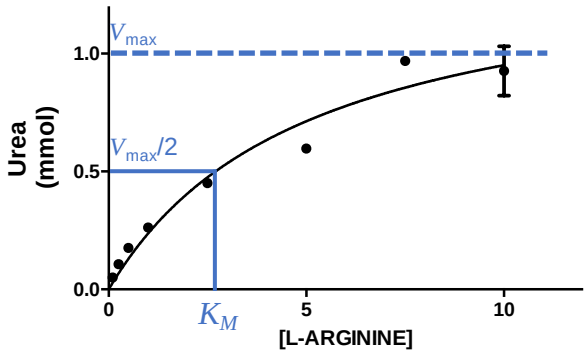

*Figure 46: determination of the Michaelis-Menten constant of L-arginine **1** for Arginase 1. All values are means (n = 3) +/- standard deviation.*

The K_M of Arg-1 for its natural substrate reported in the literature is in the range of 1 to 10 mM. These values agree with those measured in the laboratory with the commercial and produced enzymes, between 1.3 and 4.6 mM. Then, the concentration of L-arginine was fixed at 3 mM, closer to the K_M.

3.2.4.4 Poisson's law requirement

Poisson's law requires having a significant number of disintegrations per minute since this rule states that the standard deviation is calculated as the square root of the total counts detected. The confidence limit uses the 2s value (95.5% confidence limit). (Equation 2)

Equation 2: standard deviation s, confidence limit at 95.5% 2s, and expression of confidence limit in percentage %2s.

$$If \qquad \boldsymbol{s = \sqrt{total\ counts}}$$

$$Then, \quad \boldsymbol{2s = 2\sqrt{total\ counts}}$$

$$And \qquad \boldsymbol{\%2s = \frac{100 * 2 * s}{total\ counts}}$$

In our laboratory, a value of around 1,000 DPM and a counting time of 10 minutes are generally searched. In other words, we are targeting approximately 10,000 disintegrations. The root square of this target value and so the standard deviation is 100. Thus, it gives a confidence interval of 2s at 200. Therefore, the percentage of the confidence limit (%2s) for 1,000 DPM over 10 minutes is 2%, which is acceptable. Increasing the target value cannot be at the expense of a more considerable amount of radioactivity used.

We reevaluated the product production over time after the selection of the conditions. A kinetic tracing was performed by stopping the reaction after different incubation times ranging from 2 to 90 minutes. (Figure 47)

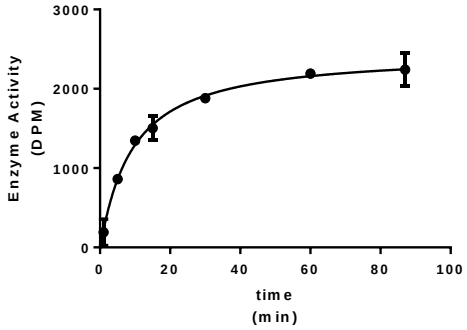

Figure 47: Study of the enzymatic activity measured as a function of the incubation time. All values are means (n = 3) +/- standard deviation.

An incubation time of five minutes for this test was in the acceptance criteria.

3.2.5 Evaluation of the influence of the dimethyl sulfoxide (DMSO)

To perform the screening of organic molecules that are usually lipophilic, DMSO, an organic solvent, is sometimes used. Nevertheless, it is necessary to verify that the presence of DMSO does not influence the activity of Arg1. (Figure 48)

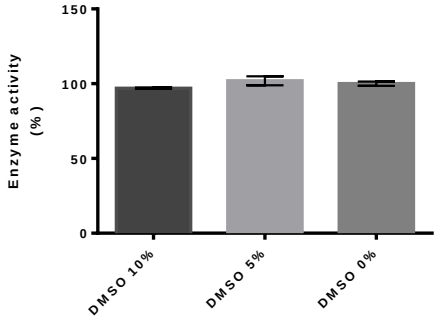

Figure 48: Quantity of product formed estimated in DPM as a function of the percentage of DMSO present in the buffer. All values are means (n = 3) +/- standard deviation.

At the end of this test, no significant difference in the enzymatic activity was observed between the three experimental conditions. Thus, the concentration of 10% (v/v) of DMSO could be retained to test the most lipophilic compounds.

3.3 VALIDATION OF THE RADIOLABELED ARG1 INHIBITION ASSAY WITH REFERENCE INHIBITORS AND TENTATIVE VALIDATION OF THE ARG1 INHIBITORY POTENCY OF THE 5-BROMOTHIAZOLE COMPOUND.

A validation of the radiolabeled assay was carried out with known inhibitors. We have chosen to carry out the first tests with two known molecules: 2(S)-Amino-6-boronohexanoic acid **42** (ABH) and S- (2-boronoethyl)-L-cysteine **43** (BEC). These two compounds are commercially available (Enzo Life Sciences and Sigma-Aldrich, respectively).

A dose-response experiment was thus carried out, and half inhibitory concentration (IC_{50}) of 1.4 [1.1-1.7] µM and 1.2 [0.6-2.3] µM were measured for ABH **42** and BEC **43**, respectively. (Figure 49)

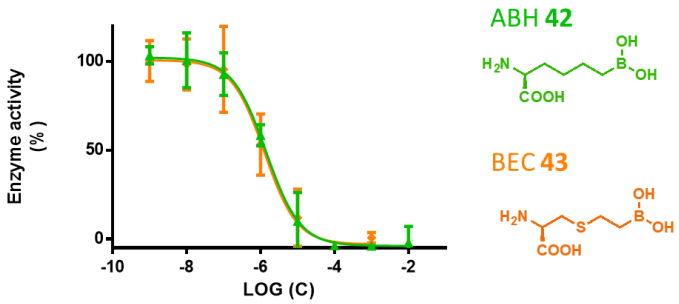

Figure 49: BEC and ABH structures and dose-response curves under the described test conditions.

For comparison, IC_{50} of 1.55 µM at pH 7.4,[104] and 0.8 µM at pH 9.0[96] are reported for ABH **42**. ABH **42** and BEC **43** exhibited similar inhibition constants K_i of 0.11 and 0.4-0.6 µM, respectively.[69] Hill Slopes were close to 1 with 0.95 and 0.98 for ABH and BEC, respectively. Thanks to this initial assay, we concluded that the test is consistent with what is found in the literature.

Based on the data presented here we were confident that we could use the radiolabeled assay to evaluate our compounds and we thus firstly undertook the validation of the 5-bromothiazole analogue previously identified using the ninhydrin assay.

The inhibition of Arg1 by the 5-bromoaminothiazole **89** was undertaken as described before but we rapidly noticed solubility issues with **89** at 100µM in the assay with the presence of a suspension in the solution. To avoid this problem, and to optimize the radiolabeled assay for more lipophilic drug that are usually more prone to aggregation, we assessed the influence of surfactant on Arg1activity. As it can be observed on Figure 50 the use of triton X-100 up to a concentration of 0.1% (v:v) does not affect Arg1 activity.

Compound **89** was thus reassessed at 100 µM in the presence of 0.01% v/v of Triton X-100 but again no inhibition was observed although the solution was clear and the compound fully soluble in these conditions. We therefore deduced from these data that the inhibition observed for **89** using the ninhydrin test were probably due to aggregation and should be considered as false-positive.

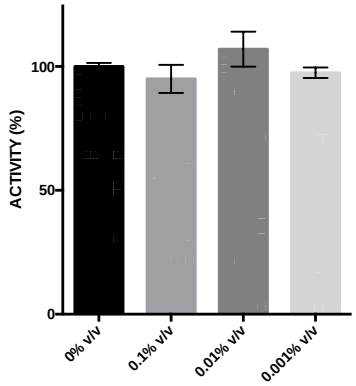

Figure 50: effect of different concentration of triton X-100 on the activity of Arg1. Triton X-100 does not affect the enzyme activity up to 0.1% v/v concentration.

3.4 PRELIMINARY CONCLUSION

In this first chapter we reported our works to produce and purify Arg1 as well as our experiments to setup a reliable inhibition assay. We selected the radioisotopic assay because it has a high sensitivity, an excellent reproducibility and

it uses low amount of Arg1. Once optimized, we confirmed the relevance of this assay with reference Arg1 inhibitors.

In a final step, our aim was to validate a series of 5-bromo-2-amino-thiazole but unfortunately the series revealed to be false-positive compounds probably due aggregation issue. Because this series of 5-bromothiazole remains of interest notably regarding the synthetic route to access these compounds, part of the time of this PhD thesis was devoted to the chemistry of 5-bromothiazoles. This work with the associated discussions and all the experimental information can be found in Annex to this thesis.

In the next chapter, a molecular modeling approach to help the discovery of new Arg1 inhibitors is presented. The compounds identified will be evaluated using the assay reported here.

4 MOLECULAR MODELING APPROACHES TO DETAIL ARG1 INHIBITION. TOWARDS STRUCTURE-BASED DRUG DESIGN

With the objective to i) give a better understanding of Arginase inhibition and ii) potentially find new hit compounds by virtual screening, we investigated a molecular modelling analysis in collaboration with the team of Pr. Gerhard Wolber from the Free University of Berlin, Germany.

4.1 INTRODUCTION

Several crystal structures of Arg1 with or without ligands are available in the Protein Data Bank (PDB) making an analysis, at the molecular level, of the structural requirements to reach a high Arg1 inhibition possible. This study might also feed a structure-based drug design approach to discover new original hits.

In this chapter, an original computer-assisted structural approach to study Arg1 and its inhibition will be detailed. First, structural analysis was conducted, notably by molecular dynamic simulations to understand the structural determinants required to inhibit Arg1. Then, original dynamic pharmacophores were investigated to possibly screen for new Arg1 hit compounds.

4.2 STRUCTURAL ANALYSIS OF PDB DATA

4.2.1 X-ray structures in PDB

A structural analysis of all the available ligand-enzyme interaction in the catalytic pocket of Arg1 was conducted using the structural data available in the Protein Data Bank (PDB). All the structures of human Arg1 with Mn^{2+} cations with or without ligand are summarized in the Table 7.

Table 7: crystallographic data from PDB. PDB codes of human Arg1 with their associated ligands, if present, are described.

Code PDB (Resolution)	Ligand
2PHA (1.90Å) 2ZAV (1.70Å)	None
3GMZ (1.43Å) (L-ornithine)	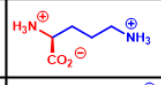 2
3LP4 (1.90Å) (L-lysine)	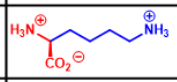 91
2AEB (1.29Å) 6Q92 (1.50Å) 6Q9P (1.66Å) (ABH)	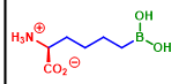 42
3F80 (1.60Å)	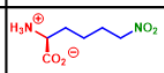 39
3DJ8 (1.51Å)	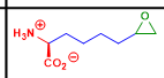 41
4FCI (1.82Å) (AGPA)	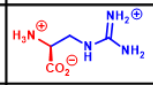 92
3MJL (1.90Å)	 93
3MFV (1.90Å)	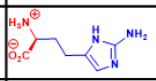 94
3MFW (1.47Å)	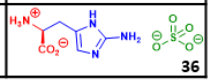 36

Code PDB (Resolution)	Ligand
2PHO (1.95Å)	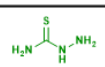 95
3GN0 (1.70Å) (DMFO)	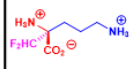 47
3LP7 (2.04Å) (NOHA)	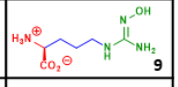 9
3KV2 (1.55Å) 1HQH (2.80Å) (nor-NOHA)	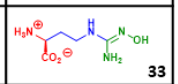 33
4HWW (1.30Å)	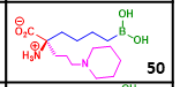 50
4HXQ (1.45Å)	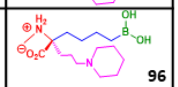 96
AIE1 (2.00Å)	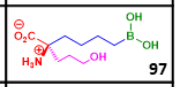 97
3SJT (1.60Å) (MABH)	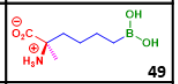 49
3SKK (1.70Å) (FABH)	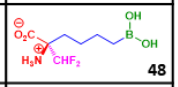 48
6QAF (1.61Å) (CB-1158)	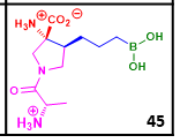 45

Code PDB (Resolution)	Ligand
6V7C (1.80Å)	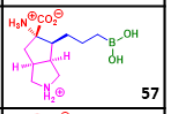 57
6V7D (1.82Å)	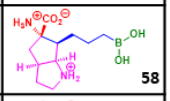 58
6V7E (1.99Å)	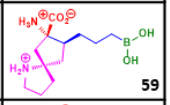 59
6V7F (2.02Å)	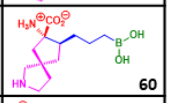 60
7K4G (1.80Å)	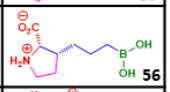 56
7K4H (1.65Å)	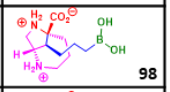 98
7K4I (1.98Å)	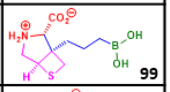 99
7K4J (1.94Å)	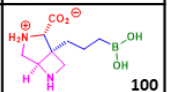 100
7K4K (2.27Å)	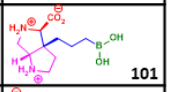 101
7KLK (1.80Å)	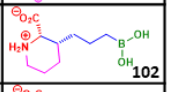 102
7KLL (2.22Å)	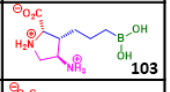 103
7KLM (2.27Å)	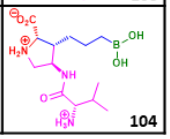 104

From Table 7, we can see that most of the ligands crystalized in Arg1 share the same pharmacophoric elements, except for 2 fragments: 2-aminoimidazole **93** in 3MJL[88] and thiosemicarbazide **95** in 2PHO[149]. 2-aminoimidazole **93** was the starting point for a further development leading to more complex inhibitors, where the fragment is couple to an amino acid moiety linked by an aliphatic chain. From this study, two other molecules were crystallized in the Arg1 pocket: L-2-aminohistidine **36** (3MFW) and L-2-aminohomohistidine **94** (3MFV). The optimized molecules from this study, A1P **37** (the structure of A1P can be found in chapter 1.2) was not co-crystallized with Arg1.[88]

Half of the ligands in Table 7 are boronic acid-based inhibitors that have only been very recently published. The clinical candidate on Arg1, X-Ray of CB-1158 **45** has only been reported in PDB in 2020,[99] as for other bicyclic structures in 2021 (**56-60** and **98-104**) on the right of Table 7. [112]

Because all the ligands are highly similar, we did not expect to see many differences in the binding of these compounds that should be very consistent from one structure to another.

4.2.2 Information from the X-ray structures

Two distinct domains of the catalytic cavity can be distinguished:

(a) the binding region of the L-amino-acid moiety that is also shared by the L-Arginine **1** substrate and the L-Ornithine **2** product by ionic interactions between the ammonium function of the amino acid and the carboxylates of Asp183 and Glu186, and H-bonds between the carboxylate function of the amino acid ligand and the Asn130 and Ser137.

(b) a cluster of interactions between the manganese ions Mn^{2+} deeply inserted in the active site cavity and the side-chains of the residues His101, Asp124, His126, Asp128, Asp232 and Asp234 (Figure 51).

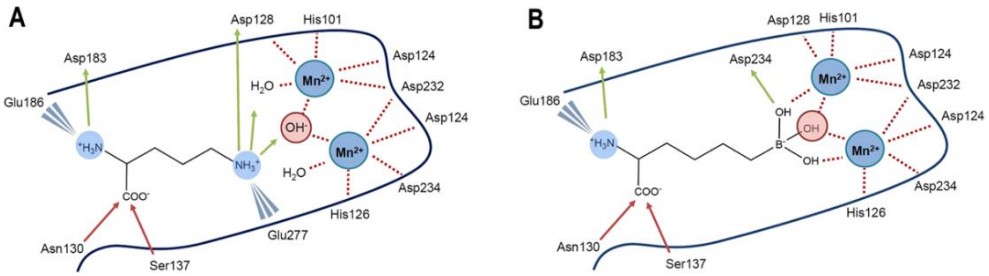

*Figure 51: Comparison of the main ligand-arginase interactions for enzymatic product L-ornithine **2** (left) and transition state analog ABH **42** (right). Interactions color code: red/green arrows for H-bonds, and blue thorns for electrostatic interactions.*

In fact, inhibitors known to bind arginase are structurally only different only at the level of the group complexing the ion cluster. The first group comprises product analogues,[102, 149] are stabilized by the hydroxide effectively bridging the ligand and the manganese ions. The hydroxide ion stays between the manganese and interacts with the ligand. The second group comprises transition state analogues like hydroxyarginines,[77, 83, 150] boronic acids,[151] or sulfonamides,[87] which displace or react with the hydroxide group to directly coordinate the two manganese ions.

Concerning CB-1158 **45** and the other bicyclic inhibitors (Table 7: **56-60** and **98-104**), the cyclisation not only constrains the molecular conformation of the inhibitor in the cleft but also makes additional interactions stabilizing the inhibitors

This analysis of the available PDB structures between Arg1 and different inhibitors also revealed a poor investigation of the influence of the central linker (in blue in Table 7) for Arg1 inhibition as most of the Arg1 inhibitors have, as linker between the two clusters of interactions, a linear aliphatic chain.

To better detail Arg1 inhibition, we undertook molecular dynamic studies to better understand Arginase dynamic and plasticity. Molecular dynamics (MD)

studies have become popular in contemporary molecular modeling to investigate the dynamic structure of macromolecules,[152] or their interactions with different binding partners.[153, 154] Due to the major impact of protein flexibility on ligand binding, a study of the conformational variability of arginase was thus performed.

4.3 MOLECULAR DYNAMICS

With all-atoms systems solvated in explicit water (TIP3P),[155] molecular simulations with three different systems from the Protein Data Bank (PDB) were conducted: (i) the apo structure of Arg1 (2PHO), (ii) the ornithine **2**-Arg1 complex (3GMZ) and (iii) the ABH **42**-Arg1 complex (2AEB). TIP3P is a rigid water model, suitable for use with any Lennard-Jones forcefield, but is especially for the OPLS family of potentials, that has a Lennard-Jones site on the oxygen and bare charge sites on the hydrogens. Each system was simulated using Desmond,[156] with OPLS (Optimized Potentials for Liquid Simulations) force field,[157] during 1 μs (5 x 200 ns) with a pressure of 1.01325 bars and a temperature of 300 K using a isothermal-isobaric ensemble or NPT ensemble (constant pressure, temperature and number of particles).

The root mean square fluctuation to the starting conformation was monitored for all alpha carbons of the three simulated systems.

4.3.1 Initial conformation

Analysis of the average deviation of alpha carbon Cα's from the initial conformation (RMSD, Figure 52) indicates that the highest measured movements were observed for the apo enzyme with a value reaching a plateau around 3 Å for all simulations.

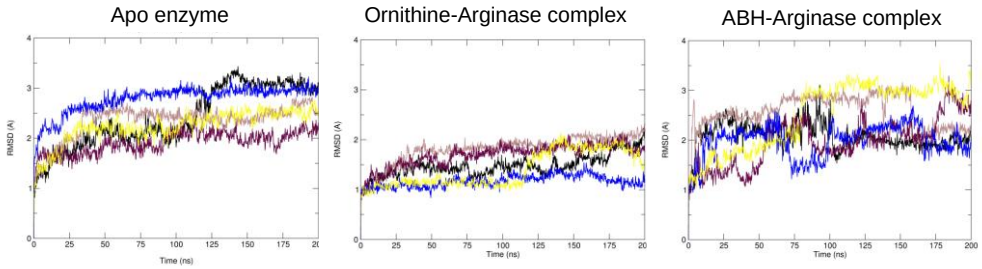

Figure 52: Root-mean square deviation (RMSD, 5 x 200 ns overlaid for each system). Colors correspond to each experiment.

Analysis of the fluctuations (RMSF) can explain how some fluctuations of a particular loop can impact the overall deviations calculated for the complete protein structure. For example, the increase RMSD of the empty enzyme after 100 ns (Figure 52, Apo enzyme, black line) correlates with an unfolding of the C-terminal chain of the protein, as illustrated with the high peak in the RMSF plot for this same simulation. Also, it is interesting to notice that an overall higher deviation from the starting conformation is observed for the ABH **42**-Arginase complex compared to the L-ornithine **2**-Arginase complex.

4.3.2 Pocket volume

Deviations observed with ligand-arginase complexes fluctuate between 1 Å and 3 Å. Interestingly, in case of the ABH **42**-arginase complex, the observed movements of the loops around the binding site indicate in some simulations a closure of the cavity around the inhibitor. Contrarily, trajectories of the L-ornithine **2**-arginase complex show a relaxation of the active site within the first nanoseconds of simulation time. Analysis of the size of the pocket volume using Povme2.0[158] illustrates the phenomenon of cavity opening (Figure 53).

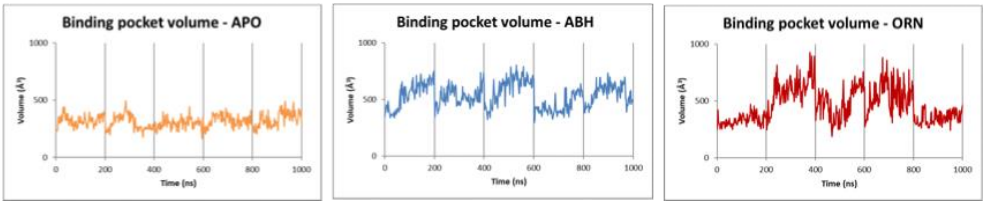

*Figure 53: Pocket volume calculation for apoenzyme (in yellow), and Arg1 with ABH **42** (in blue) and L-ornithine **2** (in red), where 200 ns repeats are separated by a vertical line*

Analysis of the pocket volume confirms these tendencies simulations with the highest volumes (> 750 Å^3) measured for three out of five 200 ns trajectories, while the volume of the same pocket remains below 500 Å^3 with the apo form of arginase. This phenomenon of cavity opening is observed with ABH **42** (middle, in blue Figure 53) and L-ornithine **2** (right, in red Figure 53), while the same volume remains constant in the case of the apo enzyme (left, in yellow Figure 53). These results show that the presence of a ligand in the active site can induce a different effect on its surrounding protein structure.

4.3.3 Identification of the most dynamic regions

After examination of the average fluctuations of all Cα (RMSF), the most dynamic regions of the protein structure were identified (graph on the left, Figure 54).

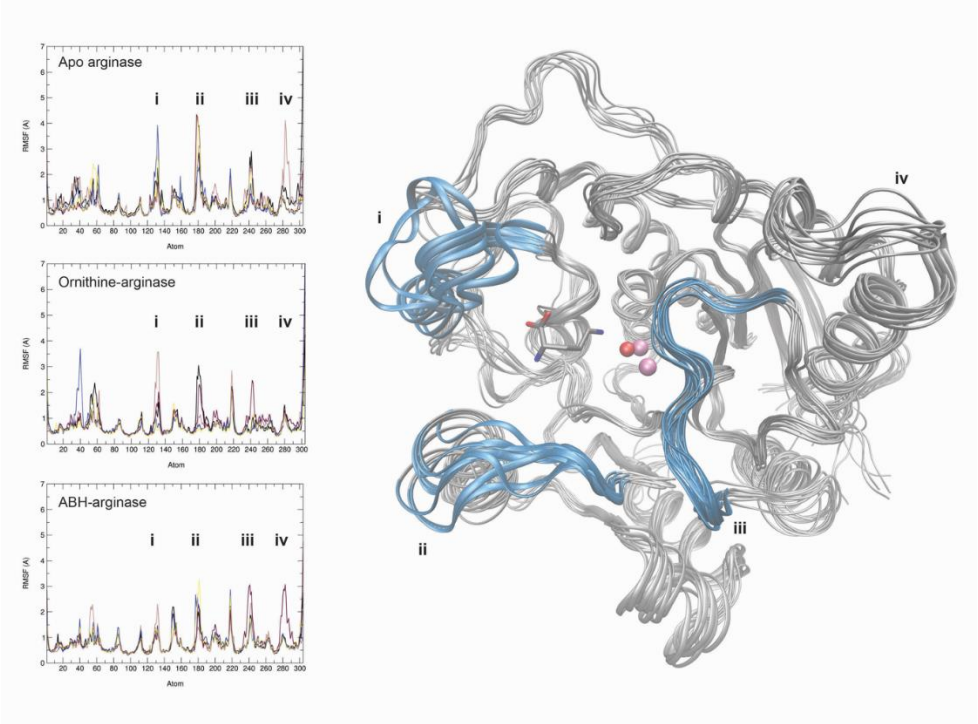

*Figure 54: Root mean square fluctuations (RMSF) overlay for the five 200 ns repeats conducted with the same three different systems (left) and superposition of 10 protein conformations extracted from 200 ns simulation of the L-ornithine **2**-Arginase 1 complex (right). The three flexible loops responsible for the opening of the binding pocket are highlighted in blue in the 3D view. Loops surrounding the active site cavity are labelled with roman numbers (i–iv). Carbons are represented in grey, Mn^{2+} atoms in light purple, and the hydroxide group, in red.*

As expected, all systems displayed a high flexibility in regions at the surface of the protein and solvent exposed (loops including residues 212–225, 153–162 and 60–62), but also in the region of the binding site (loops 130–136, 175–183, and 240–246).

The three loops at the entrance of the cavity (in blue in the representation on the right of Figure 54) are (i) the region binding to the carboxylic acid of arginine **1** (residues 130–136), (ii) the region binding to the neighboring primary amine (residues 175–183), and (iii) the loop forming the lid of the cavity above the ion cluster (residues 240–246).

Analysis of the fluctuations observed in the regions of the three loops involved in ligand-arginase interactions clearly indicate a similar level of flexibility (RMSF of 3 Å or below for loops around residues 130, 180 and 240). In comparison, these three loops are more dynamic in simulations with the Apo form of Arginase (RMSF reaching 4 Å). This result indicates that the differences in the RMSD between the ABH **42**-Arginase and the L-ornithine **2**-Arginase complexes are resulting from movements involving loops at the surface of the protein (such as loops at positions 85, 150 and 280), while both systems show a very similar dynamic of the enzymatic pocket.

The orientation of these three key loops determinate whether the pocket entrance will be open or closed, as illustrated in Figure 54 with the arginase-ornithine complex. Comparison of Cα fluctuations confirm larger movements with empty arginase as with arginase-ligand complexes. This observation is particularly true for loops directly interacting with the ligands, indicating a stabilization of the enzyme structure when bound to a small molecule. Contrarily, very little mobility is observed in the regions surrounding the ions cluster, *i.e*., residues 101, 124–128, and 232–234.

4.4 DYNAMIC PHARMACOPHORES

To investigate and report in detail interactions involved in the stabilization of the studied ligands, a pharmacophore-based analysis method was developed. Since even local protein flexibility plays a major role in ligand recognition, we aimed at the development of an approach that can reflect conformational variability of the enzyme near the active site in a simple manner. Just like a fixed-in-time ligand-protein complex can be represented by a 3D-pharmacophore model,[154] identical recognition patterns in a dynamic environment can be collected as weighted interaction fields in a 3D-dynamic pharmacophore, or *dynophore*. The novelty of this approach is to integrate, in one single 3D-pharmacophore, all interactions detected throughout a complete MD simulation, including information on occurrence

time and frequency. For each frame of the resulting trajectories with the two arginase-ligand complexes, a point-based pharmacophore was generated and collected on a three-dimensional weighted interaction field. For each interaction, the frequency of its occurrence in the trajectory is illustrated in *bar codes*, while distance distributions are represented in histograms (*experimental part, 8.3*).

Dynophore fields were built from all interactions detected in the MD simulation of Arg1 in complex with L-ornithine **2** (Figure 55) and with ABH **42** (Figure 56). To confirm that the observed results are not biased by the computational method, the ornithine-arginase system was simulated using the Gromacs MD suite[153] and Amber 99sb[159] force field. The generated dynophore and the detected interactions were very similar to those described below.

4.4.1 Ornithine-Arg1 complex dynophore.

This dynamic 3D-model for ornithine **2**-arg1 complex clearly shows local flexibility in the arginase binding site and how the interaction pattern with a weak binder like L-ornithine **2** fluctuates.

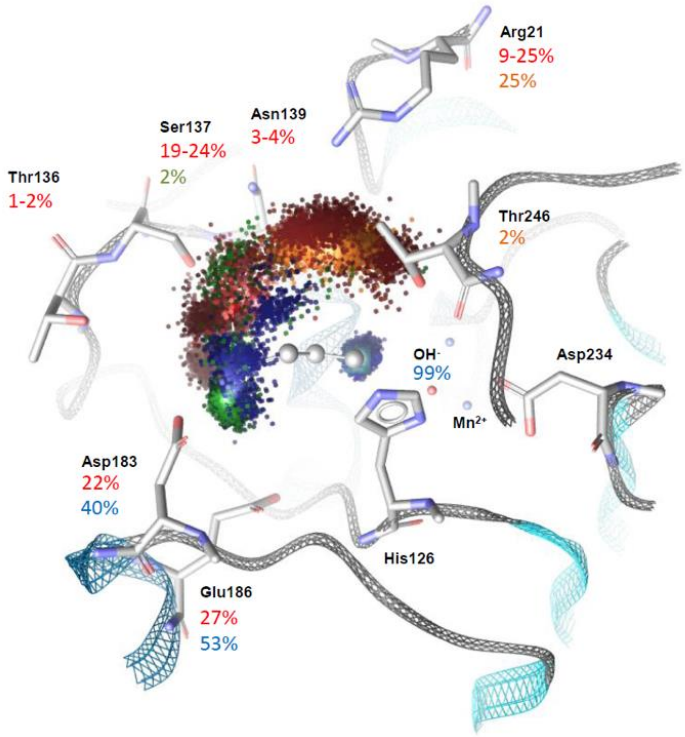

*Figure 55. Dynophore constructed with frames from 1 µs MD simulation with enzymatic product L-ornithine **2**. Percent are observation occurrence in simulation frames. Color code: red for H-bond acceptor, orange for negative ionizable feature, green for H-bond donor, blue for positive ionizable moiety and yellow for hydrophobic contact. The manganese ions are represented by lavender spheres and the hydroxide group is in red. Carbons of the ligand are represented by grey balls.*

On one side of the cavity, H-bonds (in green in Figure 55), and coulomb interactions (in blue in Figure 55) are detected during the entire simulation time between the hydroxide and the primary amine on the side-chain of L-ornithine **2**. On the other side, detected interactions involving the carbonate and amino groups of the amino acid moiety show a larger range of interaction partners, represented by a spread cloud of blue (positive charges) and red dots (negative charges). Interactions involving the amino group are H-bonds (45.2% of simulation time) and electrostatic interactions (57.9% of simulation time). H-bond donor NH_3^+ interacts mostly with Asp183 and Glu186, when oriented as observed in its crystallized conformation.[102] The carboxylate group of ornithine interacts through electrostatic interactions (24.7%) as well as H-bonds (64.4% and 62.9% for each oxygen, respectively).

Residues from loop 130–139 (mostly Ser137 and Asn130) are involved in the stabilization of the initial ligand conformation through H-bonds with the carboxylate. When the active site opens, residues further away like Thr246 and mostly Arg21 become the main interaction partners. To reach this region while maintaining an interaction with the ions cluster, the ligand must operate a clockwise rotation around the hydroxide. We surmise that this movement, coupled with the opening of the cavity, is the initiating drive to expel the reaction product out of the arginase active site.

4.4.2 ABH-arg1 complex dynophore

In the dynophore resulting from 1 μs simulation of the ABH **42**-arginase complex two main interacting groups are also clearly distinguished: The amino acid moiety and the boronate (Figure 56).

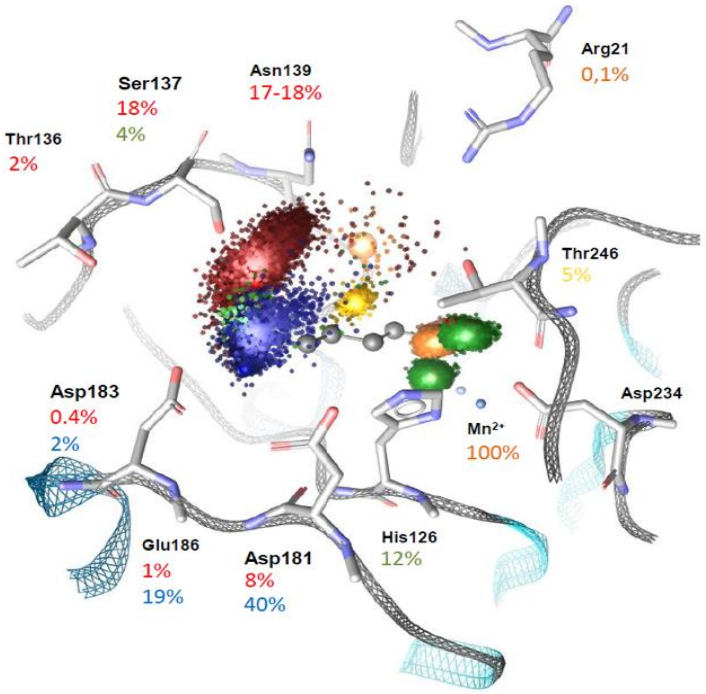

*Figure 56. Dynophores constructed with frames from 1 µs MD simulation with inhibitor ABH **42**. Percent are observation occurrence in simulation frames. Color code: red for H-bond acceptor, orange for negative ionizable feature, green for H-bond donor, blue for positive ionizable moiety and yellow for hydrophobic contact. The manganese ions are represented by lavender spheres and the hydroxide group is in red. Carbons of the ligand are represented by grey balls.*

Firstly, interactions involving the amino acid group are spread over a large volume, confirming the flexibility of the enzyme in this region. Loops *i* (residues 130–139) and *ii* (residues 175–186) binding to the carboxylate and the amine, respectively, can operate a movement towards the solvent resulting in an opening of the cavity, as shown previously with ornithine **2** (Figure 54). The dynophore shows that the bound inhibitor ABH **42** can follow this movement. The cloud of interactions detected in this region indicates the presence of H-bonds (in red and green in Figure 56) between the carboxylate of ABH **42** and residues 130–139 during 36.8% to 36.9% of the simulation time. H-bonds were mostly involving Ser137, but also Asn130, Thr135, Thr136 and Asn139. Interestingly, Thr246 and Arg21 are almost never reached by the carboxylate (< 1%). Instead, the carboxylate of ABH **42** is hold

in the region of loop 130–139, allowing the ligand to conserve an ideal orientation for complexation of the ion cluster by the boronate. This major difference between the dynamic binding of ABH **42** and ornithine **2** is illustrated by an interaction cloud more concentrated around this loop for ABH **42**.

Secondly, the amino moiety interacts as a positive ionizable feature (in blue in Figure 56). Charge interactions were detected for 26.5% of simulation time with residues Glu186, Asp183 and Asp181. H-bonds stabilizing the amino group were detected less frequently (7.6% of the analyzed frames, mostly with Ser137).

Finally, the boronate is depicted in the dynophore as 3 H-bonds donors (in green in Figure 56) at the level of the 3 hydroxyl groups as well as one H-bond acceptor and one negative ionizable feature (in orange in Figure 56) on the boron atom. These features illustrate the tight cloud of interactions detected between the boronate and the neighboring partners (arginase residues and manganese ions), indicating very little flexibility in this region, which agrees with a strong anchoring of the ligand at the bottom of the cavity.

Interestingly, hydrophobic contacts (in yellow in Figure 56) with the side-chain of Thr246 were detected at the level of the aliphatic chain of ABH **42** that links the amino acid to the boronic acid. Even if observed sporadically (5.2% of simulation time), the detection of this interaction indicates the possibility of creating hydrophobic contacts between the ligand and the enzyme in this region, despite a rather hydrophilic cavity.

We then decided to use the data we collected by the structural analysis and the dynamics by assessing a library a molecule by a virtual screening. A 3D-pharmacophore model describing key interactions identified for the binding of a transition state analogue was constructed and the model was used to screen databases of commercial compounds

4.5 VIRTUAL SCREENING BASED ON COLLECTED DATA OF THE STRUCTURE-BASED DRUG DESIGN

4.5.1 Pharmacophore model creation

With a view to identify essential features required for an optimal ligand-enzyme interaction in the catalytic pocket of Arg1, all co-crystallized inhibitors available from the Protein Data Bank (PDB) were collected and 3D-pharmacophore models were created for each of them. Shared features from all models describing ligand-enzyme interactions where the hydroxide ion is displaced were selected and compiled in one pharmacophore model.

Using the dynophore approach has many advantages over rigid or even flexible docking. Rigid docking does not take into account the movement of the enzyme or the flexibility of its residues. Flexible docking was then developed to overcome this limit. Although flexible docking is slower and required a higher computational power, it is generally more accurate when the target shows important degrees of freedom. Nevertheless, it can also lead to inconsistent results with the unfolding of the protein, creating cavities that do not exist. Solutions do exist, however. For example, semi-rigid approach could be used to avoid such issue when the binding site is known. Only the studied part of the protein is therefore considered with a rigid docking with a soft interface.[160] For more complex systems, such as those with opening-closing phenomenon, dynamic is generally recommended or required to consider such movement.[161] The creation of a pharmacophore that consider multiple conformations would assess more precisely the volume of the cavity as well as the interactions in it.

The ability to discriminate between inhibitors and non-inhibitors was assessed and improved using a dataset of 27 active compounds and 24 inactive compounds assembled from the literature, the Chembl database and *in house* activity data. Multi-conformational screening of these compounds was carried out. After a

stepwise iterative development, the final 3D-pharmacophore model was able to discriminate all inactive compounds and retain 23 of the active ones.

4.5.2 Virtual screening using the 3D-pharmacophore model

A virtual screening (VS) of commercial libraries comprising over 10^6 drug-like compounds (from providers such as Asinex, Vitas M, Life Chemicals, Chembridge, Maybridge, Specs, Enamine and Prestwick) was conducted and the model picked 63 hits, among which the amino acids glutamate and asparagine. In the Prestwick database, levodopa and methyldopa were identified. Levodopa is dopamine receptors agonist used in the clinical treatment of Parkinson's disease. Glutamic acid, asparagine, levodopa and methyldopa were not included in the final selection because of their expected low specificity. All retrieved hits were re-docked using the docking software GOLD and ranked based on the quality of their 3D-superposition with the pharmacophore model, using LigandScout. The best 19 compounds (**105-123**, Figure 57) were purchased and arginase residual activity was tested experimentally in presence of inhibitor using the radiometric assay measuring arginine consumption.

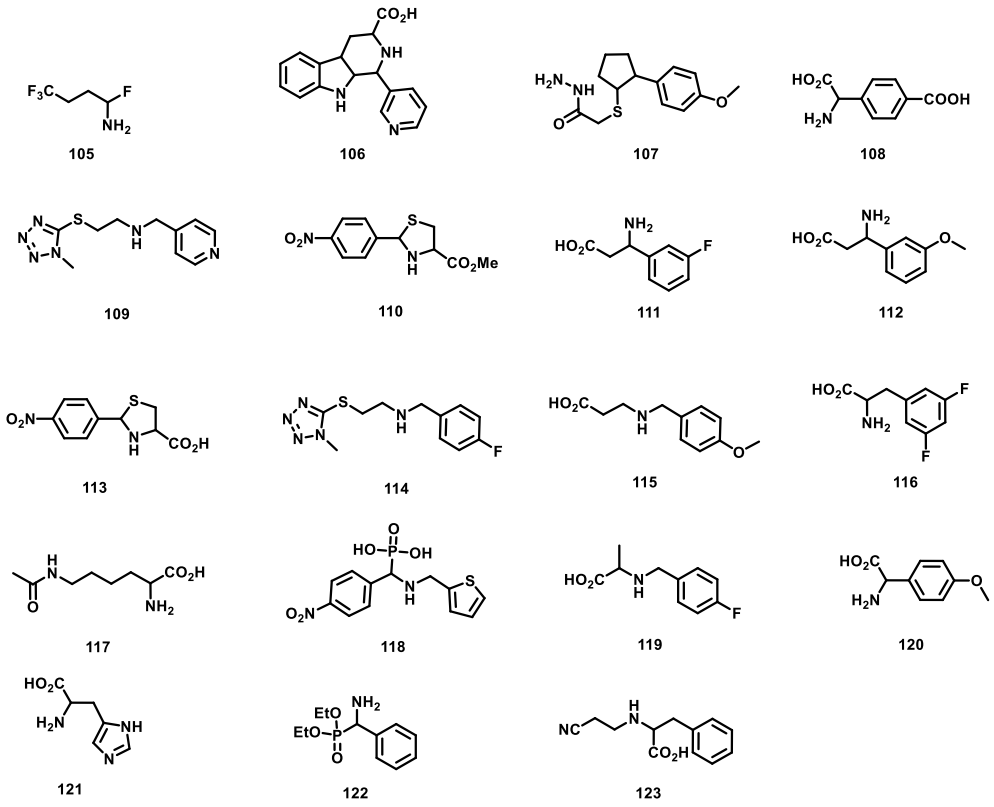

Figure 57: molecules selected and tested after virtual screening on Arg1

The number of identified molecules was very low (below 0.06%) but highlighted the difficulty of targeting this cavity which very small and hydroxylic. Moreover, due to the nature of the available ligands of Arg1 that were described in the literature, a bias could appear. Most of these compounds are amino acids. And unsurprisingly, these virtual screening results in the selection of molecules that are very similar, i.e., amino acids or mimetics. However, sometimes else also stands out. Most of these molecules possess an aromatic ring (17 on 19 identified hits): phenyl or 5-membered heterocycle thiophene and imidazole.

All these identified virtual hits were assessed for the Arg1 inhibition using the radioisotopic test described in the previous chapter, at a single concentration of 1 mM, in triplicate. As a result, no compound inhibited more than 20% of arginase

activity compared to full inhibition observed with the reference Arg1 inhibitor BEC **43** (Figure 58).

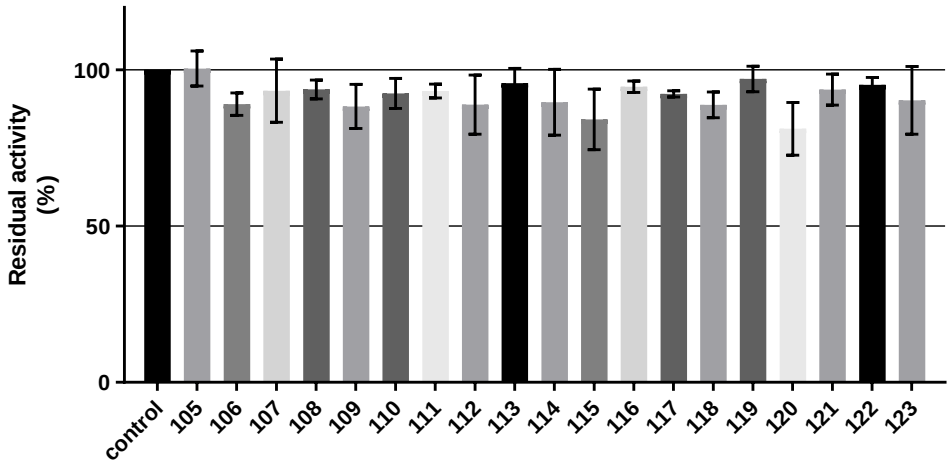

*Figure 58: Residual activity of human Arg1 in presence of the selected compounds (**105-123**) at a concentration of 1mM*

Although these results were disappointing, as all selected compounds (**105-123**) had excellent 3D-alignment with features extracted from validated inhibitors and thus share similar structural attribute to be Arginase inhibitors, we set out to analyze these data in more details to better understand the mechanisms of arginase inhibition.

The most trivial explanation for the lack of affinity of most molecules for Arg1 is that a strong binder is required to displace the hydroxide and replace it in the manganese coordination network. Nevertheless, the arginase pocket size is another critical point. Crystal structures of arginase cavity indicate a small volume, allowing little structural diversity between the metal coordinating and the amino acid moiety of the ligand. In the design reported by Ilies *et al*.,[83] one fragment (2-aminoimidazole **93**) binding to the ion cluster becomes 1000-fold more potent when bound to a L-amino acid side-chain (A1P **37**), but completely loses this activity if one extra carbon is inserted between the two key interacting groups. These structural particularities confirm that designing potent arginase inhibitors requires high precision.

4.6 PRELIMINARY CONCLUSION

In conclusion, this molecular modeling approach combining molecular dynamic analysis and pharmacophore modeling highlights the flexibility of Arg1 through a closing and opening phenomenon. The movement of three loops at the edge of the pocket, where the amino acid moiety of the ligand binds, affects the size of the pocket as well as the interaction, depending on the ligand. In practice, discovery and design of new compounds can be orientated towards bulkier molecules.

In contrast, regions coordinating the ion cluster remained more static. Moreover, reaction with the hydroxide bound the manganese cores rather than its displacement appears to be preferable for maximizing the inhibition.

The structural information reported in this study sustain the importance to consider protein flexibility for structure-based drug design approach. These observations could not have emerged from static arginase-ligand complexes and lead to the hypothesis that bulkier compound can be accommodated by the enzyme.

Unfortunately, the use of the novel dynamic pharmacophore for Arg1 inhibition did not result in the discovery of new hit fragments but this might also be due to the rather limited set of inhibitors investigated in the study.

This part of the work was in part published in: Mortier, J.; Prevost, J. R. C.; Sydow, D.; Teuchert, S.; Omieczynski, C.; Bermudez, M.; Frédérick, R.*; Wolber, G.*, Arginase Structure and Inhibition: Catalytic Site Plasticity Reveals New Modulation Possibilities. Sci Rep **2017**, 7 (1), 13616.

All the dynamics were performed by Jérémie Mortier. Results were discussed with CMFA team members (Julien R. C. Prevost and Raphaël Frédérick) and compared with results obtained during *in silico* and with docking performed on CMFA laboratory. Both laboratory results converged to the same conclusions. All the enzymatic assessment and their interpretation were performed only at the CMFA laboratory.

5 FRAGMENT-BASED DRUG DESIGN: SCREENING FOR HITS DISCOVERY

5.1 INTRODUCTION

The *in silico* study of Arginase1 clearly gives new insights on the arginase structure and dynamic. The binding site shows a rigid architecture at the level of the ions cluster, and more flexibility in the region interacting with the amino acid moiety.

We set out to verify if the enzyme could possibly accommodate bulkier ligands via the opening-closing phenomenon. 4-boronophenylalanine[162] is currently the only compound that does not have the standard 3- to 4- carbon aliphatic chain as a linker but does still inhibit human Arg1, although moderately (IC_{50} 6.0 ± 1.0 mM). As expected, the position of the boronic acid function on the cycle is important as the 3-boronophenylalanine regioisomer is inactive (30% inhibition at 10 mM). However, to our knowledge, no other cyclic linker was reported.

With the aim to potentially discover novel Arg1 inhibitors, Fragment-Based Drug Design (FBDD) strategy was preconized. According to this strategy, small molecules namely fragments, are used to probe a catalytic site. A fragment usually has a molecular weight below 300 $g.mol^{-1}$, a cLogP < 3 and a number of H-bond donors and acceptors < 3, hence complying to the so-called rule of 3 (RO3) typical for fragments. Because of their small sizes, fragments are more prone to fit particular pocket within an active site of a protein target, in our case arginase. Once a fragment is identified, it can undergo optimization either by growing (*growing* strategy) i.e., increasing the affinity to the target protein by increasing the size of the molecule to possible bind adjacent pockets and form additional intermolecular interactions, or it can possibly be linked (*linking* strategy) to another fragment that would have been identified in an adjacent pocket.

In our case, to consider the "biology" of our protein target, that is a metalloenzyme, we focused our library for coordinating fragments to specifically probe the pocket around the metal cluster. If a novel coordinating fragment is identified, it could then be adequately linked to an amino acid fragment by mean of an appropriate linker using the *linking* strategy.

5.2 BUILD AND SCREENING OF FRAGMENT LIBRARIES

5.2.1 In silico build of the coordinating fragment library

Our library of coordinating fragments was inspired by the one reported by Jacobsen *et al*, to target Arg1 catalytic site.[163] Our goal with this library was to search new functions, other than the boronic acid that is widely described, that can interact with the manganese cores of Arg1.

Here, the same library of 96 compounds (**124**-**219**) was used. (Figure 59)

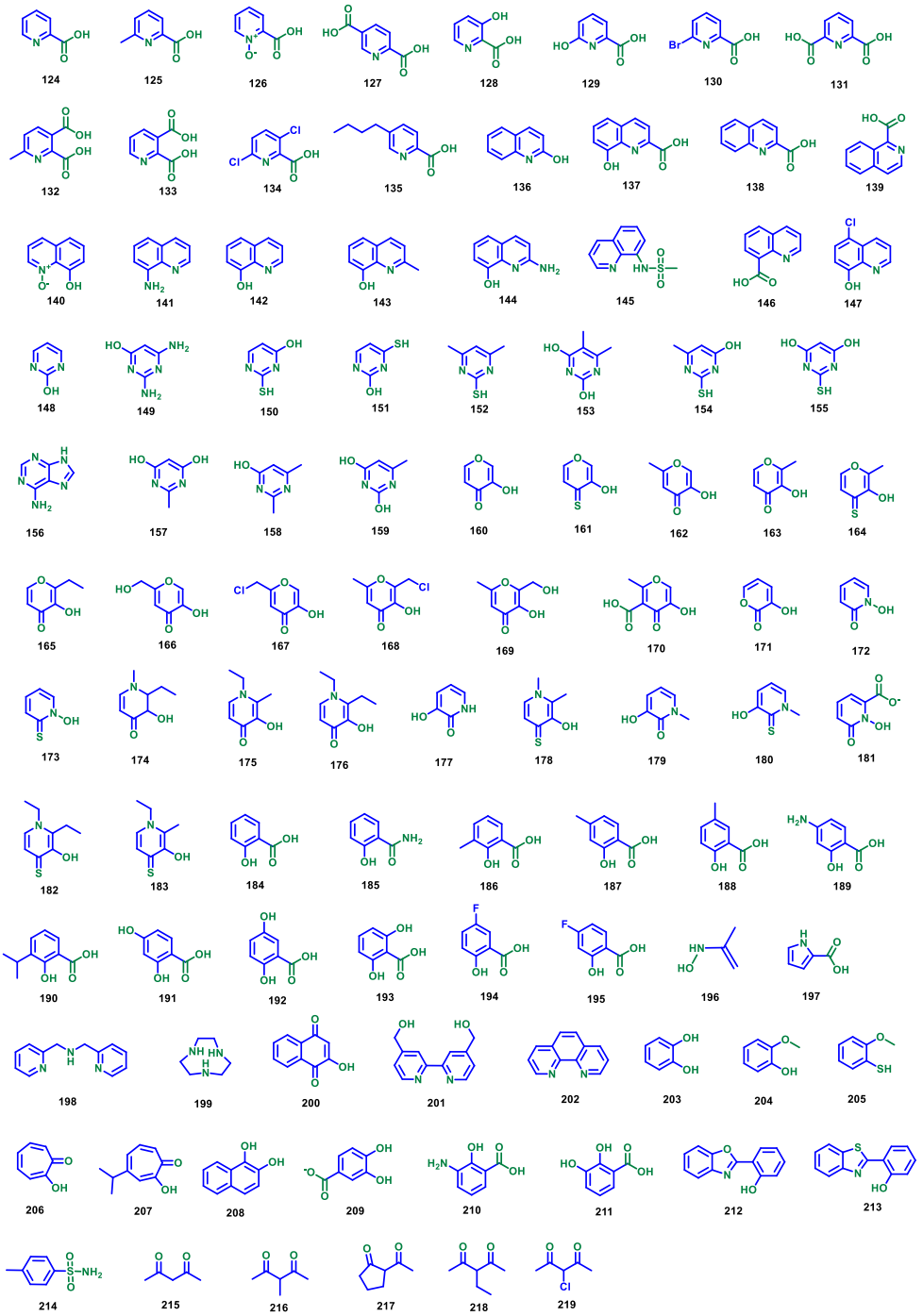

*Figure 59: list of the molecules (**124-219**) of the coordinating fragment library*

This library contains fragments with six different metal-binding classes including picolinic acids, quinolines, pyrimidines, hydroxypyrones, hydroxypyridinones, salicylic acids, and 24 other miscellaneous compounds. The fragments all have known metal-binding modes using two to four nitrogen, oxygen, and sulfur heteroatoms Moreover, all of the fragments are reported to be soluble up to 50 mM in DMSO and are easily obtained (commercially available or readily synthesized). In the study of Jacobsen, this library was used on different targets, including matrix metalloproteases (MMP), anthrax lethal factor, 5-lipoxygenase (5LO), tyrosinase, and *i*NOS, the competitive enzyme for L-arginine.

This library was also selected by its lack of multidentate ligands (bidentate, tridentate…). Thanks to our first *in silico* analysis, the pipe-like shape of the cavity disfavors such molecules. Indeed, it will force the ligands to move to the side, which creates an important steric hindrance. The choice of the chelating motifs was therefore oriented towards a library with a majority of so-called longitudinal ligands, of which only one function will be able to introduce itself to the manganese site and bind instead of the hydroxide, while limiting the probability of steric clash.

All the molecules were drawn on ChemDraw (PerkinElmer) with a protonation state at pH 7.4. Each molecule was transferred ChemBio3D (PerkinElmer) to generate 3D coordinates and the molecular conformation were minimized the MM2 forcefield. Each molecule was finally saved in separate mol2 files.

5.2.2 Docking of the coordinating fragment library

Each fragment of the library was docked with the GOLD (CCDC) software using the 2AEB crystal structure (resolution = 1.29Å), where the ligand was preliminary removed. All systems were preliminarily prepared with Gold® to add hydrogens and removed selected water molecules. A cavity of 10 Å was generated around the manganese noted MN2362.

As a docking validation experiment, ABH **42** (Figure 60) and BEC **43** were redocked and superimposed on their respective experimental binding position RMSDs below 1.0 Å were obtained, with 0.38 Å for ABH **42** and 0.93 Å for BEC **43**, respectively.

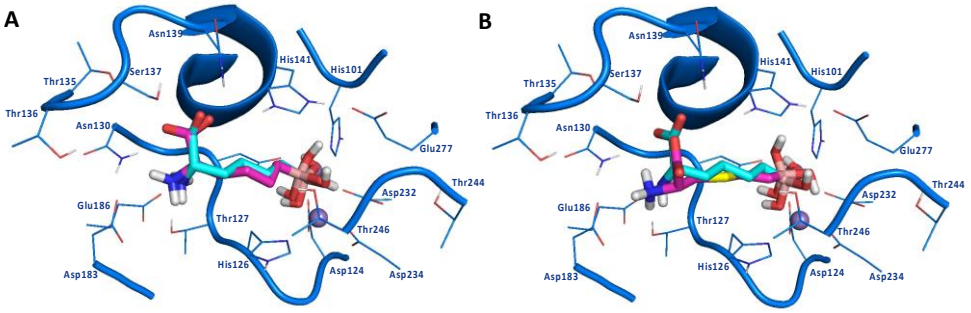

*Figure 60: A) Superposition of the generated solution for ABH **42** (pink) and co-crystalized ABH **42** (cyan) in 2AEB. B) Superposition of the generated solution for BEC **43** (pink) and co-crystalized ABH **42** (cyan) in 2AEB. Mn^{2+} are represented as purple spheres.*

Most of the variation was observed in the amino acid part, where the pocket is very hydrophilic and ionizable interactions are numerous, as described in chapter 4. In contrast, boronic acid function was very well aligned between the docked and the experimental binding positions.

Docking was then performed by generating 20 solutions for each molecule. The different docking poses were ranked according to different scoring functions (GOLDSCORE and CHEMPLP) to better appreciate the interactions, especially between the coordinating function and the metal cores of the enzyme. Of note, CHEMPLP takes the coordinating interactions with the metals into account, whereas GOLDSCORE selects the best results mainly based on polar interactions. To better compare the docking poses, the score values were normalized by doing the ratio between the score itself and the number of heavy atoms (or non-hydrogen atoms). This standardization also facilitates comparison between each fragment, regardless of the molecular weight and give access to some sort of a theoretical ligand efficiency (LE).

Among all the 96 docked molecules, the small aromatics rings score the highest. The 5- and 6-membered rings were found to be the best in terms of size. Docking results of the best fragments are summarized in Table 8.

Table 8: Outcome of the docking of the coordinating fragment library

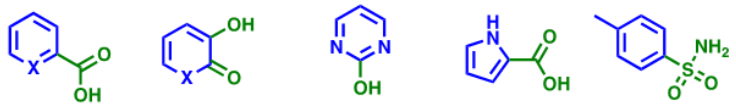

Normalized goldscore	**124** X=**N** : 7.56	**177** X=**NH** : 5.75	**148** 5.88	**197** 8.56	**214** 6.00
	126 X=**N⁺-O⁻** : 5.70	**171** X=**O** : 5.76			
	184 X=**C-OH** : 6.65				
Normalized chemplp	**124** X=**N** : 5.93	**177** X=**NH** : 5.93	**148** 6.12	**197** 5.89	**214** 6.52
	126 X=**N-O-** : 4.87	**171** X=**O** : 6.15			
	184 X=**C-OH** : 5.08				

7-membered rings and bicycles are too big for the pocket with difficulties to take a position in the pocket and interact with the metals. Indeed, bulkier fragments were found with the worst scores (high steric parameter), and outside the pocket. Benzensulfonamide **214** has the high GOLDSCORE of 6.00 and CHEMPLP score of 6.52, which was the best CHEMPLP score. Sulfonamides were studied in the past and already gave a series of inhibitors on Arg1,[87] as described in part 1.2. 5-membered cycle pyrrole-2-carboxylic acid **197** score the highest with GOLDSCORE among the fragments, with a normalized GOLDSCORE and CHEMPLP of 8.56 and 5.89, respectively. This highlights that the size is a critical

parameter thanks to a lower steric parameter revealed by the docking, as represented in Figure 61.

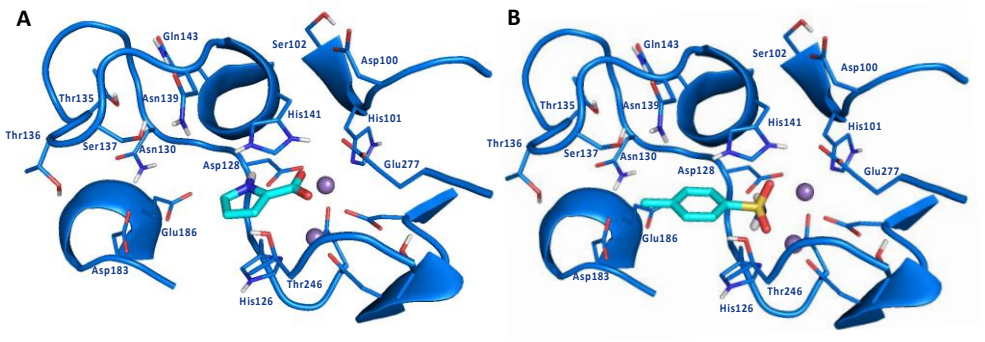

*Figure 61: docking of fragments **197** (A) and **214** (B) in arg1 active site (2AEB). Images were generated from the best solution obtained with the GOLDSCORE docking.*

Oxygen-based functions scored also very high. Phenol and carboxylate have demonstrated potent interactions due to their appropriate geometry and negative charge, respectively, and thus high scores. 6-membered platform with pyridine **173**, N-oxy-pyridine **126** and salicylic acid **184** were the best with the carboxylate as the coordinating function with pyrimidin-2-ol **148** (Figure 62A, B C and D). 3-hydroxy-2H-pyran-2-one **171** and 3-hydroxypyridin-2(1H)-one **177** suffered of the bidentate coordinating function, that introduce steric hindrance (Figure 62E and F).

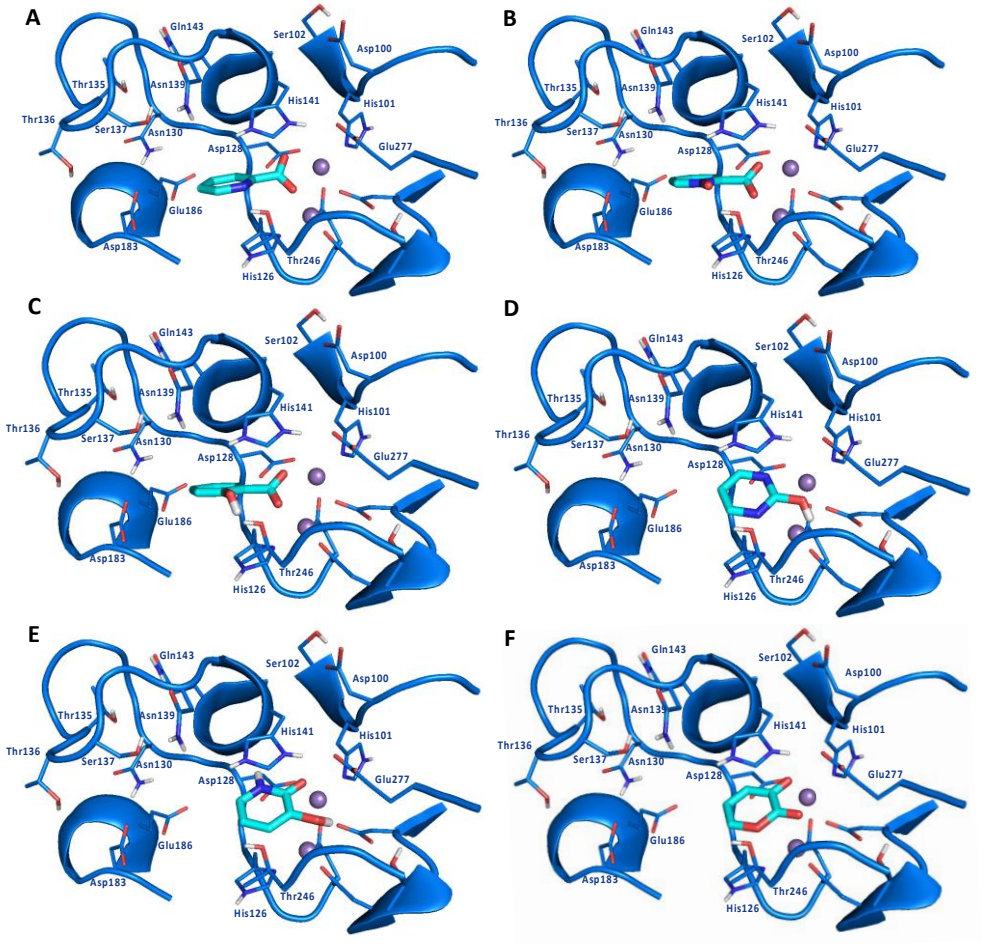

*Figure 62: docking of fragments **124** (A), 1**26** (B), **184** (C), **148** (D), **177** (E) and **171** (F) in arg1 active site (2AEB). Images were generated from the best solution obtained with the GOLDSCORE docking.*

The analysis seems to corroborate our hypothesis that other fragment than boronic acid on aliphatic linker could accommodate the Arg1 binding site. However, the position of the heteroatom seems also important to interact with surrounding residues such as Thr246, His126 and His141. The fragments scoring the highest (**124**, **171**, **184**) were the fragments with a heteroatom (oxygen or nitrogen, Figure 62A, B and F) or substituent (phenol, Figure 62B and C) pointing towards Thr246. In the others case, the fragments presented the heteroatom towards the backbone of the enzyme (Asp128 and Asn130) as represented in Figure 61A and Figure 62E.

All the compounds were finally evaluated on Arg1 using the radiometric test.

5.2.3 *In vitro* evaluation of the coordinating fragment library

In vitro assessment of the most interesting fragments was carried out following the experimental protocol set up previously. In the radiometric test, the fragments were assayed at pH 9.5 and at high concentration (1 mM) thanks to their good aqueous solubility.

Again unfortunately, no significant inhibition of Arg1 could be observed with any of the compounds. (Figure 63)

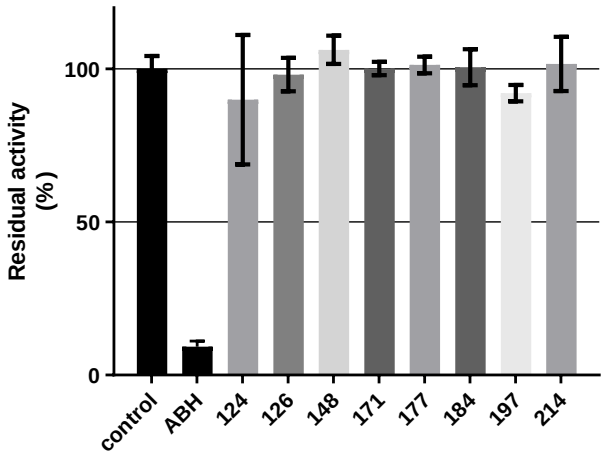

*Figure 63: Residual activity of the coordinating fragment library (at a concentration of 1mM) Residual activities and standard deviations are reported from two distinct experiments in duplicates. 2(S)-amino-6-borohexanoic acid **42** (ABH) as a positive control for Arg1 inhibition.*

The other explanation for the lack of affinity of most molecules for Arg1 is that a strong binder is required to displace the hydroxide and replace it in the manganese coordination network. In the design reported by Ilies *et al.*,[83] 2-aminoimidazole fragment **93** binding to the ion cluster becomes 10 more potent when bound to a L-amino acid side-chain (2AH, **36**) and 1000-fold when the chain has the correct length (A1P, **37**). (Figure 64)

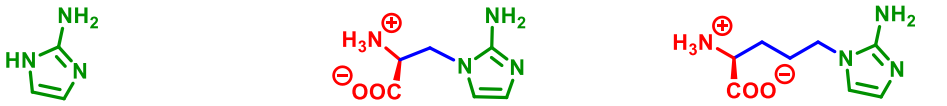

93
2-aminoimidazole
K_i = 3600 ± 20 µM

36
L-2-aminohistidine (2AH)
K_i = 300 ± 9 µM

37
2-(S)-amino-5-(2-aminoimidazol-1-yl)pentanoic acid (A1P)
K_i = 4 ± 0.2 µM

Figure 64: Activity increased for 2-aminoimidazole-based series of Arg1 inhibitors by adding the α-amino acid moiety, and correct-length linker.

5.2.4 Outcome of the coordinating fragment library

Unfortunately, again no Arg1 inhibitors could be discovered following this screening. It seems very clear that the replacement of the boronic acid function as metal coordinating moiety that can act as an anchoring point in the catalytic pocket is not necessarily a valid option. We therefore then envisioned to modulate the nature of the linker bearing the anchoring boronic acid head moiety as it seems that this moiety is among the best to inhibit arginase. We thus planned to screen various chemical structure to substitute the simple aliphatic chain and probe the linker area.

5.3 BUILD AND SCREENING OF THE BORONIC ACID LIBRARY

5.3.1 Build of the boronic acid library

A library of boronic acid compounds was thus constituted including 41 molecules (**220-260**). Since boronic acids are common reagents in organic chemistry since they are used to perform Suzuki couplings, most of the compounds were already available in our lab. The additional compounds were purchased from usual suppliers (Sigma-Aldrich (now Merck), Fluorochem, or TCI). All the selected boronic acids are fragments with a molecular weight below the 300 g.mol^{-1} limit: between 101.9 to 262.1 g.mol^{-1}. The molecules were chosen to have various platforms: aliphatic chain, aliphatic ring, 5- and 6-membered aromatic rings and bicycles. This diversity should ensure to adequately probe the catalytic pocket of Arg1. The molecules are listed in Figure 65.

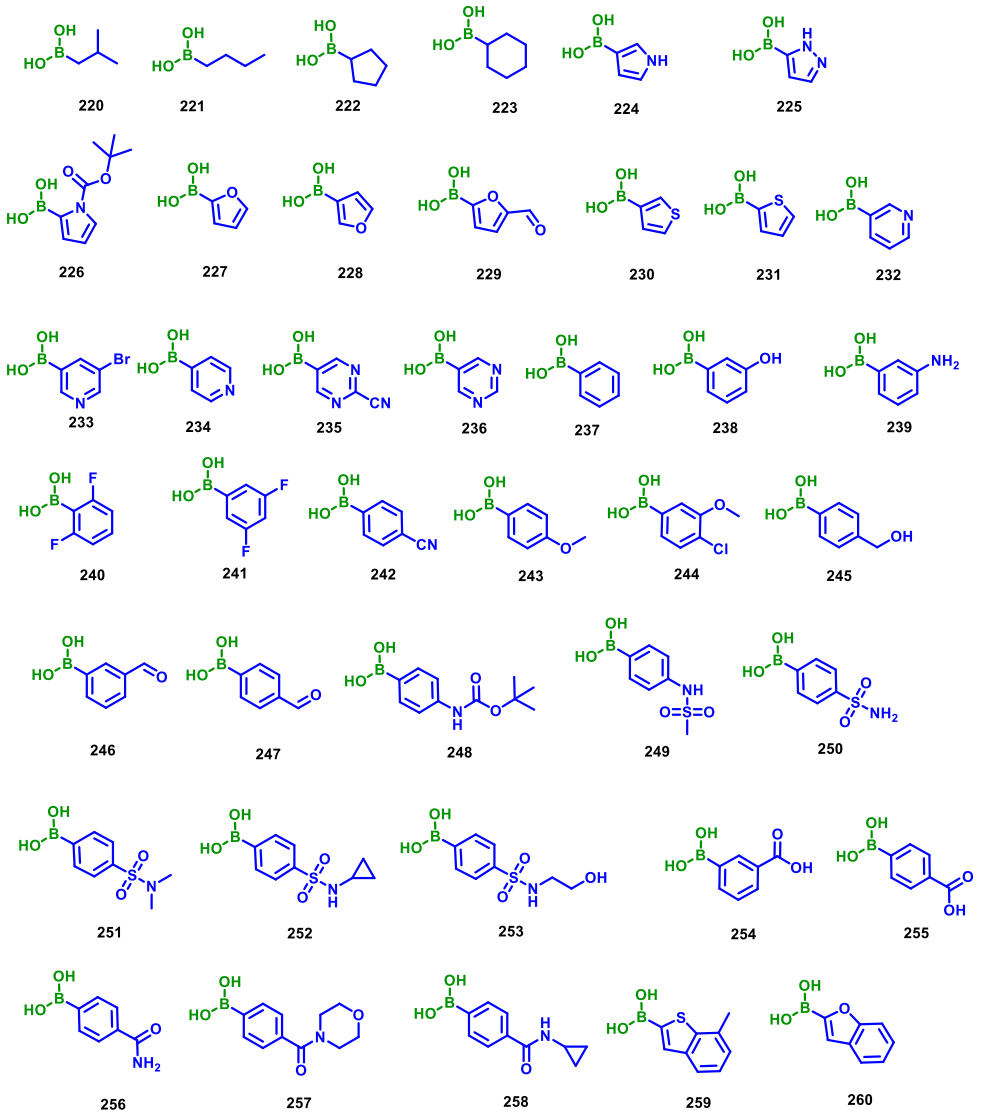

*Figure 65: Chemical structure of boronic acid fragments (**220-260**)*

5.3.2 Biochemical Evaluation of the boronic acid library

For enzymatic screening, all compounds were freshly prepared in DMSO at 10 mM for testing at 1 mM. IC_{50} were performed with stock ligand solutions freshly prepared up to 100 mM in DMSO, depending on the solubility.

We screened the selected library of boronic acids on Arg1 inhibition at a single concentration of 1 mM at pH 9.5, in triplicate. The results, expressed as a percentage of activity compared to the negative control (without inhibitor), can be found in Figure 66. ABH **42** was also included as a positive control for Arg1 inhibition (K_i = 11 nM at 9.5 and K_i = 88 nM at pH 7.5)[99] As a result, we identified five compounds (**220**, **223**, **227**, **246**, and **250**) that display *h*Arg1inhibition around 50% at 1 mM. (Figure 66A) Next, we evaluated the half-maximal inhibitory concentrations (IC_{50}) of the different hits and obtained inhibition potency ranging from 127 to 870 µM. (Figure 66B)

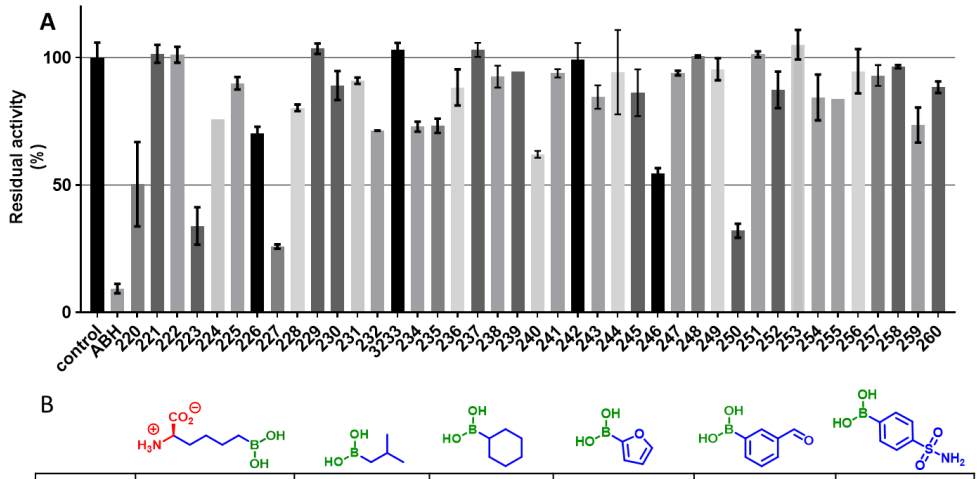

Compound	**ABH 42** 2(S)-amino-6-borohexanoic acid	**220** isobutylboronic acid	**223** cyclohexyl boronic acid	**227** 2-furanylboronic acid	**246** (3-formylphenyl) boronic acid	**250** 4-sulfamoyl benzeneboronic acid
IC_{50} [95% confidence interval]	1.5 µM [1.1-1.9 µM]	870 µM [386-1961 µM]	292 µM [166-517 µM]	127 µM [105-153 µM]	1.4 mM [0.2-8.9 mM]	403 µM [236-691 µM]

*Figure 66: A) Residual activity of the boronic acid fragment library (at a concentration of 1 mM) and chemical structures of the most potent compounds. Residual activities and standard deviations are reported from two distinct experiments in duplicates. 2(S)-amino-6-borohexanoic acid **42** (**ABH**) as a positive control for Arg1 inhibition. B) Half maximal inhibitory concentration (IC_{50}) for ABH **42**, **220**, **223**, **227**, **246**, **250**. Maximal concentration of 1 mM instead of 10 mM was used for **220**, **223, 246,** and **250** due to solubility issues. Residual activities and standard deviations are reported from two distinct experiments in triplicates.*

Among these fragments, we were pleased to identify the furan-boronic acid **227** as the most potent hit, with an IC_{50} of 127 µM. This result corroborated our

initial hypothesis that a small heteroaromatic ring should be tolerated in the *h*Arg1 binding cleft. Interestingly, despite being small and lacking an amino acid tail, which is important for Arg1 inhibition,[101] compound **227** remains a promising hit (Ligand Efficiency, LE = 1.4 pIC_{50}/Heavy Atom Count = 0.68). As a comparison, the *n*-butylboronic acid **220**, the strict analog of ABH lacking the amino acid tail, is not active, thus reinforcing the potential of the 2-furanyl boronic acid **227** for *h*Arg1inhibition.

Based on these observations, we set out to characterize the binding of these fragments within the *h*Arg1 binding site by virtual docking analysis.

5.3.3 Docking analysis

As for the previous library, the molecules were drawn as boronates on ChemDraw (PerkinElmer). MM2 energy minimization was performed with ChemBio3D (PerkinElmer), and each molecule was saved independently in MOL2 files.

Docking was performed with crystallographic structure 2AEB selected from Protein Data Bank (PDB) and with docking software GOLD® (CCDC) or AutoDock Vina.[164] For AutoDock Vina, boron atom had to be switched for *dummy* to be supported during processing as AutoDock Vina does not take into account boron in docking analysis.[165] A dummy atom is used to defined constraints such as position, geometry and length of the bond with partners. Therefore, boron was considered as sp3 carbon atom with a negative charge with similar radius and number of bonds, and its position was fixed to superpose the boronate of ABH **42**. Crystal structure with the code 2AEB was used because of its high resolution. Ligand-enzyme complexes were built in the cavity pocket by extracting and replacing the co-crystallized ligand, i.e., ABH **42** in 2AEB, with the selected molecules. All systems were preliminarily prepared with Gold® to add hydrogens and removed selected

water molecules. A cavity of 10 Å was generated around the proximal Mn^{2+} recorded as MN2362.

The scoring functions used were CHEMPLP (for the coordinating interaction with the metals), GOLDSCORE (for the polar interactions) and VINASCORE (for the hydrophobic interactions and steric fitting), with weighting by metallic atoms after determination of the most relevant function and used in combination with cross-referenced data. Scoring values were normalized by the number of "heavy atoms" (that are the number of non-hydrogen-atom). The generation of 20 solutions per molecule was obtained and visualized on a dedicated 3D screen.

The docking poses were ranked according to different scoring functions (GOLDSCORE, CHEMPLP, and VINASCORE) to better appreciate the interactions. Because the molecules are small and possess different possible interactions, using different scoring functions can help to better understand the interaction between the ligands and the enzyme. Especially between boronate and the metal cores of the enzyme. In fact, the scoring functions were chosen to cross the information between them with the aim to avoid a bias due to their respective advantages and drawback. CHEMPLP takes the coordinating interaction with the metals into account, whereas GOLDSCORE and VINASCORE select the best results based on polar interactions and hydrophobic interactions/steric fitting, respectively.

The main points of interest for the discussion regarding the docking and the inhibition, are summarized in Table 9. Compounds with boronic acid heads that are not active on Arg1, such as the thiophene **231** and pyrazole **225,** were also included as negative controls.

*Table 9: Half maximal inhibitory concentration (IC_{50}) and normalized GOLDSCORE, CHEMPLP, and VINASCORE scores from docking for ABH **42** and fragments **220**, **223**, **225**, **227**, **231**, and **237**.*

compound	IC_{50} (µM)	Ligand Efficiency	Normalized goldscore	Normalized chemplp	Normalized vinascore
ABH **42** 	1.5	0,63	6.01	6.79	5.15
220 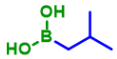	870	0.53	8.67	7.76	7.13
223 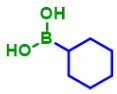	292	0.49	6.99	6.18	6.10
225 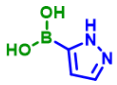	> 10 mM	-	4.47	4.54	4.93
227 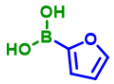	127	0.61	7.38	7.01	7.44
231 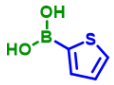	> 10 mM	-	7.82	7.01	7.44
237 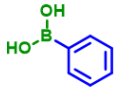	> 10 mM	-	6.46	6.78	6.50

All three scoring functions were similar with very little difference, giving fragment **220** the highest score. Interestingly, we found that excellent normalized scores characterized the small fragments **223** (Figure 67A), and **227** (Figure 67B).

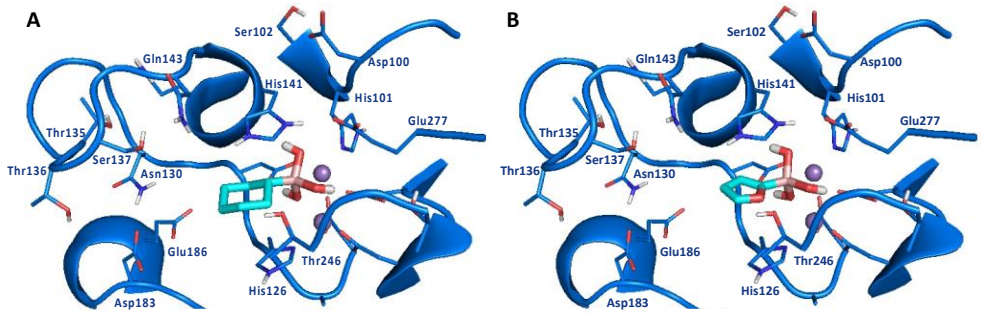

*Figure 67: Docking of **223** (A) and **227** (B) fragment in Arg1 active site (2AEB).*

3-furanylboronic acid isomer **228** only inhibited Arg1 by 20%, which is far from the inhibition of 74% of 2-isomer **227**. The main observed difference in docking is the position of the oxygen in the active site. (Figure 68)

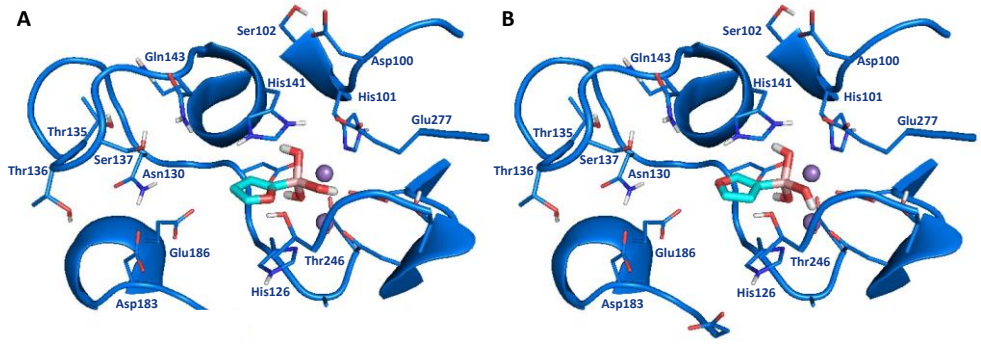

*Figure 68: Docking of **227** (A) and **228** (B) fragment in Arg1 active site (2AEB).*

The comparison of the docking of the fragments **227** and **228** highlights that the localization of the heteroatom, oxygen in this case, is important. Indeed, the furan oxygen of **227** is facing the Thr246 and its hydroxide, which could make a hydrogen bound. The absence of this interaction could explain the difference in inhibition.

The replacement of the furan by thiophenes, such as in the isomeric compounds **230**/**231** (Figure 69), although very interesting in docking with the second highest score did not provide *h*Arg1 inhibition.

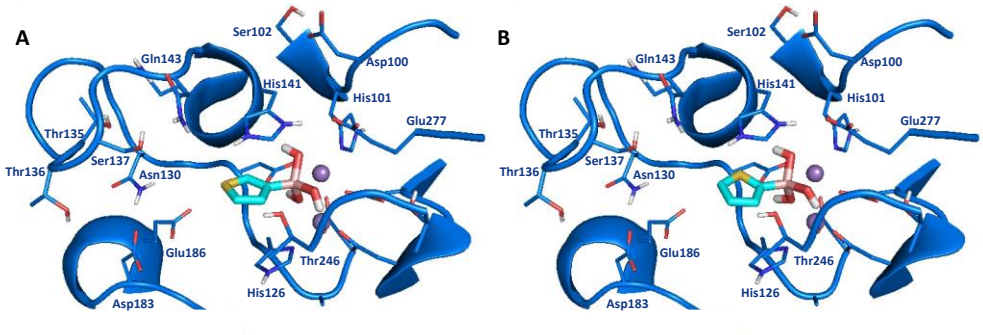

*Figure 69: Docking of **230** (A) and **231** (B) fragment in Arg1 active site (2AEB).*

In the case of thiophenes **230** and **231**, docking shows that their placement is favored when the sulfur faces away from threonine 246. Thiophene rings also seem to be a little bulkier and to be disadvantaged, as well as phenylboronic acid **237**. Pyrrole **224** (Figure 70A) and 1H-pyrazole **225** (Figure 70B) did not have high docking scores, or neither inhibition of Arg1.

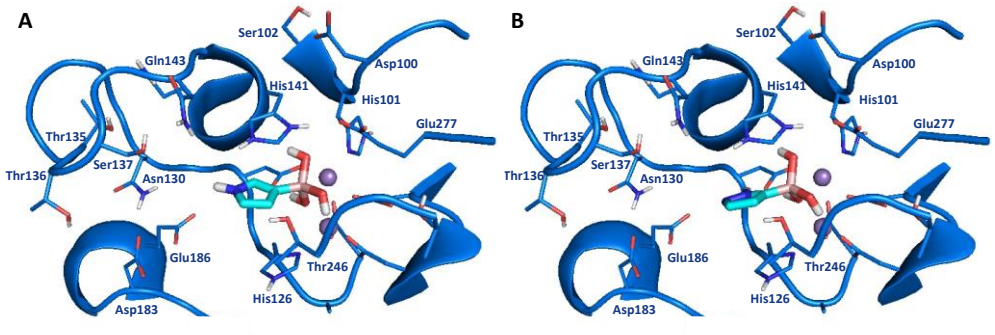

*Figure 70: Docking of **224** (A) and **225** (B) fragment in Arg1 active site (2AEB).*

The position of the nitrogen is similar in the docking as the thiophenes **230** and **231**. Although the size of the fragments **224** and **225** is small, it can be assumed that the presence of nitrogen is not favorable. At this point, it seems that only the oxygen of the furan **227** seems to bring an additional interaction and improve the inhibition.

5.3.4 Outcome of the boronic acid library

Therefore, this result validates the hypothesis resulting from the molecular dynamics study regarding the ability of this thin cavity to accommodate linkers larger than a saturated carbon chain.

These results point out that the volume accommodating the chemical linker that connects the boronic acid of the inhibitors with its amino acid group is flexible. The consequence of this finding is that the enzymatic pocket can bear a chemical development of this specific part of the ligand. More than a simple chemical link, this fragment can become an actor of the ligand-enzyme binding, for example through hydrophobic contacts as observed in the region of Thr246 with ABH **42**.

5.4 PRELIMINARY CONCLUSION

Most of the current Arginase inhibitors that have been reported so far encompass a boronic acid head linked to an amino acid tail via an aliphatic linker. In the present part, we investigated the central linker part to appraise the possibility to accommodate cyclic/aromatic scaffolds and hence potentially offer new interactions in the *h*Arg1 active site. Our study led to the identification of the cyclohexyl boronic acid **223** and 2-furanyl-boronic acid **227** fragments that revealed a promising *h*Arg1 inhibition of 292 and 127 µM, respectively. A docking study suggested that **227** could form favorable quadripolar π-stacking interactions with the imidazole rings of the His 141 and 126 residues.

Based on this analysis, we investigated the potential of the 2-furanyl-boronic acid **227** to design more elaborated *h*Arg1 inhibitors.

6 HIT OPTIMIZATION WITH BORONIC ACID FRAGMENTS

6.1 INTRODUCTION

Following the identification of some boronic acid compounds, we initiated a tentative optimization study of the two more potent boronic acid fragments identified: the cyclohexylboronic acid **272** and the 2-furanylboronic acid **276** fragments. Our idea was to further evolve these fragments to reach a higher Arg1 inhibitory potency, notably adding the amino-acid tail. The optimization strategy, inspired from the structure of ABH **42**, can be found on Figure 71.

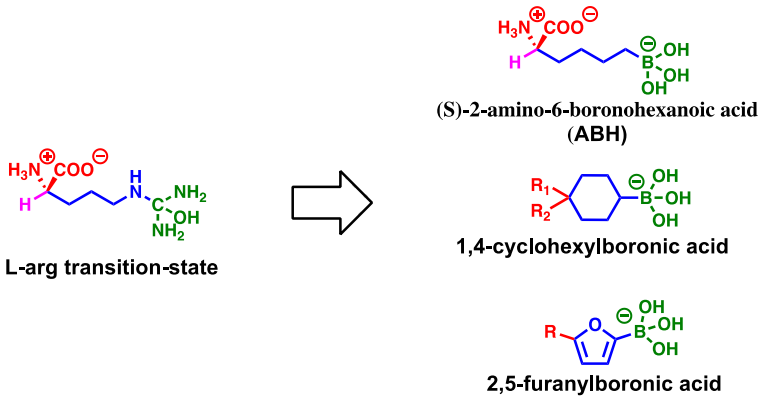

*Figure 71: Optimization of 2-furanylboronic acid and cylohexylboronic acid to mimic L-arginine transition-state as ABH **42**.*

6.2 OPTIMIZATION OF THE 2-FURANYLBORONIC ACID 227 FRAGMENT

First, the optimization of 2-furanylboronic **227** was undertaken. In the first step a molecular docking study was performed to understand the binding of the 2-furanylboronic acid compound inside the Arg1 cavity.

6.2.1 Prediction by docking of 2-furanyl derivatives

According to this docking experiment, the furan ring would be involved in two π-stacking interactions with the imidazole rings of His141 and His126, delineating the channel. A small lipophilic aromatic ring with an H-bond acceptor heteroatom thus seems tolerated in this position. Furthermore, the position of the furan oxygen also seems to contribute to the stabilization of the compound inside the binding cleft through a particular H-bond with the Thr246 hydroxyl group. Hence, the position isomer, 3-furanyl boronic acid **228,** is not an Arg1 inhibitor. It should be noted that Thr246 was also reported to interact with some Arg1 inhibitors[70, 112, 166] (ex: PDB codes 2AEB[15] or 3MFW[77]), thus corroborating the present analysis. An illustration of the binding of **227** inside Arg1 is given in Figure 72A.

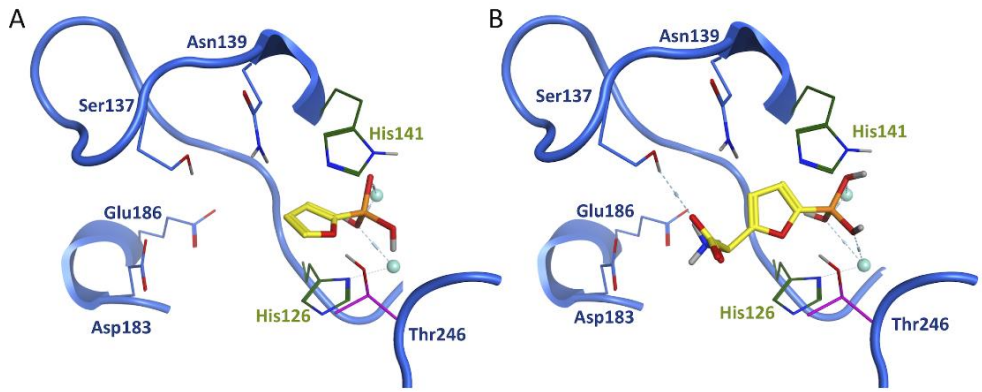

*Figure 72: Views of the docking inside the Arg1 binding cleft of (A) **227** and (B) **227** linked with the missing amino acid tail miming ABH **42**. Thr246 is highlighted in pink*

To appreciate the potency of future optimization, the missing amino-acid moiety was further linked to the furanyl part. An illustration is represented in Figure 72B, where the designed molecules revealed a good overlapping with ABH **42** overall. However, the amino acid tail forces the rigid heterocycle to rotate slightly to accommodate the pocket.

To further confirm the interest of this fragment for the elaboration of new Arg1 inhibitors, we evaluated whether the addition of a known amino acid moiety and additional arm would be, at least *in-silico*, favorable for Arg1 inhibition. To this end, we selected the three tails of the Arg1 inhibitors NED-3238 **44**, CB1158 **45**, and proline-derived inhibitor **46** and virtually linked these tails to the boronic acid fragments and performed a docking of these complete molecules (Figure 73).

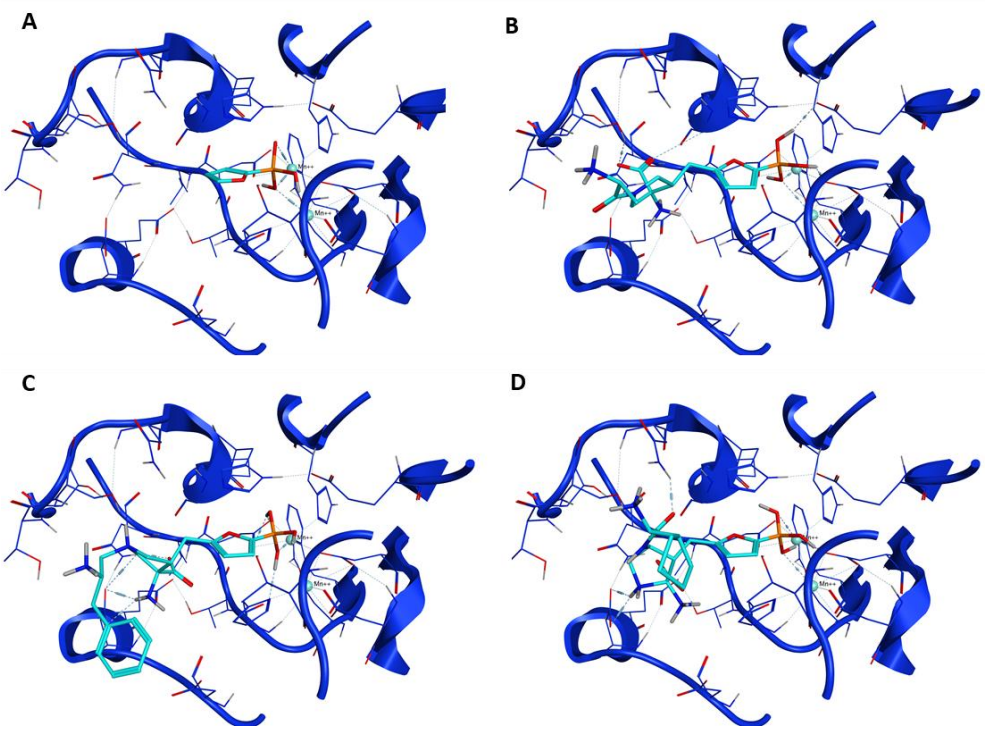

Figure 73: Views of the docking inside the Arg1 binding cleft of (A) ***227*** *(B)* ***227*** *linked with the tail of CB1158, (C)* ***227*** *linked with the tail of NED-3238 (D)* ***227*** *linked with the tail of* ***46****.*

From this analysis, compound **227** still scored very high, regardless of the tail used. **227** with the tail of **46** (Figure 73D) gave the highest VINASCORE with -9.1, followed by CB-1158 (Figure 73B) and NED-3238 (Figure 73C) tails with -8.7 and -8.6, respectively. Interestingly, compounds derived from **227** were slightly better than NED-3238 **44**, CB-1158 **45**, and proline-derived inhibitor **46** themselves.

This experiment seems to demonstrate that the furan motif could significantly increase the inhibition. However, this is only computational prediction, and the synthesis of such derivatives is needed to evaluate them.

6.2.2 2,5-disubstituted-furanylboronic acid synthesis

Based on these results, we envisioned the optimization of the furanyl compound **227** into more elaborated Arg1 inhibitors. The synthesis of furanyl boronic acid compounds bearing an amino acid tail was our first intent. However, because the synthesis of furan derivatives can reveal a hazardous task, we initially investigated the chemistry on more simple compounds. In fact, the synthesis of furan derivatives is known to be challenging,[167, 168] notably because of the furan's susceptibility to acidic conditions,[169] temperature, light exposure, and redox conditions.[170]

As a first step, we thus attempted to synthesize 2,5-disubstituted furans bearing a boronic acid on one side and an amino-alkyl group on the other side. Although deprived of the carboxylic acid function, these compounds still bear an amino group that could form stabilizing interactions with Arg1. The retrosynthetic analysis of such compounds is depicted in Figure 74. According to this scheme, the compounds could be obtained in three steps from the commercially available furfural **263** by protecting the aldehyde to the acetal **262**. Boronation of **262** gives the key boronic acid intermediate **261** that finally undergo functionalization such as reductive amination.

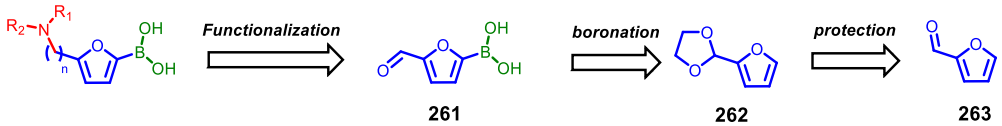

*Figure 74: Retrosynthetic pathway for 2,5-disubstituted furanylboronic acids synthesis from furfural **263**.*

The synthesis of the key intermediate **261** started from furfural **263,** which was first protected as the dioxolan **262,** and then boronated. (Figure 75) To this end, freshly distilled furfural **263** was protected with ethylene glycol using a dean-stark apparatus to afford **262** in 60 % yield. The latter was further boronated in the 2-position following lithiation using *t*-BuLi and addition of the lithiated compound to tri-isopropylborate and hydrolysis with HCl to give the (5-formylfuran-2-yl)boronic acid **261** key intermediate in 34% overall yield.

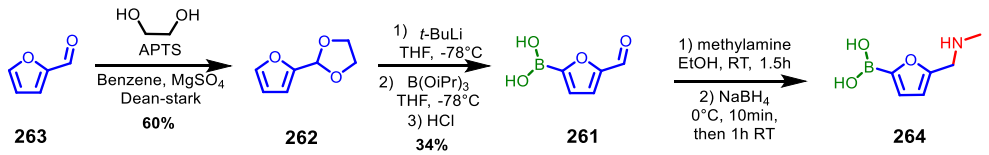

*Figure 75: synthesis of (5-((methylamino)methyl)furan-2-yl)boronic acid **264***

From **261**, we initially assessed the reductive amination reaction using methylamine. **264** could be obtained and isolated in quantitative yield in the conditions used. The obtention of **264** encouraged us to investigate the synthesis of a small series of analogs incorporating other aliphatic or cyclic amines. However, several attempts with different amines such as hydroxylamine, *O*-methylhydroxylamine, or secondary amines in the exact same conditions as for the synthesis of **264** revealed unfruitful with only black residual materials obtained, suggesting degradation or polymerization products. The loss of the boronic acid function by protodeboronation was systematically observed using NMR spectroscopy.

Protodeboronation is a mechanism of degradation of boronic acid where the boronic function is exchanged with a hydrogen. This reaction can occur in all conditions with boronic acids: solid and in solution. (Figure 76)

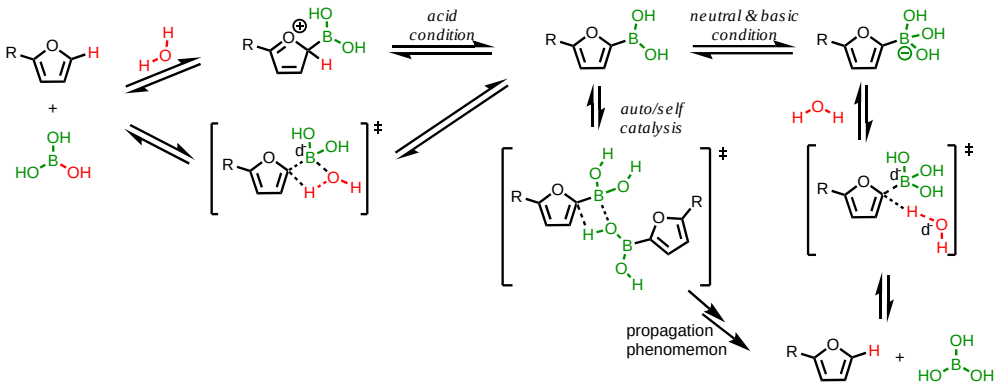

Figure 76: Mechanisms of protodeboronation of 2-5-furanyl boronic acid derivatives.

In solid state, auto/self-catalysis is observed. The rate of neat 2-furanylboronic acid **227** protodeboronation is very high, and storage of such building block is tricky.[171] The degradation in solution is strongly dependent on the conditions.[171] It depends on the solvent, the presence of water, metals or cations, and other chemical functions, as well as temperature and pH.[172] Protodeboronation in basic conditions are well reported following the interest in Suzuki-Miyaura coupling where the loss of the boronic acid function prevent the reaction.[172] After nucleophilic attack of the boronic acid by hydroxide anion, the obtained boronate can be exchange with a hydrogen of another water molecule to form boric acid and protodeboronated compound. In acidic conditions, protodeboronation occurs by protonation of the furan cycle followed by deboronation with addition of a water molecule, in 2 steps of by a concerted mechanism.[173] The mechanism of protodeboronation has attracted much attention lately and seems now better understood.[174] A stability window for 2-furanylboronic acid **227** in the neutral and mild acidic conditions should allow the synthesis of our compounds and relative stability in physiological conditions.

Novel experimental conditions were thus explored to possibly avoid the rapid degradation observed previously, notably using one-pot conditions with specific reductive agents such as sodium cyanoborohydride (Table 10**).** For the purpose of this study, we used various reaction conditions and dimethylamine as a

model compound, as illustrated in Table 10. The only condition where compound **265** could be prepared and did not readily degrade involved the use of 10 equivalents of the amine in acetic acid at pH 6. In these particular conditions, the (5-((dimethylamino)methyl)furan-2-yl)boronic acid **265** could be isolated from the crude material and characterized by ^{1}H and ^{13}C NMR. However, **265** demonstrated poor stability, especially at room temperature or in the presence of moisture.

*Table 10: Outcomes of the synthesis of (5-((dimethylamino)methyl)furan-2-yl)boronic acid **265** using different experimental conditions.*

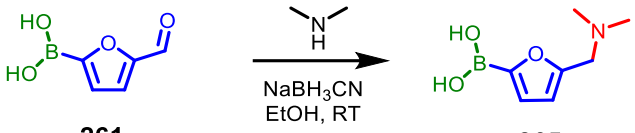

261 **265**

Entry	Equivalent of amine	condition	Conversion rate from the crude	Particular comments
1	1.1	HCl salt	complete	Not isolated, degradation
2	1.1	HCl salt, pyridine	No conversion	**261** fully recovered
3	1.1	AcOH (pH 6)	incomplete	Not isolated, protodeboronation
4	5.0	AcOH (pH 6)	complete	Not isolated, protodeboronation
5	10.0	AcOH (pH 6)	complete	Isolated yield: 20%, stable in buffer

In all attempts, degradation by protodeboronation was fast in non-buffered solution and at high concentration. Finally, because the methylamine derivative **264** could be isolated and was actually very stable in the solid-state or in solution, we reasoned that the nature of the amine used in the reaction could influence the stability of the final compounds. We thus investigated the synthesis of furan derivatives harboring variously substituted alkylamino chains using the best conditions with 10 equivalents of amine substrates in AcOH (Table 11).

Table 11: Outcomes of syntheses of 2-5-furanyl boronic acid derivatives with various amines

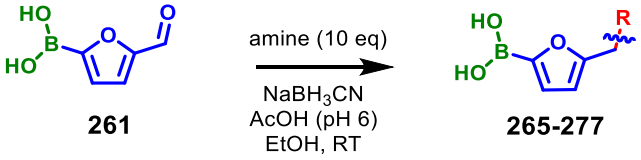

Compound	R	Conversion rate from the crude	Isolated	Particular comments
266[a]		degradation	no	Fully protodeboronated in the crude mixture
265		complete	yes	Protodeboronation of the isolated compound
267	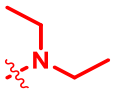	complete	yes	Protodeboronation of the isolated compound
268	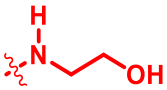	degradation	no	Fully protodeboronated in the crude mixture
269	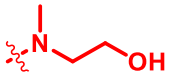	complete	no	Not purified from buffered crude
270	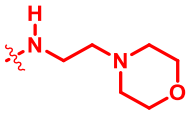	complete	no	Not purified from buffered crude
271	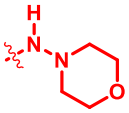	complete	no	Not purified from buffered crude
272		complete	yes	Protodeboronation of the isolated compound
273	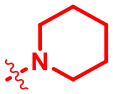	complete	yes	Protodeboronation of the isolated compound
274	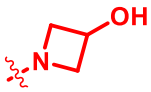	complete	no	Not purified from buffered crude
275	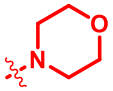	complete	yes	Protodeboronation of the isolated compound
276	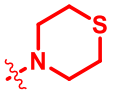	complete	yes	Protodeboronation of the isolated compound

[a] *Ammonium acetate was used instead of ammonia and glacial acetic acid*

Apart from compounds **266** and **268,** all attempts led to complete conversion to the searched products, as deducted from NMR analysis of the crude reaction mixture, but the workup and purification of these materials proved to be very challenging. Hence, only a few analogs could be isolated after purification by reversed-phase column chromatography but readily degraded by protodeboronation once evaporated to dryness. An illustration of the rapid protodeboronation is presented in Figure 77**.**

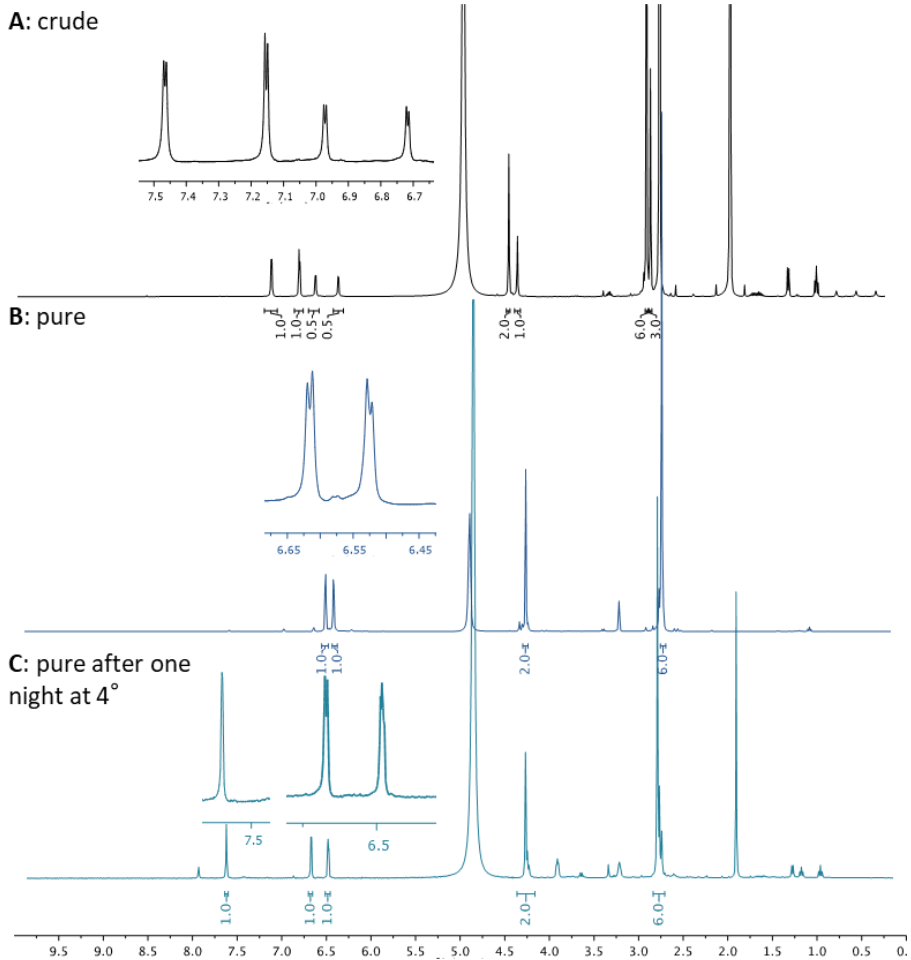

*Figure 77: NMR spectra from (A) the crude reaction mixture during the synthesis of **265**, (B) isolated **265** pure product, and (C) NMR spectra of the same sample of **265** after one-night storage at 4°C illustrating the protodeboronation. The protodeboronated product is followed by the apparition of a doublet (J=1.1 Hz) at 7.6ppm and one of the aromatic signals becomes a triplet instead of a doublet.*

NMR spectra from crude (Figure 77A) to pure **265** (Figure 77B) highlight the excellent conversion from starting material **261** and the synthesis of compound **265**. After one-night of storage at 4°C, the NMR analysis (Figure 77C) revealed, however, the unique presence of the protodeboronated compound from pure **265**. The rate of protodeboronation was even faster at room temperature.

These experiments illustrate the difficulty to work with these boronylated furans that are highly prone to degradation. Still, in our hands, only one of these furan boronic acid bearing an methylaminomethylene in the 5-position (**264**) could be isolated and was found to be highly stable. At this stage, we have no hypothesis to explain the better stability of **264** compared to other amine derivatives.

6.2.3 Biochemical and biophysical evaluation of 5-methylaminomethyl-furan-2-boronic acid 264

The biological evaluation of **264** on *h*Arg1 revealed an IC_{50} of around 400 µM [223-698]. (Figure 79A). One hypothesis that could, at least in part, explain the absence of gain in potency for **264** compared to **227** might be the additional entropic penalty of the protonated amine function. In addition, the distance between the amine and the boronate seems not optimum, with 5.1 Å for **264** and 6.8 Å for ABH **42**. In addition, in docking, the furan is flipped, and the oxygen is presented away from the Thr246, suggesting a loss of the possible hydrogen bond. (Figure 78)

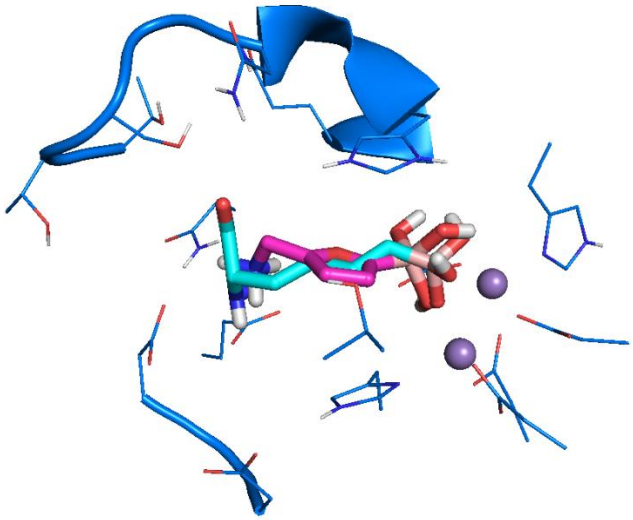

*Figure 78: docking pose of **264** (in pink) in 2AEB, compared to the co-crystalized ABH **42** (in cyan). Mn^{2+} are represented as purple spheres.*

This pose is observed to allow the amine to be in the similar environment compared to ABH **42**. It suggests the molecule is possibly too rigid with only one bond between the furan cycle and the carbon of the amine. This also seems to be confirmed by the too small distance between the boronate and amine functions.

Although not very potent, **264** remains a very interesting new scaffold for Arg1 inhibition. We thus set out to confirm that **264** binds at the active site of Arg1. To this end, we used an orthogonal biophysical method by Saturated Transfer Difference (STD) NMR spectroscopy. Because boronates generally show slow kinetics of association and dissociation on Arg1.[99] This slow exchange precludes the observation of saturation transfer using STD NMR. STD NMR need an exchange between free and bound ligand to the enzyme to observe the transfer of the saturation by nuclear Overhauser effect from the enzyme to the ligand bound to the enzyme, in our case, in the active site. Competition experiments were performed to monitor the displacement of a known active-site inhibitor by **264**. We reasoned that preincubation of *h*Arg1 with **264** could prevent the access of a known ligand to the

active site and reduce its STD signal in comparison when the known inhibitor is alone. L-ornithine with $K_i = 1.3$ mM[19] was then chosen for this experiment. Coherently, preincubation of *h*Arg1 with **264** before adding L-ornithine resulted in an approximately 50% reduction in saturation transfer compared to the conditions without **264** (Figure 79B). This reduction in STD signal likely stemmed from a competition between **264** and L-Ornithine and suggests that **264** interacts at the Arg1 active-site.

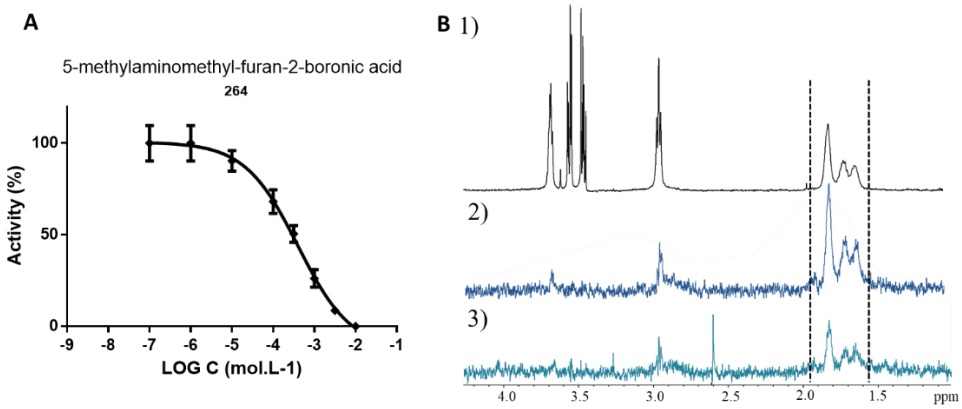

*Figure 79: A) half-maximal inhibitory concentration curves for 5-methylaminomethyl-furan-2-boronic acid **264**: IC_{50}=400 µM [223-698]. B) STD NMR competition experiment. B.1) 1H spectra of L-ornithine 2 B.2) STD NMR of L-Ornithine. C.3) STD NMR of 1 mM of 313 and L-Ornithine. The competition of 313 with L-Ornithine results in a signal reduction of around 50%.*

With the competitive inhibition demonstrated with **264**, our initial hypothesis that small aromatic boronic acid could well accommodate the Arg1 binding site seems to be validated. Although, unfortunately, the synthesis of these particular furanyl derivatives revealed challenging due to stability issues.

6.3 OPTIMIZATION OF THE CYCLOHEXYLBORONIC ACID FRAGMENT 223

The series is constituted by a cyclohexyl ring substituted in position 4 by the amino acid part. The α carbon can be fused to the ring or spaced by 1 or 2 bonds. (Figure 80)

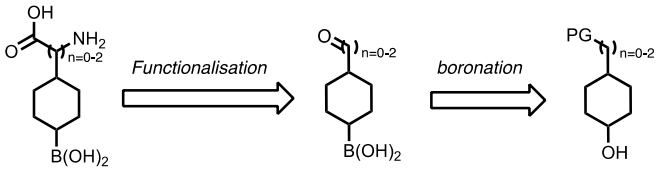

Figure 80: Retrosynthetic pathway for amino acid-substituted cyclohexylboronic acid synthesis

The 1-amino-4-boronocyclohexane-1-carboxylic acid **282** synthesis, where the α carbon is fused to the ring, was described by Kabalka.[175] (Figure 81)

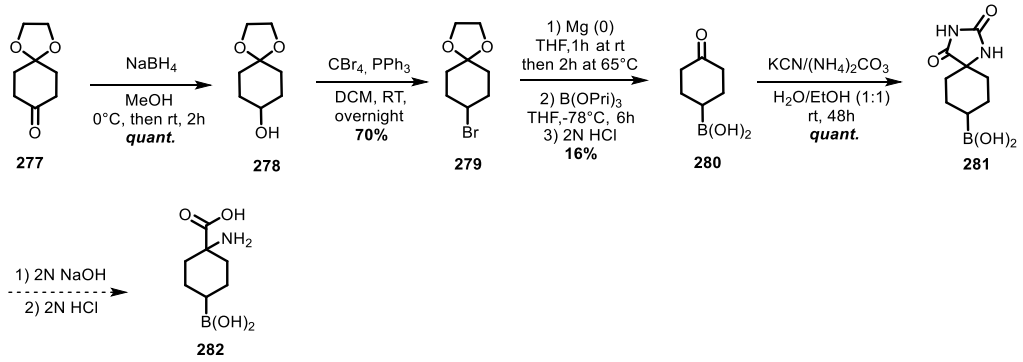

*Figure 81: synthesis of 1-amino-4-boronocyclohexane-1-carboxylic acid **282**.*

The reduction of commercially available cyclohexanedione monoethylene ketal **277** with sodium borohydride led quantitatively to the obtention of 1,4-dioxaspiro[4.5]decan-8-ol **278**. **278** was then functionalized with the Appel reaction to 8-bromo-1,4-dioxaspiro[4.5]decane **279**. Boronation of **279** was performed by passing by Grignard formation followed by its addition on triisopropyl borate in solution in THF at -78°C. After 6h of stirring at -78°C, the solution was quenched with aqueous hydrochloric acid (2M) and the resulting solution was stirred for an additional 2h. After purification, 4-boronocyclohexanone **280** was obtained with a maximum yield of 16%. Bucherer-Bergs reaction with **280** afforded the hydantoin

281 in a quantitative yield, as a white powder after purification. In the last step, hydantoin opening to afford the 1-amino-4-boronocyclohexane-1-carboxylic acid **282** was unsuccessfully attempted.

Currently, two steps are problematic. The formation of the boronic acid occurs with only 16% yield, contrary to the 70% reported. We highlighted that during the reaction, the Grignard is formed more slowly than described and the deprotection of the ketal takes place. Optimization is needed to improve the yield. The second issue with this pathway appears with the last step of deprotection of the hydantoin **281** into α-amino acid **282**. Although the hydantoin deprotection is usually straightforward, here, the spiro carbon involves very harsh conditions to break the ring. Currently, this step has not shown any conversion. Ace pressure tube or microwave could solve this issue.

The same strategy was also considered for the next molecule, where the α carbon is separated from the cycle by the presence of an additional C-C bond. (Figure 82)

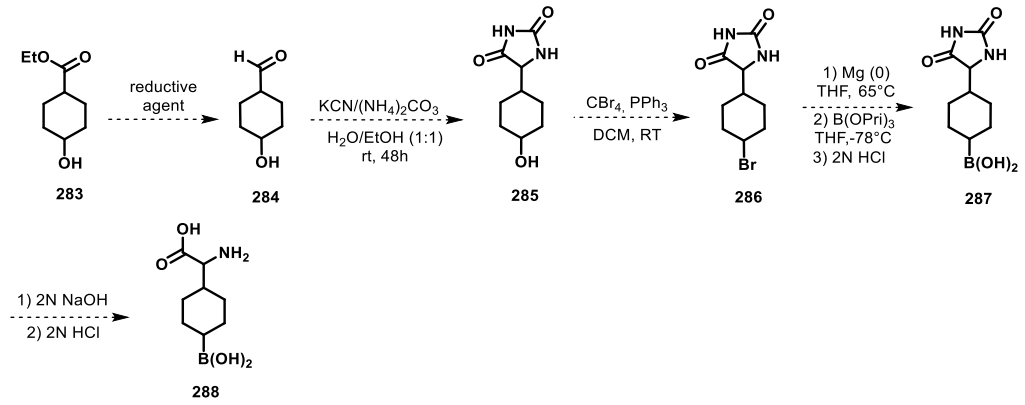

*Figure 82: synthesis of 2-amino-2-(4-boronocyclohexyl)acetic acid **288***

6.4 PRELIMINARY CONCLUSION

The synthesis of 2,5-substituted furanyl boronic acid derivatives revealed very challenging, notably because these compounds undergo protodeboronation. Hence, only the *N*-methylmethanamine derivatives **264** proved to be stable and could be evaluated on hAgr1. The study revealed an IC_{50} around 400 µM for this compound, that is slightly less potent that the unsubstituted 2-furanylboronic **227**. Competition experiments by NMR-STD confirmed the competitive profile of this compound. In conclusion, the present analysis revealed the potential of the furane scaffold for the design of Arg1 inhibitors but also highlights the challenge to work with 2-furanyl derivatives.

This work is in preparation for publication:

Prevost, J. R. C.; Kozlova, A.; Thabault, Liberelle M. and Frédérick, R. Probing the active site of Arginase 1 with aromatic boronic acids: towards the identification of novel Arg1 inhibitors.

7 GENERAL DISCUSSION AND CONCLUSIONS

7.1 MAJORS OUTCOMES AND CHALLENGES ENCOUNTERED DURING THIS THESIS

Currently, the most potent inhibitors of Arg1 are transition-state inhibitors bearing a boronic acid moiety, and there seems to be a consensus that a boronic acid is the best choice in Arg1 inhibitor design. They are all structurally similar to ABH **42** but present an additional ring to rigidify the structure and add more substituents to increase the potency towards the residues of the active site entrance.

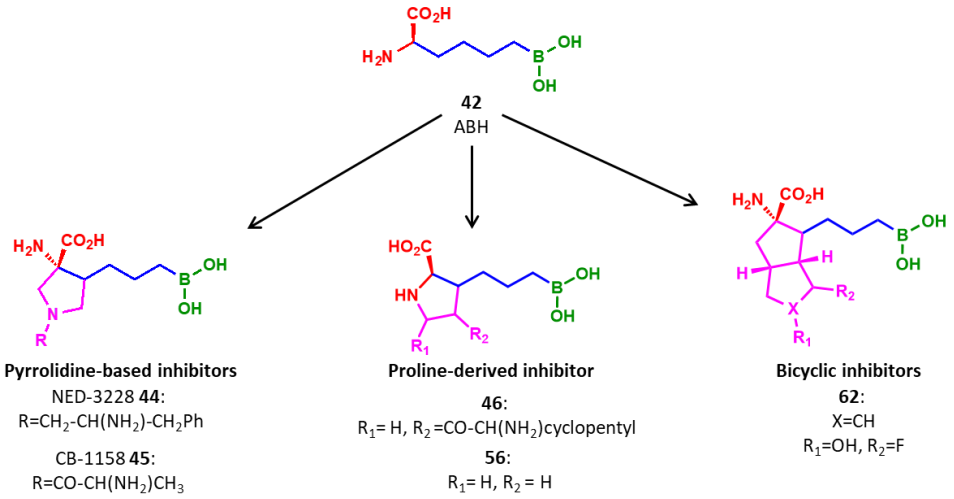

*Figure 83: current Arg1 inhibitors based on ABH **42** structure. (X=C or N, R, R_1 and R_2 are additional substituents)*

Pyrrolidine-based inhibitors improved the inhibition of Arg1 by 10-fold (IC_{50} = 110 nM when R=H vs. 1547 nM for ABH **42**). The nitrogen substitution led to more potent molecules such as NED-3228 **44** (R = CH_2-CH(NH_2)-CH_2Ph, IC_{50} = 1.3 nM).[104] CB-1158 **45** (with R = CO-CH(NH_2)CH_3) is the first compound to be investigated in clinical trials.[105, 106] Proline-derived inhibitors incorporate the amine of the amino acid function inside a cyclic structure, leading to a similar IC_{50} improvement compared to ABH **42** (**56**: IC_{50} = 16 nM vs. 311 nM for **42**). Various

substitutions were investigated on this scaffold and highlighted some very potent inhibition values with several substituents, with IC_{50} going under 1 nM (R_1 = H and R_2 = NH-CO-CH(NH_2)C(CH_3)$_3$). Bicyclic compounds were also studied and presented similar interesting results.[112] Although promising, accessing these new structures is increasingly complicated. Indeed, we note the appearance of additional chiral centers that are necessary to control. These compounds demonstrated only moderate selectivity between Arg1 and Arg2. For example, NED-3228 **44** possesses an IC_{50} of 1.3 nM on Arg1 and 8.1 nM on Arg2,[104] while CB-1158 displays IC_{50} values of respectively 86 nM and 296 nM.[105] The selectivity is difficult to obtain with this strategy targeting the similar active sites of Arg1 and Arg2. This problem is intrinsic to all orthosteric inhibitors.[176] Overall, all reported structures are relatively similar and focus only on modifications of the α or β carbon, and there are no investigations of the linker part modifications (in blue, Figure 83).

Thus, in this work, we aimed to discover novel scaffolds to design original Arg1 active site inhibitors that could be amenable to preclinical experiments and thus that lack the boronic acid warhead. For this purpose, we studied the enzyme's catalytic pocket and screened various chemical libraries to study the structure-activity relationships for extending the structural variety of existing inhibitors.

In chapter three, we discussed the selection of the enzymatic assay for this project and its setup. The selected assay using a radiolabeled substrate allowed us to evaluate our chemical libraries, the 5-bromo-2-aminothizaole series and the compounds synthesized in chapters six. Radiometric assays' advantages include their sensitivity, rapidity, reliability and allow robust enzyme activity determination,[177] while avoiding the generation of artifacts that are common with the ninhydrin colorimetric assay. 5-bromo-2-aminothiazoles revealed to be inactive, and probably false-positive hits, with this method.[178]

Chapter four detailed an original computer-assisted structural approach to study Arg1 and its inhibition.[179] First, structural analysis was conducted with existing crystallographic data in the literature. We observed that the differences between the different series of compounds designed to inhibit Arg1 were mainly in the manganese cluster area. Indeed, the guanidium part of L-arginine was modified and replaced by various chemical functions to obtain transition-state inhibitors.

Then, molecular dynamics simulations were performed to understand the structural determinants required to inhibit Arg1. Although the bottom of the pocket is very rigid, we were able to observe that a phenomenon of opening and closing of the pocket could take place, thanks to the mobility of 3 loops. We hypothesized that the discovery and design of new compounds could be oriented towards bulkier molecules. To validate our hypothesis, a 3D-pharmacophore was built, and a virtual screening was performed to discover new inhibitors, but none of the selected molecules inhibited Arg1 activity more than 20% at the single concentration of 1 mM. Our structural study concluded that this lack of affinity was due to the requirement of hydroxide displacement and replacement within the manganese coordination network. Nowadays, most of the molecules with an important inhibition on Arg1 have a boronic acid, which is the best function for this purpose.[63, 101, 109, 112]

In chapter five, a fragment-based drug design was performed to verify if the enzyme could accommodate bulkier ligands and to probe the linker of the pocket with a library of fragments. Libraries of manganese coordinating compounds and molecules with a boronic acid function were used. Using boronic acid as an anchor pattern is a head-to-tail approach that helps to prob the pocket.[180] This method led to the identification of the cyclohexyl boronic acid **223** and 2-furanyl-boronic acid **227** fragments, revealing a promising *h*Arg1 IC_{50} of 292 and 127 µM, respectively. The inhibition potency was high considering that the α-amino-acid was missing, which is associated with a significant loss of affinity as illustrated with a 5000-fold reduction in k_{cat}/K_M[17] and a decrease from 1.5 µM for nor-NOHA **33** to 450 µM for

descarboxy-nor-NOHA and > 5000 μM for desamino-nor-NOHA[93]). Molecular modeling suggested that **223** is in a hydrophobic area, and **227** could form favorable quadripolar π-stacking interactions with the imidazole rings of the His141 and His126 residues.

In chapter six, we set out to optimize these fragments to increase their inhibitory potency. The synthesis of 2-5-furanyl boronic acid derivatives proved to be challenging. Despite substitutions of 2-furanyl boronic acid with alkyl or aryl groups is quite common and bench-stable that can be used in Suzuki coupling for example,[181] substitutions with chains containing heteroatoms are rarely described.[182] Nevertheless, we described the attempt to synthesize *N*-substituted and *N*,*N*-disubstituted compounds from furfural. Only the *N*-methylmethanamine derivatives **264** proved stable enough to be evaluated on *h*Agr1 and yielded a competitive inhibition profile with an IC_{50} around 400 μM.

Overall, this work demonstrated that the search for new scaffolds targeting the Arg1 catalytic site is challenging, the first reason being the size of the active site itself. With a pipe-shaped depth of 10 Å and a volume of only 350 $Å^3$, the pocket is too small to allow significant chemical diversity. The difficulty of finding new scaffolds was highlighted in this manuscript (chapters four & five) by the virtual screening that did not result in inhibition *in vitro*, despite excellent 3D alignment. However, the size and shape of the pocket is an explanation, but the catalytic site is also very hydrophilic.[109] The part that binds the α-amino-acid consists of L-aspartate and L-glutamate side-chains.[15] Their carboxylates form a negatively charged area where the ammonium sits, and the carboxylate of the ligand interacts via bridging water molecules.[102] Secondly, docking suffers from limitations from their static treatment of the active site and the ligands.[183] We demonstrated the mobility of some chains, but some residues also demonstrated degrees of freedom as His141 with its

~90° rotation, as described in the mechanism (Figure 5). In the crystal structures, Thr146 can rotate and present the methyl (3MFW[88]) or the hydroxyl group (2AEB[15]). Thirdly, the presence and involvement of metals in the inhibition make it more difficult to model the interactions.[184] Working with boron to target the metals was also challenging. Medicinal chemistry has become more interested in Boron over the last two decades, especially since the FDA approval of Bortezomib (Velcade®), an anti-cancer agent inhibiting the proteasome.[185] While boron is probably underused, it opens up new possibilities for drug design, but its originality is also one of its drawbacks. The electron density is still poorly considered in the force fields used in molecular modeling despite recent developments.[186] Such limitations are deleterious when it comes to anticipating interactions and having a rational design.

Boron chemistry is not as well described as nitrogen, sulfur, or oxygen chemistry. Additionally, working with boron sometimes involves the need for specific equipment, as NMR that can confirm a change in the environment of boron.[187] But assuredly, the most limiting parameter in this work was the stability of the synthesized molecules. It appeared that such compounds are challenging to obtain, purify, and assess on Arg1. However, such derivatives are interesting in the Arg1 research field and probably in other topics. Stabilizing or protecting the function against protodeboronation could lead to compounds easier to purify, isolate, and use.[188, 189] Prodrugs can be designed by this approach.[190] It also makes the design of active molecules complex, especially when ADME parameters are taken into account.[108] A perspective article is currently in preparation, in which the possibility of adding boron to pharmaceutical diagnostic or treatment tools is discussed and illustrated with examples.

7.2 PERSPECTIVES

This work opens many perspectives. It is very clear from the work performed that the chemistry of furanyl boronic acids is very challenging, especially because of the poor stability of the resulting material in the final step of our synthetic procedure. To avoid this issue, an alternative retrosynthetic pathway could be envisioned. (Figure 84)

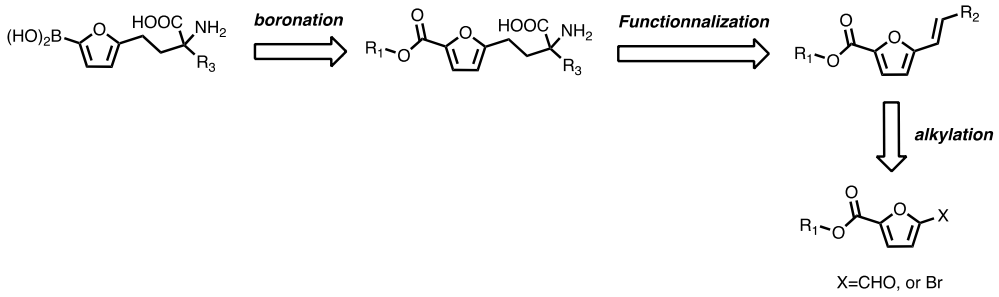

Figure 84: Retrosynthetic pathway for amino acid substituted 2-furanylboronic acids synthesis

According to this retrosynthetic scheme, a longer chain length can be envisioned to obtain a spacer between the furan ring and the amino acid part. Thus, starting from a furfural derivative (X=CHO) or a brominated derivative (X=Br), the alkylation can be performed via Knoevenagel,[191] Wittig,[192] aldol condensation for X=CHO,[193] and Heck when X=Br.[194] Then, functionalization of the previously added function (such as ester, carboxylic acid, or ketone) can be done via various reactions, depending on the starting one. Petasis reaction[195] from ketoacid or ketoester.[196] Strecker reaction[197] from aldehyde or ketone can also lead to amino acid function, as the Petasis reaction.[198] The similar Mannich reaction can lead to α and ß amino acids,[199] as the Petasis to δ amino acids.[200] Such a variety in obtaining possible products is attractive to increase the scope of pharmacomodulations. In the last step, the ester can be transform to bromine, [201] prior to the Miyaura borylation[202] of the furan to obtain boronic ester[203] or boronic acid of the desired compound.[204]

An alternative could be to stabilize the boronic acid function during the synthesis. This approach was performed for Suzuki couplings.[181] The *N*-methyliminodiacetate (MIDA) protecting group could be an elegant option (Figure 85) as it is known to generate "bench-stables" boronic acids.[167, 189, 205]

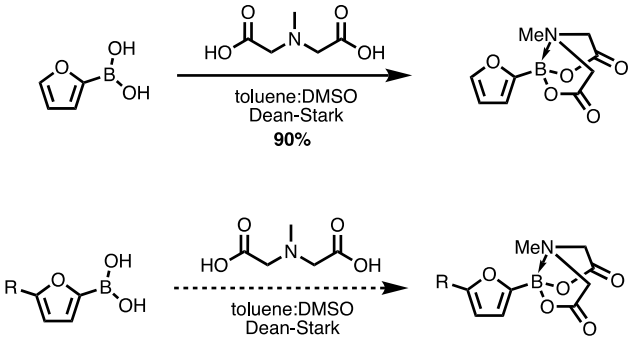

Figure 85: Protection of 2-furanyl boronic acid (top) and 2,5-disubstituted furanyl boronic acid (bottow)

Interestingly, this protecting group could open the perspective of an original Arg1 prodrug inhibitor, as this function could slowly deprotect under the mildly basic experimental conditions of the coupling.[167] A MIDA could also allow for improved pharmacological parameters such as bioavailability. This strategy was recently published in a patent of 2020, where a 3rd generation molecule was cyclized between the boronic acid and the amino acid part.[206]

Moreover, the chemistry of the 4-cyclohexylboronic acid **223** must be finalized by obtaining molecules that can be tested on Arg1.

Because targeting the catalytic site has several previously discussed drawbacks, a different approach to target oligomerization started in 2020. Our laboratory has now built a solid experience in targeting protein oligomerization. Targeting oligomerization can have many advantages, especially when catalytic site wiring is challenging, as recently reviewed by Thabault *et al.*[207] Arginase is an enzyme that is active as a trimer, but its activity partially is preserved when monomeric. Preventing the formation of the trimer or its disruption could lead to the

destruction of the enzyme by the cell, either by degron exposition or protein misfolding. (Figure 86)

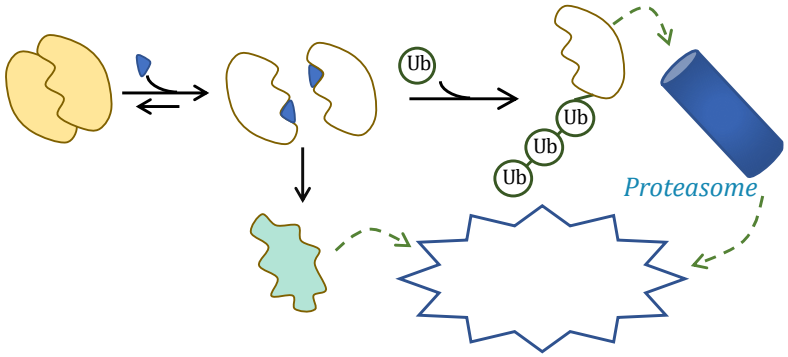

Figure 86: Homomeric disruption can promote protein degradation and misfolding. Disruption of a homomeric complex can lead to proteasome-dependent protein degradation because of degron exposition or protein misfolding resulting from intrinsic destabilization and chaperone-mediated degradation.[207]

The strategy of blocking or disrupting the oligomerization was performed in the past against lactate dehydrogenase (LDH) with stapled peptides.[208] Epitope mapping, as previously done with other targets,[209] will be performed to find the most important interfaces for trimerization and better understand the interaction pattern between each monomers. A preliminary *in silico* mapping has already been performed and has highlighted three different sequences involved in the oligomerization (Figure 87).

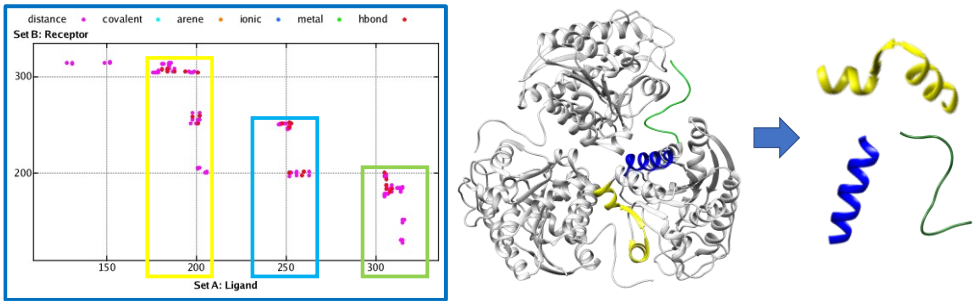

Figure 87: in silico epitope mapping of Arg1. Three different sequences have been shown to interact with another monomer. Yellow and blue sequences are helically folded, and the green sequence is the S-shaped C-terminal arm, where Arg308 is present. (Courtesy of Juhans Dechenne)

Recently, Gao et al. reported preliminary data on the effect of the C-terminal arm, in green in Figure 87, on the oligomerization of Arg1.[5] The pentapeptide with the final sequence of the arm (REGNH) showed an inhibition of 2.4 ± 0.3 mM, highlighting the real interest of this approach on Arg1.

The work of Juhans Dechenne already lead to a protocol of production and purification of Arg1 described in 3.1). Truncated Arg1 production was also performed, and optimization of biophysical methods for determination of a dissociation constant (K_D) by STD NMR, WATERLOGSY NMR, and microscale thermophoresis (MST) are in progress.

8 EXPERIMENTAL PART AND SUPPORTING INFORMATION

8.1 GENERAL INFORMATION

All chemicals were purchased from Sigma or Acros Organics and used without further purification. NMR spectra were recorded on a Bruker Ultrashield Advance II 400 MHz instrument using dimethyl sulfoxide (DMSO-d_6) or chloroform ($CDCl_3$) as deuterated solvent. Chemical shifts are reported in parts per million (ppm) and referenced to the residual solvent resonance. Coupling constants (J) are reported in hertz (Hz). Standard abbreviations indicating multiplicity were used as follows: s = singlet, d = doublet, t = triplet, dd = double doublet, q = quartet, m = multiplet, b = broad. Melting points (m.p.) were determined using an electrothermal apparatus and are reported uncorrected. LC-MS analyses were performed on an Agilent 6200 series TOF mass spectrometer equipped with ESI and APCI as ionization sources and TOF (Time Of Flight) detector, coupled with an Agilent 1200 series LC system with flux of 0.25 mL/min. High- resolution mass spectra were carried out on a Thermofisher Scientific LTQ-Orbitrap XL hybrid. X-ray diffraction data were collected at room temperature on a Gemini Ultra (Rigaku) diffractometer using Cu Ka (1.54584) radiation.

8.2 ARG1 ENZYMATIC ASSAY

Arginase inhibition was measured using a modified version of the fixed-point radioactive assay developed by Ruegg and Russell.[36] Assay mixtures contained 50 µL of 100 mM 2-(cyclohexylamino)ethanesulfonic acid (CHES)-NaOH (pH 9.0), 100 µM $MnCl_2$, 0.05 µCi of [guanidino- 14C]-L-arginine, 3 mM unlabeled L-arginine, and 5 µL of inhibitors in a 50 µL volume per centrifuge tube. Reactions were started by adding 5 µL of a 10 µg/mL recombinant human arginase

I solution. After 5 min, reactions were quenched by the addition of 400 µL of "stop" solution (0.25 mM acetic acid (pH 4.5), 7 M urea, 10 mM L-arginine, and a 1:1 (v/v) slurry of Dowex® W-X8 in water). Each reaction mixture was immediately vortexed for 30 s after adding the "stop" solution and then centrifuged at 6000 rpm for 10 min. 200 µL of the supernatant was taken and 3 mL of scintillation liquid (Ultima Gold™, PerkinElmer®) was added in preparation for liquid scintillation counting using a PerkinElmer® counter (model: Tri-Carb 2900TR). The DPM value obtained for the blank (containing no enzyme) was systematically subtracted. Results were then expressed as percent of control activity (without inhibitor), after which GraphPad prism software was used to treat the data and to analyze the dose- response curves. Inhibitor potency was expressed as IC_{50} values (Sigmoid standard curve, four parameters logistic, X is log of the concentration). Reference inhibitor ABH was purchased from Sigma- Aldrich/Merck.

8.3 EXPERIMENTAL PARTS FOR CHAPTER 4

8.3.1 Molecular dynamics

Crystal structures with the following code were retrieved from the Protein Data Bank (PDB): 3GMZ for the Arginase1-ornithine complex,[102] 2AEB for the arginase-ABH complex,[15] and 2PHA for the apo form of Arginase 1.[149] The complex cyclohexyboronic acid-arginase was manually built from the 2AEB crystal structure, replacing the amino acid and aliphatic side-chain of ABH by the cyclohexane of **272** using Molecular Operating Environment (MOE). All systems were prepared with the Maestro protein preparation tool to add hydrogens, remove the flexible and solvent exposed C-terminal loop 309-HKPIDYL-315, cap termini, and coordinate the ion cluster with zero bond order. Residues/atoms coordinating the first Mn^{2+} are HIS126/ND1, ASP234/OD1+2, ASP124/OD1, ASP232/OD2 and the second Mn^{2+} are ASP124/OD2, ASP128/OD2 HIS101/ ND1 and ASP232/OD2. Additionally, both manganese ions were coordinated by the charged oxygen of the hydroxide for

the apo form and the complex with ornithine, or the complexing oxygen of the inhibitor, OH of boronate for ABH. Using Desmond (version 11.0.014) with OPLS2005 force field, the three selected enzyme-ligand complexes were placed in an orthorhombic box filled with about explicit TIP3P water molecules and neutralizing counter ions (Na^+ or Cl^-). The total amount of atoms reached between 31k and 33k for all systems. Minimization and equilibration were performed for each system using default parameters. Then, ligand-enzyme complexes were simulated for 200 ns with periodic boundary conditions. A pressure of 1.01325 bars was kept constant using the Martyna-Tobias-Klein barostat method,[159] and a temperature of 300 K was kept constant with a Nose-Hoover thermostat.[210] Short-range electrostatic interactions were calculated up to a distance of 9 Å cut-off. and a temperature of 300 K was kept constant with a Nose-Hoover thermostat.[210] Short-range electrostatic interactions were calculated up to a distance of 9 Å cut-off. With RESPA integrator, constraints were used on all bonds with 2 fs time step length for bonded and near atoms, and 6 fs for far atoms. Each simulation was repeated five times and trajectories were concatenated before the dynophore analysis.

Using Gromacs (version 5.0.4-mpi,)[153] with Amber 99 sb force field,[211] the ornithine-Arginase1 complex was solvated with explicit water molecules (TIP3P) in a 168 nm^3 dodecahedron neutralized with Na^+ and Cl^- counterions. Topology for ornithine was generated using Antechamber[212] through the ACPYPE online platform.[213] Following steepest descent minimization, each complex was equilibrated for 0.1 ns using position restraints applied to all protein heavy atoms. Then each system was simulated for 200 ns (time step length = 2 fs), with periodic boundary conditions, using PMEelectrostatics (rcoulomb = 12 Å) with Amber 99 sb force field,[211] the ornithine-Arginase1 complex was solvated with explicit water molecules (TIP3P) in a 168 nm^3 dodecahedron neutralized with Na^+ and Cl^- counterions. Topology for ornithine was generated using Antechamber[212] through the ACPYPE online platform.[213] Following steepest descent minimization, each complex was equilibrated for 0.1 ns using position restraints applied to all protein

heavy atoms. Then each system was simulated for 200 ns (time step length = 2 fs), with periodic boundary conditions, using PMEelectrostatics (rcoulomb = 12 Å)[98] and Van der Waals interactions cut-off (rvdw = 12 Å). Constraints were used on all bonds in the peptides (LINCS algorithm)[214]. The Nosé-Hoover coupling method was used (temperature of 300 K)[210] together with the Parrinello-Rahman coupling method (pressure of 1 bar).[215] The ion cluster coordination was controlled using distance restrains and the charges of Mn^{2+} and OH^- were set manually to +2 and −1, respectively, and Van der Waals interactions cut-off (rvdw = 12 Å). Constraints were used on all bonds in the peptides (LINCS algorithm)[214]. The Nosé-Hoover coupling method was used (temperature of 300 K)[210] together with the Parrinello-Rahman coupling method (pressure of 1 bar).[215] The ion cluster coordination was controlled using distance restrains and the charges of Mn^{2+} and OH^- were set manually to +2 and −1, respectively.

Gromacs was used for all RMSD, RMSF and cluster analysis using the g_rms, g_rmsf and g_cluster tools, respectively (alignments always performed using Cα for least squares fit and RMSD calculations).[153] Pocket volume calculation was performed with Povme2.0[158]using default parameters. The coordinates of the boron atom as center of a 10 Å-radius sphere defined the pocket cavity. All simulations were conducted on a GPU, locally and on the high-performance computing system SOROBAN of the Freie Universität Berlin (http://www.zedat.fu-berlin. de/Compute).

8.3.2 Dynophore

The developed dynophore implementation automatically generates a pharmacophore for each frame of a given MD simulation and processes its pharmacophore features pursuing the following principle: Pharmacophore features detected during the simulation that are sharing the same interaction type (e.g., H-bond donor or hydrophobic contact) and the same ligand atoms are grouped into a

so-called superfeature. The occurrence of each superfeature is monitored in terms of spatial, statistical, and sequential behavior throughout the whole analyzed trajectory.

(a) Spatial information: Dynophores are built by superimposing the 3D-pharmacophores of all trajectory frames aligned on the target Cα atoms. Subsequently, each feature is reduced to the coordinates at the centroid of the detected feature sphere and the resulting dynophore is represented by clouds of points in three dimensions.

(b) Statistical information: The occurrence of each superfeature is monitored (superfeature occurrence frequency), whereby frequency is simply calculated relatively to the sum of all considered frames. Additionally, for each superfeature, all interaction with a partner on the target-side are also monitored (interaction occurrence frequency), whereby frequency is calculated relatively to the sum of the corresponding superfeature occurrences. Distance distributions are reported in histograms (interaction distance histogram) for each reported interaction.

(c) Sequential information: Occurrence of superfeatures and their interactions are described sequentially in form of bar code series (superfeature occurrence sequence and interaction occurrence sequence) as well as interaction distances in form of distances series (interaction distance sequence). The dynophore program has been implemented within the ilib/LigandScout framework.[216]

All features represented in the dynophore were extracted from 1 μs (5000 frames) of MD simulation trajectory (frames were recorded every 5 ns) with arginase 1 and L-ornithine, and arginase1 and inhibitor ABH and analyzed: Interactions of the same type detected for one single ligand atom were grouped in a so-called superfeature. For each superfeature, all detected interactions were analyzed and reported sequentially. Distances between all interaction partners were measured and plotted in a graph regarding their absolute frequency for each superfeature

Figure of the features and plots of the distances can be found in supporting information of related article: Mortier, J.; Prevost, J. R. C.; Sydow, D.; Teuchert,

S.; Omieczynski, C.; Bermudez, M.; Frederick, R.; Wolber, G., Arginase Structure and Inhibition: Catalytic Site Plasticity Reveals New Modulation Possibilities. *Sci Rep* **2017,** *7* (1), 13616.

8.3.3 Computational study of the cyclohexylboronic acid binding mode

A dynophore was created from MD simulations of arginase in complex with cyclohexylboronic acid **223** (Figure 88). Following the same method as introduced previously, Figure 88 represents the dynophore generated from 1 µs (5000 frames) of MD simulation trajectory (frames were recorded every 5 ns). All interactions of the same type detected for one single ligand atom are grouped in a superfeature. For each superfeature, all interactions are reported sequentially. Distance distributions are plotted for all interactions relatively to their absolute frequency.

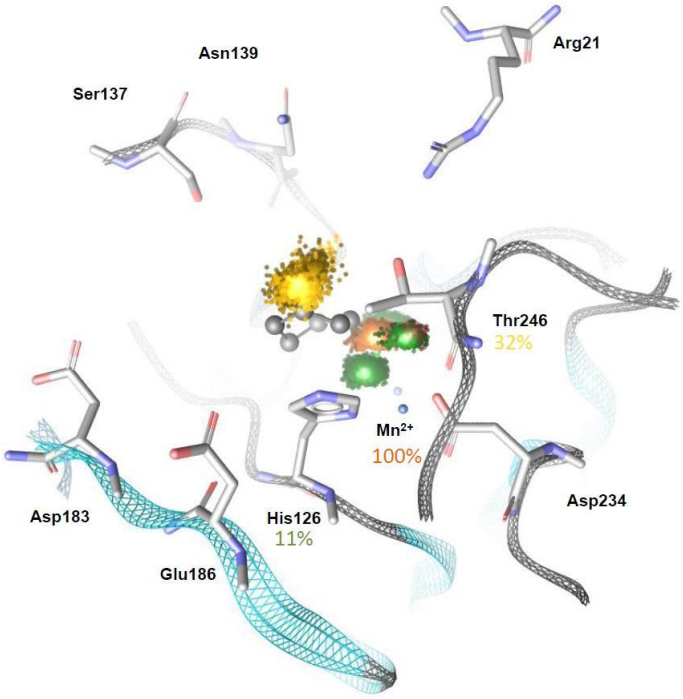

*Figure 88: Dynophore for the arginase-**223** complex (orange for negative ionizable features, green for H-bond donors, blue for positive ionizable moieties and yellow for hydrophobic contacts).*

8.4 EXPERIMENTAL PARTS FOR CHAPTERS 5 AND 6

8.4.1 Docking

All molecules of the chelating fragments library were constructed, and MM2 minimization was obtained with ChemDraw® and ChemBio3D® (PerkinElmer Informatics). Combinatory library of full compounds was built from the tail of three reference inhibitors (NED-3238 **44**,[104-106] CB1158 **45**, [105, 106] and proline-derived inhibitor **46**[108]) combined with the boronic acid fragment. Docking was performed with crystallographic structure 2AEB selected from Protein Data Bank (PDB) and with docking software GOLD® (CCDC) or AutoDock Vina.[164] For Vina, boron atom was switched for dummy carbon to be supported during processing.[165] Crystal structure with the code 2AEB was used because of its high resolution. Ligand-enzyme complexes were built in the cavity pocket by extracting and replacing the co-crystallized inhibitor ABH with the selected molecules. All systems were preliminarily prepared with Gold® to add hydrogens and removed selected water molecules. An enlarged cavity of 10 Å was generated around the proximal Mn^{2+} recorded as MN2362. Verification was conducted with co-crystallized molecules for other crystallographic structures available from the PDB. The scoring functions used were CHEMPLP (for the coordinating interaction with the metals), GOLDSCORE (for the polar interactions) and VINASCORE (for the hydrophobic interactions and steric fitting), with weighting by metallic atoms after determination of the most relevant function and used in combination with cross-referenced data. The generation of 20 solutions per molecule was obtained and visualized on a dedicated 3D screen.

8.4.2 Biological evaluation and docking results

Table 12: outcomes of biological evaluation crossed with in Silico analysis from docking

compound	MW (boronic acid)	Number of heavy atoms (boronate)	inhibition (mean) at 1mM	inhibition (SD) at 1mM	Goldscore	Normalized Goldscore	Chemplp	Normalized Chemplp	VinaScore	Normalized VinaScore
ABH	192	13	9,3	2	78,13	6,01	88,21	6,79	-6,7	5,15
220	119,088	8	50,3	17	69,32	8,67	62,05	7,76	-5,7	7,13
221	101,94	8	101,5	4	58,42	7,30	61,88	7,74	-5,7	7,13
222	131,088	9	101,2	3	66,58	7,40	64,99	7,22	-6,1	6,78
223	145,104	10	33,9	7	69,85	6,99	61,8	6,18	-6,1	6,10
224	128,052	15	75,8	0	66,6	4,44	62,41	4,16	-6,5	4,33
225	129,047	14	90	2	62,55	4,47	63,55	4,54	-6,9	4,93
226	228,104	16	70,3	3	65,34	4,08	68,27	4,27	-6,3	3,94
227	129,036	9	25,8	1	66,41	7,38	63,08	7,01	-6,7	7,44
228	129,036	9	80,3	1	63,89	7,10	68,95	7,66	-6,5	7,22
229	157,031	11	103,6	2	68,86	6,26	66,75	6,07	-7	6,36
230	145,013	9	89,1	6	70,27	7,81	63,68	7,08	-6,5	7,22
231	145,013	9	91	1	70,34	7,82	67,77	7,53	-6	6,67
232	140,052	10	71,4	0	64,28	6,43	60,73	6,07	-6,6	6,60
233	217,962	11	103,1	3	66	6,00	67,79	6,16	-6,8	6,18
234	140,052	10	72,9	2	65,22	6,52	65	6,50	-6,5	6,50
235	166,042	12	73,3	3	65,1	5,43	64,99	5,42	-6,9	5,75
236	141,047	10	88,3	7	66,3	6,63	65,98	6,60	-6,7	6,70
237	139,057	10	103,1	3	64,64	6,46	67,75	6,78	-6,5	6,50
238	155,052	11	92,6	4	71,86	6,53	67,48	6,13	-6,3	5,73
239	154,068	11	94,6	0	57,23	5,20	36,63	3,33	-6,5	5,91
240	175,038	12	62,1	1	58,09	4,84	56,73	4,73	-6,1	5,08
241	175,038	12	93,9	2	65,91	5,49	66,83	5,57	-6,8	5,67
242	164,052	12	99,2	7	67,77	5,65	66,51	5,54	-6,7	5,58
243	169,067	12	84,6	5	63,45	5,29	51,56	4,30	-6,8	5,67
244	203,028	13	94,3	17	52,33	4,03	69,96	5,38	-7,1	5,46
245	169,067	12	86,2	9	67,64	5,64	66,86	5,57	-6,8	5,67
246	167,052	12	54,6	2	65,65	5,47	70,31	5,86	-6,8	5,67
247	167,052	12	94	1	65,79	5,48	73,37	6,11	-6,9	5,75
248	254,12	18	100,5	0	59,41	3,30	72,56	4,03	-7,5	4,17
249	218,029	15	95,5	4	72,35	4,82	76,06	5,07	-7,4	4,93
250	246,061	14	32,1	3	68,69	4,91	69,11	4,94	-7,7	5,50
251	258,061	14	101,3	1	67,61	4,83	77,23	5,52	-7,5	5,36
252	262,056	15	87,4	7	66,09	4,41	75	5,00	-7,8	5,20
253	232,045	15	105,1	6	55,78	3,72	61,85	4,12	-7,6	5,07
254	182,039	13	84,4	9	56,5	4,35	70,23	5,40	-7,6	5,85
255	182,039	13	83,7	0	65,58	5,04	67,54	5,20	-7,1	5,46
256	182,062	14	94,7	9	63,25	4,52	60,78	4,34	-7,2	5,14
257	252,104	18	93	4	28,98	1,61	69,93	3,89	-8	4,44
258	222,094	16	96,5	1	63,04	3,94	64,93	4,06	-7,3	4,56
259	209,044	14	73,6	7	59,62	4,26	64,88	4,63	-7	5,00
260	161,95	13	88,4	2	66,72	5,13	60,78	4,68	-8,2	6,31

Inhibition and standard deviation (SD) are expressed in %

Normalized Goldscore and Chemplp are obtained with the following equation: Score/Number of Heavy atoms

*Normalized Vinascore is obtained with the following equation: (-10)*score/ Number of Heavy atoms.*

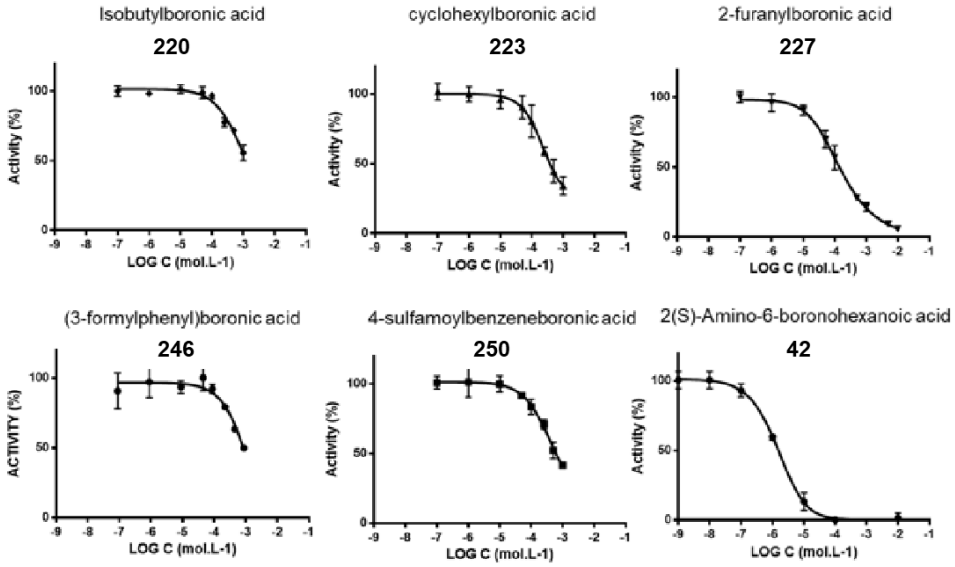

*Figure 89: Half maximal inhibitory concentration (IC_{50}) for **ABH 42**, **220**, **223**, **227**, **246** **250**. Maximal concentration of 1 mM instead of 10 mM was used for **220**, **223, 246,** and **250** due to solubility issues. Residual activities and standard deviations are reported from two distinct experiments in triplicates.*

8.4.3 Biological evaluation and comparison of furfurylamine and furanylcarboxylic acid

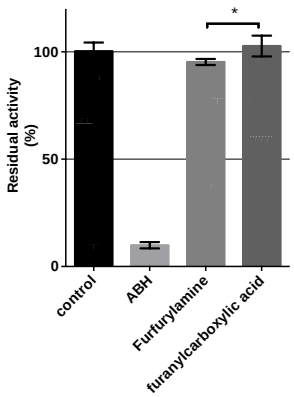

Figure 90: residual activity (%) of furfurylamine and 2-furanylcarboxylic acid on Arg1 at 1 mM

8.4.4 Biophysical evaluation

Saturation-Transfer Difference NMR. All experiments were performed on a Bruker Ascend Avance III 600 MHz system equipped with a broadband cryoprobe (BBO H&F) (Bruker). Samples were prepared in PBS containing 10% D_2O and 100 µM $MnCl_2$. The concentration of Arg1 was set to 15 µM of monomer. Ligand binding was detected using an STD stddiffesgp.3 sequence with a 2 s saturation time. Water signal suppression was achieved using an excitation-sculpting scheme, and a 50 ms spinlock was used to suppress protein background signals. Experiments were performed at 298 K. For each experiment, 1024 scans were collected on (0 ppm) and off-resonance (40 ppm) to yield a 32k points free induction decay (FID).

Signal reduction was measured by the integration of ornithine signals between 1.8 and 2.0 ppm. Spectrum of L-ornithine and Arg1 is in red and the top. Spectrum of the competition between 1 mM of **264** and L-ornithine is in blue on the bottom. Integration is decreased of 50% by the competition with **264**.

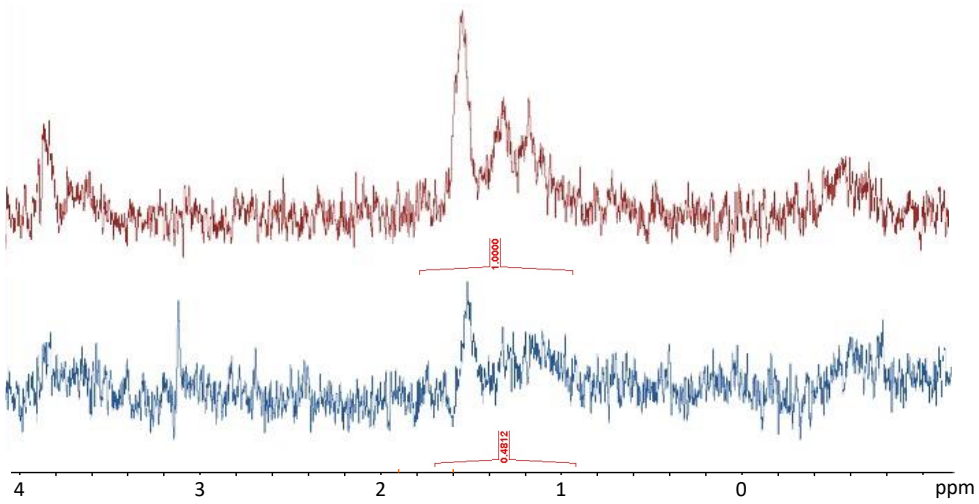

*Figure 91: STD of L-Orn **2** . Spectrum of L-ornithine **2** and Arg1 is in red and the top. Spectrum of the competition between 1 mM of **264** and L-ornithine is in blue at the bottom.*

8.4.5 Synthesis procedure

General procedure for the synthesis of (5-tertiary-amine-methylfuran-2-yl)boronic acid:

To a solution of 5-formyl-2-furanylboronic acid (1.0 eq, 0.5 mmol, 75 mg) in methanol (5 mL) was added the amine (10 eq, 5 mmol) and pH was adjusted with acetic acid (±0.5 mL). Sodium cyanoborohydride (0.6 eq, 0.6 mmol, 43 mg) was then added in one portion to the solution. The solution was stirred at room temperature until completion, followed by TLC.

Note: in the following NMR reports, the carbon linked to the boron is generally note reported due to its long relaxing time.

(5-formylfuran-2-yl)boronic acid **261**

A solution of 2-(furan-2-yl)-1,3-dioxolane (1.0 eq., 3.34 mL, 28.3 mmol) in THF (43 mL) was cooled at -78°C with an acetone/dry ice bath under inert conditions (N_2 atmosphere). Tertio-butyllithium (1.7 M in pentane, 25 mL, 1.5 eq., 42.5 mmol) was added dropwise. The solution was then stirred for 1h30. Triisopropylborate (1.0 eq., 12.8 mmol) was added dropwise, and the solution was stirred for an additional 2h. Methanol (23 mL) was carefully added, the mixture was stirred for 15 min, before the reaction was warmed up slowly at 0°C (ice bath) for the slow addition of aqueous hydrochloric acid (2 M, 40 mL). The solution was concentrated, and the resulting oil was purified by silica column (DCM/MeOH) to obtain a light-brown powder. Yield: 34% ^{1}H NMR (400 MHz, DMSO) δ 9.67 (s, 1H), 7.48 (d, J = 3.5 Hz, 1H), 7.23 (d, J = 3.5 Hz, 1H). ^{13}C NMR (101 MHz, DMSO) δ 179.56 (1C), 155.40 (1C), 123.45 (1C), 122.95 (1C).

2-(furan-2-yl)-1,3-dioxolane **262**

To a solution of freshly distilled furfural (1.0 eq, 4.14 mL, 50 mmol) in benzene (50 mL) was added dry sulfate magnesium (12 g), ethylene glycol (2 eq, 5.58 mL, 10 mmol) and PTSA (0.025 eq) as catalyst. The flask was fitted with a Dean-Stark

trap and reflux condenser. The mixture was stirred at reflux overnight. After filtration and wash with toluene, the solution was concentrated. The resulting oil was purified on silica gel chromatography (cyclohexane/ethyl acetate) to give the pure product as colorless oil. Yield: 60% ^{1}H NMR (400 MHz, CDCl3) δ 7.42 (d, J = 0.8 Hz, 1H), 6.45 (d, J = 3.1 Hz, 1H), 6.35 (dd, J = 3.1, 1.8 Hz, 1H), 5.92 (s, 1H), 4.27 – 3.92 (m, 4H). ^{13}C NMR (101 MHz, CDCl3) δ 151.03 (1C), 143.18 (1C), 110.15 (1C), 108.78 (1C), 97.71 (1C), 65.16 (2C).

(5-((methylamino)methyl)furan-2-yl)boronic acid **264**

(5-formylfuran-2-yl)boronic acid (1 eq, 500 mg, 3.6 mmol) and methyl amine (3.0 eq, 0.9 mL, 0.4 M, 33% in ethanol, 10.9 mmol) were dissolved in dry MeOH under inert atmosphere and 3 Å molecular sieves (1 g) were added. The mixture was stirred at room temperature for 1h30, where the mixture was cooled to 0°C in an ice bath. $NaBH_4$ (1.1 eq, 152 mg, 4 mmol) was added portion wise. After the addition, the mixture was stirred for 10 min at 0°C, and then 1h30 at room temperature. After filtration and concentration, the crude mixture was purified by trituration with MeCN to afford the pure product as very hydroscopic white powder. Quantitative. ^{1}H NMR (400 MHz, Methanol-d4) δ 6.25 (d, J = 3.1 Hz, 2H), 3.92 (s, 2H), 2.48 (s, 3H). ^{13}C NMR (101 MHz, MeOD) δ 147.72 (1C), 112.91 (1C), 109.00 (1C), 46.05 (1C), 32.43 (1C).

General procedure for synthesis (5-tertiary-amine-methylfuran-2-yl)boronic acid **265-277**

To a solution of 5-formyl-2-furanylboronic acid (1.0 eq, 0.5 mmol, 75 mg) in methanol (5 mL) was added the amine (10 eq, 5 mmol) and pH was adjusted with acetic acid (0.5 mL). Sodium cyanoborohydride (0.6 eq, 0.6 mmol, 43 mg) was then added in one portion to the solution. The solution was stirred at room temperature until completion, followed by TLC.

Note:

Conversion of the starting material (5-formyl-2-furanylboronic acid **261**) was observed by NMR analysis. However, due to product stability issue (protodeboronation), all ^{13}C NMR data were not obtained due to the longer acquisition time needed.

Example: (5-((dimethylamino)methyl)furan-2-yl)boronic acid **265** spectra are reported bellow. Crude mixture, pure product and protodeboronated compound spectra are present.

(5-((dimethylamino)methyl)furan-2-yl)boronic acid **265**

The title compound was prepared following the general procedure. ^{1}H NMR (400 MHz, methanol-d_4) δ 6.62 (d, J = 3.2 Hz, 3H), 6.52 (d, J = 3.2 Hz, 3H), 4.43 (d, J = 12.8 Hz, 1H), 4.37 (s, 6H), 2.92 – 2.81 (m, 2H), 2.85 (s, 6H). ^{13}C NMR (101 MHz, methanol-d_4) δ 144.19 (1C), 116.27 (1C), 113.99 (1C), 52.87 (1C), 41.21 (2C). HRMS: calc. for $C_7H_{13}BNO_3$ $(M+H)^+$: 170.09830, found: 170.09779.

(5-(aminomethyl)furan-2-yl)boronic acid **266**

As described, the compound was not obtained in these conditions

(5-((diethylamino)methyl)furan-2-yl)boronic acid **267**

The title compound was prepared following the general procedure. ^{1}H NMR (400 MHz, MeOD) 6.51 (d, J = 3.0 Hz, 1H), 6.25 (d, J = 3.1 Hz, 1H), 4.34 (s, 2H), 3.14 (q, J = 7.1 Hz, 4H), 1.33 (t, J = 7.0 Hz, 6H). ^{13}C NMR (101 MHz, MeOD) δ 153.25 (1C), 141.69 (1C), 113.24 (1C), 107.19 (1C), 56.35 (1C), 46.80 (2C), 41.92 (2C). HRMS: calc. for $C_9H_{17}BNO_3$ $(M+H)^+$: 198.04845, found: 198.10839.

(5-(((2-hydroxyethyl)amino)methyl)furan-2-yl)boronic acid **268**

As described, the compound was not obtained in these conditions

(5-(((2-hydroxyethyl)(methyl)amino)methyl)furan-2-yl)boronic acid **269**

As described, the compound was not purified from the buffered crude.

(5-(((2-morpholinoethyl)amino)methyl)furan-2-yl)boronic acid **270**

As described, the compound was not purified from the buffered crude.

(5-((morpholinoamino)methyl)furan-2-yl)boronic acid **271**

As described, the compound was not purified from the buffered crude.

(5-(pyrrolidin-1-ylmethyl)furan-2-yl)boronic acid **272**

The title compound was prepared following the general procedure. ^{1}H NMR (400 MHz, methanol-d_4) δ 7.04 (d, J = 3.4 Hz, 1H), 6.69 (d, J = 3.3 Hz, 1H), 4.48 (s, 2H), 3.60 – 3.47 (m, 2H), 3.29 – 3.17 (m, 2H), 2.39 – 1.95 (m, 4H). HRMS: calc. for $C_9H_{15}BNO_3$ $(M+H)^+$: 196.11395, found: 196.11352

(5-(piperidin-1-ylmethyl)furan-2-yl)boronic acid **273**

The title compound was prepared following the general procedure. ^{1}H NMR (400 MHz, methanol-d_4) δ 7.05 (d, J = 3.4 Hz, 1H), 6.71 (d, J = 3.4 Hz, 1H), 4.39 (s, 2H), 3.47 (dd, J = 12.2, 3.2 Hz, 2H), 2.96 (td, J = 12.6, 3.2 Hz, 2H), 2.11 – 1.71 (m, 6H). HRMS: calc. for $C_{10}H_{17}BNO_3$ $(M+H)^+$: 210.12960, found: 210.12925.

(5-((3-hydroxyazetidin-1-yl)methyl)furan-2-yl)boronic acid **274**

As described, the compound was not purified from the buffered crude.

(5-(morpholinomethyl)furan-2-yl)boronic acid **275**

The title compound was prepared following the general procedure. ^{1}H NMR (400 MHz, D_2O) δ 6.86 (d, J = 3.5 Hz, 1H), 6.51 (d, J = 3.4 Hz, 1H), 4.57 (s, 2H), 4.07 (m, 2H), 3.74 (m, 2H), 2.97 (m, 4H). ^{13}C NMR (101 MHz, D_2O) δ 148.51 (1C),

142.32 (1C), 121.70 (1C), 113.98 (1C), 64.41 (2C), 52.81 (1C), 51.37 (2C). HRMS: calc. for $C_9H_{15}BNO_3$ $(M+H)^+$: 212.10886, found: 212.10839.

(5-(thiomorpholinomethyl)furan-2-yl)boronic acid **276**

The title compound was prepared following the general procedure.^{1}H NMR (400 MHz, methanol-d_4) δ 6.61 (d, J = 3.1 Hz, 1H), 6.50 (d, J = 3.0 Hz, 1H), 4.49 (s, 2H), 3.33 (s, 8H). HRMS: calc. for $C_9H_{15}BNO_3$ $(M+H)^+$: 228.08602, found: 228.08500.

8.4.6 NMR spectra

2-(furan-2-yl)-1,3-dioxolane **262**

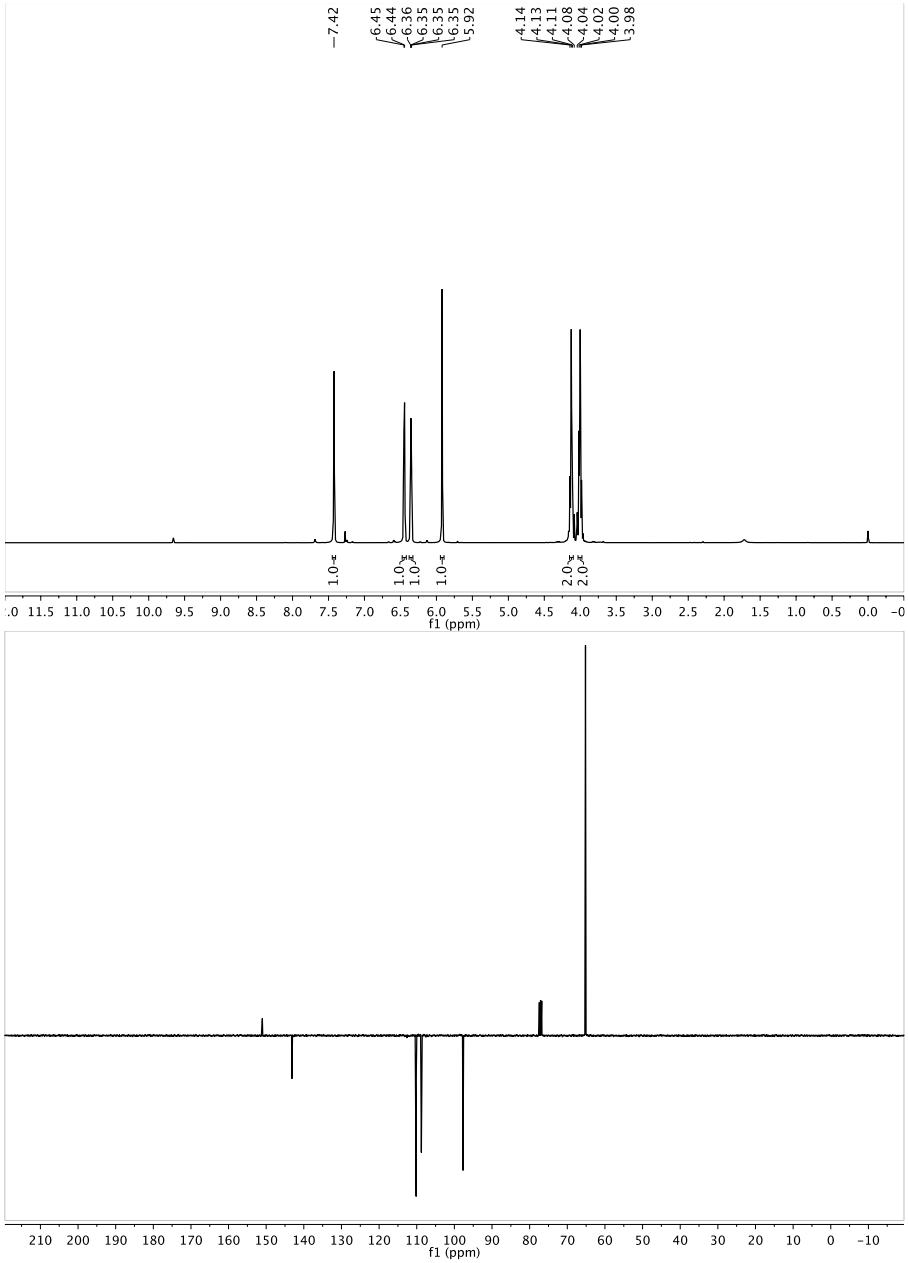

(5-formylfuran-2-yl)boronic acid **263**

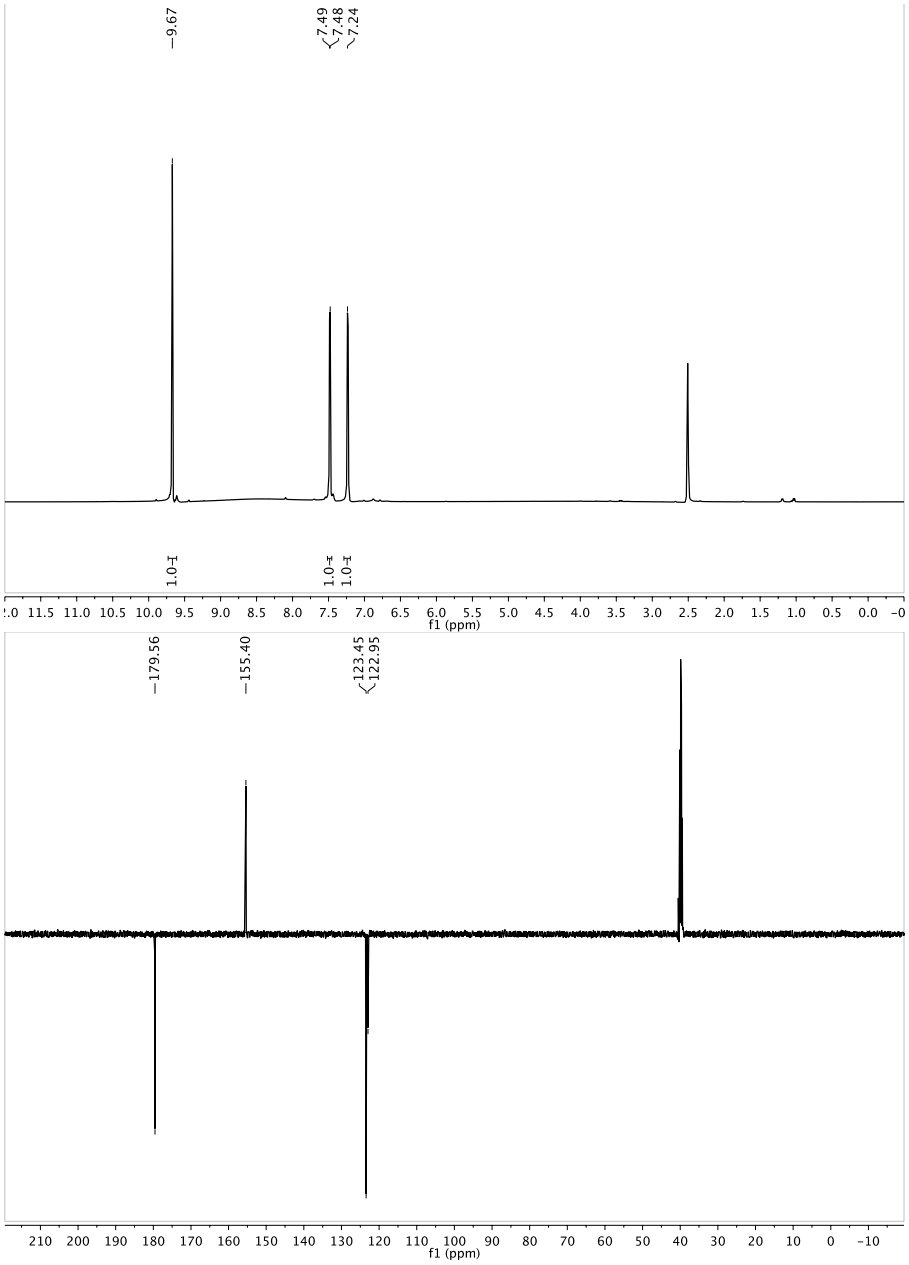

(5-((methylamino)methyl)furan-2-yl)boronic acid **264**

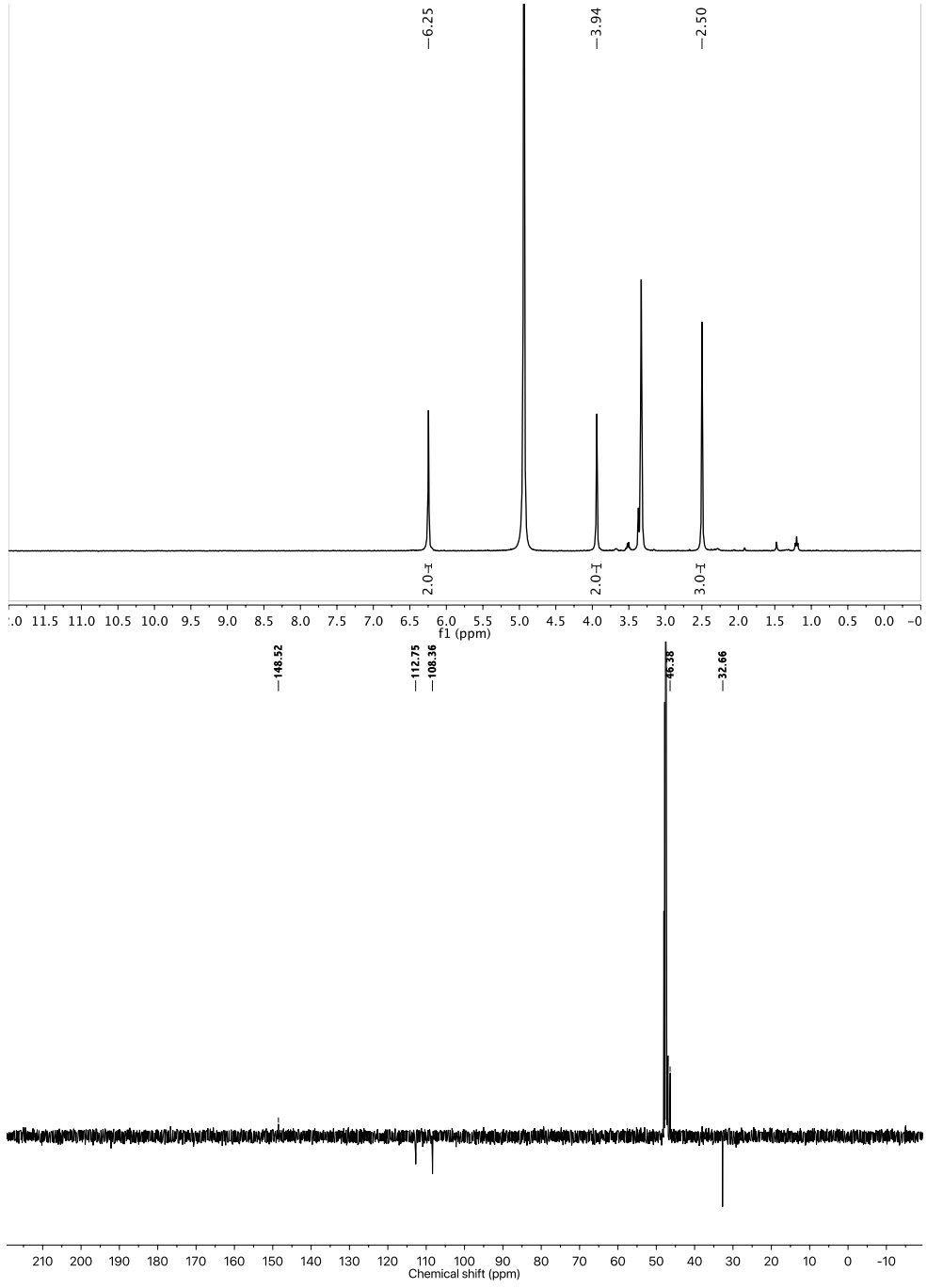

(5-((dimethylamino)methyl)furan-2-yl)boronic acid **265**:

Crude mixture after concentration (in MeOD):

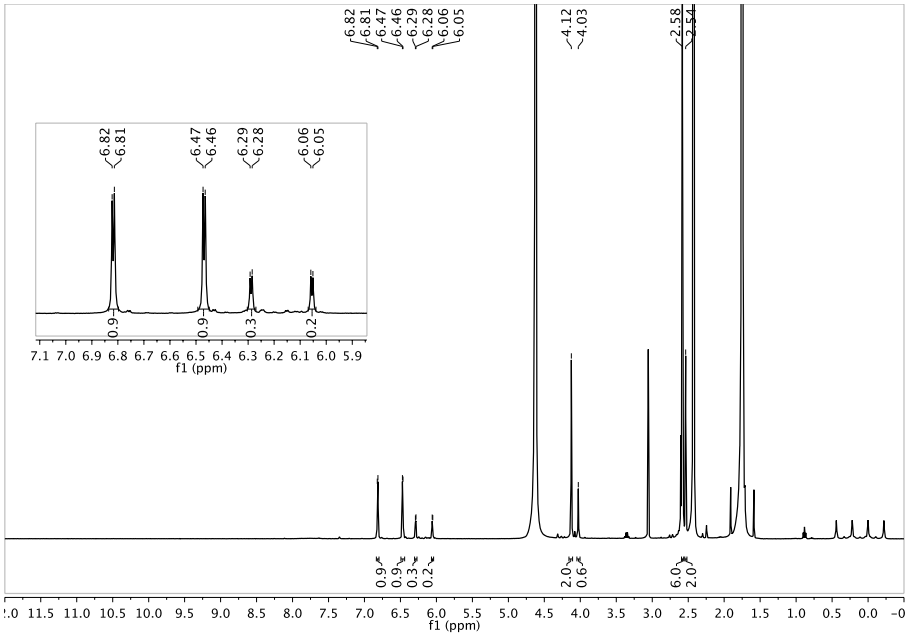

(5-((dimethylamino)methyl)furan-2-yl)boronic acid **265**: Pure: ^{1}H

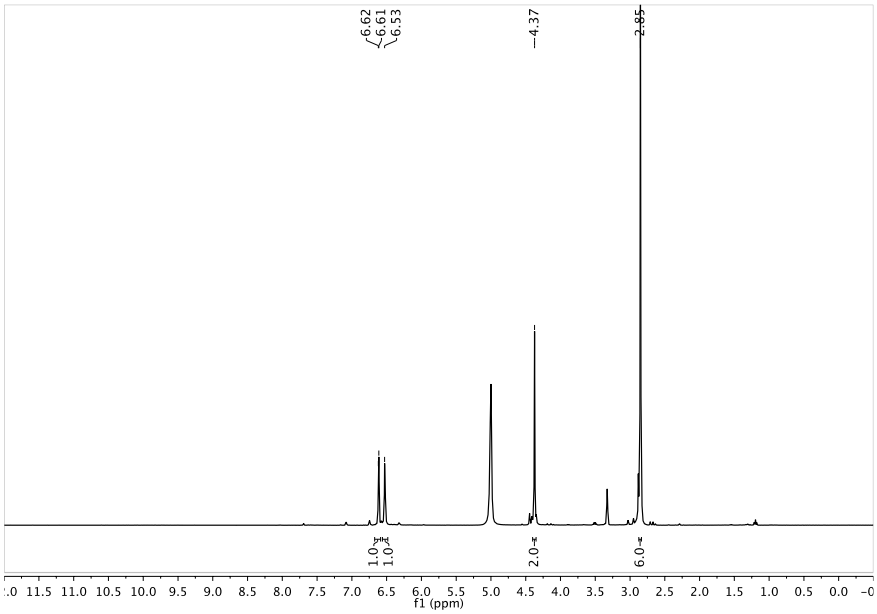

(5-((dimethylamino)methyl)furan-2-yl)boronic acid **265**: Pure^{13}C

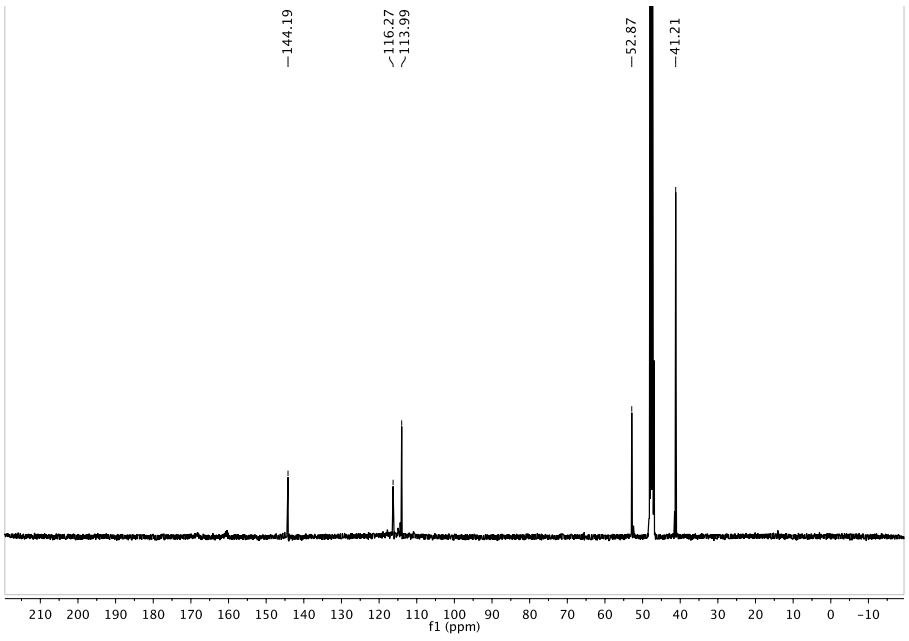

(5-((dimethylamino)methyl)furan-2-yl)boronic acid **265**: HMBC

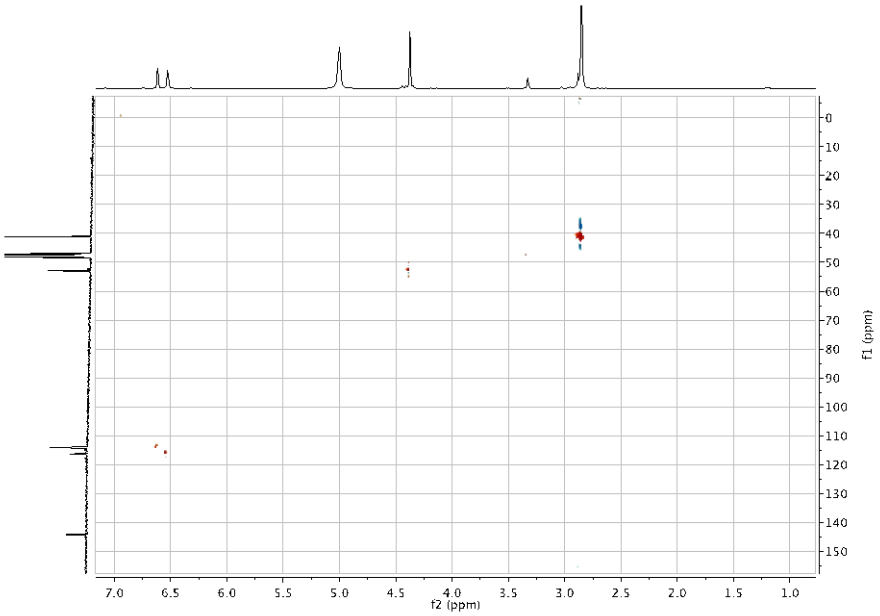

(5-((dimethylamino)methyl)furan-2-yl)boronic acid **265**: HSQC

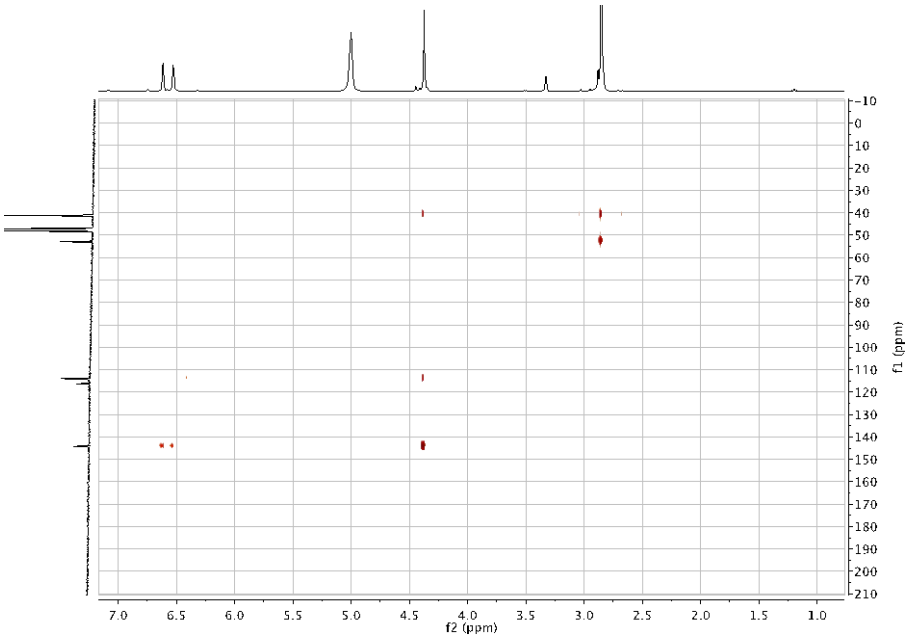

Protodeboronated product from synthesis' crude of **265**:

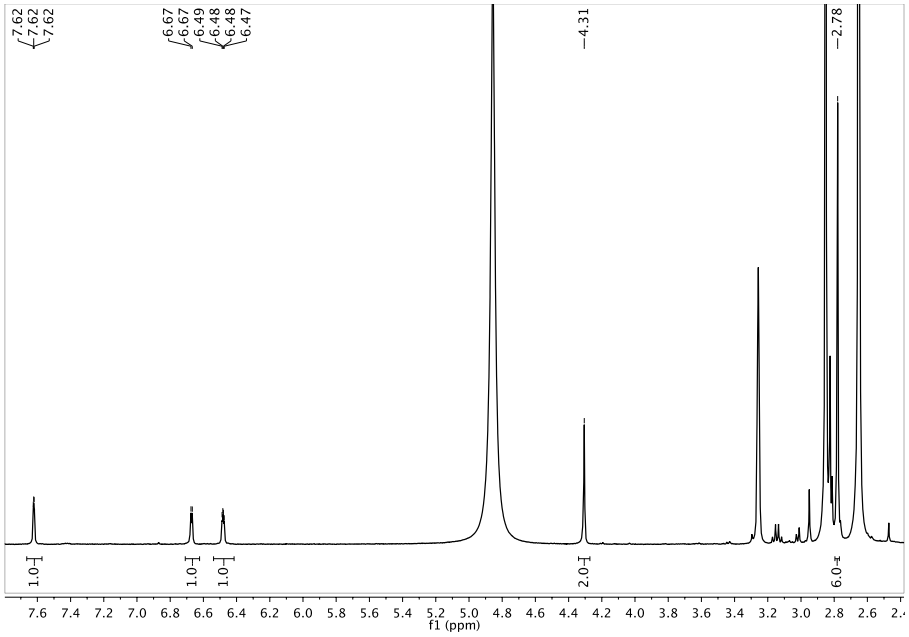

Isolated protodeboronated product from synthesis of **265**:

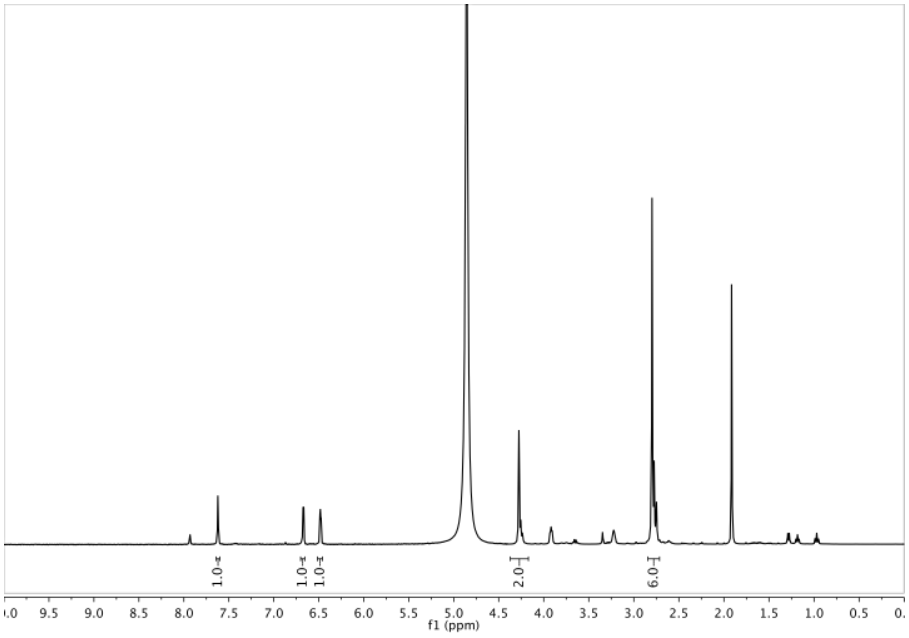

9 REFERENCES

(1) Lavulo, L. T.; Sossong, T. M., Jr.; Brigham-Burke, M. R.; Doyle, M. L.; Cox, J. D.; Christianson, D. W.; Ash, D. E. Subunit-subunit interactions in trimeric arginase. Generation of active monomers by mutation of a single amino acid. *J Biol Chem* **2001**, *276* (17), 14242-14248.
(2) Mora, A.; del Ara Rangel, M.; Fuentes, J. M.; Soler, G.; Centeno, F. Implications of the S-shaped domain in the quaternary structure of human arginase. *Biochim Biophys Acta* **2000**, *1476* (2), 181-190.
(3) Garcia, D.; Uribe, E.; Lobos, M.; Orellana, M. S.; Carvajal, N. Studies on the functional significance of a C-terminal S-shaped motif in human arginase type I: essentiality for cooperative effects. *Arch Biochem Biophys* **2009**, *481* (1), 16-20.
(4) Kanyo, Z. F.; Chen, C. Y.; Daghigh, F.; Ash, D. E.; Christianson, D. W. Crystallization and oligomeric structure of rat liver arginase. *J Mol Biol* **1992**, *224* (4), 1175-1177.
(5) Gao, K.; Lunev, S.; van den Berg, M. P. M.; Al-Dahmani, Z. M.; Evans, S.; Mertens, D.; Meurs, H.; Gosens, R.; Groves, M. R. A synthetic peptide as an allosteric inhibitor of human arginase I and II. *Mol Biol Rep* **2021**, *48* (2), 1959-1966.
(6) Kanyo, Z. F.; Scolnick, L. R.; Ash, D. E.; Christianson, D. W. Structure of a unique binuclear manganese cluster in arginase. *Nature* **1996**, *383* (6600), 554-557.
(7) Christianson, D. W. Arginase: structure, mechanism, and physiological role in male and female sexual arousal. *Acc Chem Res* **2005**, *38* (3), 191-201.
(8) D'Antonio, E. L.; Hai, Y.; Christianson, D. W. Structure and function of non-native metal clusters in human arginase I. *Biochemistry* **2012**, *51* (42), 8399-8409.
(9) Shishova, E. Y.; Di Costanzo, L.; Emig, F. A.; Ash, D. E.; Christianson, D. W. Probing the specificity determinants of amino acid recognition by arginase. *Biochemistry* **2009**, *48* (1), 121-131.
(10) G, S. C.; van Waarde, A.; I, F. A.; Domling, A.; P, H. E. Arginase as a Potential Biomarker of Disease Progression: A Molecular Imaging Perspective. *Int J Mol Sci* **2020**, *21* (15).
(11) Grauffel, C.; Lim, C. Factors governing when a metal-bound water is deprotonated in proteins. *Phys Chem Chem Phys* **2018**, *20* (47), 29625-29636.

(12) Cavalli, R. C.; Burke, C. J.; Kawamoto, S.; Soprano, D. R.; Ash, D. E. Mutagenesis of rat liver arginase expressed in Escherichia coli: role of conserved histidines. *Biochemistry* **1994**, *33* (35), 10652-10657.
(13) Jackson, V. E.; Felmy, A. R.; Dixon, D. A. Prediction of the pKa's of aqueous metal ion +2 complexes. *J Phys Chem A* **2015**, *119* (12), 2926-2939. Gilson, R.; Durrant, M. C. Estimation of the pKa values of water ligands in transition metal complexes using density functional theory with polarized continuum model solvent corrections. *Dalton Trans* **2009**, (46), 10223-10230.
(14) D'Antonio, E. L.; Christianson, D. W. Crystal structures of complexes with cobalt-reconstituted human arginase I. *Biochemistry* **2011**, *50* (37), 8018-8027.
(15) Di Costanzo, L.; Sabio, G.; Mora, A.; Rodriguez, P. C.; Ochoa, A. C.; Centeno, F.; Christianson, D. W. Crystal structure of human arginase I at 1.29-A resolution and exploration of inhibition in the immune response. *Proc Natl Acad Sci U S A* **2005**, *102* (37), 13058-13063.
(16) Vockley, J. G.; Goodman, B. K.; Tabor, D. E.; Kern, R. M.; Jenkinson, C. P.; Grody, W. W.; Cederbaum, S. D. Loss of function mutations in conserved regions of the human arginase I gene. *Biochem Mol Med* **1996**, *59* (1), 44-51.
(17) Reczkowski, R. S.; Ash, D. E. Rat liver arginase: kinetic mechanism, alternate substrates, and inhibitors. *Arch Biochem Biophys* **1994**, *312* (1), 31-37.
(18) Maarsingh, H.; Zaagsma, J.; Meurs, H. Arginase: a key enzyme in the pathophysiology of allergic asthma opening novel therapeutic perspectives. *Br J Pharmacol* **2009**, *158* (3), 652-664.
(19) Nick Pace, C.; Landers, R. A. Arginase inhibition. *Biochimica et Biophysica Acta (BBA) - Enzymology* **1981**, *658* (2), 410-412.
(20) Pernow, J.; Jung, C. Arginase as a potential target in the treatment of cardiovascular disease: reversal of arginine steal? *Cardiovasc Res* **2013**, *98* (3), 334-343.
(21) Ryoo, S.; Lemmon, C. A.; Soucy, K. G.; Gupta, G.; White, A. R.; Nyhan, D.; Shoukas, A.; Romer, L. H.; Berkowitz, D. E. Oxidized low-density lipoprotein-dependent endothelial arginase II activation contributes to impaired nitric oxide signaling. *Circ Res* **2006**, *99* (9), 951-960.
(22) Xiong, Y.; Yepuri, G.; Forbiteh, M.; Yu, Y.; Montani, J. P.; Yang, Z.; Ming, X. F. ARG2 impairs endothelial autophagy through regulation of MTOR and PRKAA/AMPK signaling in advanced atherosclerosis. *Autophagy* **2014**, *10* (12), 2223-2238.

(23) Schaaf, M. B.; Houbaert, D.; Mece, O.; Agostinis, P. Autophagy in endothelial cells and tumor angiogenesis. *Cell Death Differ* **2019**, *26* (4), 665-679.
(24) Steppan, J.; Nyhan, D.; Berkowitz, D. E. Development of novel arginase inhibitors for therapy of endothelial dysfunction. *Front Immunol* **2013**, *4*, 278.
(25) Iyer, R. K.; Yoo, P. K.; Kern, R. M.; Rozengurt, N.; Tsoa, R.; O'Brien, W. E.; Yu, H.; Grody, W. W.; Cederbaum, S. D. Mouse model for human arginase deficiency. *Mol Cell Biol* **2002**, *22* (13), 4491-4498.
(26) Sin, Y. Y.; Ballantyne, L. L.; Mukherjee, K.; St Amand, T.; Kyriakopoulou, L.; Schulze, A.; Funk, C. D. Inducible arginase 1 deficiency in mice leads to hyperargininemia and altered amino acid metabolism. *PLoS One* **2013**, *8* (11), e80001.
(27) Ballantyne, L. L.; Sin, Y. Y.; Al-Dirbashi, O. Y.; Li, X.; Hurlbut, D. J.; Funk, C. D. Liver-specific knockout of arginase-1 leads to a profound phenotype similar to inducible whole body arginase-1 deficiency. *Mol Genet Metab Rep* **2016**, *9*, 54-60.
(28) Marti, I. L. A. A.; Reith, W. Arginine-dependent immune responses. *Cell Mol Life Sci* **2021**, *78* (13), 5303-5324. Keshet, R.; Szlosarek, P.; Carracedo, A.; Erez, A. Rewiring urea cycle metabolism in cancer to support anabolism. *Nat Rev Cancer* **2018**, *18* (10), 634-645.
(29) Aktan, F. iNOS-mediated nitric oxide production and its regulation. *Life Sci* **2004**, *75* (6), 639-653.
(30) Mori, M. Regulation of nitric oxide synthesis and apoptosis by arginase and arginine recycling. *J Nutr* **2007**, *137* (6 Suppl 2), 1616S-1620S.
(31) Jensen, J. V.; Wendisch, V. F. Ornithine cyclodeaminase-based proline production by Corynebacterium glutamicum. *Microb Cell Fact* **2013**, *12*, 63.
(32) Szefel, J.; Danielak, A.; Kruszewski, W. J. Metabolic pathways of L-arginine and therapeutic consequences in tumors. *Adv Med Sci* **2019**, *64* (1), 104-110.
(33) Fleming, V.; Hu, X.; Weber, R.; Nagibin, V.; Groth, C.; Altevogt, P.; Utikal, J.; Umansky, V. Targeting Myeloid-Derived Suppressor Cells to Bypass Tumor-Induced Immunosuppression. *Front Immunol* **2018**, *9*, 398.
(34) Yoshimura, A.; Naka, T.; Kubo, M. SOCS proteins, cytokine signalling and immune regulation. *Nat Rev Immunol* **2007**, *7* (6), 454-465.
(35) Bagnost, T.; Ma, L.; da Silva, R. F.; Rezakhaniha, R.; Houdayer, C.; Stergiopulos, N.; Andre, C.; Guillaume, Y.; Berthelot, A.; Demougeot, C. Cardiovascular effects of arginase inhibition in spontaneously hypertensive rats with fully developed hypertension. *Cardiovasc Res* **2010**, *87* (3), 569-577.

(36) Lorenzen, J. M.; Uckert, S.; Scheller, F.; Haller, H.; Kuczyk, M. A. Effects of arginase inhibitors on the contractile and relaxant responses of isolated human penile erectile tissue. *World J Urol* **2009**, *27* (6), 805-810.
(37) Romero, M. J.; Platt, D. H.; Tawfik, H. E.; Labazi, M.; El-Remessy, A. B.; Bartoli, M.; Caldwell, R. B.; Caldwell, R. W. Diabetes-induced coronary vascular dysfunction involves increased arginase activity. *Circ Res* **2008**, *102* (1), 95-102.
(38) Santhanam, L.; Christianson, D. W.; Nyhan, D.; Berkowitz, D. E. Arginase and vascular aging. *J Appl Physiol (1985)* **2008**, *105* (5), 1632-1642.
(39) Jung, C.; Gonon, A. T.; Sjoquist, P. O.; Lundberg, J. O.; Pernow, J. Arginase inhibition mediates cardioprotection during ischaemia-reperfusion. *Cardiovasc Res* **2010**, *85* (1), 147-154. Yang, Z.; Ming, X. F. Functions of arginase isoforms in macrophage inflammatory responses: impact on cardiovascular diseases and metabolic disorders. *Front Immunol* **2014**, *5*, 533.
(40) Chung, J. H.; Moon, J.; Lee, Y. S.; Chung, H. K.; Lee, S. M.; Shin, M. J. Arginase inhibition restores endothelial function in diet-induced obesity. *Biochem Biophys Res Commun* **2014**, *451* (2), 179-183. El Assar, M.; Angulo, J.; Santos-Ruiz, M.; Ruiz de Adana, J. C.; Pindado, M. L.; Sanchez-Ferrer, A.; Hernandez, A.; Rodriguez-Manas, L. Asymmetric dimethylarginine (ADMA) elevation and arginase up-regulation contribute to endothelial dysfunction related to insulin resistance in rats and morbidly obese humans. *J Physiol* **2016**, *594* (11), 3045-3060.
(41) D'Antonio, E. L.; Ullman, B.; Roberts, S. C.; Dixit, U. G.; Wilson, M. E.; Hai, Y.; Christianson, D. W. Crystal structure of arginase from Leishmania mexicana and implications for the inhibition of polyamine biosynthesis in parasitic infections. *Arch Biochem Biophys* **2013**, *535* (2), 163-176.
(42) Wesolowski, R.; Markowitz, J.; Carson, W. E., 3rd. Myeloid derived suppressor cells - a new therapeutic target in the treatment of cancer. *J Immunother Cancer* **2013**, *1*, 10. Raber, P.; Ochoa, A. C.; Rodriguez, P. C. Metabolism of L-arginine by myeloid-derived suppressor cells in cancer: mechanisms of T cell suppression and therapeutic perspectives. *Immunol Invest* **2012**, *41* (6-7), 614-634.
(43) Gabrilovich, D. I.; Nagaraj, S. Myeloid-derived suppressor cells as regulators of the immune system. *Nat Rev Immunol* **2009**, *9* (3), 162-174.

(44) Elliott, L. A.; Doherty, G. A.; Sheahan, K.; Ryan, E. J. Human Tumor-Infiltrating Myeloid Cells: Phenotypic and Functional Diversity. *Front Immunol* **2017**, *8*, 86. Ouzounova, M.; Lee, E.; Piranlioglu, R.; El Andaloussi, A.; Kolhe, R.; Demirci, M. F.; Marasco, D.; Asm, I.; Chadli, A.; Hassan, K. A.; et al. Monocytic and granulocytic myeloid derived suppressor cells differentially regulate spatiotemporal tumour plasticity during metastatic cascade. *Nat Commun* **2017**, *8*, 14979. Youn, J. I.; Gabrilovich, D. I. The biology of myeloid-derived suppressor cells: the blessing and the curse of morphological and functional heterogeneity. *Eur J Immunol* **2010**, *40* (11), 2969-2975.
(45) Xu, L.; Hilliard, B.; Carmody, R. J.; Tsabary, G.; Shin, H.; Christianson, D. W.; Chen, Y. H. Arginase and autoimmune inflammation in the central nervous system. *Immunology* **2003**, *110* (1), 141-148.
(46) Veglia, F.; Perego, M.; Gabrilovich, D. Myeloid-derived suppressor cells coming of age. *Nat Immunol* **2018**, *19* (2), 108-119.
(47) Yu, T.; Gan, S.; Zhu, Q.; Dai, D.; Li, N.; Wang, H.; Chen, X.; Hou, D.; Wang, Y.; Pan, Q.; et al. Modulation of M2 macrophage polarization by the crosstalk between Stat6 and Trim24. *Nat Commun* **2019**, *10* (1), 4353.
(48) Bronte, V.; Serafini, P.; Mazzoni, A.; Segal, D. M.; Zanovello, P. L-arginine metabolism in myeloid cells controls T-lymphocyte functions. *Trends Immunol* **2003**, *24* (6), 302-306. Rotondo, R.; Barisione, G.; Mastracci, L.; Grossi, F.; Orengo, A. M.; Costa, R.; Truini, M.; Fabbi, M.; Ferrini, S.; Barbieri, O. IL-8 induces exocytosis of arginase 1 by neutrophil polymorphonuclears in nonsmall cell lung cancer. *Int J Cancer* **2009**, *125* (4), 887-893.
(49) Sharda, D. R.; Yu, S.; Ray, M.; Squadrito, M. L.; De Palma, M.; Wynn, T. A.; Morris, S. M., Jr.; Hankey, P. A. Regulation of macrophage arginase expression and tumor growth by the Ron receptor tyrosine kinase. *J Immunol* **2011**, *187* (5), 2181-2192.
(50) Vergadi, E.; Ieronymaki, E.; Lyroni, K.; Vaporidi, K.; Tsatsanis, C. Akt Signaling Pathway in Macrophage Activation and M1/M2 Polarization. *J Immunol* **2017**, *198* (3), 1006-1014.
(51) Xu, H.; Chen, J.; Si, X.; Chen, M.; Pei, F.; Qiu, C.; Wu, J.; Guan, X. PKR inhibition mediates endotoxin tolerance in macrophages through inactivation of PI3K/AKT signaling. *Mol Med Rep* **2018**, *17* (6), 8548-8556.
(52) Dantonio, P. M.; Klein, M. O.; Freire, M.; Araujo, C. N.; Chiacetti, A. C.; Correa, R. G. Exploring major signaling cascades in melanomagenesis: a rationale route for targetted skin cancer therapy. *Biosci Rep* **2018**, *38* (5).
(53) Trikha, P.; Carson, W. E., 3rd. Signaling pathways involved in MDSC regulation. *Biochim Biophys Acta* **2014**, *1846* (1), 55-65.

(54) Schleicher, U.; Paduch, K.; Debus, A.; Obermeyer, S.; Konig, T.; Kling, J. C.; Ribechini, E.; Dudziak, D.; Mougiakakos, D.; Murray, P. J.; et al. TNF-Mediated Restriction of Arginase 1 Expression in Myeloid Cells Triggers Type 2 NO Synthase Activity at the Site of Infection. *Cell Rep* **2016**, *15* (5), 1062-1075.
(55) Miret, J. J.; Kirschmeier, P.; Koyama, S.; Zhu, M.; Li, Y. Y.; Naito, Y.; Wu, M.; Malladi, V. S.; Huang, W.; Walker, W.; et al. Suppression of Myeloid Cell Arginase Activity leads to Therapeutic Response in a NSCLC Mouse Model by Activating Anti-Tumor Immunity. *J Immunother Cancer* **2019**, *7* (1), 32.
(56) Vissers, Y. L.; Dejong, C. H.; Luiking, Y. C.; Fearon, K. C.; von Meyenfeldt, M. F.; Deutz, N. E. Plasma arginine concentrations are reduced in cancer patients: evidence for arginine deficiency? *Am J Clin Nutr* **2005**, *81* (5), 1142-1146.
(57) Feng, S.; Cheng, X.; Zhang, L.; Lu, X.; Chaudhary, S.; Teng, R.; Frederickson, C.; Champion, M. M.; Zhao, R.; Cheng, L.; et al. Myeloid-derived suppressor cells inhibit T cell activation through nitrating LCK in mouse cancers. *Proc Natl Acad Sci U S A* **2018**, *115* (40), 10094-10099.
(58) Albaugh, V. L.; Pinzon-Guzman, C.; Barbul, A. Arginine-Dual roles as an onconutrient and immunonutrient. *J Surg Oncol* **2017**, *115* (3), 273-280.
(59) Jin, X.; Dai, L.; Ma, Y.; Wang, J.; Liu, Z. Implications of HIF-1alpha in the tumorigenesis and progression of pancreatic cancer. *Cancer Cell Int* **2020**, *20*, 273. Semenza, G. L. Targeting HIF-1 for cancer therapy. *Nat Rev Cancer* **2003**, *3* (10), 721-732. Pezzuto, A.; Carico, E. Role of HIF-1 in Cancer Progression: Novel Insights. A Review. *Curr Mol Med* **2018**, *18* (6), 343-351. Jun, J. C.; Rathore, A.; Younas, H.; Gilkes, D.; Polotsky, V. Y. Hypoxia-Inducible Factors and Cancer. *Curr Sleep Med Rep* **2017**, *3* (1), 1-10.
(60) Ke, X.; Chen, C.; Song, Y.; Cai, Q.; Li, J.; Tang, Y.; Han, X.; Qu, W.; Chen, A.; Wang, H.; et al. Hypoxia modifies the polarization of macrophages and their inflammatory microenvironment, and inhibits malignant behavior in cancer cells. *Oncol Lett* **2019**, *18* (6), 5871-5878. Werno, C.; Menrad, H.; Weigert, A.; Dehne, N.; Goerdt, S.; Schledzewski, K.; Kzhyshkowska, J.; Brune, B. Knockout of HIF-1alpha in tumor-associated macrophages enhances M2 polarization and attenuates their pro-angiogenic responses. *Carcinogenesis* **2010**, *31* (10), 1863-1872.
(61) Grzywa, T. M.; Sosnowska, A.; Matryba, P.; Rydzynska, Z.; Jasinski, M.; Nowis, D.; Golab, J. Myeloid Cell-Derived Arginase in Cancer Immune Response. *Front Immunol* **2020**, *11*, 938.
(62) Kossel, A.; Dakin, H. D. Über die Arginase. *Hoppe-Seyler´s Zeitschrift für physiologische Chemie* **1904**, *41* (4), 321-331.

(63) Pudlo, M.; Demougeot, C.; Girard-Thernier, C. Arginase Inhibitors: A Rational Approach Over One Century. *Med Res Rev* **2017**, *37* (3), 475-513.
(64) Pethe, S.; Boucher, J. L.; Mansuy, D. Interaction of anions with rat liver arginase: specific inhibitory effects of fluoride. *J Inorg Biochem* **2002**, *88* (3-4), 397-402.
(65) Kim, S. W.; Cuong, T. D.; Hung, T. M.; Ryoo, S.; Lee, J. H.; Min, B. S. Arginase II inhibitory activity of flavonoid compounds from Scutellaria indica. *Arch Pharm Res* **2013**, *36* (8), 922-926.
(66) dos Reis, M. B.; Manjolin, L. C.; Maquiaveli Cdo, C.; Santos-Filho, O. A.; da Silva, E. R. Inhibition of Leishmania (Leishmania) amazonensis and rat arginases by green tea EGCG, (+)-catechin and (-)-epicatechin: a comparative structural analysis of enzyme-inhibitor interactions. *PLoS One* **2013**, *8* (11), e78387.
(67) da Silva, E. R.; Castilho, T. M.; Pioker, F. C.; Tomich de Paula Silva, C. H.; Floeter-Winter, L. M. Genomic organisation and transcription characterisation of the gene encoding Leishmania (Leishmania) amazonensis arginase and its protein structure prediction. *Int J Parasitol* **2002**, *32* (6), 727-737.
(68) Girard-Thernier, C.; Pham, T. N.; Demougeot, C. The Promise of Plant-Derived Substances as Inhibitors of Arginase. *Mini Rev Med Chem* **2015**, *15* (10), 798-808.
(69) Pham, T. N.; Liagre, B.; Girard-Thernier, C.; Demougeot, C. Research of novel anticancer agents targeting arginase inhibition. *Drug Discov Today* **2018**, *23* (4), 871-878.
(70) Pham, T. N.; Bordage, S.; Pudlo, M.; Demougeot, C.; Thai, K. M.; Girard-Thernier, C. Cinnamide Derivatives as Mammalian Arginase Inhibitors: Synthesis, Biological Evaluation and Molecular Docking. *Int J Mol Sci* **2016**, *17* (10).
(71) Garcia, A. R.; Oliveira, D. M. P.; Claudia, F. A. A.; Jesus, J. B.; Renno Sodero, A. C.; Souza, A. M. T.; Supuran, C. T.; Vermelho, A. B.; Rodrigues, I. A.; Pinheiro, A. S. Leishmania infantum arginase: biochemical characterization and inhibition by naturally occurring phenolic substances. *J Enzyme Inhib Med Chem* **2019**, *34* (1), 1100-1109.
(72) Handler, N.; Wolkerstorfer, A.; Buschmann, H. Selective Optimization of Side Activities: An Alternative and Promising Strategy for Lead Generation. In *Lead Generation*, Methods and Principles in Medicinal Chemistry, 2016; pp 221-258.
(73) Wermuth, C. G. Selective optimization of side activities: the SOSA approach. *Drug Discov Today* **2006**, *11* (3-4), 160-164.

(74) Iyamu, E. W.; Ekekezie, C.; Woods, G. M. In vitro evidence of the inhibitory capacity of chloroquine on arginase activity in sickle erythrocytes. *Br J Haematol* **2007**, *139* (2), 337-343.
(75) Iyamu, E. W.; Perdew, H.; Woods, G. M. Modulation of Arginase Pathway by Chloroquine and Its Congener May Underlie the Enhanced Cell Commitment towards Erythroid Differentiation. *Blood* **2007**, *110* (11), 3394-3394.
(76) Lisi, L.; Pizzoferrato, M.; Miscioscia, F. T.; Topai, A.; Navarra, P. Interactions between integrase inhibitors and human arginase 1. *J Neurochem* **2017**, *142* (1), 153-159.
(77) Di Costanzo, L.; Ilies, M.; Thorn, K. J.; Christianson, D. W. Inhibition of human arginase I by substrate and product analogues. *Arch Biochem Biophys* **2010**, *496* (2), 101-108.
(78) Edlbacher, S.; Zeller, A. Optische Spezifität und Aktivierung der Arginase. *Hoppe-Seyler´s Zeitschrift für physiologische Chemie* **1936**, *242* (5-6), 253-260.
(79) Dabir, S.; Dabir, P.; Somvanshi, B. The kinetics of inhibition of Vigna catjang cotyledon and buffalo liver arginase by L-proline and branched-chain amino acids. *J Enzyme Inhib Med Chem* **2006**, *21* (6), 727-731.
(80) Rao, K. V. K.; Reddy, S. R. R.; Swami, K. S. The inhibition of sheep liver arginase by some l-amino-acids. *Int J Biochem* **1973**, *4* (19), 62-70. Hunter, A.; Downs, C. E. The Inhibition of Arginase by Amino Acids. *J Biol Chem* **1945**, *157* (2), 427-446.
(81) Sen, D. K. Uraemia and its treatment by arginase inhibitor. *Nature* **1959**, *184(Suppl 7)*, 459-460.
(82) Hrabak, A.; Bajor, T.; Temesi, A. Comparison of substrate and inhibitor specificity of arginase and nitric oxide (NO) synthase for arginine analogues and related compounds in murine and rat macrophages. *Biochem Biophys Res Commun* **1994**, *198* (1), 206-212.
(83) Boucher, J. L.; Custot, J.; Vadon, S.; Delaforge, M.; Lepoivre, M.; Tenu, J. P.; Yapo, A.; Mansuy, D. N omega-hydroxyl-L-arginine, an intermediate in the L-arginine to nitric oxide pathway, is a strong inhibitor of liver and macrophage arginase. *Biochem Biophys Res Commun* **1994**, *203* (3), 1614-1621.
(84) Moali, C.; Brollo, M.; Custot, J.; Sari, M. A.; Boucher, J. L.; Stuehr, D. J.; Mansuy, D. Recognition of alpha-amino acids bearing various C=NOH functions by nitric oxide synthase and arginase involves very different structural determinants. *Biochemistry* **2000**, *39* (28), 8208-8218.

(85) Custot, J.; Moali, C.; Brollo, M.; Boucher, J. L.; Delaforge, M.; Mansuy, D.; Tenu, J. P.; Zimmermann, J. L. The New α-Amino Acid Nω-Hydroxy-nor-l-arginine: a High-Affinity Inhibitor of Arginase Well Adapted To Bind to Its Manganese Cluster. *J Am Chem Soc* **1997**, *119* (17), 4086-4087.
(86) Custot, J.; Boucher, J.-L.; Vadon, S.; Guedes, C.; Dijols, S.; Delaforge, M.; Mansuy, D. Nω-Hydroxyamino-α-amino acids as a new class of very strong inhibitors of arginases. *J Biol Inorg Chem* **1996**, *1* (1), 73-82.
(87) Cama, E.; Shin, H.; Christianson, D. W. Design of amino acid sulfonamides as transition-state analogue inhibitors of arginase. *J Am Chem Soc* **2003**, *125* (43), 13052-13057.
(88) Ilies, M.; Di Costanzo, L.; North, M. L.; Scott, J. A.; Christianson, D. W. 2-aminoimidazole amino acids as inhibitors of the binuclear manganese metalloenzyme human arginase I. *J Med Chem* **2010**, *53* (10), 4266-4276.
(89) Shin, H.; Cama, E.; Christianson, D. W. Design of amino acid aldehydes as transition-state analogue inhibitors of arginase. *J Am Chem Soc* **2004**, *126* (33), 10278-10284.
(90) Zakharian, T. Y.; Di Costanzo, L.; Christianson, D. W. (S)-2-amino-6-nitrohexanoic acid binds to human arginase I through multiple nitro-metal coordination interactions in the binuclear manganese cluster. *J Am Chem Soc* **2008**, *130* (51), 17254-17255.
(91) Zakharian, T. Y.; Di Costanzo, L.; Christianson, D. W. Synthesis of (2S)-2-amino-7,8-epoxyoctanoic acid and structure of its metal-bridging complex with human arginase I. *Org Biomol Chem* **2008**, *6* (18), 3240-3243.
(92) Ilies, M.; Dowling, D. P.; Lombardi, P. M.; Christianson, D. W. Synthesis of a new trifluoromethylketone analogue of l-arginine and contrasting inhibitory activity against human arginase I and histone deacetylase 8. *Bioorg Med Chem Lett* **2011**, *21* (19), 5854-5858.
(93) Cama, E.; Pethe, S.; Boucher, J. L.; Han, S.; Emig, F. A.; Ash, D. E.; Viola, R. E.; Mansuy, D.; Christianson, D. W. Inhibitor coordination interactions in the binuclear manganese cluster of arginase. *Biochemistry* **2004**, *43* (28), 8987-8999.
(94) Colleluori, D. M.; Ash, D. E. Classical and slow-binding inhibitors of human type II arginase. *Biochemistry* **2001**, *40* (31), 9356-9362.
(95) Havlinova, Z.; Hroch, M.; Nagy, A.; Sispera, L.; Holecek, M.; Chladek, J. Single- and multiple-dose pharmacokinetics of arginase inhibitor Nomega-hydroxy-nor-L-arginine, and its effect on plasma amino acids concentrations in Wistar rats. *Gen Physiol Biophys* **2014**, *33* (2), 189-198.

(96) Baggio, R.; Elbaum, D.; Kanyo, Z. F.; Carroll, P. J.; Cavalli, R. C.; Ash, D. E.; Christianson, D. W. Inhibition of Mn2+2-Arginase by Borate Leads to the Design of a Transition State Analogue Inhibitor, 2(S)-Amino-6-boronohexanoic Acid. *J Am Chem Soc* **1997**, *119* (34), 8107-8108.
(97) Kim, N. N.; Cox, J. D.; Baggio, R. F.; Emig, F. A.; Mistry, S. K.; Harper, S. L.; Speicher, D. W.; Morris, S. M., Jr.; Ash, D. E.; Traish, A.; et al. Probing erectile function: S-(2-boronoethyl)-L-cysteine binds to arginase as a transition state analogue and enhances smooth muscle relaxation in human penile corpus cavernosum. *Biochemistry* **2001**, *40* (9), 2678-2688.
(98) Cox, J. D.; Kim, N. N.; Traish, A. M.; Christianson, D. W. Arginase-boronic acid complex highlights a physiological role in erectile function. *Nat Struct Biol* **1999**, *6* (11), 1043-1047.
(99) Grobben, Y.; Uitdehaag, J. C. M.; Willemsen-Seegers, N.; Tabak, W. W. A.; de Man, J.; Buijsman, R. C.; Zaman, G. J. R. Structural insights into human Arginase-1 pH dependence and its inhibition by the small molecule inhibitor CB-1158. *J Struct Biol X* **2020**, *4*, 100014.
(100) Nagagarajan, S.; Xue, F.; MacKerell, A. D., Jr. Impact of substrate protonation and tautomerization states on interactions with the active site of arginase I. *J Chem Inf Model* **2013**, *53* (2), 452-460.
(101) Ivanenkov, Y. A.; Chufarova, N. V. Small-molecule arginase inhibitors. *Pharm Pat Anal* **2014**, *3* (1), 65-85.
(102) Ilies, M.; Di Costanzo, L.; Dowling, D. P.; Thorn, K. J.; Christianson, D. W. Binding of alpha,alpha-disubstituted amino acids to arginase suggests new avenues for inhibitor design. *J Med Chem* **2011**, *54* (15), 5432-5443.
(103) Van Zandt, M. C.; Whitehouse, D. L.; Golebiowski, A.; Ji, M. K.; Zhang, M.; Beckett, R. P.; Jagdmann, G. E.; Ryder, T. R.; Sheeler, R.; Andreoli, M.; et al. Discovery of (R)-2-amino-6-borono-2-(2-(piperidin-1-yl)ethyl)hexanoic acid and congeners as highly potent inhibitors of human arginases I and II for treatment of myocardial reperfusion injury. *J Med Chem* **2013**, *56* (6), 2568-2580.
(104) Van Zandt, M. C.; Jagdmann, G. E.; Whitehouse, D. L.; Ji, M.; Savoy, J.; Potapova, O.; Cousido-Siah, A.; Mitschler, A.; Howard, E. I.; Pyle, A. M.; et al. Discovery of N-Substituted 3-Amino-4-(3-boronopropyl)pyrrolidine-3-carboxylic Acids as Highly Potent Third-Generation Inhibitors of Human Arginase I and II. *J Med Chem* **2019**, *62* (17), 8164-8177.
(105) Steggerda, S. M.; Bennett, M. K.; Chen, J.; Emberley, E.; Huang, T.; Janes, J. R.; Li, W.; MacKinnon, A. L.; Makkouk, A.; Marguier, G.; et al. Inhibition of arginase by CB-1158 blocks myeloid cell-mediated immune suppression in the tumor microenvironment. *J Immunother Cancer* **2017**, *5* (1), 101.

(106) Papadopoulos, K. P.; Tsai, F. Y.-C.; Bauer, T. M.; Muigai, L.; Liang, Y.; Bennett, M. K.; Orford, K. W.; Fu, S. CX-1158-101: A first-in-human phase 1 study of CB-1158, a small molecule inhibitor of arginase, as monotherapy and in combination with an anti-PD-1 checkpoint inhibitor in patients (pts) with solid tumors. *J Clin Oncol* **2017**, *35* (15_suppl), 3005-3005.
(107) GK, I. B. J.; Corporation, I. A Study of INCMGA00012, INCB001158, and the Combination in Japanese Participants With Advanced Solid Tumors. https://ClinicalTrials.gov/show/NCT03910530: 2019.
(108) Borek, B.; Gajda, T.; Golebiowski, A.; Blaszczyk, R. Boronic acid-based arginase inhibitors in cancer immunotherapy. *Bioorg Med Chem* **2020**, *28* (18), 115658.
(109) Lu, M.; Zhang, H.; Li, D.; Childers, M.; Pu, Q.; Palte, R. L.; Gathiaka, S.; Lyons, T. W.; Palani, A.; Fan, P. W.; et al. Structure-Based Discovery of Proline-Derived Arginase Inhibitors with Improved Oral Bioavailability for Immuno-Oncology. *ACS Med Chem Lett* **2021**, *12* (9), 1380-1388.
(110) Achab, A. A.; Childers, M., L.; Cimming, J., N.; Fischer, C.; Gathiaka, S.; Gunaydin, H.; Lesburg, C., A.; Derun, L.; Min, L.; Palani, A.; et al. WO2019177873 - arginase inhibitors and methods of use. WO/2019/177873, 2019.
(111) Sabnis, R. W. Novel Arginase Inhibitors for Treating Cancer and Respiratory Inflammatory Diseases. *ACS Med Chem Lett* **2020**, *11* (12), 2370-2371.
(112) Mitcheltree, M. J.; Li, D.; Achab, A.; Beard, A.; Chakravarthy, K.; Cheng, M.; Cho, H.; Eangoor, P.; Fan, P.; Gathiaka, S.; et al. Discovery and Optimization of Rationally Designed Bicyclic Inhibitors of Human Arginase to Enhance Cancer Immunotherapy. *ACS Med Chem Lett* **2020**, *11* (4), 582-588.
(113) Eric B. Sjogren; Jim Li; Michael Van Zandt; Darren Whitehouse. US10851118B2-Compositions and methods for inhibiting arginase activity. 2018.

(114) Grzybowski, M. M.; Stanczak, P. S.; Peczkowicz-Szyszka, J.; Wolska, P.; Zdziarska, A. M.; Mazurkiewicz, M.; Brzezinska, J.; Blaszczyk, R.; Gołebiowski, A.; Dobrzanski, P.; et al. Abstract P71: Novel dual arginase 1/2 inhibitor OATD-02 (OAT-1746) improves the efficacy of immune checkpoint inhibitors. *Ann. Oncol.* **2017**, *28*, xi20. Grzybowski, M. M.; Stanczak, P. S.; Peczkowicz-Szyszka, J.; Wolska, P.; Zdziarska, A. M.; Mazurkiewicz, M.; Brzezinska, J.; Blaszczyk, R.; Gołebiowski, A.; Dobrzanski, P.; et al. Abstract P1180: development of OAT-1746: a novel arginase 1 and 2 inhibitor for cancer immuntherapy. *Ann. Oncol.* **2017**, *28*, v418. Grzybowski, M. M.; Stanczak, P. S.; Peczkowicz-Szyszka, J.; Wolska, P.; Zdziarska, A. M.; Mazurkiewicz, M.; Brzezinska, J.; Blaszczyk, R.; Gołebiowski, A.; Dobrzanski, P.; et al. Abstract B003: Development of OAT-1746, a novel arginase 1 and 2 inhibitor for cancer immunotherapy. *Mol Cancer Ther* **2018**, *17*, B0003. Grzybowski, M. M.; Peczkowicz-Szyszka, J.; Stanczak, P. S.; Wolska, P.; Stanczak, P. S.; Welzer, M.; Nikolaev, E.; Siwinska, A. M.; Blaszczyk, R.; Borek, B.; et al. Abstract P1973: Targeting ARG2 as a novel therapeutic approach for cancer. *Ann. Oncol.* **2019**, *30*, v793. Pilanc-kudlek, P.; Cyranowski, S.; Wojnicki, K.; Ochocka, N.; Grzybowski, M.; Stańczak, P.; Pomper, P.; Błaszczyk, R.; Gołębiowski, A.; Dobrzański, P.; et al. Novel arginase inhibitor alone and in combination with an immune check point inhibitor reduces tumour growth in murine experimental gliomas. *Annals of Oncology* **2019**, *30*, xi56-xi57.
(115) Corporation, I. A Study to Evaluate the Safety, Tolerability, and Antitumor Activity of INCB001158 Plus Epacadostat, With or Without Pembrolizumab, in Advanced Solid Tumors. https://ClinicalTrials.gov/show/NCT03361228: 2018.
(116) Study to Evaluate the Safety of CB-280 in Patients With Cystic Fibrosis. https://ClinicalTrials.gov/show/NCT04279769.
(117) Doshi, A., Cantin, S., Secinaro, M. Abstract A769: Inhibition of arginase in combination with anti-PDL1 leads to increased infiltration and activation of CD8+ T cells, NK cells, and CD103+ dendritic cells in the mouse syngeneic MC38-OVA tumor model. *J Immunother Cancer*, **2019**, P769. Schuller, A.; Doshi, A.; Cantin, S.; Secinaro, M.; Wang, Y.; Prickett, L.; Tentarelli, S.; Gangl, E.; Ghadially, H.; Ilieva, K.; et al. Abstract 4523: Inhibition of arginase in combination with anti-PDL1 leads to increased infiltration and activation of CD8+ T cells, NK cells, and CD103+ dendritic cells in mouse syngeneic tumor models. *Cancer Res* **2020**, *80*, 4523.
(118) Corporation, I. A Phase 1/2 Study of INCB001158 in Combination With Chemotherapy in Subjects With Solid Tumors. https://ClinicalTrials.gov/show/NCT03314935: 2017.

(119) Javle, M. M.; Bridgewater, J. A.; Gbolahan, O. B.; Jungels, C.; Cho, M. T.; Papadopoulos, K. P.; Thistlethwaite, F. C.; Canon, J.-L. R.; Cheng, L.; Ioannidis, S.; et al. A phase I/II study of safety and efficacy of the arginase inhibitor INCB001158 plus chemotherapy in patients (Pts) with advanced biliary tract cancers. *J Clin Oncol* **2021**, *39* (3_suppl), 311-311.
(120) Corporation, I. Arginase Inhibitor INCB001158 as a Single Agent and in Combination With Immune Checkpoint Therapy in Patients With Advanced/Metastatic Solid Tumors. https://ClinicalTrials.gov/show/NCT02903914: 2016.
(121) Chinard, F. P. Photometric estimation of proline and ornithine. *J Biol Chem* **1952**, *199* (1), 91-95.
(122) McCaldin, D. J. The Chemistry of Ninhydrin. *Chem Rev* **1960**, *60* (1), 39-51.
(123) Kim, H. R.; Rho, H. W.; Park, J. W.; Park, B. H.; Kim, J. S.; Lee, M. W. Assay of ornithine aminotransferase with ninhydrin. *Anal Biochem* **1994**, *223* (2), 205-207.
(124) Wahl, O.; Holzgrabe, U. Amino acid analysis for pharmacopoeial purposes. *Talanta* **2016**, *154*, 150-163.
(125) Tommasi, S.; Elliot, D. J.; Da Boit, M.; Gray, S. R.; Lewis, B. C.; Mangoni, A. A. Homoarginine and inhibition of human arginase activity: kinetic characterization and biological relevance. *Sci Rep* **2018**, *8* (1), 3697.
(126) Fawcett, J. K.; Scott, J. E. A rapid and precise method for the determination of urea. *J Clin Pathol* **1960**, *13*, 156-159. Bolleter, W. T.; Bushman, C. J.; Tidwell, P. W. Spectrophotometric Determination of Ammonia as Indophenol. *Anal Chem* **2002**, *33* (4), 592-594.
(127) Watt, G. W.; Chrisp, J. D. Spectrophotometric Method for Determination of Urea. *Anal Chem* **2002**, *26* (3), 452-453.
(128) Geiger, P. J. The use of p-dimethylaminobenzaldehyde for the microdetermination of urea in urine. *Microchem* **1968**, *13* (3), 481-490.
(129) Cline, R. E.; Fink, R. M. Investigation of Color Reaction between p-Dimethylaminobenzaldehyde and Urea or Ureido Acids. *Anal Chem* **2002**, *28* (1), 47-52.
(130) Fearon, W. R. The carbamido diacetyl reaction: a test for citrulline. *Biochem J* **1939**, *33* (6), 902-907.
(131) Archibald, R. M. Colorimetric Determination of Urea. *J Biol Chem* **1945**, *157* (2), 507-518.
(132) Greenberg, D. M. *[49] Arginase:*; 1955.
(133) Phillips, R. F.; Pitt, B. M. The Use of Xanthydrol as a Reagent for the Characterization of Primary Amides. *J Am Chem Soc* **2002**, *65* (7), 1355-1357.

(134) Mackenzie, C. P. An evaluation of the xanthydrol reaction and the "urastrat" system for the rapid estimation of blood urea. *Vet Rec* **1967**, *80* (21), 621-624.
(135) Clark, S.; Francis, P. S.; Conlan, X. A.; Barnett, N. W. Determination of urea using high-performance liquid chromatography with fluorescence detection after automated derivatisation with xanthydrol. *J Chromatogr A* **2007**, *1161* (1-2), 207-213.
(136) Jung, D.; Biggs, H.; Erikson, J.; Ledyard, P. U. New Colorimetric reaction for end-point, continuous-flow, and kinetic measurement of urea. *Clin Chem* **1975**, *21* (8), 1136-1140.
(137) Zawada, R. J.; Kwan, P.; Olszewski, K. L.; Llinas, M.; Huang, S. G. Quantitative determination of urea concentrations in cell culture medium. *Biochem Cell Biol* **2009**, *87* (3), 541-544.
(138) Ruegg, U. T.; Russell, A. S. A rapid and sensitive assay for arginase. *Anal Biochem* **1980**, *102* (1), 206-212.
(139) Kepka-Lenhart, D.; Ash, D. E.; Morris, S. M. Determination of mammalian arginase activity. *Methods Enzymol* **2008**, *440*, 221-230.
(140) Ellman, G. L. Tissue sulfhydryl groups. *Arch Biochem Biophys* **1959**, *82* (1), 70-77.
(141) Baggio, R.; Cox, J. D.; Harper, S. L.; Speicher, D. W.; Christianson, D. W. A new chromophoric assay for arginase activity. *Anal Biochem* **1999**, *276* (2), 251-253.
(142) Deng, H. H.; Shi, X. Q.; Peng, H. P.; Zhuang, Q. Q.; Yang, Y.; Liu, A. L.; Xia, X. H.; Chen, W. Gold Nanoparticle-Based Photoluminescent Nanoswitch Controlled by Host-Guest Recognition and Enzymatic Hydrolysis for Arginase Activity Assay. *ACS Appl Mater Interfaces* **2018**, *10* (6), 5358-5364.
(143) Deng, H.-H.; Shi, X.-Q.; Wang, F.-F.; Peng, H.-P.; Liu, A.-L.; Xia, X.-H.; Chen, W. Fabrication of Water-Soluble, Green-Emitting Gold Nanoclusters with a 65% Photoluminescence Quantum Yield via Host–Guest Recognition. *Chem Mater* **2017**, *29* (3), 1362-1369.
(144) Kailasa, S. K.; Nguyen, T. P.; Baek, S. H.; Tu Phan, L. M.; Rafique, R.; Park, T. J. Assembly of 6-aza-2-thiothymine on gold nanoparticles for selective and sensitive colorimetric detection of pencycuron in water and food samples. *Talanta* **2019**, *205*, 120087.
(145) Campeau, L. C.; Stuart, D. R.; Leclerc, J. P.; Bertrand-Laperle, M.; Villemure, E.; Sun, H. Y.; Lasserre, S.; Guimond, N.; Lecavallier, M.; Fagnou, K. Palladium-catalyzed direct arylation of azine and azole N-oxides: reaction development, scope and applications in synthesis. *J Am Chem Soc* **2009**, *131* (9), 3291-3306.

(146) https://resources.nanotempertech.com/brochures/nanotemper-tycho-brochure (accessed. March 20, 2022)
(147) Bhat, R.; Xue, Y.; Berg, S.; Hellberg, S.; Ormo, M.; Nilsson, Y.; Radesater, A. C.; Jerning, E.; Markgren, P. O.; Borgegard, T.; et al. Structural insights and biological effects of glycogen synthase kinase 3-specific inhibitor AR-A014418. *J Biol Chem* **2003**, *278* (46), 45937-45945.
(148) Huber, V.; Camisaschi, C.; Berzi, A.; Ferro, S.; Lugini, L.; Triulzi, T.; Tuccitto, A.; Tagliabue, E.; Castelli, C.; Rivoltini, L. Cancer acidity: An ultimate frontier of tumor immune escape and a novel target of immunomodulation. *Semin Cancer Biol* **2017**, *43*, 74-89. Hirschhaeuser, F.; Sattler, U. G.; Mueller-Klieser, W. Lactate: a metabolic key player in cancer. *Cancer Res* **2011**, *71* (22), 6921-6925.
(149) Di Costanzo, L.; Pique, M. E.; Christianson, D. W. Crystal structure of human arginase I complexed with thiosemicarbazide reveals an unusual thiocarbonyl mu-sulfide ligand in the binuclear manganese cluster. *J Am Chem Soc* **2007**, *129* (20), 6388-6389.
(150) Kotthaus, J.; Schade, D.; Topker-Lehmann, K.; Beitz, E.; Clement, B. N(delta)-Methylated L-arginine derivatives and their effects on the nitric oxide generating system. *Bioorg Med Chem* **2008**, *16* (5), 2305-2312.
(151) Cama, E.; Colleluori, D. M.; Emig, F. A.; Shin, H.; Kim, S. W.; Kim, N. N.; Traish, A. M.; Ash, D. E.; Christianson, D. W. Human arginase II: crystal structure and physiological role in male and female sexual arousal. *Biochemistry* **2003**, *42* (28), 8445-8451. Bivalacqua, T. J.; Hellstrom, W. J.; Kadowitz, P. J.; Champion, H. C. Increased expression of arginase II in human diabetic corpus cavernosum: in diabetic-associated erectile dysfunction. *Biochem Biophys Res Commun* **2001**, *283* (4), 923-927.
(152) Rakers, C.; Bermudez, M.; Keller, B. G.; Mortier, J.; Wolber, G. Computational close up on protein-protein interactions: how to unravel the invisible using molecular dynamics simulations? *Wiley Interdiscip Rev Comput Mol Sci* **2015**, *5* (5), 345-359.
(153) Abraham, M. J.; Murtola, T.; Schulz, R.; Páll, S.; Smith, J. C.; Hess, B.; Lindahl, E. GROMACS: High performance molecular simulations through multi-level parallelism from laptops to supercomputers. *SoftwareX* **2015**, *1-2*, 19-25.
(154) Mortier, J.; Rakers, C.; Frederick, R.; Wolber, G. Computational tools for in silico fragment-based drug design. *Curr Top Med Chem* **2012**, *12* (17), 1935-1943.
(155) Boonstra, S.; Onck, P. R.; Giessen, E. CHARMM TIP3P Water Model Suppresses Peptide Folding by Solvating the Unfolded State. *J Phys Chem B* **2016**, *120* (15), 3692-3698.

(156) Bowers, K. J.; Sacerdoti, F. D.; Salmon, J. K.; Shan, Y.; Shaw, D. E.; Chow, E.; Xu, H.; Dror, R. O.; Eastwood, M. P.; Gregersen, B. A.; et al. Molecular dynamics---Scalable algorithms for molecular dynamics simulations on commodity clusters. In Proceedings of the 2006 ACM/IEEE conference on Supercomputing - SC '06, 2006.
(157) Kaminski, G. A.; Friesner, R. A.; Tirado-Rives, J.; Jorgensen, W. L. Evaluation and Reparametrization of the OPLS-AA Force Field for Proteins via Comparison with Accurate Quantum Chemical Calculations on Peptides. *J Phys Chem B* **2001**, *105* (28), 6474-6487.
(158) Durrant, J. D.; Votapka, L.; Sorensen, J.; Amaro, R. E. POVME 2.0: An Enhanced Tool for Determining Pocket Shape and Volume Characteristics. *J Chem Theory Comput* **2014**, *10* (11), 5047-5056.
(159) Martyna, G. J.; Tobias, D. J.; Klein, M. L. Constant pressure molecular dynamics algorithms. *J Chem Phys* **1994**, *101* (5), 4177-4189.
(160) Andrusier, N.; Mashiach, E.; Nussinov, R.; Wolfson, H. J. Principles of flexible protein-protein docking. *Proteins* **2008**, *73* (2), 271-289.
(161) Sydow, D.; Burggraaff, L.; Szengel, A.; van Vlijmen, H. W. T.; AP, I. J.; van Westen, G. J. P.; Volkamer, A. Advances and Challenges in Computational Target Prediction. *J Chem Inf Model* **2019**, *59* (5), 1728-1742.
(162) Busnel, O.; Carreaux, F.; Carboni, B.; Pethe, S.; Goff, S. V.; Mansuy, D.; Boucher, J. L. Synthesis and evaluation of new omega-borono-alpha-amino acids as rat liver arginase inhibitors. *Bioorg Med Chem* **2005**, *13* (7), 2373-2379.
(163) Jacobsen, J. A.; Fullagar, J. L.; Miller, M. T.; Cohen, S. M. Identifying chelators for metalloprotein inhibitors using a fragment-based approach. *J Med Chem* **2011**, *54* (2), 591-602.
(164) Trott, O.; Olson, A. J. AutoDock Vina: improving the speed and accuracy of docking with a new scoring function, efficient optimization, and multithreading. *J Comput Chem* **2010**, *31* (2), 455-461.
(165) Tiwari, R.; Mahasenan, K.; Pavlovicz, R.; Li, C.; Tjarks, W. Carborane clusters in computational drug design: a comparative docking evaluation using AutoDock, FlexX, Glide, and Surflex. *J Chem Inf Model* **2009**, *49* (6), 1581-1589.
(166) Muller, J.; Cardey, B.; Zedet, A.; Desingle, C.; Grzybowski, M.; Pomper, P.; Foley, S.; Harakat, D.; Ramseyer, C.; Girard, C.; et al. Synthesis, evaluation and molecular modelling of piceatannol analogues as arginase inhibitors. *RSC Med Chem* **2020**, *11* (5), 559-568.

(167) Bagutski, V.; Del Grosso, A.; Carrillo, J. A.; Cade, I. A.; Helm, M. D.; Lawson, J. R.; Singleton, P. J.; Solomon, S. A.; Marcelli, T.; Ingleson, M. J. Mechanistic studies into amine-mediated electrophilic arene borylation and its application in MIDA boronate synthesis. *J Am Chem Soc* **2013**, *135* (1), 474-487.
(168) Kwiecień, H.; Wodnicka, A. Five-Membered Ring Systems: Furans and Benzofurans. Progress in Heterocyclic Chemistry, 2020; pp 281-323. Ke, Z.; Tsui, G. C.; Peng, X.-S.; Yeung, Y.-Y. Five-Membered Ring Systems. Progress in Heterocyclic Chemistry, 2016; pp 219-274.
(169) Amarnath, V.; Amarnath, K. Intermediates in the Paal-Knorr Synthesis of Furans. *J Org Chem* **2002**, *60* (2), 301-307.
(170) Vermeire, F. H.; Carstensen, H.-H.; Herbinet, O.; Battin-Leclerc, F.; Marin, G. B.; Van Geem, K. M. The thermal decomposition of furfural: molecular chemistry unraveled. *Proc Combust Inst* **2019**, *37* (1), 445-452.
(171) Noonan, G.; Leach, A. G. A mechanistic proposal for the protodeboronation of neat boronic acids: boronic acid mediated reaction in the solid state. *Org Biomol Chem* **2015**, *13* (9), 2555-2560.
(172) Lozada, J.; Liu, Z.; Perrin, D. M. Base-promoted protodeboronation of 2,6-disubstituted arylboronic acids. *J Org Chem* **2014**, *79* (11), 5365-5368.
(173) Kuivila, H. G.; Nahabedian, K. V. Electrophilic Displacement Reactions. X. General Acid Catalysis in the Protodeboronation of Areneboronic Acids1-3. *J Am Chem Soc* **2002**, *83* (9), 2159-2163. Florentin, D.; Fournié-Zaluski, M. C.; Callanquin, M.; Roques, B. P. Etude des pKaet de la protodéboronation des acides furanneboroniques. *J Heterocycl Chem* **1976**, *13* (6), 1265-1272. Klingensmith, L. M.; Bio, M. M.; Moniz, G. A. Selective protodeboronation: synthesis of 4-methyl-2-thiopheneboronic anhydride and demonstration of its utility in Suzuki–Miyaura reactions. *Tetrahedron Lett* **2007**, *48* (46), 8242-8245.
(174) Cox, P. A.; Leach, A. G.; Campbell, A. D.; Lloyd-Jones, G. C. Protodeboronation of Heteroaromatic, Vinyl, and Cyclopropyl Boronic Acids: pH-Rate Profiles, Autocatalysis, and Disproportionation. *J Am Chem Soc* **2016**, *138* (29), 9145-9157. Cox, P. A.; Reid, M.; Leach, A. G.; Campbell, A. D.; King, E. J.; Lloyd-Jones, G. C. Base-Catalyzed Aryl-B(OH)2 Protodeboronation Revisited: From Concerted Proton Transfer to Liberation of a Transient Aryl Anion. *J Am Chem Soc* **2017**, *139* (37), 13156-13165.

(175) Kabalka, G. W.; Yao, M. L.; Marepally, S. R.; Chandra, S. Biological evaluation of boronated unnatural amino acids as new boron carriers. *Appl Radiat Isot* **2009**, *67* (7-8 Suppl), S374-379. Kabalka, G. W.; Wu, Z. Z.; Yao, M. L.; Natarajan, N. The syntheses and in vivo biodistribution of novel boronated unnatural amino acids. *Appl Radiat Isot* **2004**, *61* (5), 1111-1115. Kabalka, G. W.; Das, B. C.; Das, S. Synthesis of novel boron containing unnatural cyclic amino acids as potential therapeutic agents. *Tetrahedron Lett* **2001**, *42* (41), 7145-7146.
(176) Nussinov, R.; Tsai, C. J. The different ways through which specificity works in orthosteric and allosteric drugs. *Curr Pharm Des* **2012**, *18* (9), 1311-1316.
(177) Oldham, K. G. Radiometric Methods of Enzyme Assay. In *Methods of Biochemical Analysis*, Methods of Biochemical Analysis, 2006; pp 191-286.
(178) Prevost, J. R. C.; Kozlova, A.; Es Saadi, B.; Yildiz, E.; Modaffari, S.; Lambert, D. M.; Pochet, L.; Wouters, J.; Dolušić, E.; Frédérick, R. Convenient one-pot formation of highly functionalized 5-bromo-2-aminothiazoles, potential endocannabinoid hydrolase MAGL inhibitors. *Tetrahedron Lett* **2018**, *59* (49), 4315-4319.
(179) Mortier, J.; Prevost, J. R. C.; Sydow, D.; Teuchert, S.; Omieczynski, C.; Bermudez, M.; Frederick, R.; Wolber, G. Arginase Structure and Inhibition: Catalytic Site Plasticity Reveals New Modulation Possibilities. *Sci Rep* **2017**, *7* (1), 13616.
(180) Supuran, C. T. Structure-based drug discovery of carbonic anhydrase inhibitors. *J Enzyme Inhib Med Chem* **2012**, *27* (6), 759-772.
(181) Lennox, A. J.; Lloyd-Jones, G. C. Selection of boron reagents for Suzuki-Miyaura coupling. *Chem Soc Rev* **2014**, *43* (1), 412-443.
(182) Rosenthal, A. S.; Tanega, C.; Shen, M.; Mott, B. T.; Bougie, J. M.; Nguyen, D. T.; Misteli, T.; Auld, D. S.; Maloney, D. J.; Thomas, C. J. Potent and selective small molecule inhibitors of specific isoforms of Cdc2-like kinases (Clk) and dual specificity tyrosine-phosphorylation-regulated kinases (Dyrk). *Bioorg Med Chem Lett* **2011**, *21* (10), 3152-3158.
(183) Gioia, D.; Bertazzo, M.; Recanatini, M.; Masetti, M.; Cavalli, A. Dynamic Docking: A Paradigm Shift in Computational Drug Discovery. *Molecules* **2017**, *22* (11). Singh, S.; Bani Baker, Q.; Singh, D. B. Molecular docking and molecular dynamics simulation. In *Bioinformatics*, 2022; pp 291-304.

(184) Lin, Y. F.; Cheng, C. W.; Shih, C. S.; Hwang, J. K.; Yu, C. S.; Lu, C. H. MIB: Metal Ion-Binding Site Prediction and Docking Server. *J Chem Inf Model* **2016**, *56* (12), 2287-2291. Sciortino, G.; Rodriguez-Guerra Pedregal, J.; Lledos, A.; Garribba, E.; Marechal, J. D. Prediction of the interaction of metallic moieties with proteins: An update for protein-ligand docking techniques. *J Comput Chem* **2018**, *39* (1), 42-51. Smith, R. D.; Engdahl, A. L.; Dunbar, J. B., Jr.; Carlson, H. A. Biophysical limits of protein-ligand binding. *J Chem Inf Model* **2012**, *52* (8), 2098-2106.
(185) Das, B. C.; Thapa, P.; Karki, R.; Schinke, C.; Das, S.; Kambhampati, S.; Banerjee, S. K.; Van Veldhuizen, P.; Verma, A.; Weiss, L. M.; et al. Boron chemicals in diagnosis and therapeutics. *Future Med Chem* **2013**, *5* (6), 653-676. Vinas, I. T. C. The uniqueness of boron as a novel challenging element for drugs in pharmacology, medicine and for smart biomaterials. *Future Med Chem* **2013**, *5* (6), 617-619. Hunter, P. Not boring at all. Boron is the new carbon in the quest for novel drug candidates. *EMBO Rep* **2009**, *10* (2), 125-128. Kahlert, J.; Austin, C. J. D.; Kassiou, M.; Rendina, L. M. The Fifth Element in Drug Design: Boron in Medicinal Chemistry. *Aust J Chem* **2013**, *66* (10). Soriano-Ursua, M. A.; Das, B. C.; Trujillo-Ferrara, J. G. Boron-containing compounds: chemico-biological properties and expanding medicinal potential in prevention, diagnosis and therapy. *Expert Opin Ther Pat* **2014**, *24* (5), 485-500. Smoum, R.; Rubinstein, A.; Dembitsky, V. M.; Srebnik, M. Boron containing compounds as protease inhibitors. *Chem Rev* **2012**, *112* (7), 4156-4220.
(186) Kurt, B.; Temel, H. Parameterization of Boronates Using VFFDT and Paramfit for Molecular Dynamics Simulation. *Molecules* **2020**, *25* (9). Kurt, B.; Temel, H. Development of AMBER parameters for molecular dynamics simulations of boron compounds containing aromatic structure. *Chem Phys Let* **2021**, *775*.
(187) Eaton, G. R. NMR of boron compounds. *J Chem Educ* **1969**, *46* (9). Ruman, T.; Dlugopolska, K.; Rode, W. Synthesis and NMR properties of the first boron analogues of uracil. *Bioorg Chem* **2010**, *38* (1), 33-36. Ruman, T.; Dlugopolska, K.; Jurkiewicz, A.; Rydel, K.; Les, A.; Rode, W. The synthesis and NMR investigation on novel boron derivatives of stavudine. *Bioorg Chem* **2010**, *38* (3), 87-91.

(188) Gillis, E. P.; Burke, M. D. A simple and modular strategy for small molecule synthesis: iterative Suzuki-Miyaura coupling of B-protected haloboronic acid building blocks. *J Am Chem Soc* **2007**, *129* (21), 6716-6717. Reilly, M. K.; Rychnovsky, S. D. DABO Boronates: Stable Heterocyclic Boronic Acid Complexes for Use in Suzuki-Miyaura Cross-Coupling Reactions. *Synlett* **2011**, *2011* (16). Lai, S.; Takaesu, N.; Lin, W. X.; Perrin, D. M. Suzuki coupling of aroyl-MIDA boronate esters – A preliminary report on scope and limitations. *Tetrahedron Lett* **2021**, *74*.
(189) Grob, J. E.; Nunez, J.; Dechantsreiter, M. A.; Hamann, L. G. One-pot reductive amination and Suzuki-Miyaura cross-coupling of formyl aryl and heteroaryl MIDA boronates in array format. *J Org Chem* **2011**, *76* (12), 4930-4940.
(190) Skarbek, C.; Serra, S.; Maslah, H.; Rascol, E.; Labruere, R. Arylboronate prodrugs of doxorubicin as promising chemotherapy for pancreatic cancer. *Bioorg Chem* **2019**, *91*, 103158.
(191) van Beurden, K.; de Koning, S.; Molendijk, D.; van Schijndel, J. The Knoevenagel reaction: a review of the unfinished treasure map to forming carbon–carbon bonds. *Green Chem Let Rev* **2020**, *13* (4), 349-364.
(192) Ouellette, R. J.; Rawn, J. D. Aldehydes and Ketones: Nucleophilic Addition Reactions. In *Organic Chemistry*, 2018; pp 595-623. Byrne, P. A.; Gilheany, D. G. The modern interpretation of the Wittig reaction mechanism. *Chem Soc Rev* **2013**, *42* (16), 6670-6696.
(193) Bielski, R.; Grynkiewicz, G. Furan platform chemicals beyond fuels and plastics. *Green Chemistry* **2021**, *23* (19), 7458-7487.
(194) Karlinskii, B. Y.; Kostyukovich, A. Y.; Kucherov, F. A.; Galkin, K. I.; Kozlov, K. S.; Ananikov, V. P. Directing-Group-Free, Carbonyl Group-Promoted Catalytic C–H Arylation of Bio-Based Furans. *ACS Catalysis* **2020**, *10* (19), 11466-11480.
(195) Wu, P.; Givskov, M.; Nielsen, T. E. Reactivity and Synthetic Applications of Multicomponent Petasis Reactions. *Chem Rev* **2019**, *119* (20), 11245-11290.
(196) Blackwell, J. H.; Kumar, R.; Gaunt, M. J. Visible-Light-Mediated Carbonyl Alkylative Amination to All-Alkyl alpha-Tertiary Amino Acid Derivatives. *J Am Chem Soc* **2021**, *143* (3), 1598-1609.
(197) Strecker, A. Ueber die künstliche Bildung der Milchsäure und einen neuen, dem Glycocoll homologen Körper. *Annalen der Chemie und Pharmacie* **1850**, *75* (1), 27-45.
(198) Masamba, W. Petasis vs. Strecker Amino Acid Synthesis: Convergence, Divergence and Opportunities in Organic Synthesis. *Molecules* **2021**, *26* (6).

(199) Chowdari, N. S.; Suri, J. T.; Barbas, C. F., 3rd. Asymmetric synthesis of quaternary alpha- and beta-amino acids and beta-lactams via proline-catalyzed mannich reactions with branched aldehyde donors. *Org Lett* **2004**, *6* (15), 2507-2510.
(200) Lenci, E.; Bellini Puglielli, R.; Bucaletti, E.; Innocenti, R.; Trabocchi, A. A Glucose-Derived α-Hydroxy Aldehyde for the Petasis Reaction: Facile Access to Polyfunctional δ-Amino Acids. *Eur J of Org Chem* **2020**, *2020* (27), 4227-4234.
(201) Shiotani, S.; Morita, H.; Ishida, T.; In, Y. Furopyridines.IX. Syntheses and properties of 3-ethoxy derivatives of furo[2,3-b]-, furo[3,2-b]-, furo[2,3-c]- and furo[3,2-c]pyridine. *J Heterocycl Chem* **1988**, *25* (4), 1205-1213.
(202) Leermann, T.; Leroux, F. R.; Colobert, F. Highly efficient one-pot access to functionalized arylboronic acids via noncryogenic bromine/magnesium exchanges. *Org Lett* **2011**, *13* (17), 4479-4481. Barroso, S.; Joksch, M.; Puylaert, P.; Tin, S.; Bell, S. J.; Donnellan, L.; Duguid, S.; Muir, C.; Zhao, P.; Farina, V.; et al. Improvement in the Palladium-Catalyzed Miyaura Borylation Reaction by Optimization of the Base: Scope and Mechanistic Study. *J Org Chem* **2021**, *86* (1), 103-109.
(203) Inglesby, P. A.; Agnew, L. R.; Carter, H. L.; Ring, O. T. Diethanolamine Boronic Esters: Development of a Simple and Standard Process for Boronic Ester Synthesis. *Org Process Res Dev* **2020**, *24* (9), 1683-1689. Collins, B. S. L.; Wilson, C. M.; Myers, E. L.; Aggarwal, V. K. Asymmetric Synthesis of Secondary and Tertiary Boronic Esters. *Angew Chem Int Ed Engl* **2017**, *56* (39), 11700-11733.
(204) Silva, M. P.; Saraiva, L.; Pinto, M.; Sousa, M. E. Boronic Acids and Their Derivatives in Medicinal Chemistry: Synthesis and Biological Applications. *Molecules* **2020**, *25* (18).
(205) Fyfe, J. W.; Valverde, E.; Seath, C. P.; Kennedy, A. R.; Redmond, J. M.; Anderson, N. A.; Watson, A. J. Speciation control during Suzuki-Miyaura cross-coupling of haloaryl and haloalkenyl MIDA boronic esters. *Chemistry* **2015**, *21* (24), 8951-8964.
(206) Christianson, D. W.; Tomczuk, B. E.; Pottorf, R. S.; Colasanti, A., V,; Olson, G., L. US20200223871A1-Arginase inhbitiors and methods of use. 2020.
(207) Thabault, L.; Liberelle, M.; Frederick, R. Targeting protein self-association in drug design. *Drug Discov Today* **2021**, *26* (5), 1148-1163.
(208) Thabault, L.; Brisson, L.; Brustenga, C.; Martinez Gache, S. A.; Prevost, J. R. C.; Kozlova, A.; Spillier, Q.; Liberelle, M.; Benyahia, Z.; Messens, J.; et al. Interrogating the Lactate Dehydrogenase Tetramerization Site Using (Stapled) Peptides. *J Med Chem* **2020**, *63* (9), 4628-4643.

(209) Thabault, L.; Liberelle, M.; Koruza, K.; Yildiz, E.; Joudiou, N.; Messens, J.; Brisson, L.; Wouters, J.; Sonveaux, P.; Frederick, R. Discovery of a novel lactate dehydrogenase tetramerization domain using epitope mapping and peptides. *J Biol Chem* **2021**, *296*, 100422. Kozlova, A.; Thabault, L.; Liberelle, M.; Klaessens, S.; Prevost, J. R. C.; Mathieu, C.; Pilotte, L.; Stroobant, V.; Van den Eynde, B.; Frederick, R. Rational Design of Original Fused-Cycle Selective Inhibitors of Tryptophan 2,3-Dioxygenase. *J Med Chem* **2021**, *64* (15), 10967-10980.
(210) Nosé, S. An extension of the canonical ensemble molecular dynamics method. *Mol Phys* **1986**, *57* (1), 187-191. Hoover, W. G. Canonical dynamics: Equilibrium phase-space distributions. *Phys Rev A Gen Phys* **1985**, *31* (3), 1695-1697.
(211) Lindorff-Larsen, K.; Piana, S.; Palmo, K.; Maragakis, P.; Klepeis, J. L.; Dror, R. O.; Shaw, D. E. Improved side-chain torsion potentials for the Amber ff99SB protein force field. *Proteins* **2010**, *78* (8), 1950-1958.
(212) Wang, J.; Wolf, R. M.; Caldwell, J. W.; Kollman, P. A.; Case, D. A. Development and testing of a general amber force field. *J Comput Chem* **2004**, *25* (9), 1157-1174.
(213) Sousa da Silva, A. W.; Vranken, W. F. ACPYPE - AnteChamber PYthon Parser interfacE. *BMC Res Notes* **2012**, *5*, 367.
(214) Hess, B.; Bekker, H.; Berendsen, H. J. C.; Fraaije, J. G. E. M. LINCS: A linear constraint solver for molecular simulations. *J Comput Chem* **1997**, *18* (12), 1463-1472.
(215) Parrinello, M.; Rahman, A. A Molecular-Dynamics Study of Crystal-Structure Transformations. *B Am Phys Soc* **1981**, *26* (3), 380-380.
(216) Wolber, G.; Langer, T. LigandScout: 3-D pharmacophores derived from protein-bound ligands and their use as virtual screening filters. *J Chem Inf Model* **2005**, *45* (1), 160-169.

Annexe

Tetrahedron Letters 59 (2018) 4315–4319

Contents lists available at ScienceDirect

Tetrahedron Letters

journal homepage: www.elsevier.com/locate/tetlet

Convenient one-pot formation of highly functionalized 5-bromo-2-aminothiazoles, potential endocannabinoid hydrolase MAGL inhibitors

Julien R.C. Prevost [a], Arina Kozlova [a], Bouazza Es Saadi [a], Esra Yildiz [a], Sara Modaffari [b,1], Didier M. Lambert [a], Lionel Pochet [b], Johan Wouters [b], Eduard Dolušić [b,2], Raphaël Frédérick [a,*]

[a] Medicinal Chemistry Research Group (CMFA), Louvain Drug Research Institute (LDRI), Université Catholique de Louvain (UCL), 73 Avenue Mounier, B1.73.10, 1200 Brussels, Belgium
[b] Namur Medicine & Drug Innovation Center (NAMEDIC-NARILIS), University of Namur (UNamur), 61 rue de Bruxelles, 5000 Namur, Belgium

ARTICLE INFO

Article history:
Received 3 August 2018
Revised 17 October 2018
Accepted 24 October 2018
Available online 25 October 2018

Keywords:
Electrophilic aromatic substitution
Oxidation
Halogenation
Thiazoles
Monoacylglycerol lipase

ABSTRACT

Highly functionalized 5-bromo-2-amino-1,3-thiazoles bearing various substituents could be easily prepared by a rapid and efficient one-pot method, using simple starting materials and mild conditions while avoiding the use of metal catalysts or inconvenient reagents such as elemental halogens. These useful products can serve as starting materials for other reactions or as pharmacologically interesting compounds. In our work we have shown that the resulting 5-bromothiazole compounds could lead to monoacylglycerol lipase (MAGL) inhibition in the μM range.

During an attempt to prepare substituted thiazole *N*-oxides [1] in our laboratory, we unexpectedly found that treatment of 2-aminothiazoles with *m*-chloroperoxybenzoic acid (*m*CPBA) in ethanol did not afforded the desired product **1** (Scheme 1). Spectral analyses proved that the corresponding 5-bromo-2-amino-thiazole **2** was formed instead in a very good yield (>90%).

This observation can be explained by the fact that the starting compound was, in fact, obtained as a hydrobromide salt. Thus, rapid oxidative bromination mediated by *m*CPBA occurred in the 5-position of the thiazole ring. We decided to explore this interesting transformation in more detail, especially because thiazoles are present in many natural products possessing biological activity, such as anti-mycobacterial agents [2–5]. A growing body of medicinal chemistry literature reports thiazole derivatives as candidates for the treatment of various pathologies [6–15]. These heteroaromatics have also found applications in materials science, e.g. as liquid crystals [16,17] Furthermore, halogenated thiazoles are useful synthetic intermediates for introducing this heterocyclic scaffold into more complex molecules [18]. The older method of using elemental bromine for bromination of the thiazole ring [19–21] has still occasionally been used in the recent years [22–24]. However, this approach has drawbacks such as toxicity, low atom economy, corrosiveness, handling issues and a relatively high cost. Apart from the application of *N*-halosuccinimides [25], more recent methods for thiazole halogenation include the use of copper(II) halides [26], metalations of the thiazole ring followed by quenching the reactive intermediates with electrophiles [27] and transition metal catalysis [28]. In general, despite the modern development in aromatic halogenation [29,30], there still remains a need for new procedures operating under mild conditions. Environmentally friendly and atom-economic oxidative halogenation holds a lot of promise in this respect [31].

We firstly examined the influence of the nature of the oxidant on the yield of bromothiazole **2**. The brominated compound **2** vs. non-brominated compound **3** system was chosen as the benchmark and the absolute yields of the two thiazoles were determined by LC/MS analysis. As observed from Table 1, compared to *m*CPBA (Entry 1), all the other oxidants, such as hydrogen peroxide (entry 2), sodium hypochlorite (entry 5), and sodium periodate (entry 10) gave a lower yield of **2**. Moreover, even Oxone® (entry 4), which works fine in some other oxidative halogenations [32–39], did not give satisfying results in our experiments, permitting a 6% yield on **2**.

With the evidence of *m*CPBA being the best oxidant agent, the next part of this study examined the amount of oxidant. Adding up to 1 equivalent of *m*CPBA improved the bromination ratio, but

* Corresponding author.
E-mail address: raphael.frederick@uclouvain.be (R. Frédérick).

[1] This paper is dedicated to the memory of Mrs Sara Modaffari, a very nice and brilliant student, who passed away in March 9, 2018, aged 34.

[2] Present address: Federal agency for medicines and health products (Belgium), 40 Place Victor Horta, 1060 Brussels, Belgium.

https://doi.org/10.1016/j.tetlet.2018.10.055
0040-4039/

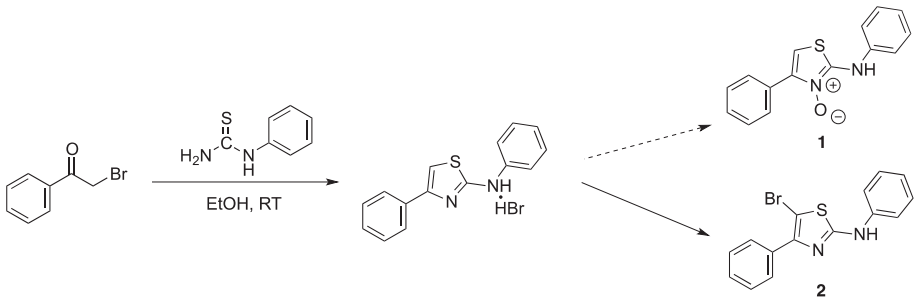

Scheme 1. *m*CPBA-mediated 5-bromo-2-amino-1,3-thiazole formation.

Table 1
Yield optimization studies for the formation of the bromothiazole 2.

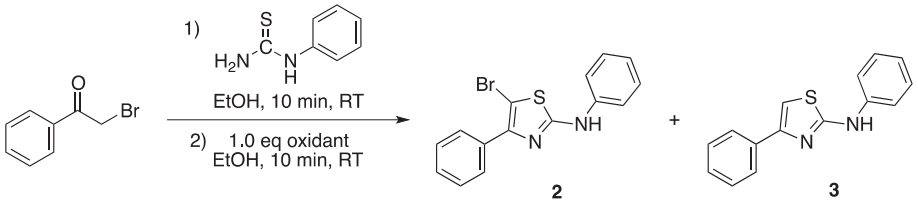

Entry	Oxidant	Equivalent	η (**2**) (%)[a]	η (**3**) (%)[a]
1	*m*CPBA	1.0	93	7
2	H_2O_2 50% aq.	1.0	6	93
3	UHP*	1.0	3	97
4	Oxone®**	1.0	6	94
5	$NaClO_2$	1.0	58	25
6	$NaBiO_3$	1.0	19	68
7	*t*-BuOOH	1.0	traces	69
8	MnO_2	1.0	12	64
9	$Na_2CO_3 \cdot 1.5\ H_2O$	1.0	traces	74
10	$NaIO_4$	1.0	77	20

*Urea hydrogen peroxide adduct.
**2 $KHSO_5 \cdot KHSO_4 \cdot K_2SO_4$.
[a] Yields determined by LC/MS analysis.

further increase of its quantity caused a drop in yields. We secondly aimed at exploring the influence of solvent. As depicted in Table 2, polar solvents such as ethanol and DMF (Table 2, entry 1, and 7) worked best, permitting high yields (>93%). In fact, the highest yield of 5-bromo derivative **2** is obtained when using DMF (Table 2, entry 7). Using acetone, dichloromethane, 1,4-dioxane, toluene or acetonitrile lead to poor global yields (Table 2, entries 2, 4, 5, 6 and 7).

Table 2
Investigation of the solvent and the reaction times for the formation of (5-bromo-4- phenyl-thiazol-2-yl)-phenylamine **2**.

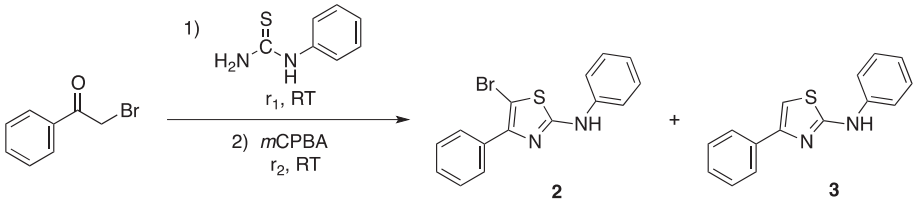

entry	solvent	Reaction time (min, r1 + r2)	η (**2**) (%)[a]	η (**3**) (%)[a]
1	EtOH	10 + 10	93	7
2	acetone	10 + 10	52	29
3	CH_2Cl_2	10 + 10	47	10
4	1,4-dioxane	10 + 10	43	22
5	toluene	10 + 10	10	12
6	MeCN	10 + 10	33	30
7	DMF	10 + 10	>99	<1
7′	DMF	5 + 5	99	1
7″	DMF	0 + 10	5	69

[a] Yields determined by LC/MS analysis.

Reduction of the r_1 and r_2 reaction time was also evaluated using DMF as solvent (Table 2, entry 7, 7′ and 7″). Reaction times limited at 5 min per step at room temperature is sufficient to obtain the desired compound **2** in a very good yield (99%). However, a one-pot operation adding *m*CPBA simultaneously with the α-bromoketone and thiourea (Table 2, entry 7″) caused a sharp drop in the yield of **2**, as well as in total thiazole (**2** + **3**). In most cases, a maximum of 10 min with *m*CPBA at room temperature was enough for the completion of the oxidative bromination reaction. Being more practical to handle than DMF, ethanol was chosen for all subsequent experiments and the chosen conditions were applied to probe the syntheses of a range of brominated thiazoles along with their non-brominated counterparts.

A suggested mechanism of the formation of the halogenation products includes the oxidation of halide to a reactive halogen derivative (Scheme 2) after reaction with the *m*- chloroperoxybenzoic acid. This *in situ* formed electrophilic hypobromous acid could then be attacked by the thiazole ring system in an electrophilic aromatic substitution reaction, giving the product brominated at C5 after aromatization. In fact, polarity inversion (umpolung) of the bromine is the key step for the addition-elimination reaction on the nucleophilic position of the thiazole ring. The formation of the diatomic elemental halogen X_2 with radical reaction seems to not occur due to the strict need of a stoichiometric amount of *m*CPBA to react with bromine. ^{13}C NMR studies showed easy identification thanks to a chemical shift for the carbon linked with the bromine in the brominated derivative around 90 ppm, against 115 ppm for none brominated compound. 2D NMR experiments (COSY, HSQC and HMBC) also led to the same conclusion.

Various methods of purification were also tried. Because of the very small differences between the retention values (R_f) for the thiazole and the 5-bromo-thiazole, flash chromatography did not reveal to be successful. After several attempts, we found that the best way to obtain an easy and rapid isolation was by precipitation. Briefly, to a solution of the compounds in methanol or ethanol, addition of water led to the precipitation of the brominated derivative first. In case of mixture after precipitation, a second recrystallisation allowed to obtain the desired products in very high purity (>95%).

Finally, using standard conditions (0.3 M of all reagents in ethanol), the syntheses of a range of brominated thiazoles was undertaken (Table 3). Briefly, *m*CPBA was added and the mixture was stirred for 30 min at room temperature to allow completion of the first (Hantzsch) step reaction. Conversion rates and absolute

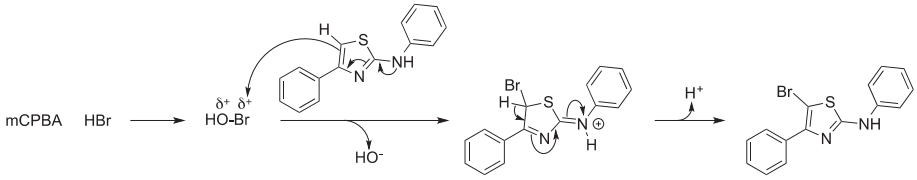

Scheme 2. Suggested mechanism of the 5-bromo derivatives formation.

Table 3
Outcomes of syntheses of 5-bromo-thiazoles with various substitution patterns (**Compound**, Yield[a] %).

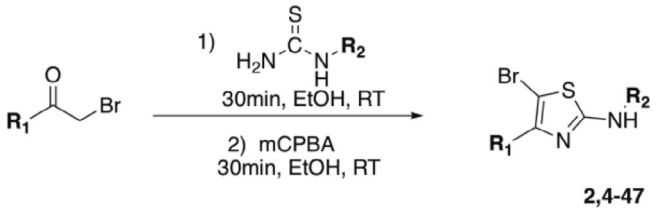

2,4-47

R_1	R_2								
		F	F	F	Cl	Cl	Cl		
	2 63%	**4** 74%	**5** 70%	**6** 71%	**7** 71%	**8** 78%	**9** 39%	**10** 36%	**11** 82%
	12 14%	**13** 51%	**14** 47%	**15** 28%	**16** 76%	**17** 87%	**18** 91%	**19** 77%	**20** 77%
	21 25%	**22** 27%	**23** 51%	**24** 41%	**25** 60%	**26** 45%	**27** 35%	**28** 51%	**29** 55%
O_2N	**30** 45%	**31** 36%	**32** 53%	**33** 45%	**34** 61%	**35** 49%	**36** 45%	**37** 85%	**38** 85%
NC	**39** 71%	**40** 36%	**41** 53%	**42** 45%	**43** 61%	**44** 49%	**45** 45%	**46** 85%	**47** 85%

[a] Yields determined by LC/MS analysis.

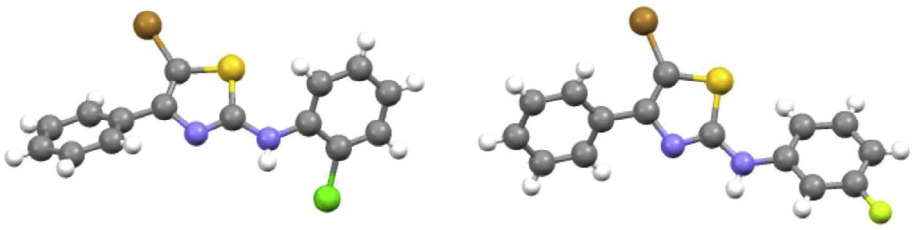

Figure 1. Solid state crystallographic structures of **5** (left) and **7** (right).

yields of the brominated vs. non-brominated derivatives were determined by LC/MS. In all cases, conversion rates proved to be quantitative with complete disparition (>99%) of the starting materials. As observed from Table 3, the absolute yields (non-optimized) ranged from 14% for **12** up to 91% for **18**, most of the transformation leading to a yield of brominated compounds >50%.

To further illustrate the scope of this reaction, the influence of electro-donating groups on R_1 and R_2 (Table 3) was also investigated. To this end, the 5-bromo-*N*-(4-methoxyphenyl)-4-phenylthiazol-2-amine **48**, the 5-bromo-*4*-(4-methoxyphenyl)-*N*-phenylthiazol-2-amine **49**, and the 5-bromo-*N,4-bis* (4-methoxyphenyl)-thiazol-2-amine **50,** containing a methoxy group on R_1 and/or R_2 were prepared and yields of, respectively, 86%, 76% and 73% were obtained, thus corroborating the versatility of this reaction.

In the case of the fluorinated (**5**) and chlorinated (**7**) compounds (see Table 3 above), crystals suitable for X-ray measurements were obtained (Fig 1). X-Ray data analysis unambiguously confirmed the structures of the newly synthesized molecules and the insertion of the bromine in the 5-position on the thiazole core.

Next, we investigated the potential of 5-bromothiazole as enzyme inhibitors. To this end, the brominated parent compound **2** was screened on various targets available in our lab and we found that this compound was interestingly a relatively potent inhibitor of the monoacylglycerol lipase (MAGL) [40] with > 60% inhibition at 100 μM. The compounds displayed in Table 3 were thus assayed on MAGL and 6 derivatives **6**, **8**, **11**, **14**, **15** and **19** proved to be more potent than the initial compound **2** with half maximal inhibitory concentration (IC_{50}) determined to be in the range of 10–55 μM [41–45]. Interestingly, the adamantyl and the phenyl on the left part of the molecules (R_1) seem better tolerated. The biological evaluation of these derivatives on MAGL can be found in the associated contents available.

In conclusion, our work describes a new, original and easy preparation of 5-bromo-thiazoles that can be synthesized efficiently following a one-pot procedure from simple starting materials, α-bromomethyl-ketones and thiosemicarbazides, and without using expensive catalysts or harsh conditions and reagents. The nature of the oxidant to perform the reaction, of the solvent and of the reaction time was evaluated. The initial compound **2** proved to be potentially interesting to target monoacylglycerol lipase (MAGL). A small library of 5-bromo-2-amino-thiazoles was thus elaborated and demonstrated promising although very preliminary inhibitory potency of MAGL.

Experimental

General information

All chemicals were purchased from Sigma or Acros Organics and used without further purification. NMR spectra were recorded on a Bruker Ultrashield Advance II 400 MHz instrument using dimethyl sulfoxide (DMSO d_6) or chloroform ($CDCl_3$) as deuterated solvent. Chemical shifts are reported in parts per million (ppm) and referenced to the residual solvent resonance. Coupling constants (J) are reported in hertz (Hz). Standard abbreviations indicating multiplicity were used as follows: s = singlet, d = doublet, t = triplet, dd = double doublet, q = quartet, m = multiplet, b = broad. Melting points (m.p.) were determined using an electrothermal apparatus and are reported uncorrected. LC-MS analyses were performed on an Agilent 6200 series TOF mass spectrometer equipped with ESI and APCI as ionization sources and TOF (Time Of Flight) detector, coupled with an Agilent 1200 series LC system with flux of 0.25 mL/min. High- resolution mass spectra were carried out on a Thermofisher Scientific LTQ-Orbitrap XL hybrid. X- ray diffraction datas were collected at room temperature on a Gemini Ultra (Rigaku) diffractometer using Cu Ka (1.54584) radiation.

MAGL esterase activity assay

MAGL activity was measured by following [^{3}H]-2-oleoyl glycerol ([^{3}H]-2-OG) hydrolysis, as previously described (cf ref 37, Morera, L.; et al. *Bioorganic and Medicinal Chemistry* **2012**, 20, 6260–6275). Briefly, 6 ng of pure human MAGL was preincubated during 30 min at room temperature in the presence of the inhibitor at various concentrations (Tris buffer 50 mM, BSA 0.15% w/v, pH 8.0, inhibitor dissolved in 10 μL DMSO). 2-OG (10 μM final concentration; [^{3}H]-2-OG 50,000 dpm, American Radiolabeled Chemicals; 200 μL total volume assay) was then added and the tubes were placed at 37 °C for 10 min. The reaction was stopped by adding 400 μL of a cold methanol- chloroform (1–1) mixture and, after 5 min centrifugation at 700*g*, the radioactivity was measured in the organic phase by liquid scintillation. The dpm value obtained for a blank (containing no enzyme) was systematically subtracted. Results were then expressed as percent of control activity (without inhibitor), after which GraphPad prism software was used to treat the data and to analyze the dose-response curves.

MAGL rapid dilution assay

The reversibility of MAGL inhibition by synthesized compounds was investigated using the rapid dilution assay. The enzyme (800 ng in 38 μL of a buffer containing Tris 50 mM, BSA 0.15%, pH 8.0) was incubated during 30 min at room temperature with 2 μL of compound **19** (concentration of 10^{-4} M and 10^{-5} M in the mixture) dissolved in DMSO. The enzyme-inhibitor mixture was then diluted 300-fold with the buffer. After 15 min of incubation, the enzyme activity was measured on a 150 μL aliquot (corresponding to 10 ng of enzyme) according to the above-described standard procedure.

Intermediate thioureas synthesis

To a solution of a (substituted)-phenylisothiocyanate derivative (0.6 M) in MeCN was added aqueous ammonia (25%, 1.5 eq). The solution was stirred at room temperature for 3 h. The reaction mixture was then concentrated. Purification was done by precipitation

from a mixture of *n*-hexane/ethyl acetate mixture (3/2). The pure product was recovered as a powder after filtration in a quantitative yield.

2-Amino-5-bromothiazole derivatives synthesis

To a solution of the intermediate thioureas (1 eq., 0.1 M) in EtOH was added 2-bromoacetophenone (1.25 eq). The solution was stirred at room temperature until completion of the reaction followed by TLC. Then *m*CPBA (1 eq., 3 M in EtOH) was added and the solution was stirred until completion. The reaction mixture was then concentrated. The resulting powder was dissolved in CH_2Cl_2 and extracted with water. The organic phases were combined, dried over Na_2SO_4 and evaporated. Purification by precipitation was performed: to the resulting powder was added a solution of 10% water in methanol until obtention of a cloudy solution. After cooling at 4 °C, precipitation of the product occurred over time. Filtration afforded the pure products as powders.

*5-Bromo-N,4-diphenylthiazol-2-amine **2**/N,4-diphenylthiazol-2-amine **3** system synthesis and LC/MS analysis procedure*

A mixture of the synthesized thiourea and variously substituted haloketones (0.3 mmol of each) in an appropriate solvent (900 µL) is reacted under the indicated experimental conditions. The oxidant in ethanol solution (0.3 mmol in 100 µL)) is added and the mixture is stirred. Then 1 mL of acetone is added and 20 µL of the mixture is added to 980 µL of acetonitrile. A second dilution with 20 µL of the previously prepared solution is added to 980 µL of acetonitrile to give a sample from 0 (0% yield) to 60 µM (100% yield) of either thiazole, which is then analyzed by LC/MS (measurement of UV absorption at 254 nm).

Acknowledgments

We are grateful to Arnaud Mars for his contribution to this project, Dr. Marie-France Herent and Prof. Giulio Muccioli (UCLouvain, LDRI, BPBL, Belgium) for helpful discussions and assistance with HRMS and Nikolay Tumanov (PC^2 platform, UNamur, Belgium) for assistance with X-ray diffraction experiments. This work was supported by the Université catholique de Louvain (UCLouvain, Belgium), the National Fund for Scientific Research (F.R.S.-FNRS, Belgium) from which RF is an honorary research associate, the Télévie (Belgium), the Fonds Maisin (Belgium), the Fonds Spéciaux de Recherche (FSR, Belgium), the Actions de Recherche Concertées (ARC, Belgium) and the Fondatioun Kriibskrank Kanner (Luxembourg). RF and ED shares the last authorship position.

Appendix A. Supplementary data

Supplementary data to this article can be found online at https://doi.org/10.1016/j.tetlet.2018.10.055.

References

[1] L. Campeau, D.R. Stuart, J. Leclerc, M. Bertrand-Laperle, E. Villemure, H. Sun, S. Lasserre, N. Guimond, M. Lecavallier, K. Fagnou, J. Am. Chem. Soc. 131 (2009) 3291–3306.
[2] R.S. Roy, A.M. Gehring, J.C. Milne, P.J. Belshaw, C.T. Walsh, Nat. Prod. Rep. 16 (1999) 249–263.
[3] K.-H. Altmann, B. Pfeiffer, S. Arseniyadis, B.A. Pratt, K.C. Nicolaou, ChemMedChem 2 (2007) 396–423.
[4] Z. Jin, Nat. Prod. Rep. 23 (2006) 464–496.
[5] M.C. Bagley, J.W. Dale, E.A. Merritt, X. Xiong, Chem. Rev. 105 (2005) 685–714.
[6] Y.-S.E. Lee, S.-H. Chuang, L.Y.L. Huang, C.-L. Lai, Y.-H. Lin, J.-Y. Yang, C.-W. Liu, S. Yang, H.-S. Lin, C. Chang, J.-Y. Lai, P.-S. Jian, K. Lam, J.-M. Chang, J.Y.N. Lau, J.-J. Huang, J. Med. Chem. 57 (2014) 4098–4110.
[7] J. Yuan, S. Wang, Z. Luo, H. Qiu, P. Wang, X. Zhang, Y. Yang, Y. Yin, F. Zhang, H. Zhu, Bioorg. Med. Chem. Lett. 24 (2014) 2324–2328.
[8] J. Louvel, D. Guo, M. Agliardi, T.A.M. Mocking, R. Kars, T.P. Pham, L. Xia, H. de Vries, J. Brussee, L.H. Heitman, A.P. Ijzerman, J. Med. Chem. 57 (2014) 3213–3222.
[9] L. Lohrey, T.N. Uehara, S. Tani, J. Yamaguchi, H.-U. Humpf, K. Itami, Eur. J. Org. Chem. (2014) 3387–3394.
[10] R. Bhat, Y. Xue, S. Berg, S. Hellberg, M. Ormö, Y. Nilsson, A.-C. Radesäter, E. Jerning, P.-O. Markgren, T. Borgegård, M. Nylöf, A. Giménez-Cassina, F. Hernández, J.J. Lucas, J. Díaz-Nido, J. Avila, J. Biol. Chem. 278 (2003) 45937–45945.
[11] E.A. Ilardi, E. Vitaku, J.T. Njardarson, J. Med. Chem. 57 (2013) 2832–3842.
[12] H. Shao, S. Shi, S. Huang, A.J. Hole, A.Y. Abbas, S. Baumli, X. Liu, F. Lam, D.W. Foley, P.M. Fischer, M. Noble, J.A. Endicott, C. Pepper, S. Wang, J. Med. Chem. 56 (2013) 640–659.
[13] H. Mohammad, A.S. Mayhoub, A. Ghafoor, M. Soo, R.A. Alajlouni, M. Cushman, M.N. Seleem, J. Med. Chem. 247 (2014) 1609–1615.
[14] S.J. Kashyap, V.K. Garg, P.K. Sharma, N. Kumar, R. Dudhe, J.K. Gupta, Med. Chem. Res. 21 (2012) 2123–2132.
[15] N.P. Shah, C. Tran, F.Y. Lee, P. Chen, D. Norris, L. Charles, Science 305 (80) (2016) 399–401.
[16] A.A. Kiryanov, P. Sampson, A.J. Seed, J. Org. Chem. (2001) 7925–7929.
[17] A. Mori, A. Sekiguchi, K. Masui, T. Shimada, M. Horie, K. Osakada, M. Kawamoto, T. Ikeda, J. Am. Chem. Soc. 125 (2003) 1700–1701.
[18] S. Schröter, C. Stock, T. Bach, Tetrahedron 61 (2005) 2245–2267.
[19] G.N. Mahapatra, J. Am. Chem. Soc. 79 (1957) 988–991.
[20] B.P.T. Kaye, G.D. Meakins, C. Willbe, P.R. Williams, J. Chem. Soc. Perkin Trans. I (1981) 2335–2339.
[21] M. Begtrup, L.B.L. Hansen, Acta Chem. Scand. 46 (1992) 372–383.
[22] J. Hämmerle, M. Spina, M. Schnürch, M.D. Mihovilovic, P. Stanetty, Synthesis (Stuttg). 19 (2008) 3099–3107.
[23] Q. Dang, Y. Liu, D.K. Cashion, S.R. Kasibhatla, T. Jiang, F. Taplin, J.D. Jacintho, H. Li, Z. Sun, Y. Fan, J. DaRe, F. Tian, W. Li, T. Gibson, R. Lemus, PD Van Poelje, O.S. C. Potter, M.D. Erion, J. Med. Chem. (2011) 153–165.
[24] A.M. Grubb, M.J. Schmidt, A.J. Seed, P. Sampson, Synthesis (Stuttg). 44 (2012) 1026–1029.
[25] M.D. Altman, K.L. Arrington, J. Burch, B. Cote, J.-F. Fournier, J.Y. Gauthier, S. Kattar, S.L. Knowles, J. Lim, M.R. Machacek, A.B. Northrup, M.H. Reutershan, J.S. Robichaud, A.J. Schell, K.B. Spencer 2012. U.S. Patent 20120309735A1.
[26] F.G. Siméon, M.T. Wendahl, V.W. Pike, J. Org. Chem. 74 (2009) 2578–2580.
[27] C. Dunst, P. Knochel, J. Org. Chem. 76 (2011) 6972–6978.
[28] X. Wang, Y. Hu, S. Bonacorsi, Y. Hong, R. Burrell, J. Yu, J. Am. Chem. Soc. 135 (2013) 10326–10329.
[29] G. Wang, J. Gao, Green Chem. 14 (2012) 1125–1131.
[30] A. Bose, P. Mal, Tetrahedron Lett. 55 (2014) 2154–2156.
[31] G. Rothenberg, J.H. Clark, Green Chem. 2 (2000) 248–251.
[32] N. Narender, P. Srinivasu, S.J. Kulkarni, K.V. Raghavan, Synth Commun. 32 (2002) 279–286.
[33] M.M. Aborways, W.J. Moran, Tetrahedron Lett. 55 (2014) 2127–2129.
[34] S. Madabhushi, R. Jillella, K. Kumar, R. Mallu, K.R. Godala, Tetrahedron Lett. 54 (2013) 3993–3996.
[35] A.K. Macharla, R.C. Nappunni, N. Nama, Tetrahedron Lett. 53 (2012) 1401–1405.
[36] H. Umemoto, M. Umemoto, C. Ohta, M. Dohshita, H. Tanaka, S. Hattori, H. Hamamoto, Y. Miki, Heterocycles. 78 (2009) 2845–2850.
[37] H. Hussain, I.R. Green, I. Ahmed, Chem Rev. 113 (2013) 3329–3371.
[38] V.V.K. Mohan Kandepi, N. Narender, Synthesis (Stuttg) 44 (2012) 15–26.
[39] B.V. Tamhankar, U.V. Desai, R.B. Mane, P.P. Wadgaonkar, A.V. Bedekar, Synth Commun. 31 (2001) 2021–2027.
[40] W. Tuo, N. Leleu-Chavain, J. Spencer, S. Sansook, R. Millet, P. Chavatte, J Med Chem. 60 (2017) 4–46.
[41] N. Matuszak, G.G. Muccioli, G. Labar, D.M. Lambert, J Med Chem. 52 (2009) 7410–7420.
[42] C.N. Kapanda, J. Masquelier, G. Labar, G.G. Muccioli, J.H. Poupaert, D.M. Lambert, J Med Chem. 55 (2012) 5774–5783.
[43] G. Labar, C. Bauvois, F. Borel, J.L. Ferrer, J. Wouters, D.M. Lambert, ChemBioChem. 11 (2010) 218–227.
[44] C.N. Kapanda, G.G. Muccioli, G. Labar, J.H. Poupaert, D.M. Lambert, J Med Chem. 52 (2009) 7310–7314.
[45] L. Morera, G. Labar, G. Ortar, D.M. Lambert, Bioorg Med Chem. 20 (2012) 6260–6275.